



HAL
open science

Electrophysiological studies of(1) the regulation of G protein-gatedpotassium channels by δ -opioid receptors and(2) the function of viral rhodopsins

Ana Sofia Eria Oliveira

► **To cite this version:**

Ana Sofia Eria Oliveira. Electrophysiological studies of(1) the regulation of G protein-gatedpotassium channels by δ -opioid receptors and(2) the function of viral rhodopsins. Structural Biology [q-bio.BM]. Université Grenoble Alpes [2020-..], 2022. English. NNT : 2022GRALV053 . tel-04276361

HAL Id: tel-04276361

<https://theses.hal.science/tel-04276361v1>

Submitted on 9 Nov 2023

HAL is a multi-disciplinary open access archive for the deposit and dissemination of scientific research documents, whether they are published or not. The documents may come from teaching and research institutions in France or abroad, or from public or private research centers.

L'archive ouverte pluridisciplinaire **HAL**, est destinée au dépôt et à la diffusion de documents scientifiques de niveau recherche, publiés ou non, émanant des établissements d'enseignement et de recherche français ou étrangers, des laboratoires publics ou privés.

THÈSE

Pour obtenir le grade de

DOCTEUR DE L'UNIVERSITÉ GRENOBLE ALPES

Spécialité : Biologie Structurale et Nanobiologie

Arrêté ministériel : 25 mai 2016

Présentée par

Ana Sofia ERIA OLIVEIRA

Thèse dirigée par **Michel VIVAUDOU**

préparée au sein du **Groupe Channels, Institut de Biologie Structurale**
dans l'**École Doctorale Chimie et Sciences du Vivant**

Etudes électrophysiologiques de
(1) la régulation des canaux potassiques GIRK
par les récepteurs δ -opioïdes et
(2) la fonction des rhodopsines virales

Electrophysiological studies of
(1) the regulation of G protein-gated
potassium channels by δ -opioid receptors and
(2) the function of viral rhodopsins

Thèse soutenue publiquement le **21 avril 2022**,
devant le jury composé de :

Monsieur Michel VIVAUDOU

INGENIEUR HDR, CEA centre de Grenoble,
Directeur de thèse

Madame Meritxell CANALS

PROFESSEUR, University of Nottingham,
Rapporteuse

Monsieur Félix VIANA

CHERCHEUR, Universidad Miguel Hernández,
Rapporteur

Monsieur Franck FIESCHI

PROFESSEUR DES UNIVERSITES, Université Grenoble Alpes,
Président

Monsieur Guillaume SANDOZ

DIRECTEUR DE RECHERCHE, CNRS délégation Côte d'Azur,
Examineur



Electrophysiological studies of (1) the regulation of G protein-gated potassium channels by δ -opioid receptors and (2) the function of viral rhodopsins

By

Ana Sofia ERIA OLIVEIRA

A dissertation submitted in fulfilment of
the requirements for the degree of
DOCTOR OF PHILOSOPHY



UNIVERSITÉ GRENOBLE ALPES
École Doctorale de Chimie et Sciences du Vivant

Acknowledgments

To the members of the jury who willingly agreed (twice) to spend some of their time to evaluate and discuss my work, Dr. Félix Viana, Pr. Meritxell Canals, Dr. Guillaume Sandoz and Pr. Franck Fieschi, I would like to reemphasize my sincere gratitude.

I would like to acknowledge as well both Dr. Guillaume Lebon and Dr. Guillaume Sandoz, the members of my *Comité de Suivi Individuelle*, for the fruitful discussions through the years of the thesis.

On the same note, I would like to express my appreciation to the people with whom I had the opportunity to collaborate. Again, I have to mention Dr. Guillaume Sandoz and his team, for hosting me in his lab and for contributing directly to the experiments of both projects on this thesis. I am likewise thankful to Dr. Valentin Gordelyi and Dimitrii Zabelskii for trusting me with the viral rhodopsins.

Completing this thesis would not have been possible without my dear supervisor Michel Vivaudou. A statement - obvious as it is – that I find necessary to assert again. Thank you for creating an environment where we can thrive, for pushing us to share our work with other people, for showing us incredible analytical skills, and for giving us what I found to be the best blend of guidance and autonomy. P.S. Thank you for the unwavering support during what I can only describe as a finish line panic-induced full on meltdown. I could not have asked for a better supervisor.

A special mention to the previous and current members of the Channels Group - Mathilde Folacci, Jean Revilloud, Zlatomir Todorov - and to the members of Dr. Christophe Moreau's team, Loli, Léa, Guillaume and Justine, with whom I had the pleasure of sharing a lab and who assisted me in a way or another.

I want to give a shout-out to the students I had the heartfelt joy of guiding: Leon, Rosie, and Maria. You were real troopers and helped me so much with little coercion needed.

Of course, I could never forget all the fantastic friends (dare I say family) I made in Grenoble, which I will not venture to list not to have to choose an order. I have to thank you all for making

this journey so much smoother. My Ph.D. memories will forever be associated with all of you and the amazing moments we spent laughing together around infinite tables of Spanish, Greek, French, and Slovak food.

My 24/7 support system and personal cheerleader Rita Grenho deserves mention in everything I do, and so here it is.

Finally to my mother and father: obrigado pelo vosso apoio incondicional. Nunca me vou esquecer que só cheguei aqui porque vocês estão sempre prontos a ajudar-me. Espero um dia poder repagar tudo o que fizeram por mim.

Abstract

In this manuscript, the regulation of G protein-gated potassium channels by δ -opioid receptors, and the function of viral rhodopsins, are probed with molecular and electrophysiological approaches using the *Xenopus* oocyte heterologous expression system. The studies are presented as two independent projects:

Project A – Dual mechanism of regulation of G protein-gated potassium channels by δ -opioid receptors

The regulation of G protein-gated inwardly rectifying potassium channels (GIRK or Kir3 channels) by Opioid receptors (OR) modulates pain perception. Characteristically, GIRK channels are activated by the direct binding of the G protein $\beta\gamma$ subunits released upon activation of G protein-coupled receptors like OR.

In this project, we have studied the regulation of GIRK channels by OR by coexpressing them and measuring channel activity using electrophysiological techniques.

Our data disclose an unreported inhibition of GIRK channels by δ -opioid receptors (DOR). Opioid agonists acting through DOR activate GIRK channels at nM concentrations but inhibit them at higher concentrations. Notably, inhibition of GIRK channels was revealed at high levels of expression of DOR. Control experiments performed with the closely related μ -opioid receptor did not show any sign of inhibition, even at comparable levels of expression.

Unlike channel activation, inhibition appears not to require the receptor activation of G proteins, implying that these are two independent signaling pathways. Further experiments also suggest that this fast inhibition cannot be attributed to already described mechanisms involving kinases of G protein-coupled receptors or arrestins.

These observations highlight another level of complexity in the regulation of GIRK by OR, with mechanistic and physiological implications that remain to be fully elucidated.

Project B – Shedding light on the function of viral rhodopsins

Viral rhodopsins (VR) are a monophyletic group of proteins from viral origin within the superfamily of rhodopsins. While several VR structures have been solved, their function remains elusive. As members of the rhodopsin superfamily, they are 7-transmembrane spanning proteins covalently linked to a retinal molecule, which harvest light for potentially

different functions such as ion pumping, ion channeling, sensory or kinase activities.

We have tested the function of several viral rhodopsins by expressing them in oocytes and recording the currents elicited upon their activation by light. To assess surface expression, we developed a nanoluciferase-based technique to quantify protein expression in single oocytes. VR characterization in *Xenopus* oocytes showed that they accumulate intracellularly rather than at the cell surface, and that their activation by light induces calcium release from intracellular stores. The light-induced calcium release subsequently activates downstream effectors of calcium signaling, such as calcium-activated chloride channels.

To record the channel activity of VRs directly, we were able to redirect one VR towards the cell surface by fusing it to a high-expressing G protein-coupled receptor. The fusion construct displayed photo-induced currents, but selectivity remains to be fully elucidated.

The precise release of calcium from intracellular stores mediates a large panoply of cellular processes such as gene expression, neurotransmitter release, or muscle contraction. The propensity of the VR to accumulate in internal storages and modulate calcium release makes it a great candidate as a novel optogenetic tool, with potential applications in the manipulation of many aspects of cell activity.

Résumé

Dans ce manuscrit, la régulation des canaux potassiques GIRK par les récepteurs δ -opioïdes, et la fonction des rhodopsines virales, sont sondés à l'aide d'approches moléculaires et électrophysiologiques. Ces études sont présentées comme deux projets indépendants :

Projet A - Double mécanisme de régulation des canaux potassiques GIRK par les récepteurs δ -opioïdes

La régulation des canaux potassiques GIRK (ou Kir3) par les récepteurs opioïdes (RO) module la perception de la douleur. De manière caractéristique, les canaux GIRK sont activés par la liaison directe des sous-unités $\beta\gamma$ de la protéine G libérées lors de l'activation de récepteurs couplés aux protéines G, tels que les RO.

Dans ce projet, nous avons étudié la régulation des canaux GIRK par les RO en les coexprimant dans des ovocytes de Xenopes et en mesurant l'activité des canaux à l'aide de techniques électrophysiologiques.

Nos données révèlent une inhibition non encore décrite des canaux GIRK par les récepteurs δ -opioïdes (DOR). Les agonistes opioïdes agissant par l'intermédiaire de DOR activent les canaux GIRK à des concentrations nM mais les inhibent à des concentrations plus élevées. Notamment, l'inhibition des canaux GIRK a été révélée à des niveaux élevés d'expression de DOR. Des expériences de contrôle réalisées avec le récepteur μ -opioïde, étroitement lié, n'ont révélé aucun signe d'inhibition, même à des niveaux d'expression comparables.

Contrairement à l'activation du canal, l'inhibition ne semble pas nécessiter l'activation des protéines G par le récepteur, ce qui suggère qu'il s'agit de deux voies de signalisation indépendantes. D'autres expériences suggèrent également que cette inhibition rapide ne peut pas être attribuée à des mécanismes déjà décrits impliquant des kinases de récepteurs couplés aux protéines G ou des arrestines.

Ces observations mettent en évidence un niveau inattendu de complexité dans la régulation de GIRK par les RO, avec des implications mécanistiques et physiologiques qui restent à élucider complètement.

Projet B – Étude de la fonction des rhodopsines virales

Les rhodopsines virales (RV) constituent un groupe monophylétique de protéines d'origine virale au sein de la superfamille des rhodopsines. Bien que plusieurs structures de RV aient

été résolues, leur fonction reste insaisissable. En tant que membres de la superfamille des rhodopsines, elles sont des protéines à 7-hélices transmembranaires liées de manière covalente à une molécule de rétinal capable de réagir à la lumière pour des fonctions telles que le transport actif ou passif d'ions, ou des activités sensorielles de type kinases.

Nous avons testé la fonction de plusieurs rhodopsines virales en les exprimant dans l'ovocyte de *Xenopus* et en enregistrant les courants induits par la lumière. Pour évaluer l'expression de surface des RV, nous avons développé une technique basée sur la nanoluciférase pour quantifier l'expression dans l'ovocyte.

La caractérisation dans les ovocytes de *Xenopus* a montré que les RV s'accumulent au niveau intracellulaire plutôt qu'à la surface des cellules, et que leur activation par la lumière induit une libération de calcium à partir des réserves intracellulaires. La libération de calcium induite par la lumière active ensuite les effecteurs de la signalisation calcique en aval, tels que les canaux chlorure activés par le calcium.

Pour enregistrer directement l'activité des canaux des RV, nous avons pu rediriger un RV vers la surface cellulaire en le fusionnant à un récepteur couplé à une protéine G à forte expression. La construction récepteur-RV a montré des courants photo-induits, mais la sélectivité reste à élucider.

La libération précise du calcium à partir des réserves intracellulaires est le médiateur d'une large panoplie de processus cellulaires tels que l'expression génétique, la libération de neurotransmetteurs ou la contraction musculaire. La propension du RV à s'accumuler dans les membranes internes et à moduler la libération de calcium en fait un excellent candidat comme nouvel outil optogénétique, avec des applications potentielles dans la manipulation de nombreux aspects de l'activité cellulaire.

Table of contents

Acknowledgments	iii
Abstract.....	v
Résumé.....	vii
Table of contents.....	ix
List of abbreviations	xiii
List of figures.....	xvi
List of tables	xix
List of equations	xx
Preamble.....	21
1. An open letter about electrophysiology and <i>Xenopus</i> oocytes	22
1.1 Electrophysiology and ion channels	22
1.2 <i>Xenopus</i> oocytes in the study of ion channels.....	24
2. Project A: Dual mechanism of regulation of G protein-gated potassium channels by δ -opioid receptors.....	28
2.1 Introduction	28
2.1.1 G protein-gated inwardly rectifying potassium channels (GIRK)	28
General considerations about GIRK channels and their physiological relevance	28
GIRK channel structure and modulation of activity.....	32
GIRK regulation by G protein-coupled receptors (GPCRs)	34
Other recognised mechanisms for GIRK function modulation	37
Phosphorylation.....	37
Regulators of G protein signaling (RGS).....	37
Potassium channel tetramerization domain (KCTD) proteins	37
G protein-coupled receptor kinases (GRK)	38
2.1.2 δ -Opioid receptors (DOR).....	39
General considerations about DOR as a member of the opioid-receptor family	39
DOR structure and signaling	41
Desensitization of DOR signaling.....	43
Trafficking of DOR and impact on their function.....	46
Biased agonists and modulation of response.....	47

Direct interactions with signaling members	48
Hetero and homo-dimerization of DOR	49
2.1.3 DOR and GIRK channels: their implications in pain perception.....	49
2.2 Project aim.....	51
2.3 Results.....	52
2.3.1 DOR can activate and rapidly inhibit GIRK currents depending on receptor expression and ligand concentration	52
2.3.2 Inhibition of GIRK currents is mediated by DOR but not by MOR	56
2.3.3 DOR-mediated inhibition is an independent pathway that does not require Gai/o, Gaq or Gas	57
2.3.4 DOR-mediated inhibition does not arise from the last 32 residues of its C-terminal	61
2.3.5 Receptor differences in the inhibition of GIRK are not due to differences in surface expression levels.....	63
2.3.6 Not all GIRK channels are inhibited by DOR.....	66
2.3.7. DOR inhibits Gβγ-activated GIRK currents	68
2.3.8 DOR mediated inhibition is affected by gallein.....	73
2.3.9 GRK2 and GRK3 coexpression does not affect inhibition by DOR.....	74
2.4 Discussion	78
2.4.1 Description of an unreported DOR-mediated inhibition of GIRK channels	78
2.4.2 How do these observations integrate with described mechanisms for Kir3 and DOR regulation?	81
Non-canonical coupling to non-Gi/o proteins.....	81
Homodimerization of DOR	81
Intracellular signaling by DOR.....	81
Receptor phosphorylation, β-arrestin recruitment and internalization.....	82
Fast channel desensitization.....	83
2.5 Conclusion and perspectives	87
3. Project B: Shedding light on the function of viral rhodopsins.....	88
3.1 Introduction	88
3.1.1 The study of microbial rhodopsins and the advent of optogenetics	88
3.1.2 Available optogenetic tools and their applications.....	89
3.1.3 Viral rhodopsins.....	92
A unique family of rhodopsins	92
An important ecological indicator and a potential novel optogenetic tool	94
3.2 Project aim.....	96
3.3 Results.....	97
3.3.1 Photoactivation of OLPVR1 elicits a chloride current in <i>Xenopus</i> oocytes	97
3.3.2 Other members of the VR1 family show identical photocurrent properties	99
3.3.3 OLPVR1 photoresponse is different from Channelrhodopsin-2.....	101
3.3.4 BAPTA abrogates OLPVR1 photocurrents in oocytes	103
3.3.5 OLPVR1 accumulates intracellularly rather than at the cell surface	105

3.3.6 OLPVR1 photocurrents require IP ₃ -dependent calcium stores.....	106
3.3.7 OLPVR1 integrates tightly with the calcium-signaling pathway of <i>Xenopus</i> oocytes	107
3.3.8 Addressing OLPVR1 to the membrane reveals a BAPTA-insensitive current	109
3.3.9 OLPVR1 photoresponse elicits calcium release in HEK293T cells activating exogenous calcium-activated channels	113
3.4 Discussion	116
3.4.1 Photoactivation of VR1 rhodopsins elicits the release of calcium from intracellular stores coupling with calcium-signaling effectors	116
3.4.2 OLPVR1 localizes in intracellular membranes	118
3.4.3 OLPVR1 selectivity remains to be fully elucidated	119
3.5 Conclusion and perspectives	122
4. Materials and Methods	123
4.1 Molecular Biology.....	123
Genes and expression vectors	123
Mutagenesis.....	124
Subcloning	125
Selection of positive clones and amplification of genetic material	125
<i>In vitro</i> transcription	126
4.2 Heterologous expression in <i>Xenopus</i> oocytes.....	127
Preparation of oocytes	127
RNA microinjection.....	128
4.3 Protein expression measurement by luminescence assays in <i>Xenopus</i> oocytes.....	130
Design of HiBiT fusion constructs.....	130
Experimental conditions	130
Analysis of luminescence data	131
4.4 Functional study of membrane proteins by electrophysiology techniques in <i>Xenopus</i> oocytes	132
Configuration of the TEVC setup	132
Project A	134
Experimental conditions.....	134
Bath solutions.....	134
Agonists	134
Inhibitors	135
Data processing and analysis	135
Project B	137
Experimental conditions.....	137
Bath solutions.....	137
Inhibitors	137
Data processing and analysis	138
4.5 Functional validation of OLPVR1 by electrophysiology techniques in HEK293T cells	139
References.....	140

Annexes	161
A - Supplementary figures – Project A	162
B - Supplementary figures – Project B	176
C - Extended information on the molecular biology and protein engineering	181
D – XenoGlo: Exploiting Nanoluc technology for non-destructive surface-expression measurements of single-cell <i>Xenopus</i> oocytes	188

List of abbreviations

βHK	Transmembrane segment of H ⁺ ,K ⁺ ATPase
ΔC32	Truncation of the last 32 residues of the C-terminal
2-APB	2-Aminoethoxydiphenyl borate
A1R	Adenosine 1 receptor
ACh	Acetylcholine
ADP	Adenosine diphosphate
Ani9	2-(4-Chloro-2-methylphenoxy)- <i>N</i> -(2-methoxybenzylidene)acetohydrazide
ANOVA	Analysis of variance
ATP	Adenosine triphosphate
BAPTA	1,2-Bis(o-aminophenoxy)ethane- <i>N,N,N',N'</i> -tetraacetic acid
CaCC	Calcium-activated chloride channel
cAMP	Cyclic adenosine monophosphate
CHO	Chinese hamster ovary cells
ChR	Channelrhodopsin
Ct	Carboxyl-terminal
CTD	C-terminal domain
DADLE	[D-Ala ² , D-Leu ⁵]-enkephalin
DAG	Diacylglycerol
DALE	[D-Ala ²]-Leucine-enkephalin
DAMGO	[D-Ala ² , NMe-Phe ⁴ , Gly-ol ⁵]-enkephalin
DEPC	Diethyl pyrocarbonate
DMSO	Dimethylsulfoxide
DOR	δ-opioid receptor
EGTA	Ethylene glycol-bis(2-aminoethylether)- <i>N,N,N',N'</i> -tetraacetic acid
ER	Endoplasmic reticulum
EYFP	Enhanced yellow fluorescent protein
GABA	γ-aminobutyric acid
GDP	Guanosine diphosphate
GIRK	G protein-gated inward rectifying potassium channel
GPCR	G protein-coupled receptor
GRK	G protein-coupled receptor kinase
GTP	Guanosine triphosphate

HB	HiBiT tag
HEK cells	Human embryonic kidney cells
HEPES	4-(2-Hydroxyethyl)-1-piperazineethanesulfonic acid
ICL	Intracellular loop
IL6	Interleukine-6 secretion signal sequence
IP ₃	Inositol 1,4,5-trisphosphate
KCTD	Potassium channel tetramerization domain protein
Kir	Inwardly rectifying potassium channel
M2	Muscarinic receptor 2
M3	Muscarinic receptor 3
MAPK	Mitogen-activated protein kinase
MOR	μ-opioid receptor
MONNA	2-[(4-Methoxy-2-naphthalenyl)amino]-5-nitro-benzoic acid
MT	Golgi export trafficking signal of Kir2.1 potassium channel
NA	Niflumic acid
OLPVR1	Organic lake phycodnavirus viral rhodopsin of family 1
OLPVR2	Organic lake phycodnavirus viral rhodopsin of family 2
OR	Opioid receptor
PIP ₂	Phosphatidylinositol 4,5-bisphosphate
PKA	Protein kinase A
PKC	Protein kinase C
PLC	Phospholipase C
PP1	4-Amino-5-(4-methylphenyl)-7-(t-butyl)pyrazolo[3,4-d]-pyrimidine
PTX	Pertussis toxin
RGS	Regulators of G protein signaling
SERCA	Sarco/endoplasmic reticulum Ca ²⁺ -ATPase
SEM	Standard error of the mean
SNC80	(+)-4-[(αR)-α-((2S,5R)-4-Allyl-2,5-dimethyl-1-piperazinyl)-3-methoxybenzyl]-N,N-diethylbenzamide
SOCE	Store-operated calcium entry
SS	Signal sequence of human nicotinic acetylcholine α7 receptor subunit
SU6656	(3Z)-N,N-Dimethyl-2-oxo-3-(4,5,6,7-tetrahydro-1H-indol-2-ylmethylidene)-2,3-dihydro-1H-indole-5-sulfonamide
T4L	Lysozyme of bacteriophage T4
TAE	Tris-acetate-ethylenediamine tetraacetic acid
TEVC	Two-electrode voltage clamp
TM	Transmembrane helix
TMD	Transmembrane domain

TRIS	Tris(hydroxymethyl)aminomethane
VirChR1	Viral channelrhodopsin 1
VR	Viral rhodopsin

List of figures

Figure 1.1. Calcium signaling in <i>Xenopus</i> oocytes and activation of CaCCs.....	26
Figure a.1. Plot of the current-voltage relationship of Kir3 channels.	29
Figure a.2. Different subfamilies of G proteins partake in distinct signaling pathways.....	30
Figure a.3. Crystal structure PDB:4KFM of the mouse Kir3.2 in complex with G $\beta\gamma$ by Whorton & MacKinnon 2013.....	33
Figure a.4. Activation of GIRK channels by Gi/o-coupled GPCRs.	35
Figure a.5. Gq-coupled GPCRs can regulate GIRK channels.....	36
Figure a.6. KCTD12 coupled to GABA _B receptors sequesters G $\beta\gamma$ subunits from GIRK channels.....	38
Figure a.7. GRK2 recruitment upon GPCR activation sequesters G $\beta\gamma$ subunits from Kir3 channels.....	39
Figure a.8. Inactive structures of the members of the opioid receptor family bound to antagonists.....	41
Figure a.9. Canonical opioid receptors signaling through G proteins.	42
Figure a.10. Arrestins mediate internalization, recycling and signaling of opioid receptors ..	45
Figure a.11. High expression of DOR reveals inhibition of Kir3.4* currents in high agonist concentration.....	53
Figure a.12. Inhibition of Kir3.4* currents depends on the amount of DOR RNA injected and the amount of agonist applied but not on the level of expression of the channel.....	55
Figure a.13. Inhibition of Kir3.4* by DOR reverses slowly.....	56
Figure a.14. MOR, contrary to DOR, does not inhibit Kir3.4* currents.	57
Figure a.15. Inhibition of Kir3.4* by DOR is not sensitive to PTX, contrary to the Gi/o-dependent activation.	58
Figure a.16. Inhibition of Kir3.4* by DOR is not sensitive to the Gq/Gs inhibitor YM-254890.	59
Figure a.17. Inhibition of Kir3.4* channels by DOR does not require the activation of G proteins.	61
Figure a.18. Inhibition of Kir3.4* channels by DOR does not require the last 32 residues of the C-terminal of the receptor.....	62
Figure a.19. Differences in the inhibitory capability of the receptors cannot be solely justified by differences in surface expression.....	64
Figure a.20. DOR is not able to inhibit all Kir3 channels.	67
Figure a.21. Inhibition of Kir3 channels by DOR does not involve changes in interaction with PIP ₂	69
Figure a.22. Inhibition of Kir3 channels by DOR does not arise from changes in Na ⁺ binding or differences in Kir3 C-terminal domains.....	70
Figure a.23. Inhibition of Kir3 channels by DOR requires the channel to be activated by G $\beta\gamma$	72
Figure a.24. Inhibition of Kir3.4* channels by DOR is hampered by gallein.....	73
Figure a.25. MOR can inhibit Kir3.4* currents when coexpressed with GRK3.	74
Figure a.26. Coexpressing GRK2 with Kir3.4* and DOR has no impact on the maximal effect or kinetics of the inhibition.	76
Figure a.27. Coexpressing GRK3 with Kir3.4* and DOR has no impact on the maximal effect or kinetics of the inhibition.	77

Figure b.1. Examples of optogenetic tools.	90
Figure b.2. Phylogenetic relationships of microbial rhodopsins.	93
Figure b.3. Structures of OLPVR1 and OLPVR2.	94
Figure b.4. Amplitude of photocurrents correlates with the intensity of applied light.	97
Figure b.5. Photo-activation of OLPVR1 induces chloride currents in <i>Xenopus</i> oocytes.	98
Figure b.6. Photo-induced currents of members of the VR1 family have a similar profile which is distinct from Chr2.	100
Figure b.7. Chr2 photo-activation can induce large chloride currents in <i>Xenopus</i> oocytes only at high extracellular calcium concentrations and hyperpolarizing voltages.	101
Figure b.8. OLPVR1-induced chloride currents do not require high extracellular calcium and large calcium driving forces.	103
Figure b.9. OLPVR1-induced chloride currents are abrogated by intracellular injection of BAPTA.	104
Figure b.10. OLPVR1, in contrast with Chr2, is not present at the surface of the oocytes.	105
Figure b.11. OLPVR1 response is absent after intracellular calcium depletion.	107
Figure b.12. Effect of the different calcium-signaling inhibitors on OLPVR1 photo-induced currents.	108
Figure b.13. Fusing OLPVR1 to a high-expressing GPCR allows the trafficking of the protein to the membrane and reveals a BAPTA-insensitive photocurrent.	110
Figure b.14. Current-voltage relationships of stationary currents elicited by photo-activation of OLPVR1 fused to DOR.	112
Figure b.15. OLPVR1 activates surface TMEM16A Ca ²⁺ -activated Cl ⁻ channels (CaCCs) through release of intracellular calcium in HEK293T cells.	114
Figure b.16. OLPVR1 activates surface SK1 Ca ²⁺ -activated K ⁺ channels through release of intracellular calcium in HEK293T cells.	115
Figure 4.1. <i>Xenopus</i> oocyte expression vectors.	123
Figure 4.2. Experimental protocol for <i>in vitro</i> characterization of potassium channels and light-regulated transporters in <i>Xenopus</i> oocytes.	128
Figure 4.3. HiClamp robot.	133
Figure 4.4. Example of GIRK data obtained with the HiClamp robot.	136
Supplementary figure a.1. No unspecific effects of opioid agonists in <i>Xenopus</i> oocytes.	162
Supplementary figure a.2. Control test of the Gq/Gs inhibitor YM-254890.	163
Supplementary figure a.3. Inhibition of Kir3.4* channels by DOR does not involve the phosphorylation of the receptor by GRK2/3 on residues Thr-358 and Ser-363.	164
Supplementary figure a.4. Inhibition of Kir3.4* channels by DOR does not involve the kinase activity of GRK2/3.	165
Supplementary figure a.5. Inhibition of Kir3.4* channels by DOR does not require the activity of Src tyrosine kinases.	166
Supplementary figure a.6. DOR[ΔC32], which inhibits Kir3.4* currents, has not only low surface expression, but also low total expression.	167
Supplementary figure a.7. Topology of different MOR/DOR chimeras and summary of their effects on Kir3.4* currents.	168
Supplementary figure a.8. Recordings and surface expression of different MOR/DOR chimeras discussed in Supplementary figure a.7.	170
Supplementary figure a.9. Average current values of different Kir3 channels coexpressed with DOR show intrinsic differences between the different channels.	171
Supplementary figure a.10. DOR can inhibit Kir3.4* currents activated by other Gi/o-coupled GPCRs.	171
Supplementary figure a.11. A1R can inhibit Kir3.4* currents when coexpressed with GRK3.	172
Supplementary figure a.12. Application of 1 μM DALE does not acutely affect the amount of surface DOR.	173
Supplementary figure a.13. Coexpressing regulatory proteins KCTD12, RGS4 and β-arrestin2 with Kir3.4* and DOR has no major impact on the inhibition.	174
Supplementary figure b.1. Substitution of the cation in the extracellular solution does not affect the reversal potential of OLPVR1 photo-induced currents.	176
Supplementary figure b.2. Functional validation of HiBiT and DOR fusion constructs.	177

Supplementary figure b.3. Extracellular EGTA, as well as extracellular Niflumic Acid, reduce the average peak currents induced by OLPVR1.	178
Supplementary figure b.4. Control tests of inhibitors used in this study.	179
Supplementary figure b.5. Comparison of peak currents of different OLPVR1 constructs with the luminescence after lysis of their HiBiT-tagged counterparts.....	180
Supplementary figure b.6. Surface and intracellular expressions of different rhodopsins compared to ChR2.	180
Supplementary figure c.1. Alignment of the protein sequences of MOR/DOR chimeras	183
Supplementary figure d.1. Schematic protocol for the detection of protein expression in <i>Xenopus</i> oocytes using Nanoluciferase.	190
Supplementary figure d.2. Luminescence signal reaches the peak at 10 minutes and depends on oocyte placement.	190
Supplementary figure d.3. Expression of DOR increases with the amount of RNA injected and can be followed using HiBiT tagged proteins.	191
Supplementary figure d.4. Luminescence of HiBiT-tagged Kir3.4* channel increases with the amount of RNA injected and correlates with an increase in measured currents.....	191
Supplementary figure d.5. Expression of DOR is regulated by the identity of residue 27 and can be distinguished using HiBiT tagged proteins.	192

List of tables

Table 1.1. Reported intracellular concentrations of ions in <i>Xenopus</i> oocytes (adapted from Marin 2012)	27
Table 4.1. List of agonists used in Project A	135
Table 4.2. List of inhibitors used in Project A	135
Table 4.3. List of bath solutions used in Project B.	137
Table 4.4. List of inhibitors used in Project B	138
Table c.1. Detailed information about the design of the different proteins used in Project A.	181
Table c.2. Detailed information about the design of the different proteins used in Project B.	187

List of equations

Equation 1.1. Nernst equation. 23
Equation 1.2. Goldman-Hodgkin-Katz equation. 23

Preamble

For the doctoral school, the thesis manuscript is an academic exercise that acts as proof that I learned how to produce original scientific content and share it in a clear, reproducible manner. As such, I tried to create a document that reflects the work I did in a structured and synthetic fashion. However, this manuscript is, in fact, the culmination of the last four years of my life, and the layout I chose does not suffice to convey the journey. This section is meant to give a little bit of context as I guide you through the parts of the manuscript.

I open by talking about bioelectricity, electrophysiology, and the use of *Xenopus* oocytes as model cells. It is ultimately meant to introduce the lens used for the scientific observations presented here. A lens that allows us to investigate ion channels and their interactions with other proteins at a molecular level, on the realm of what is called “structure-function”.

The next section covers a project where I try to understand the inhibition of G protein-gated potassium channels by δ -opioid receptors. It is a phenomenon that was discovered by chance, but perplexing enough to have had become my main and original thesis project. For much of my dismay, this project remains incomplete, and will most likely haunt my dreams for many years to come.

I follow up with a rather unrelated project about viral rhodopsins. A wild card of a project that started as part of a collaboration to identify novel optogenetic tools and quickly became something more. It lured my attention for the good part of two years, and for that reason, it gained a bit of space in this manuscript.

For both of these projects, I appended a section with complementary experiments. Most are tangents that serve to clarify some aspects of our findings. Not wanting to run the risk of having them distract from the main idea, I have curated them in their own special space.

A couple of other smaller projects eventually died out, but a particular endeavour is worth mentioning. Even though it is not presented as a separate project, a large part of my experimental efforts focused on optimizing a luciferase-based assay for protein-expression detection in oocytes. I ended up using this assay in both of the projects before mentioned. Thus, and to finalise, I included some of the optimization experiments at the end of the manuscript.

1. An open letter about electrophysiology and *Xenopus* oocytes

1.1 Electrophysiology and ion channels

Electrophysiology¹ is the classical discipline that studies the electrical properties and processes of living organisms. The flow of charges in biological systems – or bioelectricity – allows for a fast mechanism for signaling and communication, which is the foundation of many cellular and physiological processes. Thus, it is not surprising that the fundamental mediators of this flow of charges – ion channels - are present in all kingdoms of life.

Ion channels are macromolecular entities that insert into biological membranes and form a pore – or channel – that, when open, allows for a selective and passive flow of ions. Ion channels are classified by their ion selectivity and mode of gating. That is, they can be distinguished based on the ions they permeate and the mechanism that governs their opening and closing. Many different stimuli have been recognized to modulate the gating of ion channels: changes in membrane potential, the binding of extracellular ligands, temperature, osmotic changes, pH, pressure, secondary intracellular messengers - such as G proteins or Ca^{2+} -, and even light. The channels that are the object of this thesis fall in the last two mechanisms of gating.

It is important to note that the function of ion channels as the core of bioelectricity cannot be dissociated from their existence in biological membranes. Cells have lipid membranes, which arrange themselves into a charge-impermeable barrier. These membranes can thus separate different compartments, such as the extra and intracellular spaces, and allow them to maintain different ionic compositions. The difference in ionic compositions creates an electrochemical gradient. It is this gradient, which can be described by the Nernst equation, that governs the movement of an ion through the channels in a so-called passive manner.

¹ Although not discussed here, the historical perspective on the development of electrophysiology as a field is reviewed in Verkhatsky & Parpura, 2014. It includes and contextualizes the pivotal experiments of household names such as Hodgkin & Huxley and Neher & Sakmann.

A particular ion will flow through a channel towards its equilibrium potential. When equilibrium is reached, the two forces of the electrochemical gradient are counterbalancing each other: the electrical force created by the difference in charges across the membrane and the diffusion tendency of the ion imposed by its concentration difference between compartments. In this condition, the ion net movement becomes zero.

The equilibrium potential for a specific ion (E_{ion}) can be calculated by the arrangement of the Nernst equation shown below (Equation 1.1).

$$E_{ion} = \frac{RT}{zF} \ln \frac{[ion]_o}{[ion]_i}$$

Equation 1.1. Nernst equation.

R is the universal gas constant (8.31 J mol⁻¹ K⁻¹), T is the temperature in Kelvin, z is the valence of the ion, F is the Faraday's constant (96500 C/mol), and [ion]_o and [ion]_i are the extracellular and intracellular concentrations of the particular ion, respectively.

However, cells have channels for a variety of different ions, granting them a certain permeability for each of the ions. One can determine the electrical potential at which the net movement of charges through the cell membrane is zero, by calculating a weighted average of Nernst potentials of the permeant ions. This potential is called reversal potential (E_{rev}), or resting membrane potential, and can be calculated by the Goldman-Hodgkin-Katz equation, limited here to Na⁺, K⁺ and Cl⁻ (Equation 1.2).

$$E_{rev} = \frac{RT}{F} \ln \frac{P_{Na^+}[Na^+]_o + P_{K^+}[K^+]_o + P_{Cl^-}[Cl^-]_i}{P_{Na^+}[Na^+]_i + P_{K^+}[K^+]_i + P_{Cl^-}[Cl^-]_o}$$

Equation 1.2. Goldman-Hodgkin-Katz equation.

R is the universal gas constant (8.31 J mol⁻¹ K⁻¹), T is the temperature in Kelvin, F is the Faraday's constant (96500 C/mol), P_{ion} is the permeability of the specified ion, and [ion]_o and [ion]_i are the extracellular and intracellular concentrations of the particular ion, respectively.

Both of these equations are on the basis of all electrophysiology studies². This thesis is an example of that.

Nowadays there are a multitude of techniques that interrogate the structure and function of ion

² The electrophysiology concepts discussed in this chapter can be found in more detail in Bertil Hille's book Ion Channels of Excitable Membranes.

channels. However, to understand the biophysical properties of these proteins, voltage-clamping techniques are still the gold standard. Techniques such as Two-Electrode Voltage Clamp (TEVC) and Patch-clamp³, are often named electrophysiology techniques since their inception was at the origin of what is called modern electrophysiology. They allow a quantitative assessment of ion channel activity by measuring ion flux across the membrane as an electrical current. These techniques can fix the membrane potential at a pre-set value, i.e., clamp the voltage, and the current required to maintain that potential stable is measured as a proxy of the current crossing the membrane.

TEVC uses two intracellular electrodes. One electrode monitors the potential of the membrane, and the other injects the current necessary to keep the potential to the pre-set value. Patch-clamp, on the other hand, involves a single electrode and micropipette. It requires the formation of a high-resistance seal between the micropipette and a micro-sized patch of a cell membrane. The small surface area allows for the recording of single ion channels.

As popular as Patch-clamp has become, it is only suitable for clamping relatively small cells, since large cells might incite high current amplitudes, which cannot be compensated by the single recording electrode. TEVC is the preferred technique to clamp larger cells, in particular *Xenopus* oocytes, which are standardly used as a heterologous expression system for the study of ion channels.

1.2 *Xenopus* oocytes in the study of ion channels

Xenopus oocytes are the egg cells of the South African clawed frog *Xenopus laevis*. Historically, they have been used as model cells in various fields (reviewed in De Robertis *et al.*, 2021). However, here, we focus on the investigation of structure-function relationships of ion channels and receptors.

During oogenesis, these cells are armed for early embryonic development. They accumulate large amounts of necessary components for gene expression, such as polymerases, transcription factors, tRNAs, histones, and ribosomes (reviewed in Woodland, 1982 and Keiper, 2003). Together with their large size (1-1.2 mm), these characteristics make them particularly amenable to direct injection of DNA or mRNA and expression of heterologous proteins (Gurdon *et al.*, 1971).

³ Bertil Hille discusses the contributions of Marmont, Cole, Hodgkin and Huxley for the development of TEVC, as well as the contributions of Neher and Sakmann for the development of Patch-clamp in the book *Ion Channels of Excitable Membranes*.

Indeed, translated heterologous mRNAs are often: functional proteins, highly expressed, with the correct post-translationally modifications, docked in the appropriate site and orientation, and exhibit the expected pharmacological and electrophysiological properties (reviewed in Colman *et al.*, 1984; Theodoulou & Miller, 1995; Kapur *et al.*, 2007).

Additionally, *Xenopus* oocytes display promiscuous expression, enabling the study of proteins from different origins, including the mammalian and viral proteins studied in this thesis. An approach commonly used to further boost expression is to substitute the untranslated regulatory regions of the mRNA of interest with those of β -globin of *Xenopus* (Krieg & Melton, 1984).

A particular advantage of this expression system is that direct injection of mRNAs allows for precise control of ratios of different proteins or subunits of multimeric complexes. Subunit stoichiometry of certain proteins determines their functional properties, and *Xenopus* oocytes have been exploited in that context (Boorman *et al.*, 2000; Durisic *et al.*, 2012). Similar control of stoichiometry can be much more challenging in other expression systems. However, it is integral to mention that the impact of different translation efficiencies on protein stoichiometry was never examined. Furthermore, in relatively rare but reported cases, oocytes may support protein subunit combinations not generally found in native tissues (as in Nelson *et al.*, 2003).

When studying ion channels, one should consider that the oocyte itself is equipped with a full set of transport systems - a drawback that is shared with all other expression systems. A comprehensive understanding of the oocyte's endogenous channels is critical to predict and avoid possible misinterpretations of the results. Sobczak *et al.* (2010) and Terhag *et al.* (2010) offer in-depth reviews of the transport proteins in *Xenopus* oocytes.

Regardless of the diversity of channels at the oocyte's surface, endogenous currents are typically very small. Often, heterologously expressed ion channels can be distinguished by the sheer amplitude of their currents, which mask any smaller currents from endogenous channels.

However, one particular endogenous channel cannot be ignored - the Calcium-activated chloride channel (CaCC, also called TMEM16A or Ano1) (Barish, 1983; Schroeder *et al.*, 2008). Contrary to most channels, CaCCs are highly expressed and show strong outward rectification, i.e., stronger currents outward than inward⁴ (Machaca & Hartzell, 1998).

⁴ In the case of chloride, being a negatively charged ion, strong outward currents (i.e., strong outward movement of positive charges) means strong inward movement (or entry) of chloride.

As the name implies, these channels respond to Ca^{2+} signaling. Physiologically, their activation induces depolarization in the oocyte that blocks polyspermy (Machaca *et al.*, 2002; Wozniak *et al.*, 2018).

Mechanistically, large chloride currents can be elicited upon the release of Ca^{2+} from intracellular stores, such as the endoplasmic reticulum (ER), or by the entry of Ca^{2+} from the extracellular space. Figure 1.1 details the multi-step process of the activation of CaCCs.

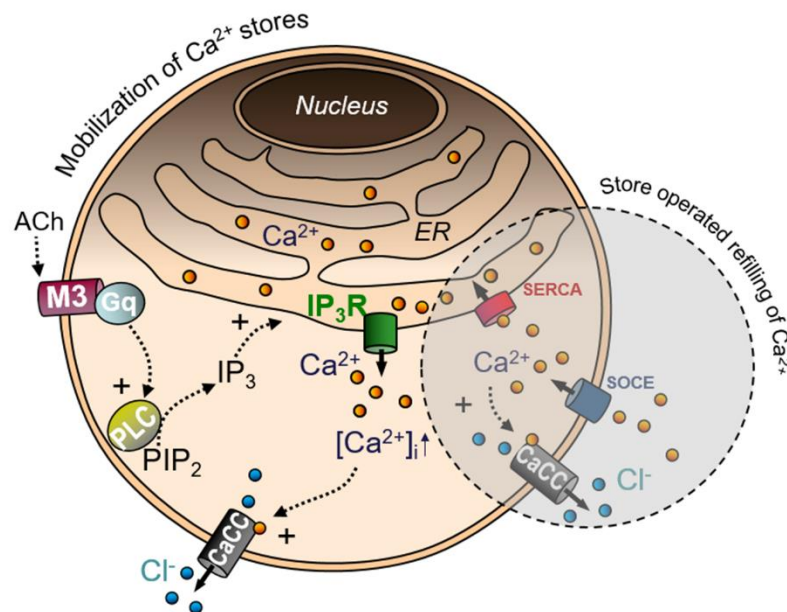


Figure 1.1. Calcium signaling in *Xenopus* oocytes and activation of CaCCs.

Activating a receptor coupled to the G protein Gq, such as the Muscarinic 3 receptor (M3), triggers the release of Ca^{2+} from intracellular stores. The release of calcium is a consequence of the activation of phospholipase C (PLC), which cleaves phosphatidylinositol-4,5-bisphosphate (PIP_2) into diacylglycerol (DAG) and inositol 1,4,5-trisphosphate (IP_3). IP_3 , in turn, acts on IP_3 receptors (IP_3R) at the endoplasmic reticulum (ER) to stimulate the release of Ca^{2+} . The increase in intracellular Ca^{2+} ultimately activates CaCCs at the membrane, inducing chloride currents. Interestingly, *Xenopus* oocytes lack other canonical calcium channels on the endoplasmic reticulum, such as ryanodine receptors (RyRs). The return to the baseline ER Ca^{2+} concentration relies on a refilling mechanism that imports Ca^{2+} from the extracellular space. This mechanism is called Store-operated calcium entry (SOCE). The depletion of ER Ca^{2+} leads to the unfolding of an ER luminal protein that acts as a Ca^{2+} sensor. This protein, then, aggregates in puncta, i.e., regions of close proximity between the ER and the plasma membrane (10–20 nm) (Luik *et al.*, 2008). Aggregates consequently recruit and activate specific membrane Ca^{2+} channels generating a microdomain of Ca^{2+} entry, which is ultimately pumped into the ER through SERCA (sarco/endoplasmic reticulum Ca^{2+} -ATPase pump). The entry of Ca^{2+} through these store-operated calcium channels can further activate CaCCs (Reviewed in Courjaret & Machaca, 2016 and in Marin, 2012).

When CaCCs may pose a problem for experimentation, one can inject calcium chelators like EGTA (Miledi *et al.*, 1984) or BAPTA (Hartzell, 1996) or use CaCC inhibitors such as niflumic acid (White *et al.*, 1990), MONNA (Oh *et al.*, 2013) or the highly specific Ani9⁵ (Seo *et al.*, 2016).

⁵ EGTA (Ethylene glycol-bis(2-aminoethylether)-N,N,N',N'-tetraacetic acid); BAPTA (1,2-Bis(o-aminophenoxy)ethane-N,N,N',N'-tetraacetic acid); MONNA (2-[(4-Methoxy-2-naphthalenyl)amino]-5-nitro-benzoic acid); Ani9 (2-(4-Chloro-2-methylphenoxy)-N'-(2-methoxybenzylidene)acetohydrazide); 2-APB (2-Aminoethoxydiphenyl borate).

2-APB (Maruyama *et al.*, 1997; Wozniak *et al.*, 2018) has also been used extensively to block calcium signaling in *Xenopus* oocytes. These compounds are helpful when specific currents need to be studied in isolation, for instance, to determine ionic selectivity. Note that, total pharmacological inhibition of specific members of the calcium signaling is not trivial. Many inhibitors show different levels of promiscuity in their effect (Wozniak *et al.*, 2018).

However, often CaCCs are exploited as an indicator of calcium entry or calcium release from intracellular stores. This is the case in studies of calcium-permeable channels, where the entry of calcium will induce a much larger chloride current. Another case is the study of receptors that couple with G proteins of subclass Gq (Figure 1.1). Their activation triggers calcium release from intracellular stores and elicits large observable CaCC currents (as in Lechleiter *et al.*, 1991). Project B in this manuscript also exploits this signaling. In this context, CaCCs act as reporters and as amplifying systems (reviewed in Hatcher-Solis *et al.*, 2014).

TEVC in *Xenopus* oocytes, in combination with molecular engineering approaches, has been extensively used in probing the function and the structure of ion channels and protein receptors. This setup preserves the intracellular medium intact (see Table 1.1) and enables the integration of the studied proteins with the required secondary messengers.

In the projects presented in this manuscript, we mobilized these methods to answer our scientific questions.

Ion	Concentration (mM)
Na ⁺	4 - 23
K ⁺	76 - 148
Cl ⁻	24 - 62
Ca ²⁺	0.003 to 0.4
Mg ²⁺	>0.5

Table 1.1. Reported intracellular concentrations of ions in *Xenopus* oocytes (adapted from Marin 2012).

Knowing the intracellular concentrations of ions in *Xenopus* oocytes is relevant for the study of ion channels because the electrochemical gradient determines the direction of the passive flow of a certain ion. As seen in the table, the ranges can vary considerably. It reflects the major disadvantage of oocytes, which is their intrinsic variability. Intracellular ion concentrations, or expression efficiency, can vary significantly even between the same batch of oocytes from a single female frog.

2. Project A: Dual mechanism of regulation of G protein-gated potassium channels by δ -opioid receptors

2.1 Introduction

In this section, we introduce briefly the proteins that are the object of this study, namely G protein-gated potassium channels and δ -opioid receptors, with a focus on the recognized molecular mechanisms of their regulation.

2.1.1 G protein-gated inwardly rectifying potassium channels (GIRK)

General considerations about GIRK channels and their physiological relevance

G protein-gated inwardly rectifying potassium channels (GIRK) are also designated as Kir3 channels, delimiting a class on a much broader family of potassium channels - Kir – Potassium Inward Rectifier channels⁶.

The term "inward rectification" refers to the dramatic change in slope of the current-voltage relationship of the Kir channels, which is seen at the equilibrium potential of K^+ (see Figure a.1). This change of slope reflects their characteristically stronger inward currents (i.e., negative currents seen at voltages under the reversal potential for K^+) compared to the much smaller outward currents (i.e., positive currents seen at voltages above the reversal potential for K^+).

The underlying mechanism of the rectification has been ascribed to the obstruction of the channel by intracellular factors (e.g., Mg^{2+} , polyamines), which are pushed into the pore at potentials above the reversal potential for K^+ , effectively silencing the outward currents (Lopatin *et al.*, 1995).

⁶ The properties of Inward Rectifier channels are reviewed in detail in Hibino *et al.*, 2010.

The rectification phenomenon makes it difficult to study Kir channels in conditions where K^+ currents are outward. Thus, most often, Kir channels are functionally characterized using conditions that impose inward flux of K^+ .

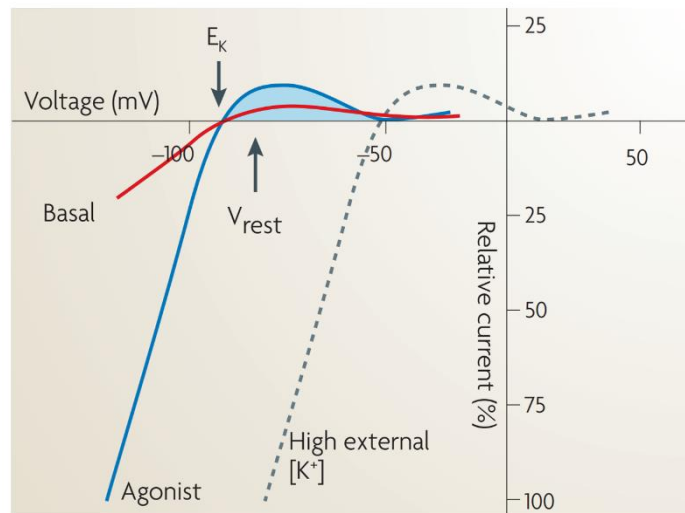


Figure a.1. Plot of the current-voltage relationship of Kir3 channels.

In physiological levels of extracellular K^+ , the current reverses (zero current) near -90 mV, which is the equilibrium potential for K^+ (E_K). The basal current of unactivated channels is shown in red. The activated current induced by an agonist acting through a receptor is shown in blue. Both show inward rectification presenting large inward currents (below 0 on the Y-axis by convention) and small outward currents (above 0 on the Y-axis). In high extracellular K^+ (for example, 20 mM K^+), the current-voltage relationship (dashed line) shifts to the right to the new equilibrium potential for K^+ , while rectification persists (adapted from Lüscher *et al.*, 2010).

The nomenclature of Kir3 channels as G protein-gated potassium channels stems from their distinctive gating by G proteins.

G proteins are heterotrimeric proteins composed of $G\alpha$, $G\beta$, and $G\gamma$ subunits. They operate as secondary messengers by functioning as molecular switches. They are "off" or "on" when bound to guanosine diphosphate (GDP) or guanosine triphosphate (GTP), respectively. G proteins are, in turn, activated by G protein-coupled receptors (GPCR). When a GPCR is activated, it catalyzes the exchange of GDP to GTP at the $G\alpha$ subunit of the trimeric G protein. This leads to the dissociation of the $G\beta\gamma$ subunits, which can directly bind and activate GIRK channels.

Numerous molecules, such as acetylcholine, adenosine, cannabinoids, dopamine, opioids, somatostatin, serotonin, and γ -aminobutyric acid (GABA) (reviewed in Jeremic *et al.*, 2021), trigger their cognate GPCRs, ultimately activating GIRK channels. Note that these receptors couple *in vivo* specifically to pertussis toxin (PTX)-sensitive G proteins, i.e., G proteins from the G_i/o subfamily (Pfaffinger *et al.*, 1985) (Figure a.2).

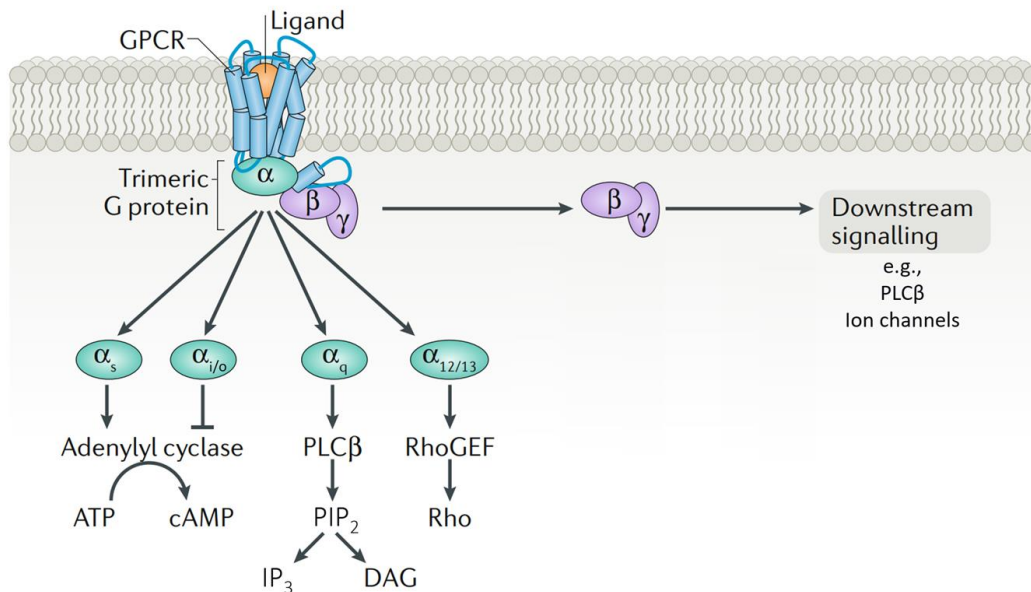


Figure a.2. Different subfamilies of G proteins partake in distinct signaling pathways.

Adapted from Pflieger *et al.*, 2019.

As for the function, GIRK channels are recognized for contributing to the resting potassium permeability of excitable cells and for regulating the triggering of action potentials.

The basal activity of GIRK channels, thought to be a result of the binding of free Gβγ subunits (Kahanovitch *et al.*, 2014), contributes to the resting potential of neurons. This contribution was evidenced by the shift (8 mV) of the resting potential of neurons in Kir3.2-null mice (Lüscher *et al.*, 1997).

When GIRK channels are activated, potassium ions exit the cell since in physiological conditions, the cell resting potential (V_{rest}) imposes outward movement of K^+ (Figure a.1). This results in a hyperpolarization⁷ of the membrane deeming the cells less active. In such a manner, GIRK channels control action potential generation and propagation by increasing the stimulus required to cross the action potential threshold. Consequently, they act as fundamental transducers of inhibitory effects in the heart and the brain.

Indeed, they regulate heartbeat (Krapivinsky *et al.*, 1995), neuronal excitability, and pain perception (Patil *et al.*, 1995). They have likewise been implicated in several conditions (reviewed in Lüscher *et al.*, 2010), such as epilepsy (Signorini *et al.*, 1997), Down syndrome

⁷ The membrane potential becomes more negative, i.e., there is an increase in negative charge on the inside leaflet of the membrane.

(Siarey *et al.*, 1999), and Parkinson's disease (Patil *et al.*, 1995). Furthermore, Kir3 channels have also been implicated in mediating alcohol and drug addiction (reviewed in Rifkin *et al.*, 2017).

Four genes coding Kir3 proteins are present in mammals, with distinct tissue-specific expression patterns (Fagerberg *et al.*, 2014). Namely, for the class members Kir3.1, Kir3.2, Kir3.3, and Kir3.4, the gene codes are KCNJ3, KCNJ6, KCNJ9, KCNJ5.

Functional Kir3 channels are tetrameric assemblies of the different Kir3 proteins. Described assemblies are either homotetramers in the case of Kir3.2 and Kir3.4, or heterotetramers such as Kir3.1/Kir3.2, Kir3.1/Kir3.3, Kir3.1/Kir3.4, and Kir3.2/Kir3.3 (reviewed in Hibino *et al.*, 2010).

Kir3.1/Kir3.4 heteromers (in a ratio of 2:2) constitute the muscarinic atrial K⁺ channel, a critical player in the regulation of heart rate (Krapivinsky *et al.*, 1995; Wickman *et al.*, 1998).

On the other hand, Kir3.1 and Kir3.2 colocalize extensively in the brain and are recognized as the prototypical neuronal GIRK channel (Koyrakh *et al.*, 2005). Nonetheless, several expression patterns were discriminated within the different neuronal populations in the rodent's nervous system. Kir3.3 expresses throughout the central nervous system (Karschin *et al.*, 1996); Kir3.1, Kir3.2, and Kir3.3 are coexpressed in several neuronal populations (Fernández-Alacid *et al.*, 2011; Cruz *et al.*, 2004; Inanobe *et al.*, 1999); and even Kir3.4 is found in a few regions, although not prominently (Aguado *et al.*, 2008).

Remarkably, wild-type Kir3.1 homotetrameric channels do not seem to exist. The Kir3.1 protein cannot correctly traffic to the plasma membrane (Krapivinsky *et al.*, 1995) unless it is partnered with other Kir3 subunits, in part because it lacks an endoplasmic reticulum (ER) export signal (Mirshahi *et al.*, 2004).

Despite the lack of ER export signal, a single point mutation (F137S) was identified in the pore region of Kir3.1 that enables the expression of homomeric channels (Chan *et al.*, 1996; Vivaudou *et al.*, 1997). The authors also showed that modification at the equivalent position in the Kir3.4(S143T) enhances the open probability of the homomeric channels. Similarly, Kir3.2 mutants (E152D) or (V188A) have higher homomeric constitutive activity (Yi *et al.*, 2001). The described mutant proteins have been used to compare the responses of homomeric versus heteromeric channels. These studies allow to clarify the contributions of each protein subunit to the biophysical properties of the GIRK channels found *in vivo*.

GIRK channel structure and modulation of activity

The Kir3.2 structure was solved by Whorton & Mackinnon in 2011. They utilized the R201A mutant, which is conductive in the absence of G protein stimulation, to capture the open conformation of the channel.

The work of Whorton & Mackinnon validated a large body of experiments that had probed the structure-function aspects of Kir3 channels for several decades (reviewed extensively in Logothetis *et al.*, 2015 and in Glaaser & Slesinger, 2015), and we now have a better understanding of how these channels are modulated.

Structurally, all members of the Kir channel family have a similar transmembrane domain (TMD) with eight α -helices (two per subunit TM1 and TM2), delimiting a water-filled transmembrane pore.

They also share a highly conserved selectivity filter. The selectivity filter refers to the quaternary structural element lining the pore that grants the ability to discriminate between potassium and other ions. The particular polypeptide motif Thr-X-Gly-Tyr/Phe-Gly is, in fact, a shared signature of all potassium channels (Heginbotham *et al.*, 1994; Bichet *et al.*, 2003).

The cytoplasmic domain (CTD) is a distinctive structural feature of Kir potassium channels, accounting for about 2/3 of the protein size. It comprises the N-terminal of each subunit as well as their C-terminals. This much larger domain hosts a series of regulatory sites, such as phosphorylation sites, pH-sensing domains, and protein binding sites. Hence, it is where most of the differences between the members of the Kir family are found.

Both TMD and CTD possess gating elements, i.e., structural features that control the passage or arrest of K^+ through the pore.

A large body of literature in the late '80s and '90s (reviewed in Logothetis *et al.*, 2015 and Glaaser & Slesinger, 2015) was concerned with identifying the factors required to activate Kir3 channels. The requirement for the simultaneous presence of $G\beta\gamma$ dimers, Na^+ and PIP_2 was eventually recognized (Sui *et al.*, 1998). In more recent work, Wang *et al.* (2014) purified and reconstituted Kir3.2 channels in planar lipid membranes and tested the effects of $G\alpha$, $G\beta\gamma$, PIP_2 and Na^+ . $G\beta\gamma$ (but not $G\alpha$) and PIP_2 must act in a concerted manner to activate Kir3.2. Na^+ , on the other hand, did not seem to be essential, merely modulating the effects of $G\beta\gamma$ and PIP_2 .

Wang *et al.* (2016) developed an assay to control G protein concentration at the membrane to show that four G $\beta\gamma$ subunits bind cooperatively to open a single Kir3.2 channel. Furthermore, they show that Na⁺ – which, in a physiological scenario, enters neurons during action potentials – boosts channel opening cooperatively. The binding of Na⁺ to the channel increases G $\beta\gamma$ affinity and, consequently, its open probability.

PIP₂, on the other hand, binds the channel and imposes conformational changes that expose the surface where G $\beta\gamma$ interacts, effectively priming the channel for opening (Niu *et al.*, 2020 by cryogenic electron microscopy).

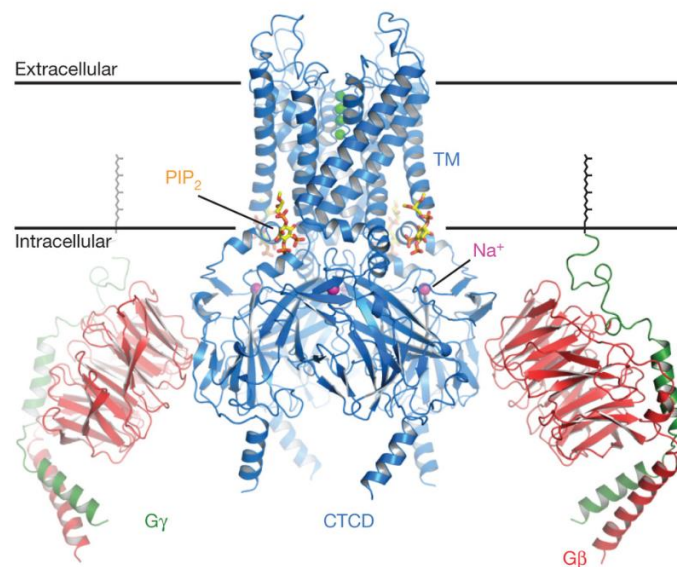


Figure a.3. Crystal structure PDB:4KFM of the mouse Kir3.2 in complex with G $\beta\gamma$ by Whorton & MacKinnon 2013.

The crystal structure PDB:4KFM of the mouse Kir3.2 in complex with G $\beta\gamma$ by Whorton & MacKinnon (2013), further revealed that all three of these cofactors bind to the CTCD (Figure a.3) and that the characteristic binding of G $\beta\gamma$ is mediated by unique residues present in the Kir3 subclass.

In contrast, the PIP₂-binding site at the C-terminal is highly-conserved in all Kir members. This interaction site is often the target of pharmacological agents and protein regulators (e.g., protein kinases and phospholipases) (reviewed in Hibino *et al.*, 2010).

Note that several features of the Kir3.1 subunit differ from the other members of the class. The Kir3.1 subunit is the largest and most divergent, sharing only 44% sequence identity with the other three members.

While it cannot function as a homomer, as previously mentioned, Kir3.1 is an integral subunit of most neuronal and cardiac GIRK channels. It has been suggested that this subunit accounts for the activation potentiation of heterotetramers due to its distinctive attributes.

For instance, Kir3.1 has a modified sequence at the Na⁺-binding site. This modification mimics the constant positive effect of bound Na⁺, constitutively increasing affinity for Gβγ (Ho *et al.*, 1999). Indeed, a mutant that exchanges the Na⁺-binding residue of Kir3.4 by the equivalent residue in Kir3.1 (D223N) acts as permanently activated and does not respond to shifts in Na⁺ (Rosenhouse-Dantsker *et al.*, 2008).

Furthermore, the Kir3.1 subunit has unique phosphorylation sites (Rusinova *et al.*, 2009) as well as interaction domains with Gβγ, Gα (Rubinstein *et al.*, 2009), and PIP₂ (Thomas *et al.*, 2006) at the C-terminal, which can modulate channel activity. At least in Rubinstein *et al.* (2009) the modulation of activation was transferable by exchanging the C-terminal of Kir3.2 with that of Kir3.1.

In addition to the canonical cofactors, GIRK channels are activated by other small molecules, but less is known about the underlying gating mechanisms. For instance, both alcohol (Lewohl *et al.*, 1999) and cholesterol (Bukia *et al.*, 2017) have been shown to bind and modulate GIRK channel activity.

As for channel blockers, only a few are known to affect the Kir family directly, but it is well recognized that they can be blocked by ions such as Ba²⁺ and Cs⁺ (Hagiwara *et al.*, 1976, 1978) or Tertiapin Q (Jin & Lu, 1998).

GIRK regulation by G protein-coupled receptors (GPCRs)

As previously mentioned, the general scheme of GIRK activation by G proteins involves a GPCR (Figure a.4). The GPCR binds an agonist, catalyzing GDP-GTP exchange at the Gα subunit of the trimeric G protein. In turn, this leads to the dissociation of the Gβγ subunit, which is now able to bind to GIRK. Together with PIP₂ and Na⁺, Gβγ imposes conformational changes that allow the opening of the channel and the passage of potassium ions through the pore. The channel closes when the agonist unbinds from the GPCR and GTP is hydrolyzed at the Gα subunit, which then re-sequesters Gβγ (Pfaffinger *et al.*, 1985; Logothetis *et al.*, 1987; Gilman 1987).

Although GIRK channels could seemingly bind G $\beta\gamma$ subunits released from all subfamilies of G proteins (Mirshahi *et al.*, 2002), it has been established that in native tissues, only G $\beta\gamma$ dimers coming from the PTX-sensitive G α_i/o -coupled receptors can activate these channels (Pfaffinger *et al.*, 1985; North *et al.*, 1987).

However, G α_z , a PTX-insensitive member of subfamily G i , can also produce slow GIRK activations by G $\beta\gamma$ donation when expressed in *Xenopus* oocytes (Vorobiov *et al.*, 2000). The same applies to G α_s when in overexpressing conditions (Hatcher-Solis *et al.*, 2014).

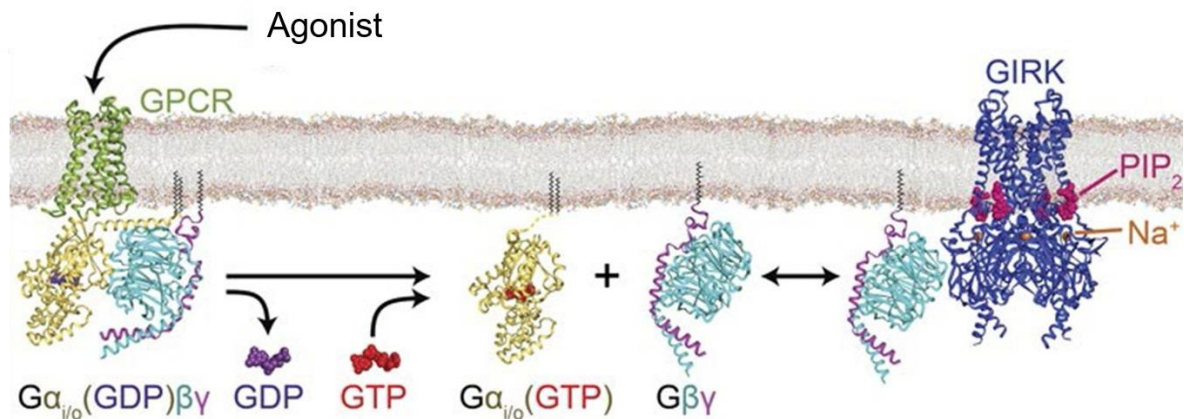


Figure a.4. Activation of GIRK channels by Gi/o-coupled GPCRs.

Adapted from. Wang *et al.*, 2016. See text for description.

This specificity towards G α_i/o donation of G $\beta\gamma$ is still not fully understood. Even though G α and GIRK channels have been shown to co-immunoprecipitate, there is no consensus on direct modulation of channel activity by G α (Clancy *et al.*, 2005). It has been proposed that specificity relies on the existence of pre-formed stable signaling complexes where the channel is coupled with the full trimeric G protein and with or without the receptor (Clancy *et al.*, 2005; Raveh *et al.*, 2009). Indeed, several lines of evidence suggest that G $\beta\gamma$ and G α_i/o can associate with GIRKs constitutively, as early as in the ER (Rebois *et al.*, 2006; Robitaille *et al.*, 2009).

Despite all the evidence suggesting constitutive interaction, a collision coupling model - where unrestricted diffusion of GPCRs, G proteins, and effectors is assumed - can account for specificity in purely kinetic terms (Touhara & Mackinnon, 2018; Berlin *et al.*, 2020). Berlin *et al.* (2020) suggest that it is conceivable that different signaling cascades may proceed in different modes.

As established in the previous section, the activation of GIRK requires interactions with PIP₂. As such, these channels can be regulated by parameters of the PIP₂ metabolism.

For instance, hydrolysis of PIP_2 by phospholipase C (PLC) inhibits GIRK channels. Thus, receptors that couple to G proteins of subfamily G_q , which activate PLC, can produce inhibitory effects on GIRK currents (Lei *et al.*, 2003, Mao *et al.*, 2004). See Figure a.5.

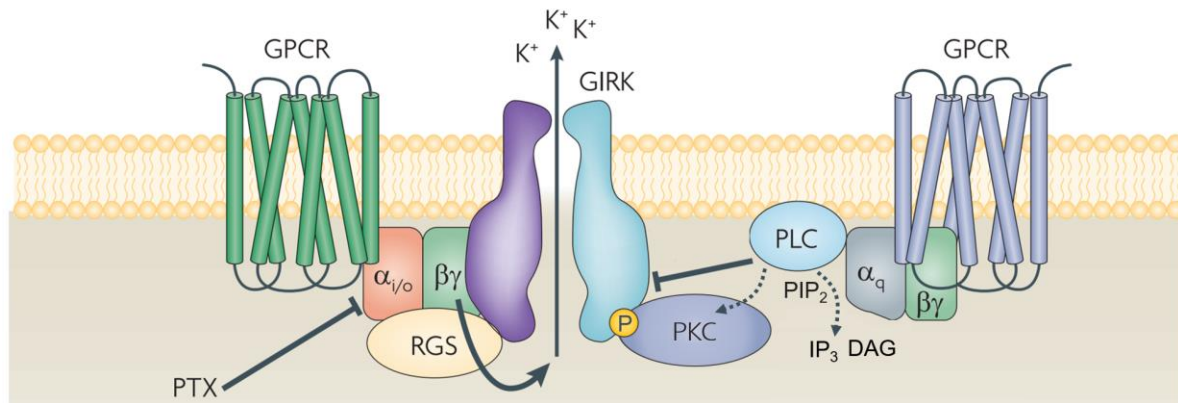


Figure a.5. G_q -coupled GPCRs can regulate GIRK channels.

Adapted from Lüscher *et al.*, 2010. See text for description. RGS – Regulator of G protein Signaling is discussed in the next sections.

Note that PLC has, in fact, a dual effect. It destabilizes the open conformation of GIRK channels by depleting PIP_2 while simultaneously reducing the channel open probability by phosphorylation via the activation of protein kinase C (PKC) (Leaney *et al.*, 2001).

Two channel mutants have been used to study the effects of the PIP_2 metabolism on the channel: Kir3.4(S191A), which shows reduced PKC inhibition (Mao *et al.*, 2004), and Kir3.4(I229L), which has stabilized PIP_2 interactions that slow down the desensitization by PIP_2 depletion (Zhang *et al.*, 1999).

These two mechanisms of activation and inhibition can intricately regulate the activity of GIRK channels. For instance, Kobrinsky *et al.* (2000) show that in native cardiac cells, stimulation of muscarinic receptors yields two simultaneous effects (just like in Figure a.5). Activation of Muscarinic Receptor 2 (M2) ($\text{G}_{\alpha i}$ -coupled) opens GIRK channels. In contrast, M1 or M3 ($\text{G}_{\alpha q}$ -coupled) trigger PLC, PIP_2 depletion, and ultimately lead to a time-delayed decrease of GIRK currents - from here on out, referred to as "desensitization".

Other recognised mechanisms for GIRK function modulation

Phosphorylation

Several proteins have been shown to phosphorylate or dephosphorylate GIRK channels, with positive or negative effects on their activity. For example, cAMP⁸-dependent protein kinase A (PKA) facilitates GIRK channel activation potentially through the specific phosphorylation of the Kir3.1 subunit (Müllner *et al.*, 2003), while protein phosphatase 2A (PP2A) dephosphorylates GIRK channels and hinders G protein-mediated activation (Medina *et al.*, 2000; Müllner *et al.*, 2003). Calmodulin kinases I and II (Medina *et al.*, 2000) as well as tyrosine kinases (Ma *et al.*, 2000) have also been reported to mediate the phosphorylation of GIRK channels (Rogalski *et al.*, 2000).

Although the implications of these phosphorylation sites are not fully understood, it seems they make GIRK-mediated signaling susceptible to many intracellular cascades, allowing it to be indirectly modulated by non-Gi/o GPCRs.

Regulators of G protein signaling (RGS)

The kinetics of GPCR to GIRK signaling is also modulated by a family of proteins known as the Regulators of G protein signaling (RGS). RGS proteins contain a GTPase-activating domain that accelerates the GTP hydrolysis activity of G α . Thus, they promote the re-formation of the inactive G protein heterotrimer, reducing the availability of active G $\beta\gamma$.

RGS proteins have been shown to accelerate both the activation and deactivation rates of GIRK channels (Doupnik *et al.*, 1997; Saitoh *et al.*, 1997) by impacting the signaling between GPCRs and GIRK (Labouèbe *et al.*, 2007 and reviewed in Doupnik, 2015). For instance, the RGS4, when coupled with GABA_B receptors, induces fast desensitization of GIRK currents within seconds of agonist application in human embryonic kidney cells (HEK) (Mutneja *et al.*, 2005).

Potassium channel tetramerization domain (KCTD) proteins

Potassium channel tetramerization domain (KCTD) proteins are a family of proteins that associate constitutively with the C-terminal of GABA_B receptors. They regulate the kinetics and

⁸ Cyclic adenosine monophosphate.

magnitude of GIRK currents activated by those same receptors.

In Turecek *et al.* (2014) and Zheng *et al.* (2019), upon activation of GABA_B receptors, KCTD12 binds and sequesters Gβγ subunits away from the GIRK channel (Figure a.6). The mechanism leads to channel closure with an onset of a few seconds and is quickly reversible.

Although KCTD12 has the intrinsic ability to inhibit GIRK currents activated by multiple GPCRs in heterologous systems, it exclusively associates with GABA_B receptors in native tissues. Thus, this KCTD-mediated desensitization of GIRK currents appears to be receptor-specific.

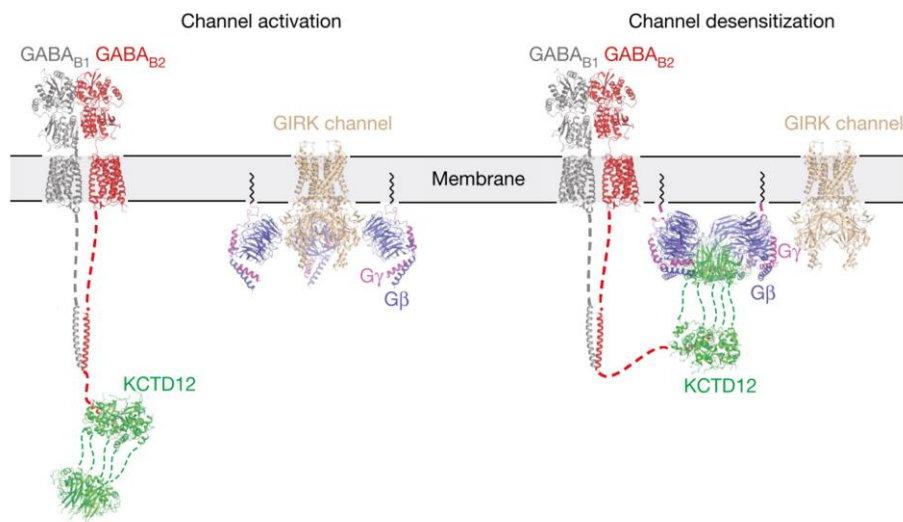


Figure a.6. KCTD12 coupled to GABA_B receptors sequesters Gβγ subunits from GIRK channels.

Adapted from Zheng *et al.*, 2019.

G protein-coupled receptor kinases (GRK)

G protein-coupled receptor kinases (GRKs) phosphorylate GPCRs upon their activation, triggering a series of processes that ultimately lead to the quenching of GPCR signaling. This function of GRKs is further discussed in the next section of the manuscript.

A direct role for GRKs on Kir3 activity has been described by Raveh *et al.* (2010). Upon the activation of the adenosine 1 receptor (A1R) or the μ-opioid receptor (MOR), GRK2 or GRK3⁹ are recruited towards the membrane and inhibit Kir3 channels. GRK-mediated desensitization of the channel is fast, PTX-insensitive, and independent of the kinase activity of GRKs (Figure a.7).

⁹ GRK2/3 are also called βARK1/2 standing for β-adrenergic receptor kinase.

Like KCTD12, described in the previous section, GRK2/3 sequester G $\beta\gamma$ away from activated Kir3 channels. Raveh *et al.* (2010) utilized the Kir3.4(S176P) mutant (Sadja *et al.*, 2001), which is non-responsive to G $\beta\gamma$ stimulation, to demonstrate that inhibition originates from the removal of G $\beta\gamma$ subunits bound to the channel. Indeed, Kir3.4(S176P) has large currents independent of G $\beta\gamma$, and, as such, they were not inhibited by GRK2.

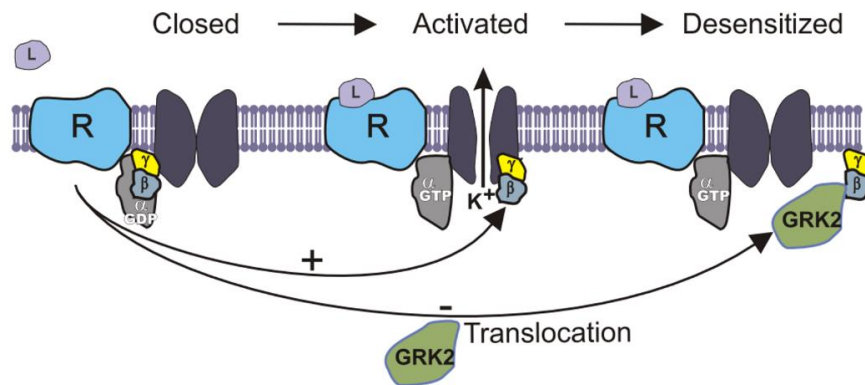


Figure a.7. GRK2 recruitment upon GPCR activation sequesters G $\beta\gamma$ subunits from Kir3 channels.

From Raveh *et al.*, 2010.

Turecek *et al.* (2014) show that, in contrast with the KCTD12-induced desensitization, the GRK2 effect was irreversible within a 10 min period. Furthermore, the GRK2 mechanism is prevented by gallein. Gallein binds with high affinity to the protein-protein interaction "hot spot" of G $\beta\gamma$, inhibiting its signaling to effectors (Lehmann *et al.*, 2008; Casey *et al.*, 2010). This evidence reinforces the idea that inhibition comes from the sequestration of G $\beta\gamma$.

As illustrated in this section, Kir3 channels possess several different modulators of activity that are bound to contribute to the complex and intricate regulation of cellular excitability.

2.1.2 δ -Opioid receptors (DOR)

General considerations about DOR as a member of the opioid-receptor family

Opioid receptors are members of the GPCR superfamily, controlling intracellular effectors, such as GIRK channels, by mobilizing G proteins.

The opioid receptor family comprises the μ - (Chen *et al.*, 1993), δ - (Evans *et al.*, 1992; Kieffer *et al.*, 1992), and κ -opioid receptors (Yasuda *et al.*, 1993) - MOR, DOR, and KOR, respectively

- which differ in ligand specificity and tissue distributions. The nociceptin/orphanin FQ receptor was classified as a member of the opioid receptor family because it is highly similar in sequence (67% in the TM) (Mollereau *et al.*, 1994). However, this receptor has negligible affinity for most opioids that activate the other family members.

Thus, apart from the nociceptin/orphanin FQ receptor, opioid receptors respond with different specificities to endogenous peptide ligands like β -endorphins, enkephalins, dynorphins, as well as opioid alkaloids such as morphine, fentanyl, oxycodone, and heroin.

Endogenous opioid peptides and receptors are widely distributed in various brain regions, the spinal cord and peripheral nerve terminals, where they regulate pain perception, well-being, and reward and addiction. They have also been shown to integrate into the immune system (Wang *et al.*, 2014), regulate gastrointestinal and respiratory function (reviewed in Corder *et al.*, 2018), and mediate cardioprotective effects (reviewed in Headrick *et al.*, 2015).

Since opioid receptors are involved in the nerve pathways that deliver nociceptive information, they have long been the focus of studies to understand their physiology, as well as to exploit them as relevant therapeutic targets for the treatment of pain.

Indeed, opioids have been used to treat pain for centuries, but they are associated with side effects that limit their use as therapeutics. Short-term side effects include constipation and respiratory depression, while the long-term side effects are tolerance and development of dependency and addiction.

MOR are the primary targets of most clinically prescribed opioids. It is now recognized that they are the major mediators of both the potent analgesia of opioids as well as their adverse effects (Charbogne *et al.*, 2014).

Conversely, ligands of KOR and DOR produce less analgesia. While KOR activation can further trigger dysphoria and stress (Van't Veer and Carlezon, 2013), DOR activation appears to have milder side effects and low abuse risk. For instance, DOR agonists do not induce physical dependence when tested in Rhesus monkeys (Brandt *et al.*, 2001). Furthermore, DOR agonists show anxiolytic and antidepressant-like actions in rodent models (reviewed in Chu Sin Chung & Kieffer, 2013), making them a particularly attractive target for the treatment of pain.

DOR is encoded by the human OPRD1 gene. The most common human polymorphism is at the residue 27 (Phe27/Cys27). The less frequent Cys27 variant has been reported to have

hindered maturation with higher retention of the receptor at the ER (Leskelä *et al.*, 2009). However, both variants have similar pharmacological and signaling properties.

The native peptide DOR agonists are the enkephalins such as [Met5]-enkephalin and [Leu5]-enkephalin and deltorphins (reviewed in Gendron *et al.*, 2016). Natural enkephalins have only moderate selectivity for DOR and are vulnerable to enzyme degradation. Thus, stable enkephalin analogs with enhanced DOR selectivity have been synthesized for the study of DOR and include, for instance, DADLE¹⁰ (Beddell *et al.*, 1977) and DALE (Szücs *et al.*, 1985).

The non-peptide DOR agonist SNC80 is also extensively used in the study of DOR, since it has high selectivity for this receptor and has demonstrated analgesic effects (reviewed in Gendron *et al.*, 2016).

DOR structure and signaling

The structures of all four opioid receptors bound to their cognate antagonists (Figure a.8) were solved in 2012 (Granier *et al.*, 2012 - DOR; Manglik *et al.*, 2012 - MOR; Thompson *et al.*, 2012 - nociceptin/orphanin FQ receptor; Wu *et al.*, 2012 - KOR).

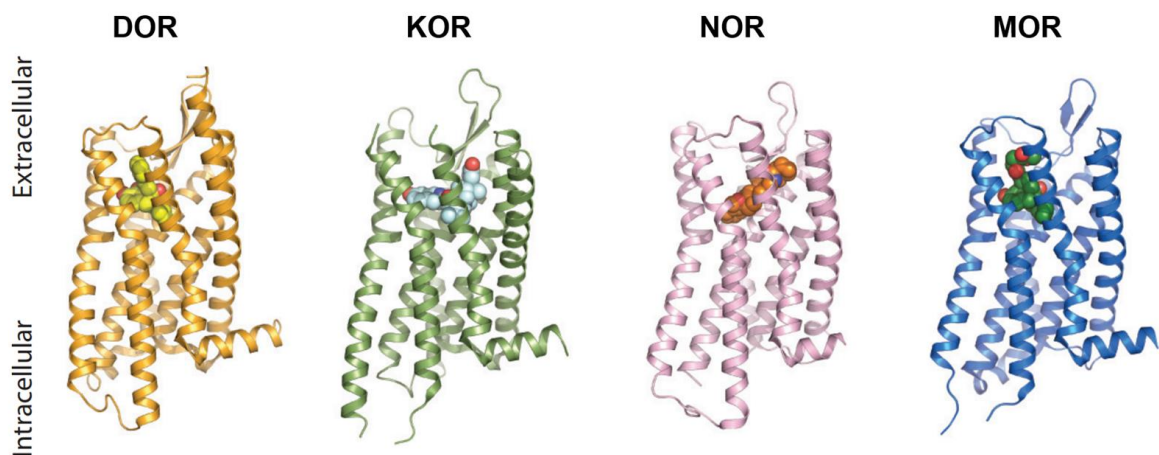


Figure a.8. Inactive structures of the members of the opioid receptor family bound to antagonists.

Adapted from Corder *et al.*, 2018.

Similar to other GPCRs of class A, they share highly conserved amino acid residues within each of the seven transmembrane domains.

¹⁰ DADLE - [D-Ala2, D-Leu5]-enkephalin ; SNC80 - (+)-4-[(α R)- α -((2S,5R)-4-Allyl-2,5-dimethyl-1-piperazinyl)-3-methoxybenzyl]-N,N-diethylbenzamide; DALE - [D-Ala2]-Leucine-enkephalin.

Between the members of the opioid receptor family, the sequence identity within their transmembrane domains is over 73%, with MOR and DOR being the most similar (76%). At the level of the structure, they share high conservation of backbone, even in regions with lower sequence identity.

The main structural differences are found at the upper part of the extracellular ligand-binding pockets, and these are the regions suggested to confer opioid specificity (Granier *et al.*, 2012).

More recently, the structure of MOR complexed with the G protein G_{ai} (Koehl *et al.*, 2018) demonstrated that the third intracellular loop - ICL3 - (between TM5 and TM6) stabilizes the interface between receptor and G protein.

Note that the structure of DOR in Granier *et al.* (2012) was obtained by the crystallization of the receptor fused to the lysozyme of phage T4 (T4L) at the ICL3. GPCR=T4L fusion proteins often facilitate crystallization of GPCRs while maintaining ligand binding unaltered. However, since the T4L is fused to the ICL3, it obstructs the binding and activation of G proteins (Rosenbaum *et al.*, 2007).

The canonical DOR signaling via G proteins is on par with that of MOR and KOR (Figure a.9).

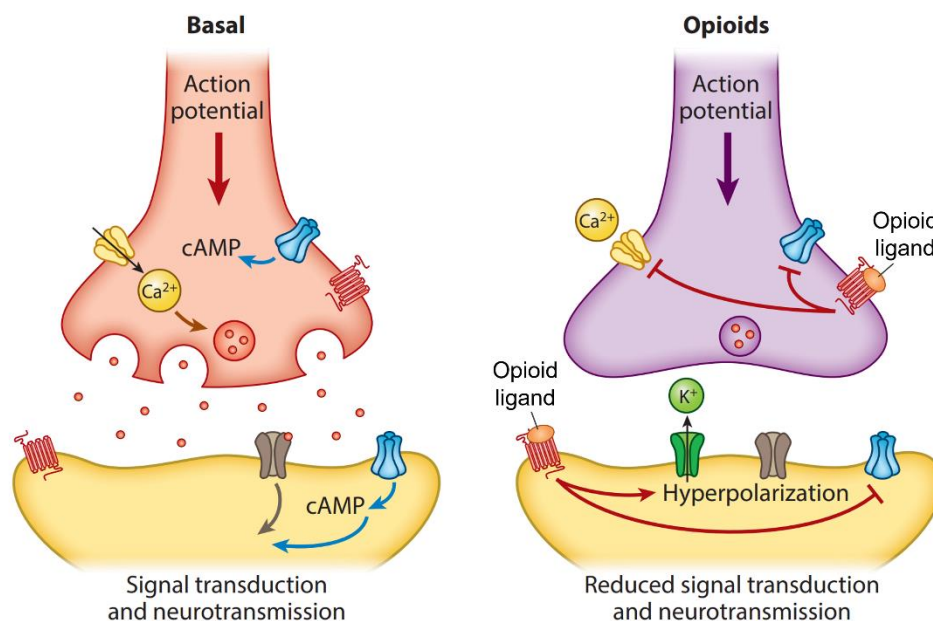


Figure a.9. Canonical opioid receptors signaling through G proteins.

Adapted from Corder *et al.*, 2018. See text for description.

Upon binding of an agonist, DOR activates trimeric G proteins from the G_{i/o} subfamily. The

G α i/o subunit is released and inhibits adenylyl cyclase (AC), decreasing its production of cyclic adenosine monophosphate (cAMP). Consequently, cAMP can no longer activate the cAMP-dependent protein kinase (PKA), effectively halting the phosphorylation of downstream proteins and channels. The G $\beta\gamma$ subunits bind and downregulate voltage-gated calcium channels in pre synapses, averting the release of neurotransmitters. In post synapses, G $\beta\gamma$ subunits bind and upregulate GIRK channels instead, causing K⁺ to exit from the cells, thus preventing depolarization.

Although DOR is only recognized to activate PTX-sensitive G α i/o proteins *in vivo*, when expressed in Chinese hamster ovary cells (CHO) (George *et al.*, 2000) or HEK293 cells (Tso *et al.*, 2000), it can activate G α z and induce PTX-insensitive signaling.

DOR can furthermore activate other downstream signaling cascades, such as the mitogen-activated protein kinase (MAPK) pathways (reviewed in Al-Hasani & Bruchas, 2011). However, the mechanisms underlying these signals seem to be ligand-specific and not fully understood.

As illustrated, DOR can engage a variety of effectors and signaling cascades, though ultimately, they integrate to depress neural functions.

Further layers of complexity at the level of DOR-function modulation can ultimately affect the signaling to its effectors (e.g., GIRK channels). The following sections discuss several mechanisms that impact DOR function.

Other aspects of DOR function modulation

Desensitization of DOR signaling

In this section, desensitization refers to the time-dependent decline in receptor signaling in the sustained presence of an agonist (reviewed in Allouche *et al.*, 2014). It is thought to serve as a mechanism to evade prolonged effects on neuronal activity.

The primary mediators of DOR desensitization are the G protein receptor kinases (GRKs), in particular, GRK2 and GRK3. They attenuate DOR function by phosphorylating the receptor in intracellular serine and threonine residues. Contrary to other kinases, GRKs kinase activity requires the active state of the GPCR and is therefore triggered by the binding of an agonist.

Mutagenesis of DOR has pinpointed the residues Thr358 and Ser363 as the target sites of

GRK2, with the caveat that Ser363 is critical for phosphorylation to proceed (Zhao *et al.*, 1997; Guo *et al.*, 2000; Kouhen *et al.*, 2000). These sites are located at the C-terminal of the receptor, and thus its truncation abolishes phosphorylation by GRK2/3 (Zhao *et al.*, 1997).

DOR phosphorylation by GRKs has a half time of around 1.5 minutes and reaches a maximum within 10 minutes (reviewed in Gendron *et al.*, 2016). Furthermore, Lowe *et al.* (2002) showed that GRK3 can desensitize DOR considerably faster (50% decrease in 5 min) than MOR (50% decrease in 45 min).

GRK modulation of opioid receptors goes further than their kinase activity. In the previous section, GRK2/3 was described as being able to quench signaling upon activation of MOR by sequestering G $\beta\gamma$ subunits directly from the effector (Raveh *et al.*, 2010). Furthermore, Brackley *et al.* (2016) demonstrate that DOR constitutively associates with GRK2 in sensory neurons *in vivo* and *in vitro*. The association chronically downregulates DOR signaling, keeping it in an incompetent state, which can be reverted by using siRNA to silence GRK2.

Phosphorylation by other kinases, such as PKC and Src kinases, has also been recognized to mediate DOR desensitization. Once again, mutagenesis of DOR allowed to identify the Ser344 and Tyr318 residues as the acting sites of PKC (Xiang *et al.*, 2001) and Src kinase (Kramer *et al.*, 2000), respectively. Since these kinases do not require the active state of DOR, their recruitment is most likely a result of downstream signaling, either triggered by DOR or other receptors. Note that, in the work of Kramer *et al.* (2000) and Xiang *et al.* (2001), desensitization was measured by following the internalization of DOR.

Indeed, the term desensitization is often used to describe the reduction in GPCR signaling caused by their (phosphorylation-triggered) internalization. As discussed below, desensitization in the broader sense does not imply internalization.

The canonical desensitization pathway of GPCRs involves first the phosphorylation of the receptor by GRKs or other kinases upon prolonged exposure to an agonist. Phosphorylation is followed by the recruitment of β -arrestins that can now bind with high affinity to the intracellular surface of the receptor, blocking the binding of G proteins. In the case of DOR, β -arrestins interact with both the ICL3 (Leu235-Ile259) and the C-terminal (Gln331- Ala372) of the receptor (Cen *et al.*, 2001). In itself, this dislodgement of G proteins contributes to desensitization. However, the binding of β -arrestins goes further and mobilizes the endocytic pathway, leading to the internalization of the receptor (Shukla *et al.*, 2014 and reviewed in Gurevich & Gurevich, 2019). See Figure a.10.

In this scenario, phosphorylation seems to be required for internalization. Yet, just as internalization is not necessary for desensitization, phosphorylation is not compulsory for β -

arrestins recruitment and internalization.

For instance, Pradhan *et al.* (2010) and Hong *et al.* (2009) have shown that long sustained exposures to specific DOR ligands (e.g., ARM390) diminish receptor signaling without promoting internalization. Indeed, the interaction of opioid receptors with β -arrestins – and the consequent down-regulation of the receptor – is not triggered consistently with every agonist or model system studied (reviewed in Allouche *et al.*, 2014).

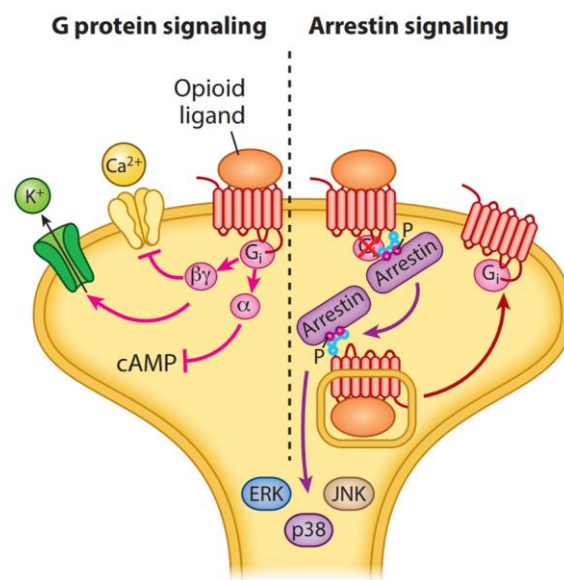


Figure a.10. Arrestins mediate internalization, recycling and signaling of opioid receptors

Adapted from Corder *et al.*, 2018. Arrestins mediate the agonist-induced internalization of the receptor, while triggering ERK, P38 and JNK which are mediators of the MAPK pathway. Internalized receptors can follow either a degradation or recycling pathway.

Furthermore, receptor phosphorylation, by itself, can desensitize the receptor by decreasing G protein engagement (Wilden, 1995) and uncoupling DOR from its effectors (e.g., Kir3 channels - Kovoov *et al.*, 1997).

On the other hand, Law *et al.* (2000), Trapaidze *et al.* (1996) and Zhang *et al.* (2005&2008) show that eliminating the GRK phosphorylation residues (by replacing them with Ala or truncating the C-terminal) does not entirely abolish receptor internalization. They suggest phosphorylation is not compulsory for internalization but instead modulates β -arrestin recruitment.

β -arrestins, although initially appointed to the internalization of the receptors, are now known to be crucial effectors of opioid signaling, triggering cascades such as the MAPK, and

mediating a broad series of cellular processes (reviewed in Corder *et al.*, 2018). See Figure a.10.

Note that internalization does not have to imply a decrease in signaling either. Receptors can continue to signal after being internalized, a mechanism that is emerging as more pervasive than previously thought (reviewed in Thomsen *et al.*, 2018). For instance, in the particular case of DOR, evidence suggests that sustained signaling from internalized receptors is at the basis of inflammatory pain relief (Jimenez-Vargas *et al.*, 2020).

Another agent of receptor signaling decrease is the Regulator of G protein signaling (RGS), already introduced in the previous section. *In vitro* pull-down experiments have determined that RGS4 can interact with the C-terminal of DOR (Karoussiotis *et al.*, 2020). Indeed, RGS4 expression in HEK293 cells reduced the agonist-triggered signaling of DOR while stimulating its internalization (Leontiadis *et al.*, 2009). The role of RGS4 in DOR desensitization is further supported by experiments where knockout mice for RGS4 show enhanced analgesia in response to SNC80 (Dripps *et al.*, 2017).

This section illustrates that the decrease in receptor signaling - or desensitization - can be found in the literature to be operated by several different intermediaries.

Trafficking of DOR and impact on their function

The cellular distribution of DOR can be a matter of debate. Several immunolabeling experiments have determined that DOR has low surface expression, accumulating intracellularly. It has led authors to suggest that the weaker analgesic potency of DOR agonists is the consequence of this lower expression at the plasma membrane (Cahill *et al.*, 2007; Pradhan *et al.*, 2011).

On the other hand, studies in sensory neurons using a DOR-GFP¹¹ fusion at the C-terminal showcase a predominant cell surface expression (reviewed in Gendron *et al.*, 2016). Since the C-terminal has so many regulatory sites for trafficking, this fusion to a large fluorescent protein raises concerns.

Regardless, authors agree that the regulation of DOR trafficking contrasts considerably with the trafficking of other GPCRs (reviewed in Gendron *et al.*, 2016). The general view is that a lower density of receptors at the membrane is the baseline for most cellular functions. Yet,

¹¹ Green fluorescent protein.

simultaneously DOR exists in intracellular reserves and can be rapidly input into the cell membrane in response to a stressor.

In support, several studies have shown that DOR can be found intracellularly close to the cell membrane, in association with the Golgi, pre-synaptic vesicles, or the sub-plasmalemmal space (Cahill & McClellan *et al.*, 2001; Wang *et al.*, 2008).

Furthermore, Cahill & Morinville *et al.* (2001) have shown that, *in vivo*, prolonged morphine exposure does not affect total DOR; instead, it increases cell surface DOR levels by recruiting intracellular DOR. On the same note, enhanced DOR signaling can result from an increase in the number of receptors at the cell membrane (Cahill & Morinville *et al.*, 2001; Pradhan *et al.*, 2009; Pradhan *et al.*, 2015; Scherrer *et al.*, 2006; Walwyn *et al.*, 2009.).

Together, the data suggest that DOR receptor signaling might be intricately connected with its density and localization.

Biased agonists and modulation of response

Biased agonism refers to the ability of different ligands to stabilize distinct conformations of a receptor, promoting differential engagement with specific signaling pathways (reviewed in Wootten *et al.*, 2018).

In support, distinct agonists have been shown to trigger DOR phosphorylation in specific sites, suggesting that their binding stabilizes receptor conformations that expose different residues to regulatory kinases (reviewed in Liggett, 2011).

In the context of biased agonism, the same receptor, depending on the ligand-bound, could preferably engage with G protein-dependent signaling or β -arrestin-dependent signaling. In such a way, different ligands can lead to distinct overall responses.

The idea that G protein signaling mediates the desirable effects of opioids while β -arrestin mediates the adverse effects has propelled the search for G protein-biased agonists (reviewed in Corder *et al.*, 2018).

However, the estimation of bias is often confounded by comparing ligands with different intrinsic efficacies and signaling kinetics (Charfi *et al.*, 2015). Furthermore, this signaling dichotomy of benefic vs. adverse effects is controversial. It reduces complex responses into

binary states, when indeed, there are several compensatory mechanisms that act to create analgesia or any of the adverse effects.

Regardless, the search for biased agonists acting through DOR has not been particularly successful (reviewed in Machelska & Celik, 2018).

Direct interactions with signaling members

GPCRs, G proteins, and channels can be regarded as isolated entities capable of communicating through a series of collisions. However, this model sometimes fails to explain certain aspects of signaling, such as the specificity between Kir3 channels and Gi/o-proteins (discussed briefly in the previous section).

Other models have been proposed to explain how these entities interact (Neubig 1994). One hypothesis is that receptors and their signaling partners may be pre-coupled even in the absence of an agonist (Wreggett *et al.*, 1984; Tian *et al.*, 1994). Evidence obtained by BRET¹² (Molinari *et al.*, 2010; Galés *et al.*, 2006), FRET¹³ (Nobles *et al.*, 2005), and co-immunoprecipitation (Audet *et al.*, 2008; Ciruela *et al.*, 2010), both in heterologous or native tissues, support this idea that DOR, G proteins and GIRK channels exist as pre-formed complexes.

Indeed, BRET and co-immunoprecipitation assays revealed that DOR associates with GIRK channel subunits in cortical neurons where they also co-internalize upon stimulation with an agonist (Nagi *et al.*, 2015).

An alternative model suggests that receptors, G proteins, and channels are compartmentalized within microdomains where all signaling members are concentrated to enable rapid interactions (Gross *et al.*, 1991; Neer, 1995; Neubig, 1994; Suzuki *et al.*, 2005; Sungkaworn *et al.*, 2017). In neurons, high densities of Kir3.2 subunits and GABA_B receptors in synapses are controlled by anchoring and scaffolding proteins (e.g., postsynaptic density protein 95 and synapse-associated protein 97), supporting the microdomain model (Choquet & Triller, 2003; Nassirpour *et al.*, 2010; Romero *et al.*, 2011; Fourie *et al.*, 2014).

Even though there are several lines of evidence to support the direct interaction of DOR and GIRK channels, the significance of this interaction is still not completely understood.

¹² BRET - Bioluminescence resonance energy transfer.

¹³ FRET – Fluorescence/ Förster resonance energy transfer.

Hetero and homo-dimerization of DOR

Besides direct interaction between channels and receptors, another way of regulating receptor to channel signaling might depend on the formation of homo- or heterodimers between receptors. Like most GPCRs, several lines of evidence support the interaction between MOR and DOR (Gomes *et al.*, 2000). Moreover, these interactions have shown functional relevance, with different pharmacology, signaling ability, and trafficking characteristics. For instance, although both MOR and DOR recruit the G protein subunit Gai, dimerization of the two receptors is associated with a shift in G protein coupling from Gai to Gaz (George *et al.*, 2000). Furthermore, the increase in heteromer formation by chronic treatment with morphine in neurons suggests this dimerization is physiologically relevant (Gupta *et al.*, 2010).

In the case of homodimers, the evidence is of the structural type, by the analysis of crystal packing contacts that show interacting parallel receptors. There is always the possibility that these are crystallographic artefacts and that they do not necessarily represent physiologically relevant interfaces. Notably, biochemical cross-linking experiments and modeling suggested the involvement of the extracellular ends of TM4 and TM5 in the dimer formation of DOR receptors. On the other hand, experiments by Cvejic & Devi (1997) suggest that the C-terminal might be necessary for the dimerization. Truncation of the last 15-residues reduced the number of dimers from cross-linking and immunoprecipitation assays in CHO cells. Nevertheless, the physiological relevance of DOR homodimers was still not demonstrated.

Evidence that opioid receptors form and can function as homomers could reveal yet another level of complexity on the opioid receptor regulation on effectors such as the GIRK channels.

2.1.3 DOR and GIRK channels: their implications in pain perception

GIRK channels are recognized to be critical players in pain perception (reviewed in Lüscher *et al.*, 2010). In the work of Blednov *et al.* (2003), Kir3.2-null male mice presented reduced analgesia upon exposure to a wide range of compounds such as ethanol, oxotremorine, baclofen, and several cannabinoids, all acting through distinct receptors. They propose that the activation of Kir3 channels is a ubiquitous mechanism of transducing analgesia through various neurotransmitters.

These findings suggest that GIRK channels could be an interesting target for the development of therapeutics for pain management. Indeed, the GIRK channel direct activator ML297

described by Kimura *et al.* (2020) showed analgesic effects. However, because GIRK channels are widespread and modulate other essential functions, such as heart rate, there is a legitimate concern that acting directly on the channels might elicit off-target effects. The alternative option is to promote the coupling between the receptors and the channel, which is, in fact, the basis of analgesic drugs such as opioids.

As previously discussed, clinically available opioids act primarily through MOR mediating analgesia but also the highly undesirable effects such as the risk of abuse. The opioid-dependency crisis, which has caused over half a million deaths in the past 25 years, has pushed the development of opioids that are devoid of these undesirable effects. Remarkably, DOR as a target has grown in attention since there is compelling evidence for lower abuse risk of DOR agonists (Brandt *et al.*, 2001). Despite this advantage, DOR ligands, such as SNC80, have not been fully explored as analgesic drugs. Depending on their rate of administration, they can lead to hippocampal hyperexcitability and induce seizures (Broom *et al.*, 2002; Jutkiewicz *et al.*, 2005 and reviewed in Quirion *et al.*, 2020).

Thus, a better understanding of DOR signaling is central to the development of safer opioid therapeutics.

The ability of DOR to activate GIRK channels has been demonstrated *in vivo* by Svoboda and Lupica (1998). Their interaction has implications in analgesia, in agreement with the pervasive action of GIRK, discussed above. The role of GIRK in opioid analgesia has been demonstrated in a similar manner, where mutant or null mice for different channel subunits show a reduction in opioid-mediated analgesia (Mitrovic *et al.*, 2003; Marker *et al.*, 2005; Ikeda *et al.*, 2000).

In specific, Chung *et al.* (2014) have demonstrated the role of GIRK on DOR-mediated analgesia by blocking GIRK channels with tertiapin Q in capsaicin-treated masseter muscle of rats. In these conditions, the analgesia triggered by the application of DPDPE, a selective DOR agonist, was reduced. Furthermore, GIRK has been suggested to underlie the convulsant effects of exogenous DOR agonists (Broom *et al.*, 2002; Jutkiewicz *et al.*, 2005).

Since many of the physiological functions attributed to DOR seem to depend on the activation of GIRK channels, the coupling of these two proteins is of major relevance in the understanding of pain perception and as a potential target for drug design.

2.2 Project aim

In the previous section, we contextualized and established the interest in understanding the coupling between GIRK channels and DOR.

In this project, we study the signaling between these two proteins by using electrophysiological techniques. The aim is to present and characterize an unreported inhibition of GIRK channels by DOR and to clarify the molecular and mechanistic aspects which lead to the inhibition, both at the side of the receptor and the channel.

2.3 Results

2.3.1 DOR can activate and rapidly inhibit GIRK currents depending on receptor expression and ligand concentration

For the purpose of studying the regulation of GIRK channels by DOR, we coexpressed both proteins in *Xenopus* oocytes. We can follow receptor function by monitoring GIRK currents through the oocyte membrane with electrophysiology techniques such as TEVC.

Kir3.4(S143T) (Vivaudou *et al.*, 1997), referred from here on as Kir3.4*, was used as a model GIRK channel since it forms highly active homotetrameric channels.

Furthermore, in oocytes, the level of expression of the different proteins can be readily controlled by the amount of injected RNA. To study the effects of the receptor density on channel regulation, we varied the amount of receptor RNA injected.

When oocytes were injected with 0.2 ng of DOR RNA (Figure a.11.A), Kir3.4* channels were activated in the presence of the opioid agonist DALE ([D-Ala2]-Leucine enkephalin). In the conditions tested (91 mM of extracellular K⁺, voltage clamped at -50 mV), activation of the channel induced inward currents. The activation was dose dependent, meaning that currents increased with the agonist concentration. By convention, inward currents are negative and, therefore, an increase, or decrease, in current amplitude is seen here as more, or less, negative current.

By increasing the amount of RNA of DOR injected from 0.2 ng to 2.5 ng, we found that DOR increases Kir3.4* currents at 10 nM of DALE but quickly decreases them ($T_{1/2}=2.5\pm 0.5$ s) when the agonist concentration is 1 μ M (Figure a.11.B & C). The decrease in currents was substantial ($P<0.0001$), reaching levels under the basal current of Kir3.4* (current in hK⁺ before agonist application). High expression of DOR seems to enable the inhibition of Kir3.4* channels under high agonist concentrations.

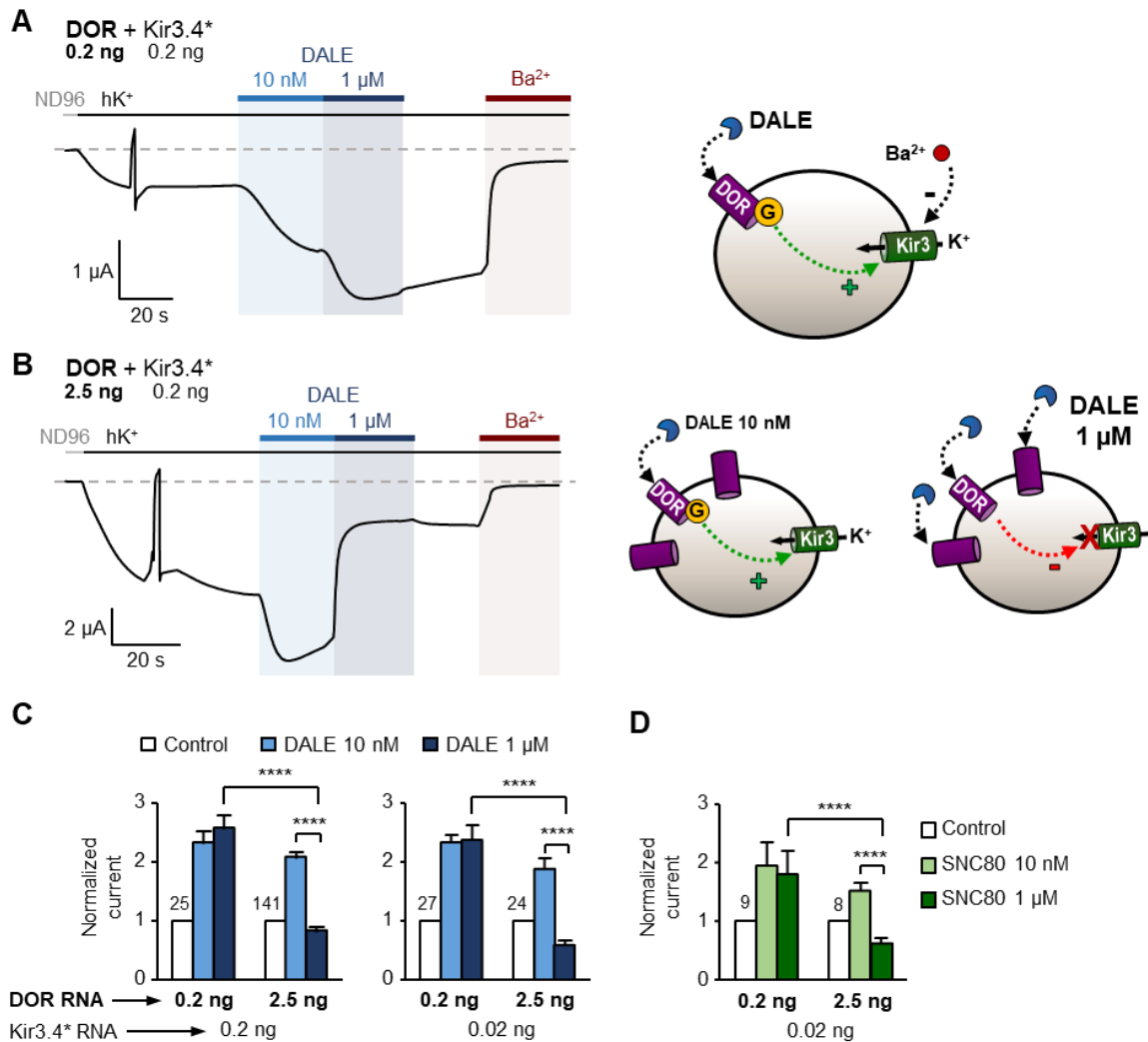


Figure a.11. High expression of DOR reveals inhibition of Kir3.4* currents in high agonist concentration.

Representative recordings of oocytes injected with 0.2 ng of Kir3.4* RNA and low amount (0.2 ng – Panel A) or high amount of DOR RNA (2.5 ng – Panel B). Recordings start in ND96 bath solution (91 mM Na⁺, 2 mM K⁺) and proceed in hK⁺ (0 Na⁺, 91mM K⁺) until the end. Voltage is clamped at -50 mV except between seconds 25 and 27, where a voltage ramp (from -50 to +50 mV) is applied. The rectifying currents measured during the voltage ramp validate the expression of Kir3 channels. DALE was applied at the concentrations indicated, and 3 mM Ba²⁺ was applied at the end of the recording. Currents blocked by the application of Ba²⁺ correspond to Kir3 currents and are thus distinguishable from leak currents.

(A) Oocytes injected with Kir3.4* and 0.2 ng of DOR respond to the agonist DALE as previously described, activating the channel in a dose-dependent manner. The activation is seen as an increase in current amplitude (negative by convention) upon application of the DOR agonist.

(B) In oocytes injected with Kir3.4* and 2.5 ng of DOR, the agonist activates the channel at low concentration (10 nM) but inhibits the channel at high concentration (1 μM). The inhibition corresponds to the fast decrease in current.

(C-D) Normalized current values correspond to the Kir3 currents measured in the different agonist concentrations normalized to the current measured in control solution hK⁺ (i.e., basal current). The numbers above the bars represent the number of oocytes tested. Error bars represent SEM. **** P<0.0001, 2-way ANOVA between the responses of 0.2 and 2.5 ng of injected DOR RNA, with Tukey's post hoc test.

(C) Average normalized currents in low (10 nM) and high (1 μM) concentrations of the agonist DALE. When DOR is highly expressed (2.5 ng of RNA) both with 0.2 or 0.02 ng of Kir3.4* RNA, the application of 1 μM DALE inhibits Kir3.4* currents.

(D) Average normalized currents in low (10 nM) and high (1 μM) concentrations of the DOR-selective agonist SNC80. When DOR is highly expressed (2.5 ng of RNA), the application of 1 μM SNC80 inhibits Kir3.4* currents.

By contrast, changing the amount of Kir3.4* channel expressed (from 0.2 ng to 0.02 ng) does not seem to affect the response of DOR (Figure a.11.C). Inhibition persisted when 2.5 ng of DOR RNA was injected, regardless of the amount of channel RNA. Inhibition is represented by the decrease in average normalized currents at 1 μ M DALE. These results suggest that the level of expression of DOR, but not the channel, modulates the inhibitory pathway.

To test the hypothesis that this signaling is ligand specific, we used two other opioid ligands, DADLE ([D-Ala², D-Leu⁵]-Enkephalin) – a synthetic opioid peptide similar to DALE (data not shown), and SNC80 – a non-peptidic selective agonist of DOR.

Inhibition of the Kir3.4* channels by DOR was not dependent on the choice of ligand (Figure a.11.D) as seen by a similar response upon application of SNC80. The data suggests that it is not the identity of the opioid agonist that is relevant for the inhibition but rather its concentration.

Figure a.12. further clarifies the effects of receptor/channel expression and ligand concentration on the inhibition.

Figure a.12.A demonstrates that increasing amounts of DOR RNA injected increased the % inhibition of Kir3.4* currents, reaching a plateau at 1 ng of receptor RNA. % Inhibition or activation was calculated as the % decrease or increase of current, respectively, elicited by 1 μ M DALE, with respect to the current in 10 nM DALE. In contrast, Figure a.12 B shows that different levels of basal current of Kir3.4*, which are indicative of channel expression, did not affect the potency of the inhibition by DOR (2.5 ng).

Figure a.12.C shows dose-response curves of oocytes expressing DOR (0.2 ng vs. 2.5 ng) and Kir3.4*. For oocytes injected with 0.2 ng DOR RNA, activation increased with DALE concentration in a dose-dependent manner with an apparent half-maximal activatory concentration $K_{1/2}$ of 2.7 nM. Oocytes injected with 2.5 ng of DOR had a similar estimated $K_{1/2}$ of activation (2.7 nM). However, the $K_{1/2}$ for the inhibition was 38 nM, reflecting two apparent affinities for DALE.

Notably, the inhibition of Kir3.4* channels by DOR also presented poor reversibility, with a small decay after two minutes and no further increase in currents upon a second application of 10 nM DALE (Figure a.13).

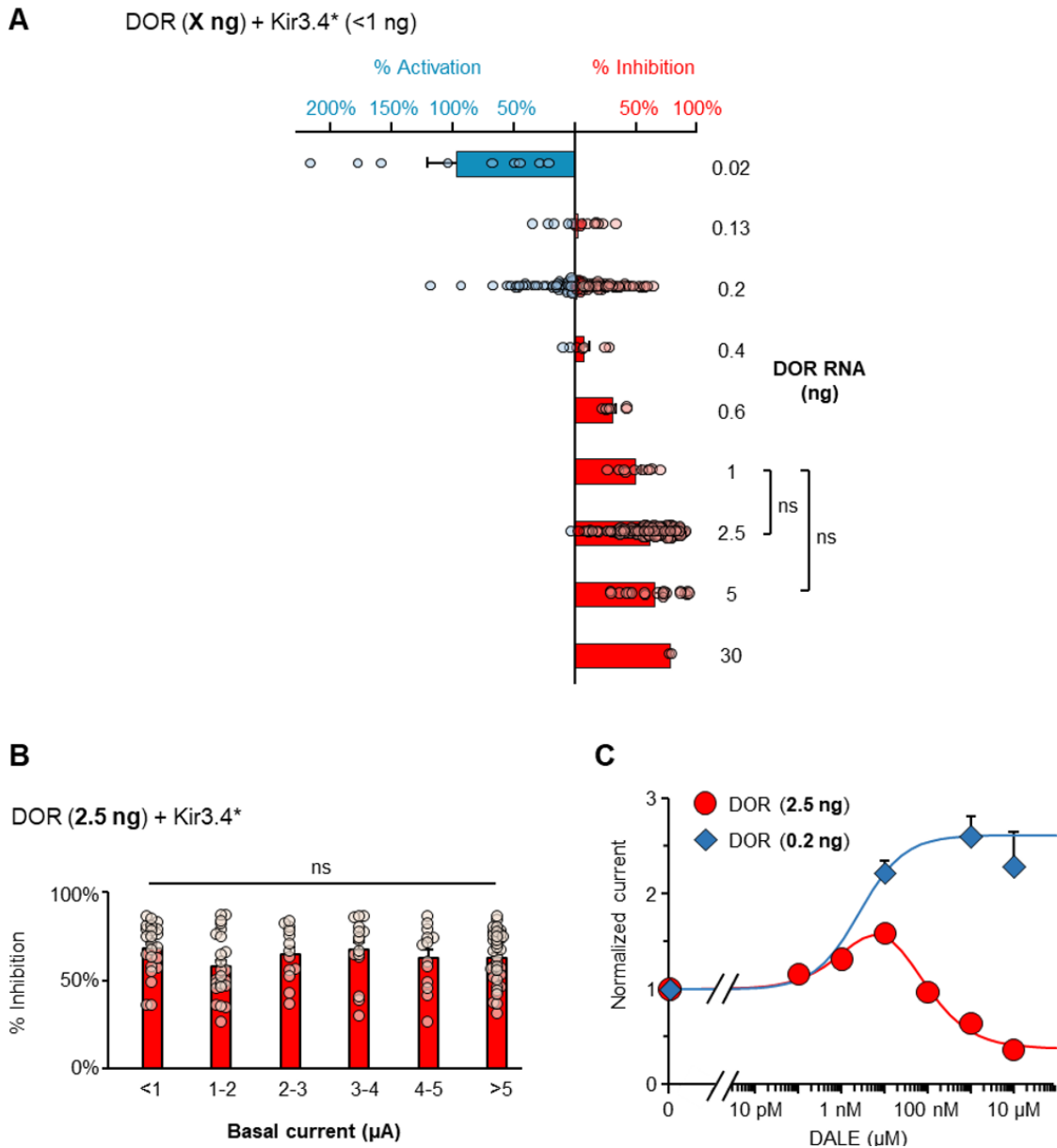


Figure a.12. Inhibition of Kir3.4* currents depends on the amount of DOR RNA injected and the amount of agonist applied but not on the level of expression of the channel.

(A) Summary of responses to 1 μM DALE of oocytes injected with the indicated amounts of DOR RNA and 0.02-1 ng Kir3.4*. Bars represent the average response, while data points represent the response of individual oocytes. % Inhibition or activation is calculated as the % decrease or increase of current, respectively, elicited by 1 μM DALE, with respect to the current in 10 nM DALE. Increasing the amount of DOR RNA injected increases the % inhibition of Kir3.4* currents. % Inhibition seems to reach a plateau at 1 ng of DOR RNA injected since higher amounts do not augment inhibition significantly.

(B) The % Inhibition of oocytes injected with 2.5 ng DOR does not change with different levels of Kir3.4* basal current. Basal current can be used as an indicator of channel expression and can vary greatly between different batches of oocytes. Inhibition is not impacted by this variability.

(C) DALE dose-response curves of oocytes expressing DOR (0.2 and 2.5 ng) and Kir3.4*. For oocytes injected with 2.5 ng DOR RNA, inhibition increases with DALE concentration in a dose-dependent manner. Solid lines represent the fits of the data, using eeFit software (Vivaudou, 2019), with a single activatory Hill equation or the sum of activatory and inhibitory equations. $K_{1/2,act}$ and $K_{1/2,inh}$ (half-maximal activatory and inhibitory concentrations) and h (Hill coefficient) were: for 0.2 ng DOR, $K_{1/2,act}=2.7$ nM, $h=0.8$; for 2.5 ng DOR, $K_{1/2,act}=2.7$ nM, $h=0.74$ and $K_{1/2,inh}=38$ nM, $h=0.71$. Error bars represent SEM. ns: not significant, one-way ANOVA with Tukey's post hoc test.

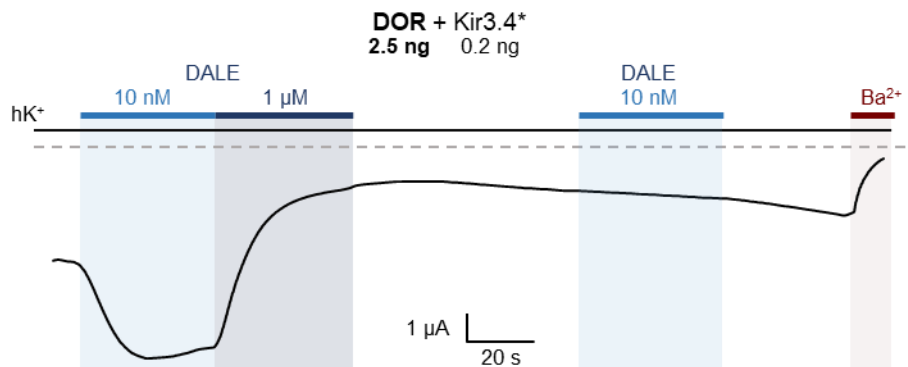


Figure a.13. Inhibition of Kir3.4* by DOR reverses slowly.

Representative recording (N=12) of an oocyte injected with 0.2 ng of Kir3.4* RNA and 2.5 ng of DOR RNA. Recording shows current in hK⁺ (0 Na⁺, 91 mM K⁺) while voltage is clamped at -50 mV. DALE was applied at the concentrations indicated, and 3 mM Ba²⁺ was applied at the end of the recording. The second application of 10 nM DALE, after 1 μM DALE, does not re-activate Kir3.4* currents if wash in between is shorter than 2 min. The data suggests inhibition persists even in the absence of the agonist and reverses slowly.

Taken together, the data demonstrate a non-canonical regulation of Kir3.4* channels by DOR. High expression of DOR reveals an inhibitory capability of the receptor upon application of a ligand at μM concentrations. Inhibition is potent, decreasing currents to sub-basal levels, with a fast onset and slow reversibility.

Control experiments to exclude unspecific effects of the agonist or DOR/Kir3.4* expression in *Xenopus* oocytes can be found in Supplementary figure a.1.

2.3.2 Inhibition of GIRK currents is mediated by DOR but not by MOR

To determine if the inhibitory mechanism was common to other opioid receptors, we tested MOR in the same conditions. MOR was chosen for sharing the highest amino-acid sequence similarities with DOR (63%).

When MOR was coexpressed with Kir3.4* channels, it did not exhibit the same inhibitory capability as DOR (Figure a.14), even when RNA amounts were increased from 2.5 ng to 30 ng and agonist concentrations were up to 10 μM. MOR increased Kir3.4* currents with the increase in agonist concentration.

Neither the application of DALE (Figure a.14.C), nor the application of the highly selective MOR agonist DAMGO (Figure a.14. A & B), was able to induce inhibition of Kir3.4* currents.

The data shows that MOR, contrary to DOR, activates Kir3.4* channels in a dose-dependent manner, even when high expression is promoted by increasing the amount of RNA injected. This suggests that, either inhibition of Kir3.4* is specific to DOR, or alternatively, MOR does not reach the same levels of expression as DOR.

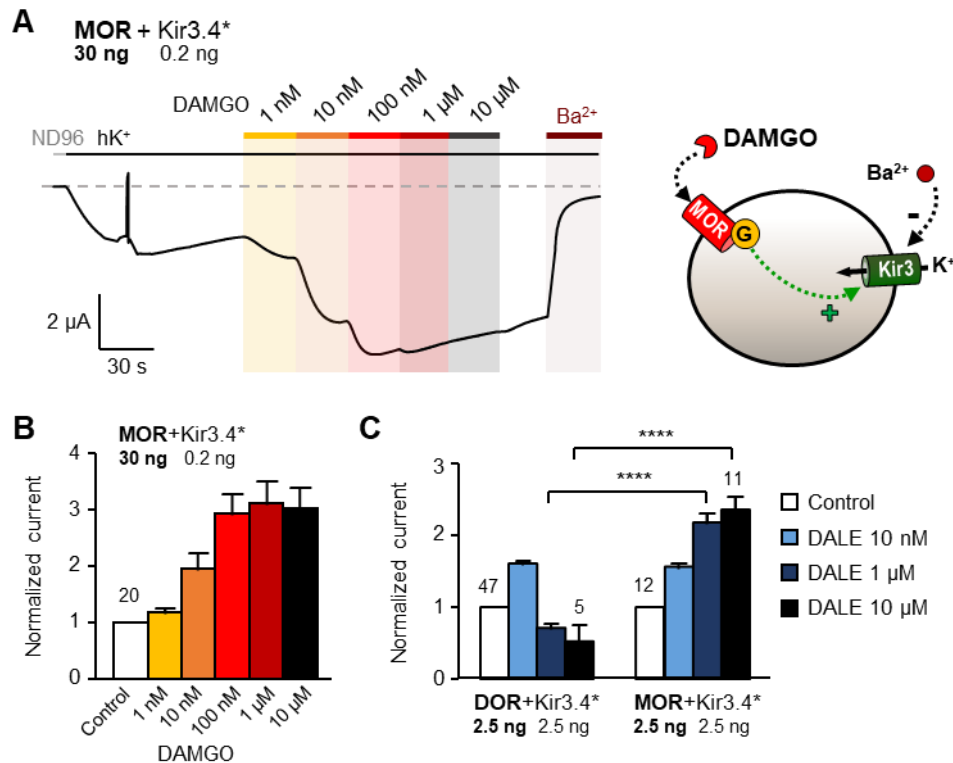


Figure a.14. MOR, contrary to DOR, does not inhibit Kir3.4* currents.

(A) Representative recording of an oocyte injected with 0.2 ng Kir3.4* RNA and 30 ng MOR RNA. Recording starts in ND96 bath solution (91 mM Na⁺, 2 mM K⁺) and proceeds in hK⁺ (0 Na⁺, 91 mM K⁺) until the end. Voltage is clamped at -50 mV except between seconds 45 and 47, where a voltage ramp (from -50 to +50 mV) is applied. The rectifying currents measured during the voltage ramp validate the expression of Kir3 channels. DAMGO, a selective MOR agonist, was applied at the concentrations indicated, and 3 mM Ba²⁺ was applied at the end of the recording. Currents blocked by the application of Ba²⁺ correspond to Kir3 currents and are thus distinguishable from leak currents. MOR, even at high expression levels (30 ng of injected RNA) responds to the agonist DAMGO as previously described, activating the channel in a dose-response manner. The activation is seen as an increase in current amplitudes.

(B) Average normalized currents of 20 oocytes tested in the same conditions as in (A).

(C) Average normalized currents in different concentrations of DALE of oocytes injected with 2.5 ng Kir3.4* and 2.5 ng of either DOR or MOR RNA. The numbers above the bars represent the number of oocytes tested. When not specified, the number of oocytes tested in a solution equals the number of oocytes in the control. Response to high concentrations of DALE (> 1 μM) is significantly different between DOR- and MOR-injected oocytes. **** P<0.0001, 2-way ANOVA between responses of DOR vs. MOR-injected oocytes, with Sidak's post hoc test.

2.3.3 DOR-mediated inhibition is an independent pathway that does not require Gai/o, Gaq or Gas

As previously described, GIRK activation by DOR involves G proteins of the type Gi/o, which are known to be sensitive to pertussis toxin (PTX). Pertussis toxin is able to ribosylate the Gα

subunit of the G protein, impairing its coupling to the receptor. To test if the same Gi/o pathway modulates inhibition, we coexpressed PTX with the receptor and channel (Vivaudou *et al.*, 1997).

When DOR and Kir3.4* were coexpressed with PTX (Figure a.15), the application of 10 nM DALE did not increase Kir3.4* currents. As expected, activation is blocked by the expression and activity of PTX. However, the application of 1 μ M DALE still induced a decrease in Kir3.4* currents. Inhibition by DOR is PTX-insensitive, contrary to activation. The two regulatory mechanisms seem to constitute independent pathways.

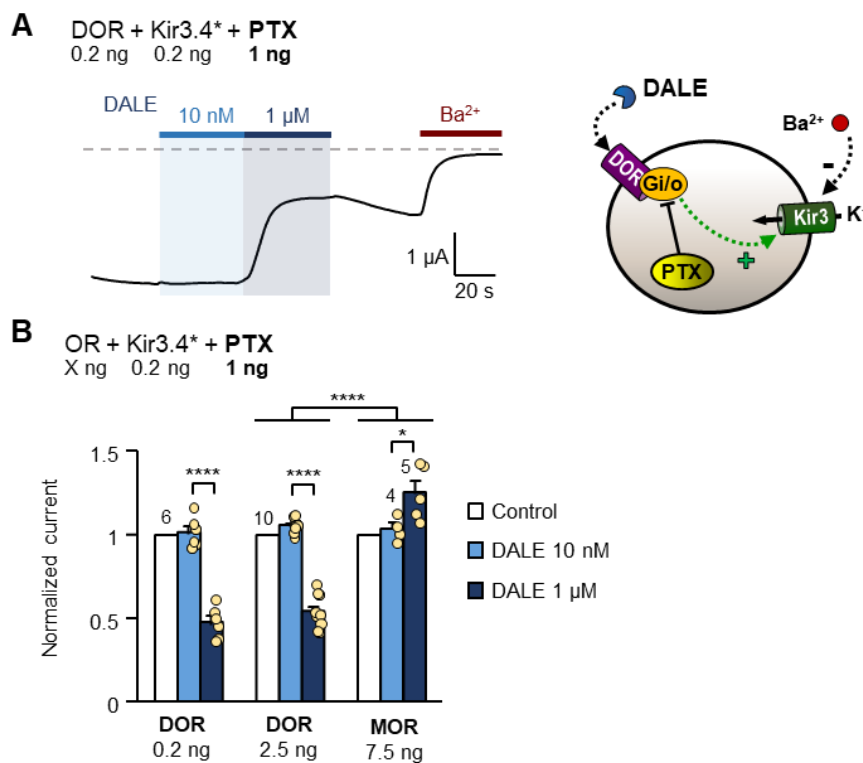


Figure a.15. Inhibition of Kir3.4* by DOR is not sensitive to PTX, contrary to the Gi/o-dependent activation.

(A) Representative recording of an oocyte injected with 0.2 ng Kir3.4* RNA, 0.2 ng DOR RNA, and 1 ng of Pertussis Toxin subunit 1 (PTX) RNA. Recording shows currents in hK⁺ (0 Na⁺, 91mM K⁺) while voltage is clamped at -50 mV. DALE was applied at the concentrations indicated, and 3 mM Ba²⁺ was applied at the end of the recording.

(B) Average normalized currents in low (10 nM) and high (1 μ M) concentrations of DALE of oocytes injected with 0.2 ng Kir3.4*, 1 ng PTX, and DOR/MOR in the amounts indicated. The numbers above the bars represent the number of oocytes tested. In the presence of PTX, there is no significant increase in current upon the application of 10 nM DALE. PTX inhibits Gi/o signaling and thus blocks DOR/MOR activation of Kir3.4*. However, inhibition of basal currents by DOR in 1 μ M DALE is still evident and significant, even at lower expressions of DOR (0.2 ng of RNA). The data suggest that DOR-mediated inhibition does not depend on Gi/o signaling. PTX response of oocytes with 2.5 ng DOR and 7.5 ng MOR is significantly different. MOR shows no inhibition of Kir3.4* currents even with PTX.

*P<0.05, ****P<0.0001, 2-way ANOVA with Tukey's post hoc tests.

Furthermore, by canceling out the activation pathway, PTX revealed that DOR could inhibit Kir3.4* channels even at lower expression levels (0.2 ng of DOR RNA - Figure a.15). The

inhibition is shown in the trace of Figure a.15.A and represented in Figure a.15.B by a decrease in the average normalized currents for oocytes injected with 0.2 ng DOR RNA. The data suggest that, rather than being a requirement, high expression of DOR potentiates the inhibitory mechanism.

In an attempt to reveal inhibition by MOR in the same manner, we coexpressed MOR, Kir3.4* and PTX. As seen in Figure a.15.B, MOR did not reveal any signs of inhibition of Kir3.4* upon application of a high concentration of DALE.

We hypothesized that overexpressing DOR in *Xenopus* might promote unspecific coupling with non-Gi/o G proteins (reported in Hatcher-Solis *et al.*, 2014; Vorobiov *et al.*, 2000).

The different mechanisms of receptor-mediated decrease of GIRK currents were discussed in the introduction. For instance, a GPCR coupled to Gq can inhibit the GIRK channels by activating phospholipase C (PLC) that (1) depletes PIP₂ and (2) activates phosphorylation of inhibitory residues of the channel by protein kinases C (PKC).

To test Gq involvement in the inhibition we used the inhibitor YM-254890, that blocks the exchange of GDP to GTP at the Gα subunit. More recently, YM-254890 has also been shown to suppress Gs signaling (Uemura *et al.*, 2009, Peng *et al.*, 2021).

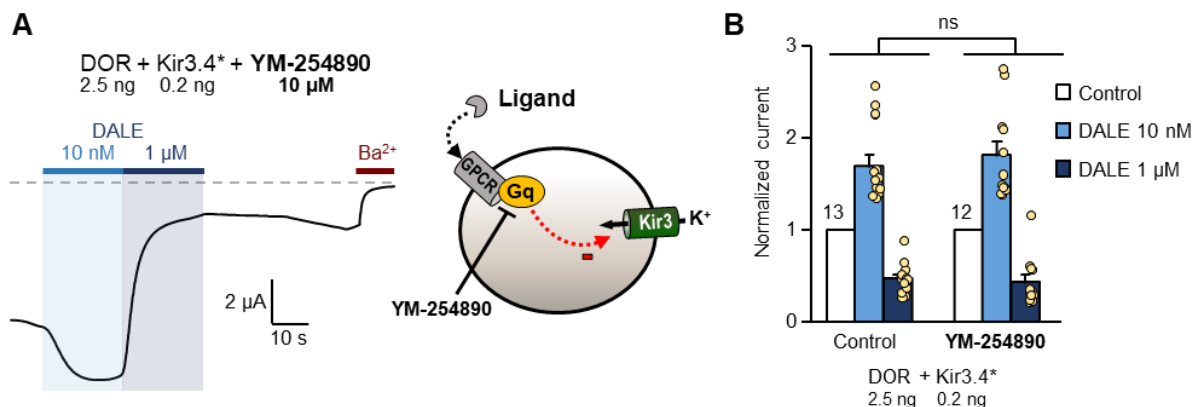


Figure a.16. Inhibition of Kir3.4* by DOR is not sensitive to the Gq/Gs inhibitor YM-254890.

(A) Representative recording of an oocyte injected with 0.2 ng Kir3.4* RNA and 2.5 ng DOR RNA after incubation for 10 minutes with the Gq/Gs inhibitor YM-254890 at 10 μM. Recording shows currents in hK⁺ (0 Na⁺, 91mM K⁺) while voltage is clamped at -50 mV. DALE was applied at the concentrations indicated, and 3 mM Ba²⁺ was applied at the end of the recording.

(B) Average normalized currents of oocytes in the same conditions as in (A) vs. oocytes not exposed to the inhibitor (Control). The numbers above the bars represent the number of oocytes tested. The responses of control oocytes and YM-254890-treated oocytes were not statistically different. The absence of effect of the Gq/Gs inhibitor suggests that DOR-mediated inhibition is not dependent of Gq/Gs.

ns: not significant, 2-way ANOVA.

We established a protocol where oocytes injected with DOR and Kir3.4* were subjected to 10 μ M of YM-254890 for 10 minutes. See Supplementary figure a.2 for tests of the inhibitor with the Gq-coupled muscarinic receptor 3 (M3).

The incubation with the Gq/Gs inhibitor did not significantly affect the inhibition of Kir3.4* channels by DOR (Figure a.16). The data suggests that the DOR-mediated decrease in Kir3.4* currents is not due to an unspecific coupling of DOR with Gq or Gs proteins.

Although we excluded the intervention of Gi/o, Gq and Gs proteins, Gz, the PTX-insensitive member of the Gi/o subfamily, was still a plausible agent. In overexpressing systems, Gz has been shown to couple with both GIRK channels (Vorobiov *et al.*, 2000) and DOR (George *et al.*, 2000; Tso *et al.*, 2000). Furthermore, heterodimerization of MOR and DOR shifts G protein coupling towards Gz (George *et al.*, 2000). We hypothesized that overexpression could promote DOR dimerization and shift its coupling preferences.

To exclude Gz involvement, we tested a construct of DOR fused to the lysozyme of phage T4 (T4L) at the intracellular loop 3 (ICL3). As previously mentioned, this construction was used for the crystallization and structural determination of DOR (Granier *et al.*, 2012). The fusion to the ICL3 of DOR, creates a steric obstruction of the binding site for G proteins. As such, it should block G protein coupling of any subfamily.

When coexpressing DOR=T4L with Kir3.4*, the application of 10 nM DALE did not lead to an increase in currents (Figure a.17). Similar to the effect of expressing PTX, the fusion effectively blocked Gi/o coupling and, consequently, the activation of Kir3.4*. When 1 μ M DALE was applied, DOR=T4L was able to inhibit Kir3.4*. The decrease in currents was modest, considering that oocytes had to be injected with 30 ng (rather than 2.5 ng). Inhibition of Kir3.4* currents by DOR (2.5 ng) was on average $58\pm 14\%$, while the inhibition by DOR=T4L was $25\pm 9\%$. The data indicates that inhibition is not mediated by G protein coupling and does not arise from the ICL3 of DOR. Inhibition was not entirely abolished by occluding the ICL3, but it was significantly impaired. The ICL3 might contribute to the recognition or binding affinity of the entity that mediates the inhibition.

The data, taken together, imply that the inhibition of Kir3.4* by DOR is a distinct and independent pathway from activation. Although it does not depend on G protein coupling, it is equally triggered by agonist binding.

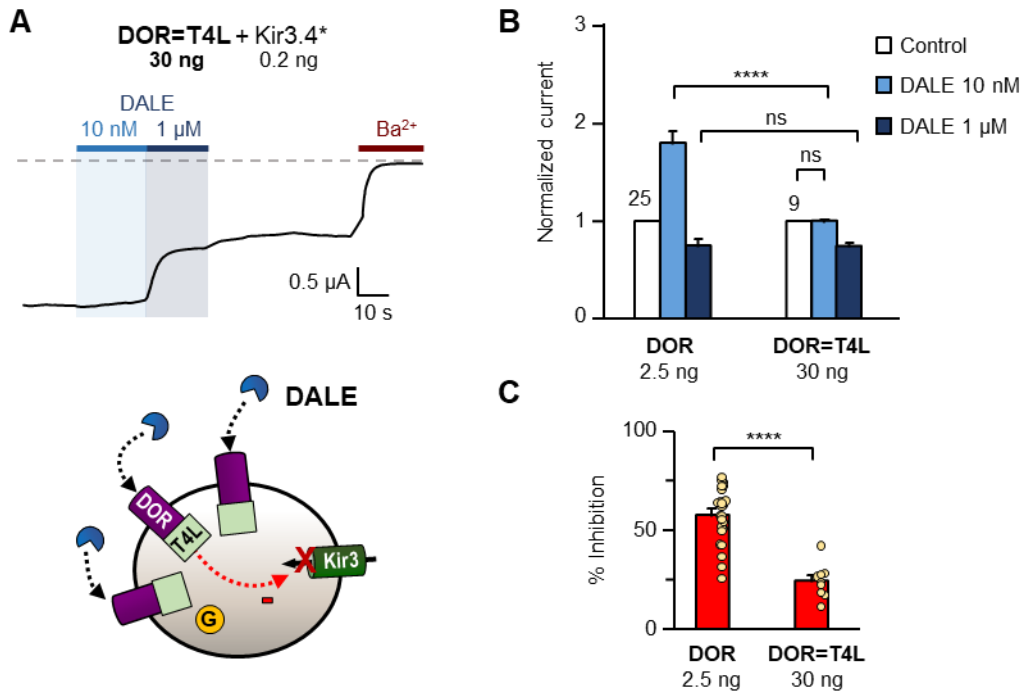


Figure a.17. Inhibition of Kir3.4* channels by DOR does not require the activation of G proteins.

DOR=T4L corresponds to the fusion of the Lysozyme of bacteriophage T4 (T4L) to the intracellular loop 3 (ICL3) of DOR. This construct was used for the crystallization and structure determination of DOR. The large T4L component on the ICL3 of DOR sterically inhibits the interaction and activation of G proteins by DOR.

(A) Representative recording of an oocyte injected with 0.2 ng Kir3.4* RNA and 30 ng DOR=T4L RNA. Recording shows currents in hK⁺ (0 Na⁺, 91mM K⁺) while voltage is clamped at -50 mV. DALE was applied at the concentrations indicated, and 3 mM Ba²⁺ was applied at the end of the recording. Inhibition of Kir3.4* is observable, as a decrease in current, upon application of 1 μM DALE. The data suggest that inhibition does not require the activation of G proteins.

(B) Average normalized currents in low (10 nM) and high (1 μM) concentrations of DALE of oocytes injected with 0.2 ng Kir3.4* RNA and DOR or DOR=T4L in the amounts indicated. The numbers above the bars represent the number of oocytes tested. Contrary to DOR, DOR=T4L does not increase currents upon application of 10 nM DALE. The fusion of DOR to T4L obstructs the interaction with G proteins and the consequent activation of the channel.

ns: not significant, ****: P<0.0001, 2-way ANOVA with Tukey's post hoc tests.

(C) Comparison of the % current inhibition elicited by DALE 1 μM (compared to current at DALE 10 nM) of DOR=T4L and DOR. DOR=T4L can inhibit Kir3.4* currents (25%±9%), but inhibition is nevertheless significantly hampered compared to DOR (58%±14%). **** P<0.0001, two-tailed Student's t-test.

2.3.4 DOR-mediated inhibition does not arise from the last 32 residues of its C-terminal

As illustrated in the introduction, the DOR C-terminal is a hub of regulatory residues. It hosts the acting sites of several kinases (GRK2 - T358/S363, PKC - S344, Src - Y318), recognition sites of β-arrestin (Q331- A372), and the interacting region with RGS4 (Y318-R330). It has also been implicated in the formation of homodimers of DOR (Cvejic & Devi, 1997), since truncation of the last 15 residues eliminates DOR dimer immunoprecipitation.

We hypothesized that inhibition of GIRK by DOR could be mediated through regulatory regions on the C-terminal. We created a DOR construct DOR[ΔC32] by truncating the last 32 residues, i.e., the whole soluble region just following intracellular helix 8.

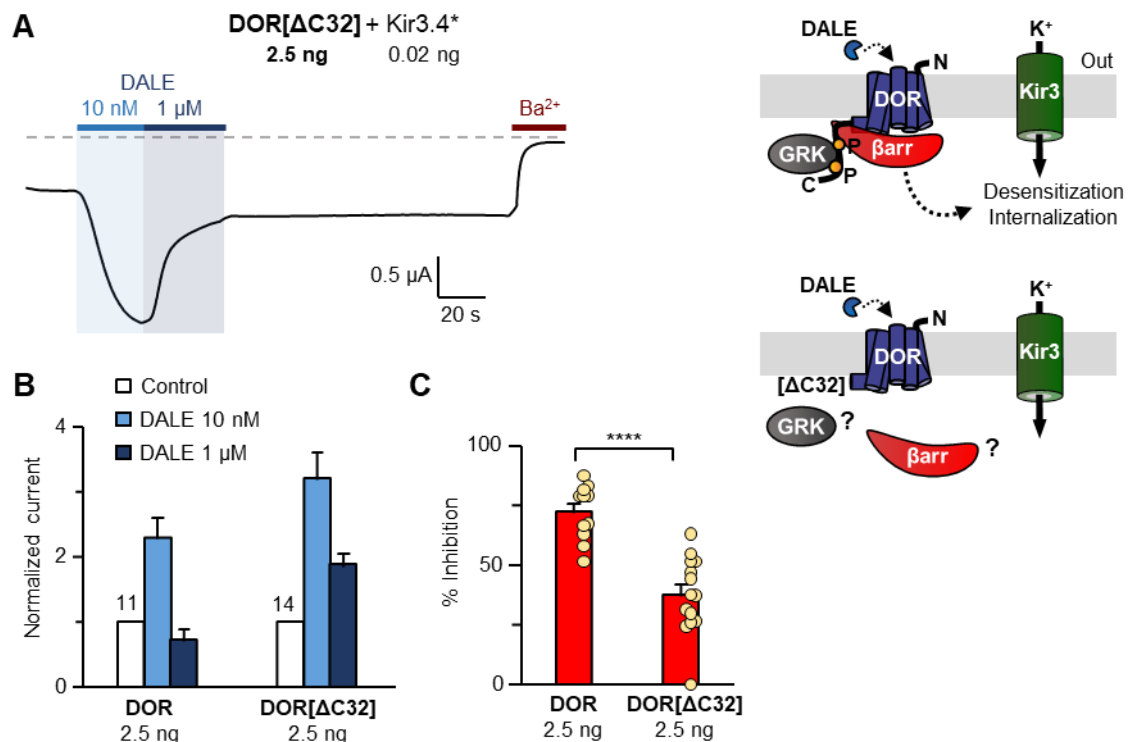


Figure a.18. Inhibition of Kir3.4* channels by DOR does not require the last 32 residues of the C-terminal of the receptor.

The C-terminal of DOR is recognized by kinases and other regulatory proteins such as β-arrestins. The deletion of the last 32 residues of the C-terminal (DOR[ΔC32]) has been shown to hamper internalization.

(A) Representative recording of an oocyte injected with 0.02 ng Kir3.4* RNA and 2.5 ng DOR[ΔC32] RNA. Recording shows currents in hK⁺ (0 Na⁺, 91 mM K⁺) while voltage is clamped at -50 mV. DALE was applied at the concentrations indicated, and 3 mM Ba²⁺ was applied at the end of the recording. Inhibition of Kir3.4* is observable upon application of 1 μM DALE. The data suggest that Kir3.4* inhibition by DOR does not require the C-terminal.

(B) Average normalized currents in low (10 nM) and high (1 μM) concentrations of DALE of oocytes injected with 0.02 ng Kir3.4* RNA and 2.5 ng DOR or DOR[ΔC32] RNA. The numbers above the bars represent the number of oocytes tested. DOR[ΔC32] can activate Kir3.4* currents in 10 nM DALE and inhibit them at 1 μM DALE.

(C) Comparison of the % current inhibition elicited by 1 μM DALE of DOR[ΔC32] and DOR. DOR[ΔC32] can inhibit Kir3.4* currents but inhibition is significantly smaller compared to DOR.

****P < 0.0001, two-tailed Student's t-test.

This protein corresponds to DOR from residue M1 to P340. It excludes GRK and PKC phosphorylation sites but not the Src phosphorylation site. It excludes part of the contact residues with β-arrestin but not the interaction region with RGS4. Furthermore, it excludes the last 15 residues implicated in DOR dimerization. Similar truncations of DOR (Trapaidze *et al.*, 1996 - 37 last residues; Guo *et al.*, 2000 - 31 last residues) have been shown to impair β-

arrestin recruitment and internalization. Furthermore, in Kovoor *et al.* (1997), the truncation of the last 33 residues of DOR eliminated desensitization mediated by GRK3 (independent of β -arrestin).

Figure a.18 shows that inhibition of Kir3.4* persisted in the construct DOR[Δ C32] when oocytes were injected with 2.5 ng RNA and upon application of 1 μ M DALE. However, inhibition by DOR[Δ C32] was significantly impaired ($37\pm 4\%$) compared to the wild-type DOR ($72\pm 3\%$).

The data suggest that inhibition does not arise from the last 32 residues of the receptor since its truncation did not entirely abolish it. Like ICL3, the C-terminal might contribute to the recognition or binding affinity of the entity that mediates the inhibition.

These experiments allowed us to exclude GRK phosphorylation at T358/S363 residues as the primary inhibitory mechanism. Likewise, we can exclude the role of PKC phosphorylation at the residue S344. In Supplementary figures a.3, a.4, we further address the implications of GRK kinases on the inhibition. Supplementary figure a.5 addresses the role of Src kinases activity.

2.3.5 Receptor differences in the inhibition of GIRK are not due to differences in surface expression levels

Although controlling the amount of RNA injected has been shown to be an acceptable way of manipulating protein expression in *Xenopus* oocytes, different translation efficiencies of individual mRNAs might confound the direct comparison between distinct proteins.

To test the implications of receptor expression on the inhibition of Kir3.4* channels, we optimized a cell luminescence-based assay for use in *Xenopus* oocytes, which we named XenoGlo. See Annex D for the validation of the method.

This method relies on the use of the HiBiT/NanoLuc system offered by Promega. The HiBiT tag is a small 11–amino acid peptide that produces bright luminescence upon high-affinity complementation with LgBiT - the large subunit of Nanoluciferase. Its use to follow GPCR expression has been demonstrated in PC3 cell lines by Boursier *et al.* (2020). They show that HiBiT-fused GPCRs had the same pharmacological properties as wild-type receptors. Furthermore, by adding an extra Interleukine 6 (IL6) secretion signal sequence, they obtained HiBiT-tagged GPCRs that trafficked to the cell surface similarly to unmodified proteins.

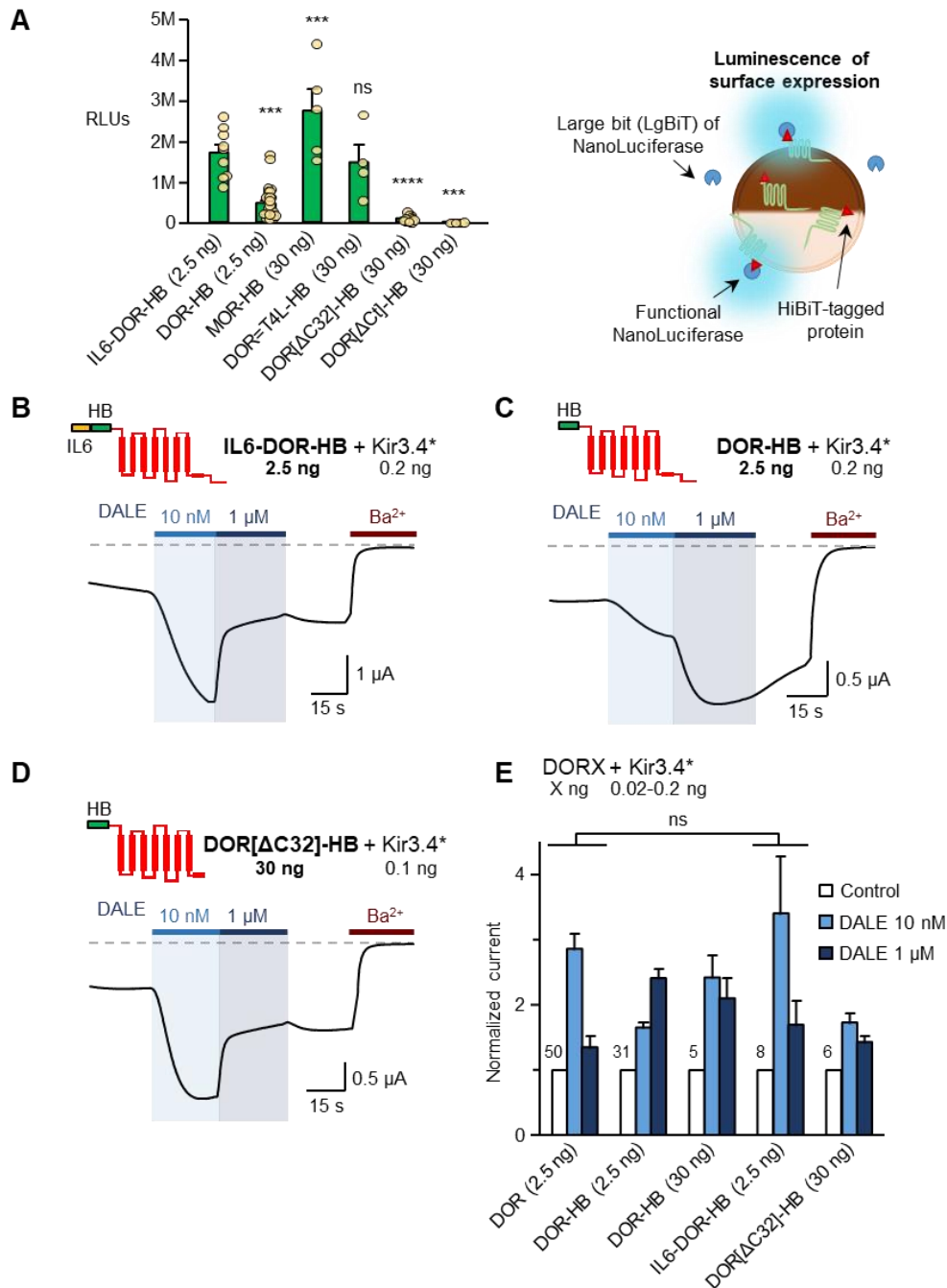


Figure a.19. Differences in the inhibitory capability of the receptors cannot be solely justified by differences in surface expression.

(A) Mean luminescence recorded in oocytes expressing the specified HiBiT-tagged (HB) receptors and 0-0.2 ng of Kir3.4* RNA. Each point represents a single oocyte.

Receptor-HB corresponds to the receptor fused to the HiBiT-tag on the N-terminal. IL6-DOR-HB corresponds to the DOR-HB construction with an added secretion signal sequence of Interleukine 6 (IL6) to improve surface expression.

DOR=T4L corresponds to the fusion of the Lysozyme of bacteriophage T4 (T4L) to the intracellular loop 3 (IL3) of DOR.

DOR[ΔC32] corresponds to the deletion of the last 32 residues of the C-terminal of DOR.

DOR[ΔCt] corresponds to the deletion of the full C-terminal of DOR (51 residues).

ns not significant, ***P<0.001, ****P<0.0001, one-way ANOVA with Dunnett's post hoc test against the control IL6-DOR-HB (2.5 ng).

(B-D) Representative recordings of oocytes injected with Kir3.4* RNA and RNA of the specified HiBiT-tagged receptors. Recordings show currents in hK⁺ (0 Na⁺, 91mM K⁺) while voltage is clamped at -50 mV. DALE was applied at the concentrations indicated, and 3 mM Ba²⁺ was applied at the end of the

recording.

(E) Average normalized currents of oocytes injected with Kir3.4* RNA and wt DOR or HiBiT-tagged constructs DOR-HB, IL6-DOR-HB, and DOR[ΔC32]-HB. DOR[ΔCt] does not respond to DALE application (not shown). The numbers above the bars represent the number of oocytes tested. ns not significant two-way ANOVA with Tukey's post hoc test.

We designed a series of constructs comprised of a receptor fused to the HiBiT tag on the N-terminal. Since the N-terminal of the receptors is extracellular, the luminescence signal upon exposure to LgBit and the Nanoluciferase substrate is a readout of surface expression of the protein.

Figure a.19.A shows surface luminescence levels (surface RLUs) in oocytes expressing the denoted receptors. 'Receptor-HB' corresponds to the specified receptor fused to the HiBiT-tag (HB) on the N-terminal (HB notation is added at the end of the name for clarity). IL6-DOR-HB corresponds to the DOR-HB construction with an extra IL6 secretion signal sequence at the beginning of the N-terminal. We compared the surface expression of HiBiT-tagged DOR, MOR, DOR=T4L, and DOR[ΔC32] (discussed in the previous sections). We also included DOR[ΔCt], which corresponds to the deletion of the full C-terminal of DOR (51 residues).

The first thing to notice is that IL6-DOR-HB and DOR-HB differ considerably in surface expression levels (≈1.5 and ≈0.9M RLUs, respectively). When coexpressed in oocytes with Kir3.4*, IL6-DOR-HB (2.5 ng) was able to inhibit the channels in a manner not statistically different from wt DOR. The same does not apply to DOR-HB (2.5 ng) (Figure a.19 traces B & C, histogram E). The HiBiT tag fusion by itself seems to hinder the expression and response of the constructs.

Nevertheless, oocytes injected with 30 ng of MOR-HB RNA express more receptors at the surface (≈2.8M RLUs) than oocytes injected with 2.5 ng of IL6-DOR-HB RNA (≈1.5M RLUs). The data suggest that the inability of MOR to inhibit Kir3.4* is not related to a lower surface expression (Figure a.19.A).

DOR=T4L (30 ng) has similar expression levels as IL6-DOR-HB (2.5 ng) with average RLU values of ≈1.3M vs. 1.5M, respectively. Thus, the difference in inhibition between the two constructs observed in the previous sections is not confounded by differences in expression. DOR=T4L decreased inhibition indeed results from the obstruction of the ICL3 by T4L.

Curiously, oocytes injected with 30 ng of DOR[ΔC32]-HB RNA show inhibition of Kir3.4* (Figure a.19.D & E), despite a dramatically lower expression (≈108K RLUs). Expression is even lower than DOR-HB (2.5 ng), which shows no inhibition. Our previous observations on

the decrease of inhibition have to be re-evaluated in light of the difference in expression levels. Previously the data seemed to suggest that DOR[Δ C32]-HB has reduced inhibitory capability when, in fact, it requires much lower levels of surface receptor to trigger the inhibition. The C-terminal might be downregulating the inhibition in the native receptor (Supplementary figure a.6 also shows DOR[Δ C32]-HB has low total expression).

The results on DOR[Δ Ct] further support the importance of the C-terminal for trafficking and function, since removing the full C-terminal of DOR made it not functional (data not shown) and significantly reduced its surface expression (\approx 6K RLU).

The data suggest that differences in surface receptor level cannot justify why MOR cannot inhibit Kir3.4* while DOR can. Inhibition seems to be specific to DOR. Just as suggested in the experiments with PTX, it seems that high expression of the receptor might not be necessary for the inhibitory pathway to be triggered. ICL3 and the last 32 residues of the C-terminal of the receptor continue to emerge as non-essential modulating domains of the inhibition of Kir3.4* by DOR.

In an attempt to exploit the sequence similarities between MOR and DOR to identify the molecular domains involved in the DOR-mediated inhibition, we created a series of MOR/DOR chimeras and screened them for inhibitory capability. We were able to transfer the inhibitory capability to MOR by substituting its intracellular regions with those of DOR. Because the results were not always consistent, limited information was obtained from these experiments. The results can be found in Supplementary figure a.7 and a.8.

2.3.6 Not all GIRK channels are inhibited by DOR

GIRK channels are homo- or hetero-tetrameric complexes of Kir3 proteins. Different channels have different tissue distributions and specific characteristics and functions. To test if DOR-mediated inhibition was generalized throughout the family of Kir3 proteins, we coexpressed different channel subunits with DOR (2.5 ng of RNA).

As seen in Figure a.20, Kir3.2 and Kir3.4 homotetrameric channels can be inhibited by DOR. This observation extends to wild-type proteins as well as to the gain-of-function mutants Kir3.2(E152D) and Kir3.1(V188A) (Yi *et al.*, 2001).

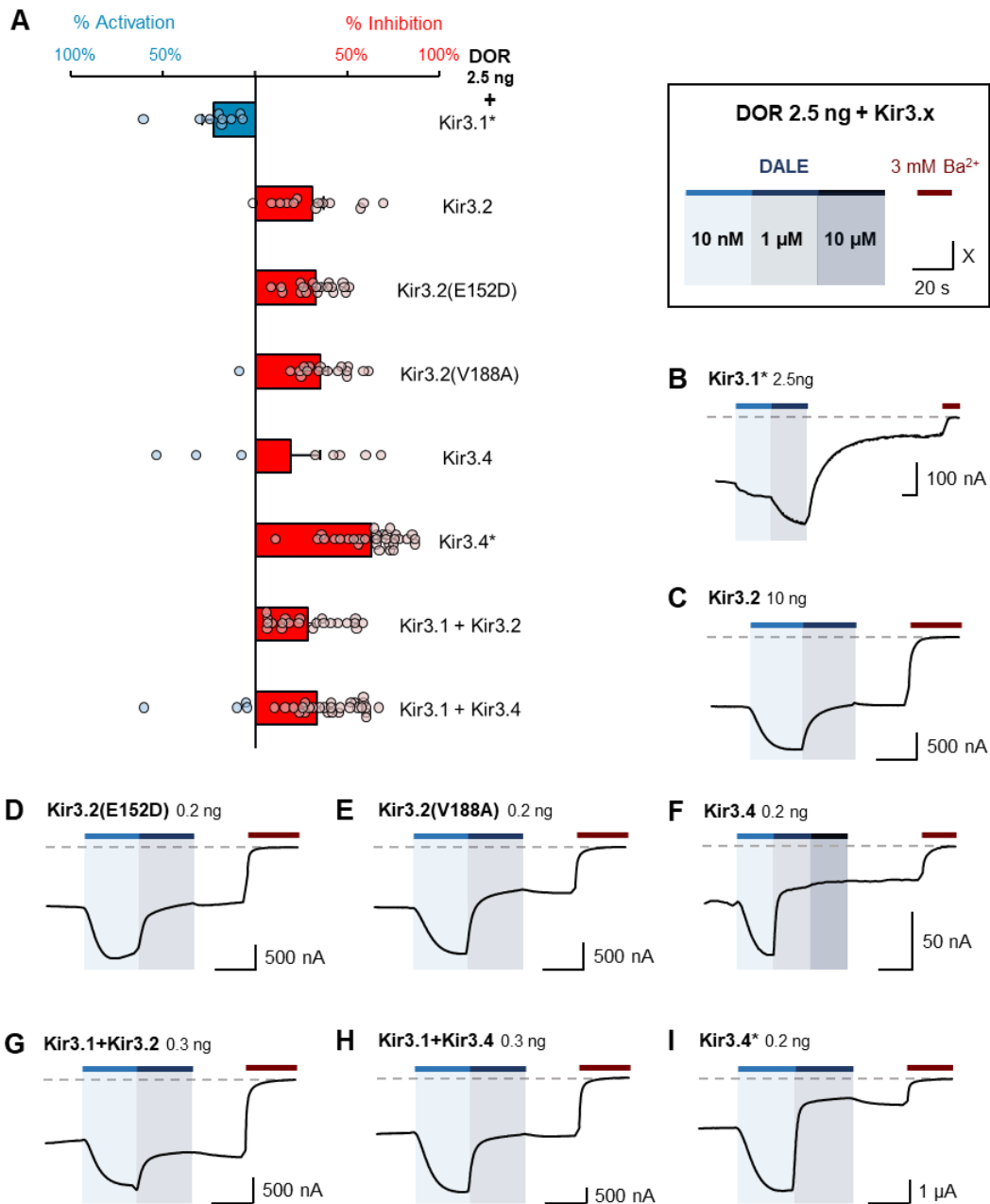


Figure a.20. DOR is not able to inhibit all Kir3 channels.

(A) Summary of responses in 1 μM DALE for oocytes injected with 2.5 ng DOR RNA and 0.1-10 ng RNA of the specified Kir3 channels. For conditions where two Kir3 channels were expressed, stoichiometry was kept at 1:1. Bars represent the average responses, while data points represent the response of individual oocytes. % Inhibition or activation is calculated as the % decrease or increase in current, respectively, elicited by 1 μM DALE, compared to the current in 10 nM DALE. The channels tested are as follows:

Kir3.1* - mutant F137S that produces active homotetrameric channels

Kir3.2 – wild-type

Kir3.2(E152D) – gain-of-function Kir3.2 mutation that impairs channel gating in the transmembrane domain

Kir3.2(V188A) – gain-of-function Kir3.2 mutation that impairs channel gating at the cytosolic domain

Kir3.4 – wild-type

Kir3.4* - mutant S143T that produces highly-active homotetrameric channels

Kir3.1 + Kir3.4 – predominant heart GIRK channel

Kir 3.1 + Kir3.2 – predominant brain GIRK channel

(B-I) Representative recordings of oocytes injected with 2.5 ng of DOR RNA and the specified amounts of the indicated Kir3 channels RNAs. Recordings show currents in hK⁺ (0 Na⁺, 91mM K⁺) while voltage is clamped at -50 mV. DALE was applied at the concentrations indicated, and 3 mM Ba²⁺ was applied at the end of the recording. All channels tested showed inhibition by DOR except for Kir3.1* (B).

Conversely, homotetrameric channels of the single-point mutant Kir3.1(F137S), designated Kir3.1*, do not show any sign of inhibition (Figure a.20.B). Despite that, when Kir3.1 wild-type is coexpressed with either Kir3.2 or Kir3.4 to form heterotetrameric channels, the inhibition by DOR remains. This information is relevant because it demonstrates that DOR can inhibit the predominant forms of native GIRK channels.

As previously discussed, Kir3.1 is remarkably different from the other Kir3 subunits. It contains unique interaction domains with G $\beta\gamma$, G α , and PIP₂ in its C-terminal, as well as unique residues that mimic constitutive Na⁺ binding (Ho *et al.*, 1999; Rosenhouse-Dantsker *et al.*, 2008; Rubinstein *et al.*, 2009; Rusinova *et al.*, 2009; Thomas *et al.*, 2006).

The stronger interactions with the cofactors and mediators of GIRK function might explain its resistance to inhibition by DOR. Not being susceptible to inhibition is consistent with the generalized view of Kir3.1 subunits as potentiators of channel activity.

For an overview of the basal and elicited currents of the different channels, see Supplementary figure a.9.

2.3.7. DOR inhibits G $\beta\gamma$ -activated GIRK currents

To understand the factors that modulate the inhibition at the level of the channel, we mobilized a series of channel mutations that affect the regulation of GIRK function by the cofactors PIP₂, Na⁺, and G $\beta\gamma$.

Figure a.21 explores the implications of PIP₂ on the inhibition of Kir3.4* by DOR. Kir3.4* mutants (S191A) and (I229L) have been described to strengthen and stabilize PIP₂ interactions, consequently reducing desensitization by PIP₂ depletion (Mao *et al.*, 2004; Zhang *et al.*, 1999). DOR seems to inhibit both mutant channels with the same efficacy as Kir3.4* (Figure a.21.D). The data suggest the inhibition by DOR is not caused by depletion of PIP₂ around the channel.

Figure a.22 focuses on the implications of Na⁺-binding and C-terminal domains of the channel on the inhibition of Kir3.4* by DOR. The Kir3.4 residue D223 is a sodium-binding residue that controls Kir3 activity. In contrast, Kir3.1 has an N residue at the equivalent position and does not respond to shifts in sodium, acting as permanently activated (Ho *et al.*, 1999). We hypothesized that sodium binding could be at the origin of the inhibition by DOR and justify why Kir3.1 fails to be inhibited. To investigate this hypothesis, we used mutant Kir3.4(D223N) that, like Kir3.1, does not respond to shifts in sodium (Rosenhouse-Dantsker *et al.*, 2008).

Figure a.22.A shows that inhibition persists when Kir3.4(D223N) is coexpressed with DOR (2.5 ng). The data suggest that sodium binding is not at the origin of the inhibition.

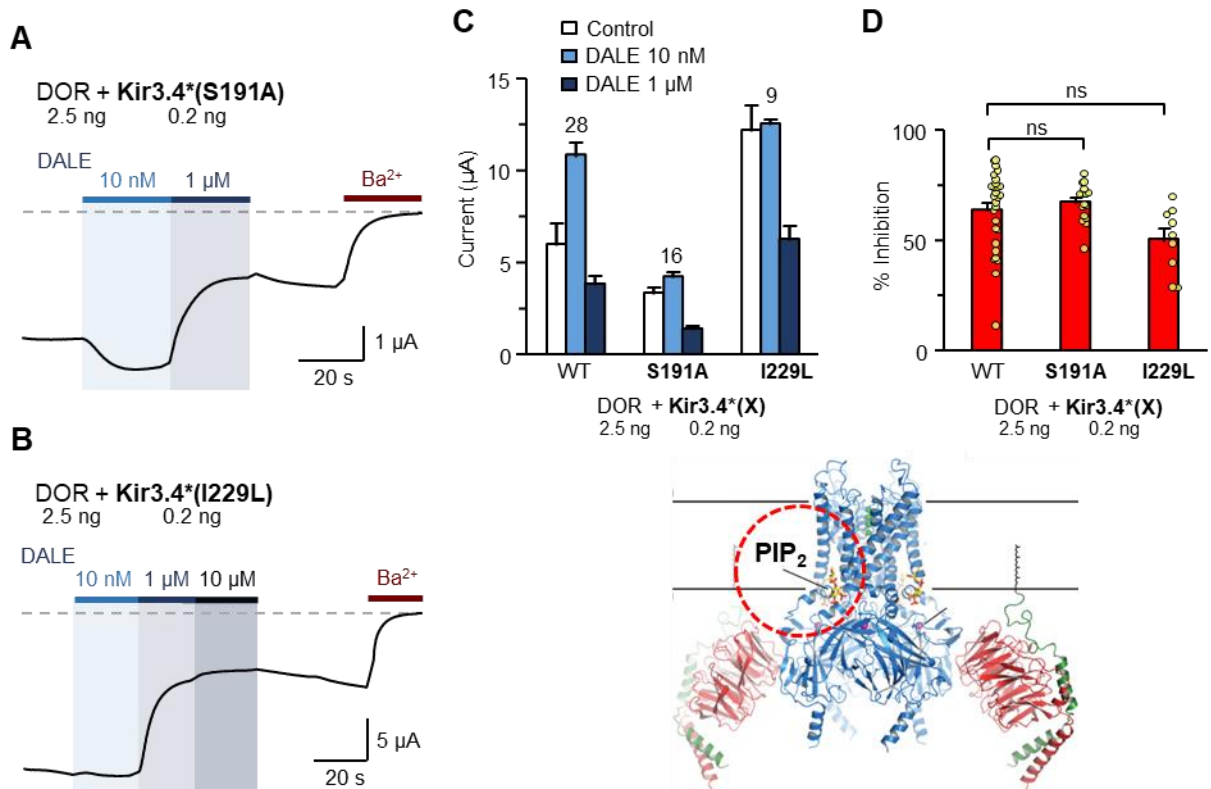


Figure a.21. Inhibition of Kir3 channels by DOR does not involve changes in interaction with PIP₂.

Kir3.4(S191A) and Kir3.4(I229L) mutants have been shown to strengthen and stabilize PIP₂ interactions and decrease desensitization by PIP₂ depletion or PKC phosphorylation.

(A-B) Representative recordings of oocytes injected with 2.5 ng of DOR RNA and 0.2 ng of RNA of the channel mutants Kir3.4*(S191A) or Kir3.4*(I229L). Recordings show currents in hK⁺ (0 Na⁺, 91mM K⁺) while voltage is clamped at -50 mV. DALE was applied at the concentrations indicated, and 3 mM Ba²⁺ was applied at the end of the recordings. Inhibition of both mutants is observable, by a decrease in current, upon application of 1 μM DALE.

(C) Average currents in low (10 nM) and high (1 μM) concentrations of DALE of oocytes injected with 2.5 ng DOR RNA and 0.2 ng RNA of the specified channel. The numbers above the bars represent the number of oocytes tested.

(D) Comparison of the % current inhibition elicited by 1 μM DALE in oocytes injected with 2.5 ng DOR RNA and 0.2 ng RNA of the specified channels. DOR inhibits both mutant channels Kir3.4*(S191A) and Kir3.4*(I229L) with the same efficacy as Kir3.4*. ns: not significant, one-way ANOVA with Dunnett's post hoc test.

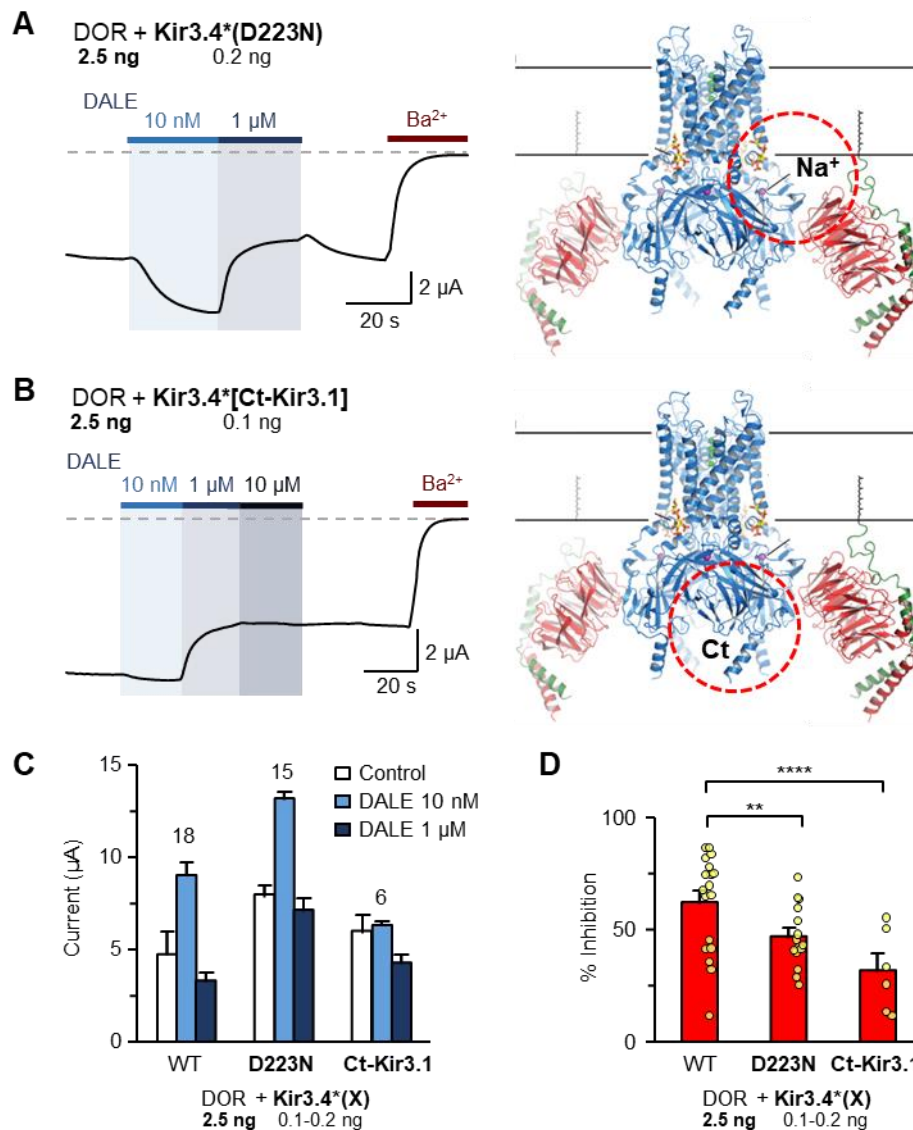


Figure a.22. Inhibition of Kir3 channels by DOR does not arise from changes in Na⁺ binding or differences in Kir3 C-terminal domains.

Upregulation of Kir3.4 by Na⁺ involves residue D223, and is abrogated in the mutant Kir3.4(D223N). Kir3.1 contains unique interaction domains with Gβγ, Gα and PIP₂ in its C-terminal, which have been shown to be transferable by replacing the C-terminal of Kir3.2 with that of Kir3.1. The mutant Kir3.4*[Ct-Kir3.1] corresponds to the substitution of Kir3.4* C-terminal with that of Kir3.1.

(A-B) Representative recordings of oocytes injected with 2.5 ng DOR RNA and the specified amounts of the channel mutants Kir3.4*(D223N) and Kir3.4*[Ct-Kir3.1]. Recordings show currents in hK⁺ (0 Na⁺, 91mM K⁺) while voltage is clamped at -50 mV. DALE was applied at the concentrations indicated, and 3 mM Ba²⁺ was applied at the end of the recordings. Inhibition of both mutants is observable as a decrease in current, upon application of 1 μM DALE.

(C) Average currents in low (10 nM) and high (1 μM) concentrations of DALE from oocytes injected with 2.5 ng DOR RNA and 0.2 ng RNA of the specified channels. The numbers above the bars represent the number of oocytes tested.

(D) Comparison of the % current inhibition elicited by 1 μM DALE in oocytes injected with 2.5 ng DOR RNA and the indicated RNA of the specified channels. Inhibition by DOR is significantly less for Kir3.4*(D223N) and for Kir3.4*[Ct-Kir3.1] than for Kir3.4*. ** P<0.01, **** P<0.0001, one-way ANOVA with Dunnett's post hoc test.

Beside the sodium binding site, there are other differences between Kir3.1 and the other subunits that could explain why DOR fails to inhibit Kir3.1 (Rubinstein *et al.*, 2009; Rusinova *et al.*, 2009; Thomas *et al.*, 2006). We focused on the C-terminal. Mutant Kir3.4*[Ct-Kir3.1] corresponds to the substitution of Kir3.4 C-terminal by that of Kir3.1. Figure a.22.B shows that DOR can inhibit Kir3.4*[Ct-Kir3.1]. Just as the sodium binding site, the C-terminal of the channel does not seem to be the primary domain involved in the inhibition. The differences in the C-terminal cannot fully justify why the Kir3.1 subunit is not inhibited by DOR.

Note that, as seen in Figure a.22.D, DOR is not able to inhibit Kir3.4*(D233N) and Kir3.4*[Ct-Kir3.1] with the same efficacy as Kir3.4* - 46±4%, 28±8%, and 63±3%, respectively. Both of these mutants potentiate channel activity by mimicking Na⁺ binding, in the case of Kir3.4*(D233N), or introducing regulatory domains that bind positive modulators, as in Kir3.4*[Ct-Kir3.1]. This potentiation could be why inhibition by DOR is not as strong.

Figure a.23 examines the implication of Gβγ in the inhibition of Kir3.4* by DOR. Mutations S176P in Kir3.4 and R201A in Kir3.2 have been described as mimicking the Gβγ-activated state of the channel, leading to high currents in the absence of G protein stimulation and almost no further increase upon G protein activation (Sadja *et al.*, 2001; Whorton & Mackinnon in 2011). Indeed, Kir3.2(R201A) was the mutant used for the structural determination of Kir3.2. Because the residue R196 of Kir3.4 aligns with the residue R201 of Kir3.2, we also tested Kir3.4*(R196A) as the equivalent mutant to Kir3.2(R201A).

As seen in Figure a.23.A & B, DOR is not able to activate Kir3.4*(S176P) and Kir3.4*(R196A) at 10 nM DALE. The lack of elicited currents is in agreement with the fact that these channels do not respond to Gβγ. Strikingly, DOR was also not able to inhibit Kir3.4*(S176P) and Kir3.4*(R196A) upon application of 1 μM DALE. That is, DOR cannot inhibit Gβγ-independent currents such as those of Kir3.4*(S176P) or Kir3.4*(R196A). The data suggest that DOR inhibition of Kir3 channels occurs downstream of the activation and requires the channel to be bound to Gβγ.

The inhibition by DOR seems to originate from the displacement of Gβγ subunits away from the Kir3.4* channel. It explains the impaired inhibition of mutants Kir3.4*(D233N) and Kir3.4*[Ct-Kir3.1] since these mutations potentiate interactions with Gβγ. Stronger interaction with Gβγ leads to a lower degree of inhibition by DOR.

Supplementary figure a.10. further supports this mechanism by demonstrating that DOR can inhibit Kir3.4* activated by other Gi/o-coupled receptors.

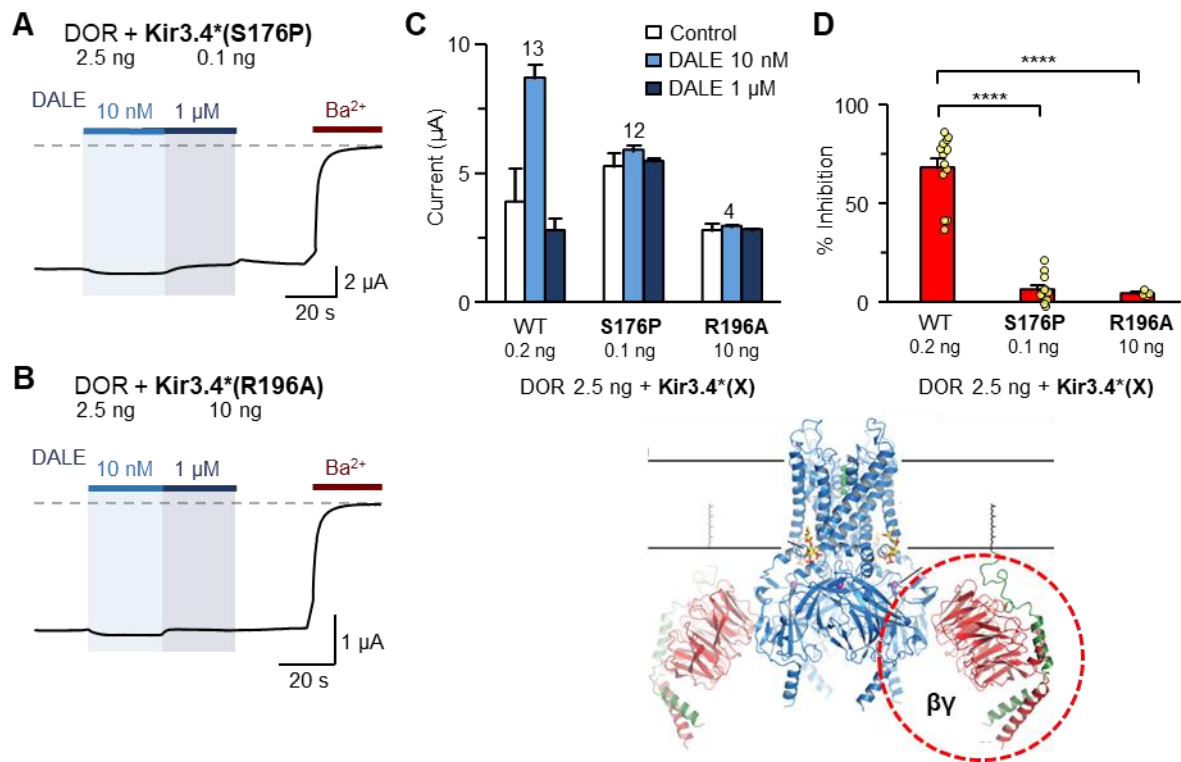


Figure a.23. Inhibition of Kir3 channels by DOR requires the channel to be activated by Gβγ.

Mutations S176P in Kir3.4 and R201A in Kir3.2 have been described as mimicking the Gβγ-activated state of the channel, leading to high currents in the absence of G-protein stimulation, and almost no further increase of current upon G-protein activation. Kir3.4*(R196A) is the equivalent mutation to Kir3.2(R201A).

(A-B) Representative recordings of oocytes injected with 2.5 ng of DOR RNA and RNA of the specified mutant channels. Recordings show currents in hK⁺ (0 Na⁺, 91mM K⁺) while voltage is clamped at -50 mV. DALE was applied at the concentrations indicated, and 3 mM Ba²⁺ was applied at the end of the recordings.

(C) Average currents in low (10 nM) and high (1 μM) concentrations of DALE of oocytes injected with 2.5 ng of DOR RNA and RNA of the specified channel. The numbers above the bars represent the number of oocytes tested.

(D) Comparison of the % current inhibition elicited by 1 μM DALE in oocytes injected with 2.5 ng DOR RNA and the specified RNA of each channel. DOR is unable to inhibit either Kir3.4*(S176P) or Kir3.4*(R196A) upon application of 1 μM DALE. **** P<0.0001, one-way ANOVA with Dunnett's post hoc test.

2.3.8 DOR mediated inhibition is affected by gallein

A similar profile of displacement of G $\beta\gamma$ from Kir3 channels has been reported for MOR and Adenosine 1 Receptor (A1R) in Raveh *et al.* (2010). As discussed in the introduction, GRK2/3 is the mediator of this action. Upon receptor activation, GRK2/3 is translocated to the membrane and sequesters G $\beta\gamma$ directly from Kir3 channels leading to a PTX-insensitive, fast, and slowly reversible channel desensitization.

Because of the similarities between the mechanism in Raveh *et al.* (2010) and our observations, we set out to investigate the role of GRK2/3 in the DOR-mediated inhibition.

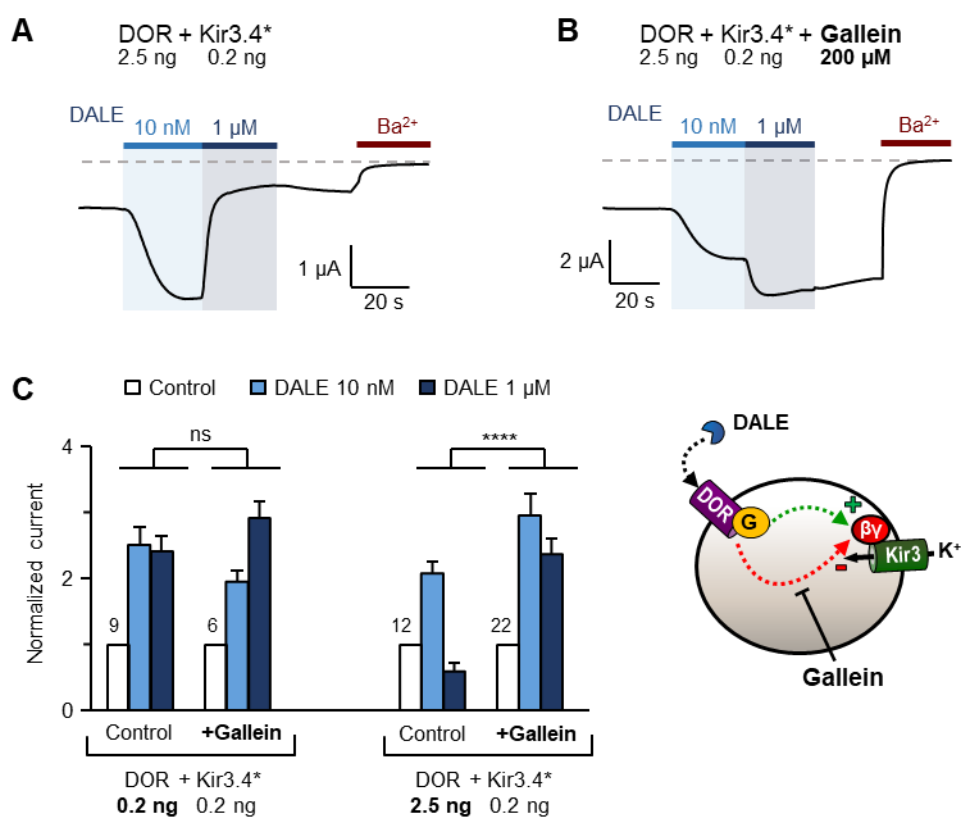


Figure a.24. Inhibition of Kir3.4* channels by DOR is hampered by gallein.

Gallein is a compound binding with high affinity to the protein-protein interaction “hot spot” of G $\beta\gamma$ subunits. It has been shown to hinder GRK2-induced desensitization (Casey *et al.*, 2010). It was proposed that gallein interferes with the sequestration of G $\beta\gamma$ bound to Kir3 by GRK2.

(A – B) Representative recordings of oocytes injected with 0.2 ng Kir3.4* RNA and 2.5 ng DOR RNA, without (A) or with (B) gallein incubation for 60 minutes (200 μ M). Recordings show currents in hK⁺ (0 Na⁺, 91mM K⁺) while voltage is clamped at -50 mV. DALE was applied at the concentrations indicated, and 3 mM Ba²⁺ was applied at the end of the recordings.

(C) Average normalized currents of oocytes tested in the same conditions as in (A - Control) and (B) with 0.2 or 2.5 ng DOR RNA. The numbers above the bars represent the number of oocytes tested. In oocytes injected with 2.5 ng DOR RNA, inhibition upon application of 1 μ M DALE was severely decreased when oocytes were incubated with gallein (from 72% in control oocytes to 15% in gallein-incubated oocytes). ns: not significant, **** P<0.0001, 2-way ANOVA with Tukey's post hoc tests.

GRK2/3-mediated desensitization is prevented by gallein (Casey *et al.*, 2010; Turecek *et al.*, 2014). This compound binds with high affinity to the protein-protein interaction domain of G β γ subunits, but does not interfere with Kir3-G β γ binding (Lehmann *et al.*, 2008). As a first experiment, we assessed the effects of gallein on Kir3.4* inhibition by DOR.

Figure a.24 shows that when oocytes were incubated with gallein, inhibition of Kir3.4* currents upon application of 1 μ M DALE was significantly decreased (from 72% in control oocytes to 15% in gallein-treated oocytes).

The data does not necessarily implicate GRK2/3, but it supports the hypothesis that DOR inhibition is a similar mechanism involving the protein-protein interaction domain of G β γ subunits.

2.3.9 GRK2 and GRK3 coexpression does not affect inhibition by DOR

Despite the similarities between the GRK2/3 mechanism and our observations, there is an important aspect that does not fit. Raveh *et al.* (2010) described the desensitization in MOR receptors. If indeed the mechanism in question is the same, it remains to be understood why we consistently observed no inhibition of Kir3.4* currents by MOR.

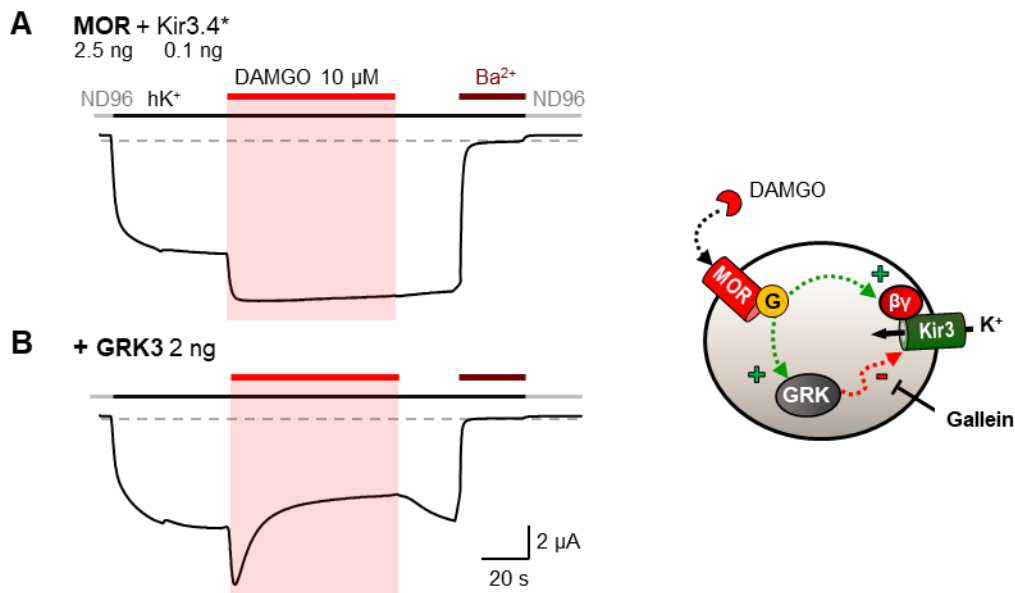


Figure a.25. MOR can inhibit Kir3.4* currents when coexpressed with GRK3.

Representative recordings (N=8) of oocytes injected with 0.1 ng Kir3.4* RNA and 2.5 ng MOR RNA, without (A) or with (B) the coexpression of GRK3 (2 ng RNA). Recordings start in ND96 bath solution (91 mM Na⁺, 2 mM K⁺) and proceed in hK⁺ (0 Na⁺, 91 mM K⁺). Voltage is clamped at -50 mV. DAMGO (10 μ M) was applied where indicated, and 3 mM Ba²⁺ was applied at the end of the recordings. DAMGO elicits an inhibition of Kir3.4* through MOR when coexpressed with GRK3.

In Figure a.25 we demonstrate that MOR can mediate inhibition of Kir3.4* upon application of 10 μ M DAMGO only when coexpressed with, in this case, GRK3. In Supplementary figure a.11 we show the same applies to the A1R adenosine receptor. This is in full agreement with Raveh *et al.* (2010) description of the non-enzymatic effects of GRK2/3 on MOR activation. In the conditions tested here, further than desensitizing, MOR effectively inhibits Kir3.4* currents to a level below the initial basal current.

Already these experiments imply a difference in mechanism since there is no requirement for GRK2/3 coexpression in the case of DOR-mediated inhibition.

To understand the implications of GRK2 and GRK3 on DOR-mediated inhibition, we coexpressed them with DOR and Kir3.4*.

Coexpressing GRK2 significantly decreased the basal currents (≈ 1.2 vs. ≈ 4.2 μ A) in oocytes expressing 2.5 ng of DOR RNA (Figure a.26.B). The decrease in basal currents is not seen with low expression of DOR (0.2 ng of RNA). This seems to suggest that the GRK2-induced decrease in basal currents with elevated DOR is not due to a decrease in channel expression or a generalized sequestration of G $\beta\gamma$ subunits. In that case the decrease should be equally evident in low DOR expression. GRK2 seems to be inhibiting Kir3 basal currents in a manner independent of DOR activation but dependent on GRK2-DOR interaction.

Despite the decrease in basal currents, coexpression of GRK2 did not affect the % inhibition (Figure a.26.C) or the $T_{1/2}$ of inhibition (Figure a.26 D) upon application of 1 μ M DALE. GRK2 overexpression, if involved in DOR-mediated inhibition, was expected to change its kinetics, as for MOR in Raveh *et al.* (2010). GRK2 did not accelerate or increase the maximum inhibitory effect, suggesting that it is not the major player in the inhibition mediated by DOR. Furthermore, the overexpression of GRK2 did not compete against the effects of gallein, which could still block the inhibition fully.

Similar to GRK2, coexpression of GRK3 decreased significantly the basal currents (≈ 0.3 vs. ≈ 4.6 μ A) in oocytes expressing 2.5 ng of DOR RNA (Figure a.27.B), it did not affect the % inhibition (Figure a.27 D), and it did not change the $T_{1/2}$ of inhibition (Figure a.27 E). The overexpression of GRK3 did not affect the surface expression/retention of DOR either (Figure a.27.C), and thus, it is not the reason for the smaller basal currents. Just as for GRK2, the reasons for this basal current decrease are unclear.

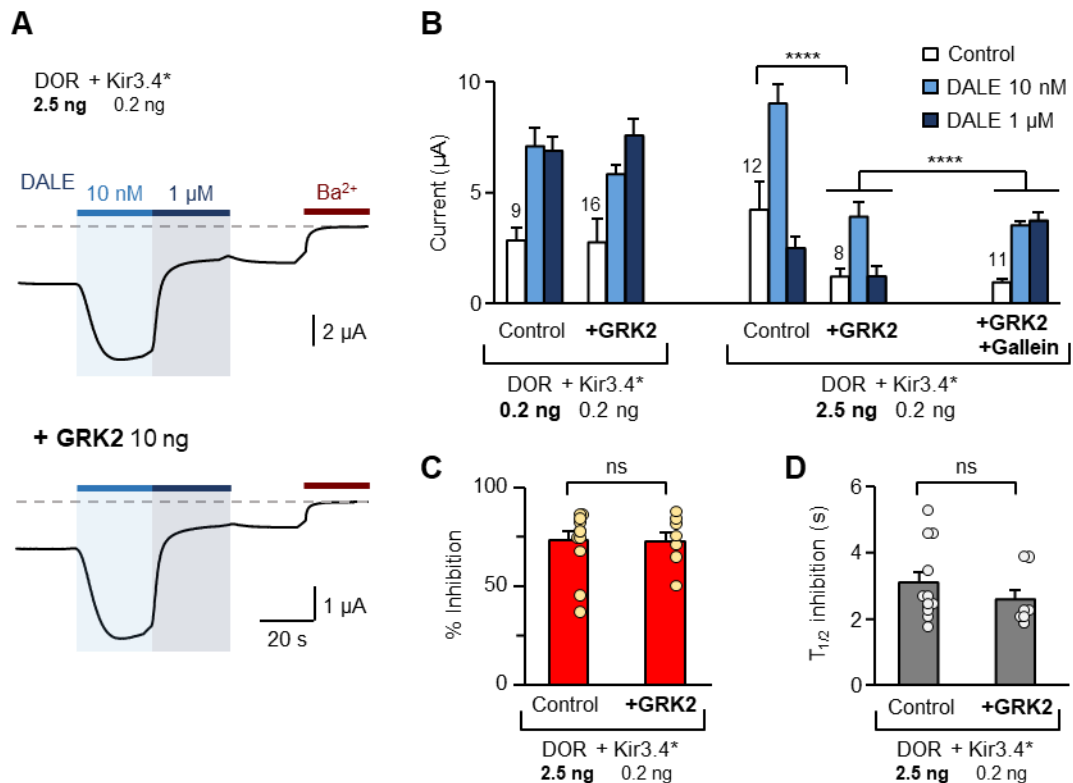


Figure a.26. Coexpressing GRK2 with Kir3.4* and DOR has no impact on the maximal effect or kinetics of the inhibition.

(A) Representative recording of an oocyte injected with 0.2 ng Kir3.4* RNA, 2.5 ng DOR RNA, and 10 ng GRK2 RNA. Recording shows current in hK⁺ (0 Na⁺, 91mM K⁺) while voltage is clamped at -50 mV. DALE was applied at the concentrations indicated, and 3 mM Ba²⁺ was applied at the end of the recording. Inhibition is evident as a decrease in current upon the application of 1 μM DALE.

(B) Average currents in 10 nM and 1 μM DALE of oocytes injected with RNA for Kir3.4*, DOR, and with or without GRK2 in the specified amounts. The numbers above the bars represent the number of oocytes tested. Note the statistically-different basal currents of oocytes injected with 2.5 ng DOR, with and without GRK2 coexpression. The right-most group shows the average currents of oocytes injected with 0.2 ng Kir3.4* RNA, 2.5 ng DOR RNA, 10 ng GRK2 and subjected to 200 μM Gallein for 60 minutes. **** P<0.0001, 2-way ANOVA with Tukey's post hoc tests.

(C) Comparison of the % current inhibition elicited by 1 μM DALE in control oocytes (2.5 ng DOR + 0.2 ng Kir3.4*) vs. oocytes coexpressing 10 ng GRK2 RNA. ns: not significant, two-tailed Student's t-test.

(D) Average half-time values of the inhibition by 1 μM DALE of control oocytes (2.5 ng DOR + 0.2 ng Kir3.4*) and oocytes coexpressing 10 ng GRK2 RNA. ns: not significant, two-tailed Student's t-test. Overexpressing GRK2 had a considerable effect on the basal currents in oocytes expressing 2.5 ng DOR RNA (B). However, it did not affect the % inhibition (C) or the T_{1/2} of inhibition (D) upon application of 1 μM DALE.

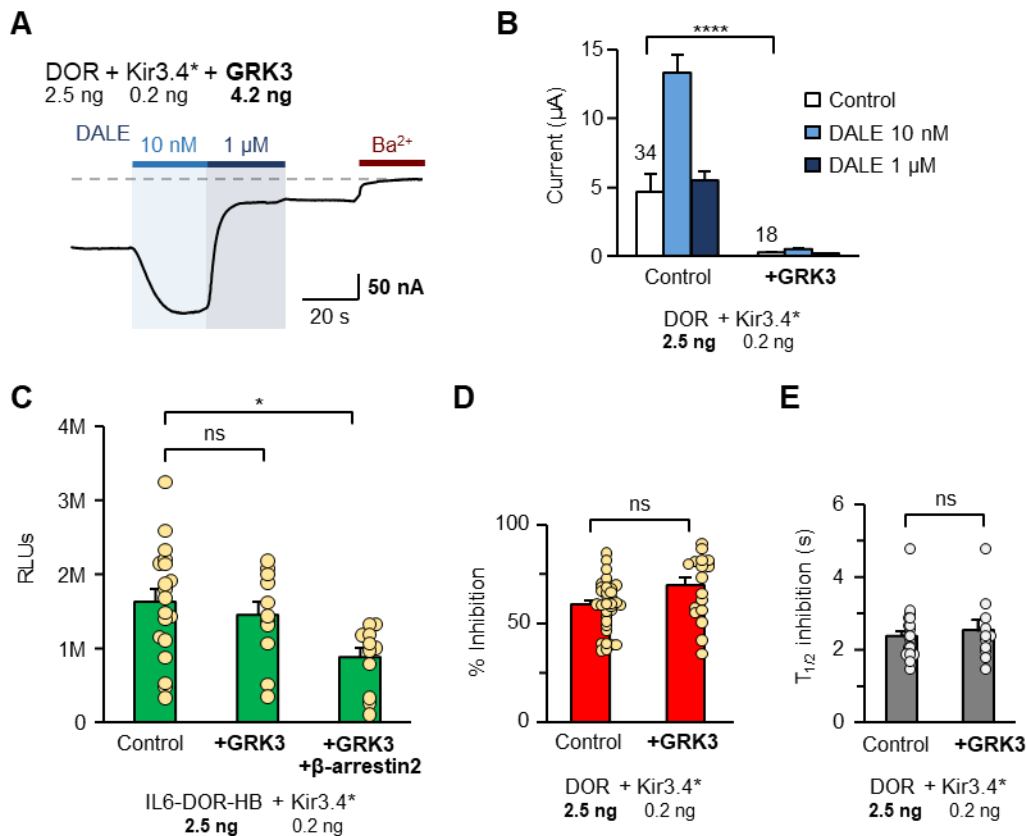


Figure a.27. Coexpressing GRK3 with Kir3.4* and DOR has no impact on the maximal effect or kinetics of the inhibition.

(A) Representative recording of an oocyte injected with 0.2 ng Kir3.4* RNA, 2.5 ng DOR RNA, and 4.2 ng GRK3 RNA. Recording shows currents in hK⁺ (0 Na⁺, 91 mM K⁺) while voltage is clamped at -50 mV. DALE was applied at the concentrations indicated, and 3 mM Ba²⁺ was applied at the end of the recording. Inhibition is evident as a decrease in current upon application of 1 μM DALE.

(B) Average currents in 10 nM and 1 μM DALE of oocytes injected with RNA for Kir3.4* (0.2 ng), DOR (2.5 ng) and, with or without GRK3 (4.2 ng). The numbers above the bars represent the number of oocytes tested. Note the smaller basal currents of oocytes coexpressing GRK3. **** P < 0.0001, 2-way ANOVA with Tukey's post hoc tests.

(C) Mean luminescence recorded in oocytes expressing 0.2 ng of untagged-Kir3.4* RNA, 2.5 ng of IL6-DOR-HB, without or with 4.2 ng of GRK3 RNA and 2.7 ng of β-arrestin2 RNA. Each point represents a single oocyte. IL6-DOR-HB corresponds to the HiBiT-tagged DOR with an added secretion signal sequence.

ns: not significant, * P < 0.05, one-way ANOVA with Dunnett's post hoc test.

(D) Comparison of the % current inhibition elicited by 1 μM DALE in control oocytes (2.5 ng DOR + 0.2 ng Kir3.4*) vs. oocytes coexpressing 4.2 ng GRK3 RNA. ns: not significant, two-tailed Student's t-test.

(E) Average half-time values of the inhibition by 1 μM DALE of control oocytes (2.5 ng DOR + 0.2 ng Kir3.4*) and oocytes coexpressing 4.2 ng GRK3 RNA. ns: not significant, two-tailed Student's t-test.

Taken together, the data demonstrate that MOR and DOR can inhibit Kir3 currents using seemingly identical mechanisms, but they might rely on different mediators to dislodge Gβγ from the channel.

2.4 Discussion

2.4.1 Description of an unreported DOR-mediated inhibition of GIRK channels

In this project, we set out to study the regulation of GIRK channels by DOR. By coexpressing the two proteins in *Xenopus* oocytes we observed a non-canonical decrease of Kir3.4* currents at μM concentrations of DOR agonists DALE and SNC80, whereas the expected increase at nM concentrations was preserved. The two mechanisms exhibited different apparent affinities for the agonist. For DALE, activation $K_{1/2}$ was ≈ 3 nM while inhibition $K_{1/2}$ was ≈ 40 nM. While some opioid ligands have been proposed to inhibit GIRK channels by binding them directly (Shirasaki *et al.*, 2004), that was not the case here. Expression of both the receptor and the channel is necessary for the ligand to induce a decrease in currents (Supplementary figure a.1).

The extent of the decrease in current was highly dependent on receptor expression levels. Increasing the amount of receptor shifts the response from a perceived activation (net increase in current) to an inhibition (net decrease in current). In contrast, channel expression levels have little effect on the overall response.

At expression levels imposed by the injection of 2.5 ng of DOR RNA, the decrease in current has a fast onset and a $T_{1/2}$ of 2.5 seconds. In the same conditions, μM concentrations of agonist consistently decreased the currents to sub-basal levels. For that reason, we address it as inhibition rather than desensitization. Although not explored in detail, inhibition was slowly reversible with, in most cases, little apparent decay after 2 minutes.

DOR, Kir3 and PTX coexpression allowed to resolve two independent signaling mechanisms triggered by agonist binding, the Gi/o-dependent activation and the PTX-insensitive inhibition. The PTX experiments also disclose that the inhibitory mechanism can occur even at low levels of receptor expression. The smaller degree of coupling with the inhibitory pathway, dictated by the low expression of the receptor, reads as a net activation. By blocking the overpowering activation, PTX was able to reveal the inhibition in low receptor expression.

The aspects of the receptor that mediate the inhibition are not completely clear. We were able to exclude the requirement of G protein binding by the observations with the DOR=T4L protein. The obstruction of the ICL3 blocks G protein binding and consequently channel activation, but not inhibition.

We were likewise able to exclude the requirement for the last 32 residues of the C-terminal by the persistence of inhibitory capability of the truncated receptor DOR[Δ C32].

The ICL3 and C32-terminal domains might not be required on their own but they modulate the inhibitory signaling. Blocking the ICL3 decreased inhibitory capability without affecting receptor expression. ICL3 seems to have a positive modulatory role. Conversely, deleting the C32-terminal enabled a net inhibitory response at much lower surface expression levels, suggesting a negative modulatory role.

We attempted to exploit the fact that DOR and MOR share high sequence similarity to explore why inhibition of Kir3.4* can be mediated by DOR but not MOR (Supplementary figure a.7 & 8). A series of chimeric proteins between the two receptors probed the molecular determinants of the inhibition. Exchanging the intracellular regions of MOR by those of DOR enabled the transfer of the inhibitory capability. It is not surprising that this could be achieved. Similar chimeric designs have been shown, for example, to translocate G protein specificity between receptors (e.g., in Siuda *et al.*, 2015).

Interestingly, MOR and DOR intracellular regions differ only on three residues of the ICL3 and on the C-terminal. Exchanging the ICL3 between DOR and MOR was insufficient to eliminate DOR inhibition or promote MOR inhibition, in support of the results with DOR=T4L. The C-terminal is the remaining molecular domain that differs in both proteins and could justify the differences between the responses. By integrating the results of DOR[Δ C32] we could further restrict the differences to a set of 9 residues at the C-terminal. However, the translocation of this short sequence into MOR was not sufficient to impart inhibitory capability (MOR/Ct-DOR[Δ C32]).

Since the results were inconsistent, it limits our interpretation of which intracellular domains of the receptor originate inhibition. It seems that rather than being restricted to a small delimited section of the protein, it involves a complex interaction with ICL3 and the C-terminal, i.e., it depends on the global structure of the receptor rather than individual sequence elements.

The mechanistic aspects of the inhibition on the side of the channel are better understood. DOR cannot inhibit channel currents independent of G $\beta\gamma$ binding, which implies inhibition results from displacing G $\beta\gamma$ directly from the channel. In support of this conclusion, channel mutations that impart higher affinity to G $\beta\gamma$ were less susceptible to inhibition (Kir3.4(D223N) and Kir3.4*[Ct-Kir3.1]). Exactly what leads to the displacement of G $\beta\gamma$ is not known. The fast onset and slow reversibility of inhibition could imply either a fast modification of the channel that uncouples G $\beta\gamma$ or a long-lived G $\beta\gamma$ sequestration by the receptor or a partner protein.

When testing the different Kir3 subunits, DOR could inhibit all, except Kir3.1. Mutants Kir3.4(D223N) and Kir3.4*[Ct-Kir3.1] addressed the idiosyncrasies of Kir3.1 related to sodium binding and extra-modulatory regions on the C-terminal. Both mutations decrease inhibition when transferred to Kir3.4, albeit not completely. It argues that neither domain can, by itself, justify the difference in response. However, we did not test if both modulatory domains together could account for the lack of inhibition of Kir3.1. More importantly, DOR can inhibit Kir3.1/3.2 and Kir3.1/3.4 channels, the predominant channel tetrameric combinations found *in vivo*.

Taken together, the data shows a fast, slowly reversible, PTX-insensitive inhibition of Kir3 channels by DOR upon μM agonist exposure, that is promoted by high receptor expression, mediated by the intracellular regions of the receptor and results from the displacement of channel-bound $\text{G}\beta\gamma$.

An obvious limitation of using heterologous expression systems is that they involve some degree of overexpression. It is not trivial to assess how the increase in protein densities might impact their function. By assuming a collision coupling model, high expression might increase the tendency of proteins to spontaneously associate. While it could lead to unspecific coupling, it could also represent physiologically relevant scenarios, since high local concentrations of signaling members are sometimes imposed by scaffolding and anchoring proteins.

Mass activity of overexpressing DOR, with the possibility of exhausting signalling molecules, is probably not sufficient to explain our observations. High expression of different receptors, including the closest member of the opioid family - MOR, does not elicit the same response, arguing that the inhibitory mechanism of DOR depends on some intrinsic characteristic. It is more likely that our set-up, while not necessarily being a direct representation of a physiological condition, allows to capture an inhibitory mechanism normally occluded by net activating currents.

Our observations demonstrate that DOR has a specific mechanism to directly quench the signaling of one of its main effectors - G protein-gated channels. By reverting the exact same signaling that it triggers, it delivers complete control of the onset and offset of the signaling, seemingly, in an agonist concentration-dependent manner. The fact that it is potentiated by DOR expression, integrates with the general view that DOR function is tightly connected with its expression and trafficking.

2.4.2 How do these observations integrate with described mechanisms for Kir3 and DOR regulation?

Non-canonical coupling to non-Gi/o proteins

DOR and GIRK have been shown to couple with PTX-insensitive G proteins in overexpressing systems. In parallel, Gq-mediated decrease of GIRK currents can have acute onsets and slow reversibility (Kobrinisky *et al.*, 2000), similar to what we observed. We addressed the implications of non-canonical G protein-coupling and showed through DOR=T4L, that G-protein coupling is not a requisite for inhibition, excluding the role of this phenomenon.

Homodimerization of DOR

Physiological implications of DOR homodimerization have not been demonstrated, but heterodimers of MOR and DOR, for instance, present distinct pharmacological and signaling profiles (George *et al.*, 2000). One could question if that is also the case for DOR homodimers.

Assuming a collision coupling model, overexpressing DOR might increase the likelihood of finding the receptor in a dimeric or oligomeric state. A shift in the signaling properties of multimers could potentially mediate the inhibition. The suggestion that the density of DOR can affect their functionality is not out of context. As discussed previously, DOR surface density seems to be highly controlled by trafficking mechanisms that can rapidly address receptors to the membrane in response to a trigger.

We did not directly assess the hypothesis that DOR dimers might mediate the inhibition. There is little information on how and if these entities form. However, the last 15 residues of the C-terminal of DOR have been implicated in the formation of receptor dimers in immunoprecipitates (Cvejic & Devi, 1997). If the formation of dimers requires the last 15 residues of the receptor, the fact that DOR[ΔC32] can still inhibit should exclude this hypothesis.

Intracellular signaling by DOR

Intracellular signaling of DOR can activate a specific subset of signaling pathways to produce physiologically relevant responses (Jimenez-Vargas *et al.*, 2020).

Could it be that intracellular accumulation and signaling, rather than surface expression, initiate inhibition? Although we did not address this question directly, we collected evidence suggesting it might not be the case.

In this context, DOR[Δ C32]-HB that can inhibit Kir3.4* at low surface expression levels would be expected to have a high intracellular accumulation that justifies the inhibitory capability. Similarly, an increase in DOR RNA amount injected should be accompanied by an increase in intracellular protein leading to more potent inhibition.

This increase in intracellular accumulation is seen for DOR-HB in Supplementary figure a.6 where we measure luminescence in lysed oocytes injected with increasing amounts of RNA. However, DOR[Δ C32]-HB total protein expression was as low as surface expression. Thus, it does not support the hypothesis that a high intracellular amount of DOR is necessary for inhibiting Kir3.

Receptor phosphorylation, β -arrestin recruitment and internalization

DOR phosphorylation, followed by β -arrestin recruitment and internalization, is a process by which receptor activation can lead to downregulation of the channel in a time scale of several minutes to hours. In particular, DOR has been shown to co-internalize with Kir3 channels (Nagi *et al.*, 2015). We collected preliminary data using IL6-DOR-HB to follow surface receptor internalization after applying DALE (Supplementary figure a.12). However, we found no noticeable decrease in surface receptor luminescence compared to the condition where no agonist was applied. Fast internalization does not explain the inhibition of Kir3 by DOR, and it does not fit with the characteristics mentioned in the previous section.

Furthermore, both phosphorylation and β -arrestin recruitment have also been implicated in independent mechanisms of desensitization of DOR signaling.

We excluded the role for receptor phosphorylation at the last 32 residues by observing inhibition by DOR[Δ C32]. This domain includes the recognized sites for GRK2/3 and PKC phosphorylation. We further demonstrated that the kinase activity of GRK2/3 or Src kinases is not necessary for the inhibition of Kir3 by DOR (Supplementary figures a.3-5).

Indeed, receptor phosphorylation with a consequent decoupling of G protein signaling does not fit the characteristics we found for the inhibition, such as:

- (1) G protein coupling is not necessary for the inhibition to be triggered, seen by DOR=T4L;
 - (2) DOR can inhibit Kir3 channels activated by other receptors (Supplementary figure a.10).
- Rather than a decrease in DOR G protein signaling induced by phosphorylation of the receptor, the inhibition is an independent mechanism triggered in parallel acting downstream the receptor.

The data suggested a modulatory role of the C-terminal and the ICL3 in the DOR-mediated inhibition. We hypothesized that it potentially contributes to the recognition or binding affinity of the entity that mediates the inhibition. Notably, the ICL3 and the C-terminal of DOR comprise recognized residues for β -arrestins interactions. Truncation of the C-terminal affects β -arrestin recruitment in a similar way that it affected DOR-mediated inhibition. It raised the question of whether β -arrestins are the agents responsible for DOR inhibition. We assessed the impact of overexpressing β -arrestin2 with both DOR and Kir3 (Supplementary figure a.13). However, we saw no apparent difference in the inhibitory capability of DOR.

It is also interesting to note that the coexpression of exogenous GRKs and β -arrestins has been shown to be necessary to reconstitute these pathways in *Xenopus* oocytes (Kovoor *et al.*, 1997; Lowe *et al.*, 2002), pointing to a low or no expression of these proteins in the egg cell. Curiously, Kovoor *et al.* (1997) demonstrated that GRK3 and β -arrestin2 coexpression with DOR and Kir3 exhibited desensitization of the channel current upon agonist application ($T_{1/2} \approx 5$ min) in *Xenopus* oocytes. The desensitization by DOR was dramatically faster than desensitization by MOR ($T_{1/2} \approx 45$ min). They also demonstrated that the C-terminal was critical for the observed DOR desensitization. Their observations are very different from ours. The difference probably stems from the fact that they injected the oocytes with 0.1 ng of DOR RNA, which we show has a predominantly activating response. Taken together, it does not seem like the classical desensitization pathway of DOR is involved in the inhibition we described, contrary to the observations in Kovoor *et al.* (1997).

Fast channel desensitization

Two phases can be resolved for Kir3 current desensitization: a slower phase that takes several minutes and is mediated by the pathway described above and a fast phase with a $T_{1/2}$ of seconds.

The fast Kir3 decrease in currents (as in cortical neurons shown by Sickmann and Alzheimer 2003) cannot be explained by the classical pathways of GPCR desensitization. The mechanisms that have emerged in the literature to justify the immediate decrease in currents depend on the direct regulation at the level of the effectors, i.e., Kir3 channels.

Fast desensitization of currents in the seconds time scale has not been reported in the context of the interaction between DOR and Kir3. However, different mechanisms have been shown involving other GPCRs: GABA_B through RGS proteins; GABA_B through KCTDs; A1R and MOR through GRK2/3.

RGS4

Several lines of evidence show that RGS4 can modulate opioid receptor desensitization in heterologous systems (Chuang *et al.*, 1998). Notably, a few characteristics of their interaction were similar to what we were observing:

- (1) RGS4 preferentially modulates DOR signaling, but not MOR, in neuroblastoma cells (Wang *et al.*, 2009);
- (2) RGS4 desensitization correlated strongly with agonist concentration (Leaney *et al.*, 2004);
- (3) RGS4 interaction with DOR seems to arise at intracellular Helix 8, a domain that was kept intact when we tested DOR[Δ C32] (Karoussiotis *et al.*, 2020).

We thus questioned if RGS4 might mediate the Kir3 inhibition shown by DOR in *Xenopus* oocytes.

For instance, with GABA_B receptor, RGS4 triggers acute desensitization of Kir3 channels upon a sustained application of GABA_B receptor agonist (Mutneja *et al.* 2005). The Kir3 currents decreased up to 60% in under 1 minute and did not arise from receptor internalization. However, in contrast with our observations, PTX eliminated the RGS4-mediated decline of the currents. It is perhaps not surprising since RGS4 decreases Kir3 currents by increasing the GTPase activity at G α , promoting the formation of the inactive G $\alpha\beta\gamma$ state (Chuang *et al.*, 1998; Mutneja *et al.*, 2005). Furthermore, just like GRKs or β -arrestins, overexpression of RGS proteins is required to reconstitute RGS4-mediated desensitization of Kir3 channels in *Xenopus* oocytes (Doupnik *et al.*, 1997; Saitoh *et al.*, 1997).

Nevertheless, we overexpressed RGS4 with Kir3 and DOR to assess its impact on the inhibition kinetics (Supplementary figure a.13). Interestingly, even though % inhibition was not affected, the T_{1/2} increased, implying RGS4 slowed down inhibition. This directly contrasts with its described mechanism of accelerating Kir3 current decrease.

Furthermore, in low expression conditions of DOR (0.2 ng), RGS4 coexpression increased the extent of activation upon 1 μ M DALE application. The increase in % activation observed when coexpressing RGS4 is most likely connected to the slowing down of the inhibition. It is unclear if RGS4 directly slows down inhibition and consequently increases apparent activation or the other way around, i.e., directly increases activation slowing down apparent inhibition. Regardless, the effects of RGS4 seem to impact the equilibrium between activation and inhibition of Kir3.4* by DOR. Ultimately, DOR-mediated inhibition requires active G $\beta\gamma$, thus it is not surprising that it is affected, to some extent, by the G protein cycle.

RGS4 does not seem to be the intermediary of DOR-mediated inhibition.

KCTDs

KCTD12 proteins natively associate with GABA_B receptors and, upon agonist application, bind and scavenge Gβγ subunits away from Kir3 channels decreasing its currents with an onset of a few seconds (Turecek *et al.*, 2014; Zheng *et al.*, 2019). Although similar to our observations, KCTD12 action is quickly reversible and not affected by gallein, contrasting with the DOR-mediated inhibition. Regardless, we tested the effects of overexpressing KCTD12 with DOR and Kir3 channels (Supplementary figure a.13). However, we observed no effect on the kinetics of the inhibition, further excluding this protein as the intermediary of DOR-mediated inhibition.

GRK2/3

GRK2/3-mediated desensitization of the Kir3 channels through activation of A1R or MOR is fast, PTX-insensitive, and, like KCTD12, results from the sequestration of Gβγ away from activated Kir3 channels (Raveh *et al.*, 2010). It shares further commonalities with the mechanism described in this project. For instance, it displays poor reversibility within a 10 min period, and it is prevented by gallein. However, as it was shown, to reconstitute this mechanism in *Xenopus* oocytes, we were required to coexpress GRK3 with MOR and A1R. The same does not apply to the DOR-mediated inhibition.

Interestingly, in the conditions tested here, GRK3 reduced Kir3 currents to sub-basal levels, both with A1R and MOR, putting in evidence another common aspect of these mechanisms. Raveh *et al.* (2010) did not assess the dependency on the concentration of the agonist or the expression of the receptor, and thus, in those aspects, we cannot compare the two mechanisms.

Curiously, overexpression of GRK2/3 with DOR and Kir3 did not change the kinetics of the inhibition like for MOR in Raveh *et al.* (2010). Instead, a dramatic decrease in basal currents of the channel was observed when DOR was highly expressed and without agonist application. Because the decrease in basal currents is not observed in low expression of DOR, we excluded generalized non-induced sequestration of Gβγ by GRK2/3. In support, the large decrease in basal currents was not observed when expressing MOR with GRK3. GRK2/3 seem to be inhibiting Kir3 basal currents in a manner independent of DOR activation but

dependent on GRK2/3-DOR interaction.

Our results do not enable us to understand the reason why this happens. However, Brackley *et al.* (2016) described a constitutive interaction between GRK2 and DOR, which stabilizes the receptor in an incompetent state. Indeed, we observed a reduction in the absolute amplitudes of response, both the activation and the inhibition, even if the proportion and speed of inhibition remained constant. How exactly this interaction translates into a decrease in Kir3 basal current is unclear. One could speculate that DOR, Kir3, and GRK2 form pre-assembled incompetent complexes.

It is curious that the observed effects of GRK2/3 on DOR response are also dependent on receptor expression. We might not be able to completely exclude GRK2/3 implications on the agonist-induced inhibition by DOR. If DOR constitutively interacts with *Xenopus* endogenous GRK2/3 proteins, but not MOR, that could potentially explain why MOR requires overexpressing conditions of GRKs to couple with this signaling.

A better understanding of the role of GRK2/3 would be accomplished by silencing GRK2/3 genes in *Xenopus*. However, our attempts to use siRNA in *Xenopus* oocytes failed (data not shown), and we could not establish a valid protocol.

Although we could not confidently ascertain the role of GRK2/3, or lack thereof, in the DOR-mediated inhibition of Kir3 channels, the mechanisms in question seem to be similar in most aspects tested.

2.5 Conclusion and perspectives

Our observations uncovered a novel, complex regulation of Kir3 channels by DOR, with mechanistic aspects equivalent to GRK2/3-mediated channel desensitization, with the extra modulation aspects of agonist concentration and receptor density. Since DOR and Kir3 interaction is intricately connected with pain perception, one could speculate this mechanism has physiological, neuroadaptive, or pathological implications, but that remains to be verified. It would be interesting to understand how this mechanism integrates with the lower analgesic or convulsive effects of DOR agonists.

We explored the advantages of the *Xenopus* oocyte as a model cell. However, further details of the inhibition will have to be validated in other model systems, although very few systems enable a control of protein expression levels as precise and simple as *Xenopus* oocytes. At a first stage, mammalian cells might allow us to evaluate the requirement for GRK2/3 through the silencing of these genes and confirm or exclude this mechanism. From there, many questions arise regarding the desensitization of Kir3 channels.

Slow mechanisms of desensitization in the continuous presence of an agonist can take minutes to hours and serve as a form of adaptation to long-lived stimuli. However, fast desensitization might serve to respond to acute shifts in agonist concentration rather than prolonged exposition. Fast mechanisms of reducing Kir3 current offer a more precise control to prevent excessive Kir3 channel activity.

We have illustrated throughout this manuscript how desensitization depends on a series of factors, including the receptor in question. There seems to be an increasing number of reports of specific fast desensitizing mechanisms, with different partner molecules being described for different receptors. In a typical cell environment populated by different receptors, specific desensitizing mechanisms might facilitate the integration of simultaneous signaling cascades. One asks if this might be a more pervasive mechanism by which each receptor type can precisely control the onset and decay of the signaling by acting directly on its effectors.

The elucidation of these mechanisms will improve our fundamental understanding of the signaling between GPCRs and Kir3 channels, with potential impacts on drug development and human health.

3. Project B: Shedding light on the function of viral rhodopsins

3.1 Introduction

In this section, we introduce the family of viral rhodopsins within the scope of the development of optogenetic tools.

3.1.1 The study of microbial rhodopsins and the advent of optogenetics

Rhodopsins are a superfamily of 7-transmembrane spanning proteins covalently linked to a retinal chromophore. They are essentially divided into two distantly related groups: microbial-type rhodopsins (type-1) and animal visual rhodopsins (type-2).

Microbial rhodopsins are considered the most widespread light energy transducers (Béjà *et al.*, 2000), since extensive metagenomic studies identified over 10 000 microbial rhodopsin genes from origins as different as archaea, bacteria, eukaryotes, and viruses.

Because microbial rhodopsins are linked to a retinal molecule, they can harvest light and convey a panoply of functions such as ion pumping, ion channeling, sensory and kinase activities (Ernst *et al.*, 2014). Yet, the specific biological functions of most microbial rhodopsins remain elusive.

The study of the function of microbial rhodopsins provided the background for the origin of optogenetics - where light, through the action of exogenous rhodopsins, is used to control neuronal activity with unprecedented time and spatial resolution.

More specifically, the discovery of Channelrhodopsin-2 (ChR2), found in the green algae *Chlamydomonas reinhardtii*, propelled the development of this strategy (Fenalti *et al.*, 2014; Miesenböck 2011). Nagel *et al.* (2003) used *Xenopus* oocytes to express ChR2 mRNA and measure membrane currents upon light application. They demonstrated that ChR2 was a

non-selective light-gated cationic channel. Indeed, ChR2 can permeate Na^+ , K^+ , H^+ and Ca^{2+} upon illumination. Notably, the entry of Ca^{2+} , imposed by high extracellular concentration of Ca^{2+} and hyperpolarizing voltages, deploys the *Xenopus* endogenous calcium-activated chloride channels (CaCCs), discussed in section 2.1.

Inspired by the properties of ChR2, Boyden *et al.* (2005), expressed this rhodopsin in neurons and observed that merely shining light on the cells could trigger neuronal firing with precise temporal control. Eventually, the development of ways to target the microbial rhodopsins and light to specific neuronal elements allowed the manipulation of live organisms and their behaviors (Adamantidis *et al.*, 2007; Tsai *et al.*, 2009).

Indeed, optogenetics enables the real-time control of cellular signaling, cells, or even neuronal circuits, deep within the brain, mediating behavior such as learning or motor function (Boyden *et al.*, 2005; Deisseroth *et al.*, 2006; Zhang *et al.*, 2007; Fenalti *et al.*, 2014; Miesenböck 2011). Optogenetic control of nerve cells represents one of the most important technological advancements in neuroscience. It has rapidly evolved and revolutionized the field by addressing numerous fundamental questions that were not possible before through electrical stimulations or pharmacological methods (reviewed in Tye & Deisseroth, 2012).

3.1.2 Available optogenetic tools and their applications

The standard optogenetic tools are microbial rhodopsins that depolarize or hyperpolarize the membranes upon illumination, consequently exciting or inhibiting the neurons.

Within the most used microbial rhodopsins, there are light-driven pumps and light-gated channels, mediating active or passive flow of ions, respectively. Light-gated channels have the advantage of generally eliciting larger currents than light-driven pumps - in which one photon is coupled to the translocation of a single ion. In contrast, light-driven pumps are less dependent on the electrochemical gradient of the cell than light-gated channels.

ChR2 remains to date, one of the most popular tools in optogenetics. It is a light-gated cationic channel that, upon illumination, enables the entry of cations, depolarizing and consequently activating neurons (Figure b.1). Through the years, a series of optimizations of ChR2 has emerged: faster response to light (Gunaydin *et al.*, 2010; Hight *et al.*, 2015); bistable switching of open and close states (Berndt *et al.*, 2009); different spectra of activation (Zhang *et al.*, 2008); and different permeability to distinct ions (Berndt *et al.*, 2014; Kato *et al.*, 2012; Kleinlogel, Feldbauer *et al.*, 2011; Wietek *et al.*, 2014; Zhang *et al.*, 2011).

For instance, Kleinlogel, Feldbauer *et al.* (2011) described a variant of ChR2 70-fold more efficient than the wild-type in terms of neuronal activation by light. The dramatic increase originated from an improved Ca^{2+} permeability. Raising intracellular Ca^{2+} elevates the internal surface potential, activating voltage-gated Na^+ channels that indirectly potentiate the response.

A different approach focused on redirecting ChR2 to organelles, specifically the ER. Fusing ChR2 with the fourth transmembrane helix of the ryanodine receptor enabled the retention of ChR2 at the ER. As a consequence of this retention, ChR2 was able to mediate the release of Ca^{2+} from intracellular stores upon illumination (Asano *et al.*, 2018). The implications of this tool were not fully explored.

While ChR2 is the prototypical neuronal activator, neuronal silencing has been achieved using proton pumps and chloride pumps (Han & Boyden, 2007; Zhang *et al.*, 2007; Chow *et al.*, 2010).

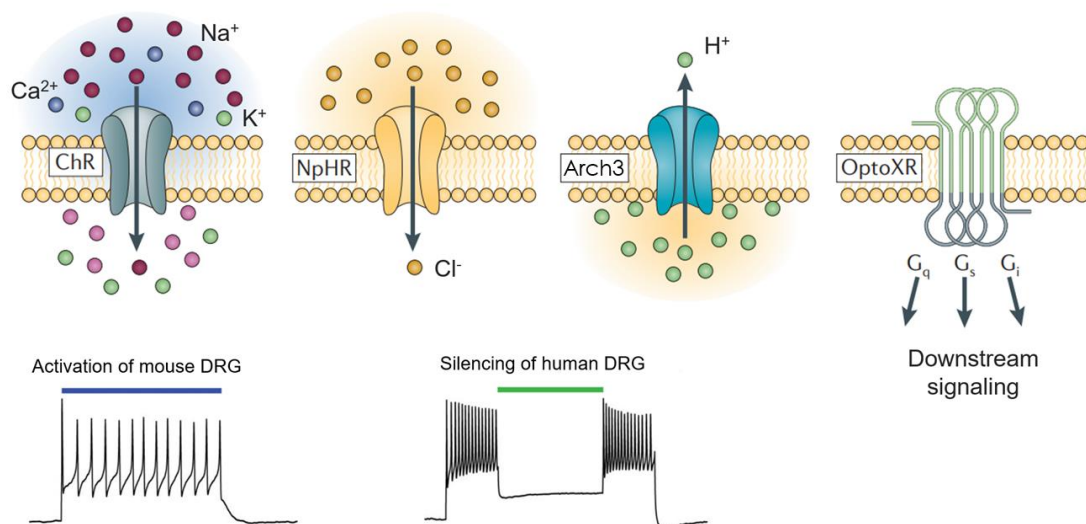


Figure b.1. Examples of optogenetic tools.

ChR - Channelrhodopsin; NpHR - *Natronomonas pharaonis* halorhodopsin; Arch3 – H^+ pump archaerhodopsin from *Halorubrum sodomense*; OptoXR – OptoXReceptor; DRG – Dorsal root ganglion. Adapted from Tye & Deisseroth, 2012 and Copitis *et al.*, 2016.

Most of the experiments silencing neurons utilized the H^+ pump archaerhodopsin (Arch3) from *Halorubrum sodomense* (Figure b.1) (Chow *et al.*, 2010). Upon application of yellow-green light, protons exit the cell, hyperpolarizing and consequently silencing the neurons.

However, because of its superior expression in neurons, *Natronomonas pharaonis* halorhodopsin (NpHR) has been exploited for neuronal inhibition *in vivo* (Figure b.1). NpHR is a Cl^- pump that allows reliable silencing of neurons under yellow light by pumping chloride

inside the cell, hyperpolarizing it (Zhang *et al.*, 2007). The increase in the functional expression of NpHR was accomplished by fusing it to (1) the N-terminal signal peptide from the β -subunit of the nicotinic acetylcholine receptor and (2) the C-terminal ER export sequence from the potassium channel Kir2.1 (Gradinaru *et al.*, 2008). These approaches are commonly used in attempts to improve the surface expression of rhodopsins.

Other microbial rhodopsins have also been exploited in optogenetics, albeit less extensively: H⁺ pump "Mac" from *Leptosphaeria maculans* (Husson *et al.*, 2012); crux-halorhodopsin Cl⁻ pump "Jaws" from *Haloarcula salinarum* (Chuong *et al.*, 2014); Cl⁻ channelrhodopsins "MerMAIDS" from metagenomic studies (Oppermann *et al.*, 2019); light-driven Na⁺ pump "KR2" from *Krokinobacter eikastus* (Gushchin *et al.*, 2015).

Optogenetics had such a profound impact on the scientific community that it inspired a series of tangents in different fields that capitalize on the spatiotemporal precision of light delivery. Nowadays, optogenetics does not focus solely on the study of neurons¹⁴, and it is not constricted to the use of microbial rhodopsins.

With the adoption of other genetically encoded light-responsive proteins, the optogenetic toolkit has expanded to include a wide collection of regulatory proteins and, consequently, cellular functions, which can now be controlled with light.

Tischer & Weiner (2014) review a set of optogenetic tools where proteins that change conformation in response to light are adopted to induce, for instance, gene expression or protein association and sequestering.

Another fascinating approach explores the similarities between different GPCRs and visual rhodopsins, which are, in fact, also GPCRs. Because of the structural similarities, replacing the intracellular loops of a visual rhodopsin with those of a specific GPCR, creates a protein that can be activated by light and selectively trigger specific intracellular pathways (Figure b.1- OptoXR) (Airan *et al.*, 2009). For instance, upon light application, a MOR/rhodopsin chimeric receptor was demonstrated to couple to the same signaling cascades as wild-type receptors, including Gi-mediated inhibition of cAMP and G $\beta\gamma$ activation of GIRK channels (Siuda *et al.*, 2015).

Optopharmacology has emerged as another strategy that utilizes light-sensitive compounds rather than proteins. Chemical tools include caged agonists and antagonists and reversibly

¹⁴ Farenzi *et al.* (2019) review the development of cardiac optogenetics.

photoswitchable ligands (reviewed in Kramer *et al.*, 2013).

As illustrated in this section, the enormous variety of optogenetic tools creates opportunities to study virtually any function of excitable cells. The impact of optogenetics for brain research is demonstrated by the identification of neuronal populations in mice involved in seemingly every behavioral aspect: sleep, hunger, thirst, maternal behavior, aggression, locomotion, learning, and memory, among others (reviewed in Deisseroth 2015).

Optogenetics also brought the promise of a new approach for the restoration of function in blindness patients. In 2021, the expectation finally culminated with the first description of partial recovery of visual function in a patient with retinitis pigmentosa. It was accomplished by intraocular injection of an adeno-associated viral vector encoding a red-shifted ChR, backed by engineered goggles (Sahel *et al.*, 2021).

Scientific progress will continue to be driven by the development of more efficient optogenetic tools that can be customized for any experimental requirement.

3.1.3 Viral rhodopsins

A unique family of rhodopsins

Microbial rhodopsins are encoded in all domains of life. Indeed, Yutin & Koonin (2012) identified microbial rhodopsins genes in the genome of the Organic Lake Phycodnavirus - a giant virus infecting marine algae. Giant viruses have genome sizes comparable to some bacteria and contain many genes involved in cellular life, although their roles are not fully understood.

Metagenomic and phylogenetic sequence analysis show that viral rhodopsins are extremely abundant in marine environments. They form a monophyletic group of proteins within the rhodopsin superfamily that further splits into two distinct branches: Viral Rhodopsins of type 1 (VR1) and Viral Rhodopsins of type 2 (VR2) (Yutin & Koonin, 2012; López *et al.*, 2017). As seen in Figure b.2, viral rhodopsins show only distant sequence similarity to microbial rhodopsins with known functions such as ChR2.

The structure and function of viral rhodopsins have been investigated only recently.

In 2019 Needham *et al.* solved the structure of VirRDTS, a member of the VR1 family, and demonstrated that it pumps protons when expressed in *E. coli*.

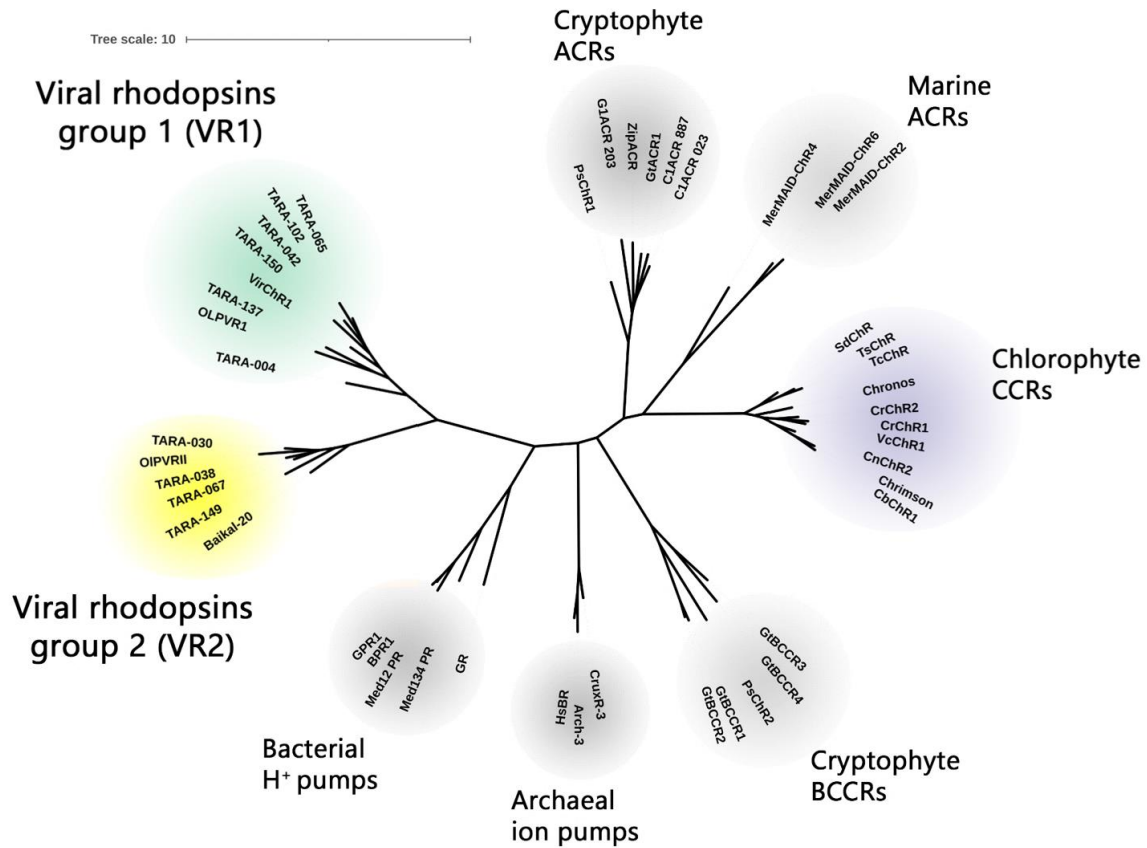


Figure b.2. Phylogenetic relationships of microbial rhodopsins.

In the same year, Bratanov *et al.* (2019) reported that OLPVR2 (or OLPVR1I), a member from the VR2 family found in the genome of the Organic Lake Phycodnavirus, also showed proton-pumping capability. Curiously, the crystal structure of OLPVR2 was unique. OLPVR2 forms pentamers in lipid membranes that look analogous to a pentameric ligand-gated ion channel (Figure b.3). Authors suggest that OLPVR2 could be a light-gated pentameric ion channel with predicted chloride selectivity. However, this was not experimentally verified.

In 2020, Zabelskii *et al.* solved the structure of OLPVR1 (Figure b.3), a member from the VR1 family found in the genome of the Organic Lake Phycodnavirus. It has low structural similarity with known rhodopsins such as ChR2, but they share some conserved residues essential for the ion channeling function, implying OLPVR1 is a channel. However, membrane expression of OLPVR1 in mammalian cells was unsuccessful, and according to fluorescence microscopy data, it failed to localize at the cell surface. Thus, the function of OLPVR1 remains to be elucidated.

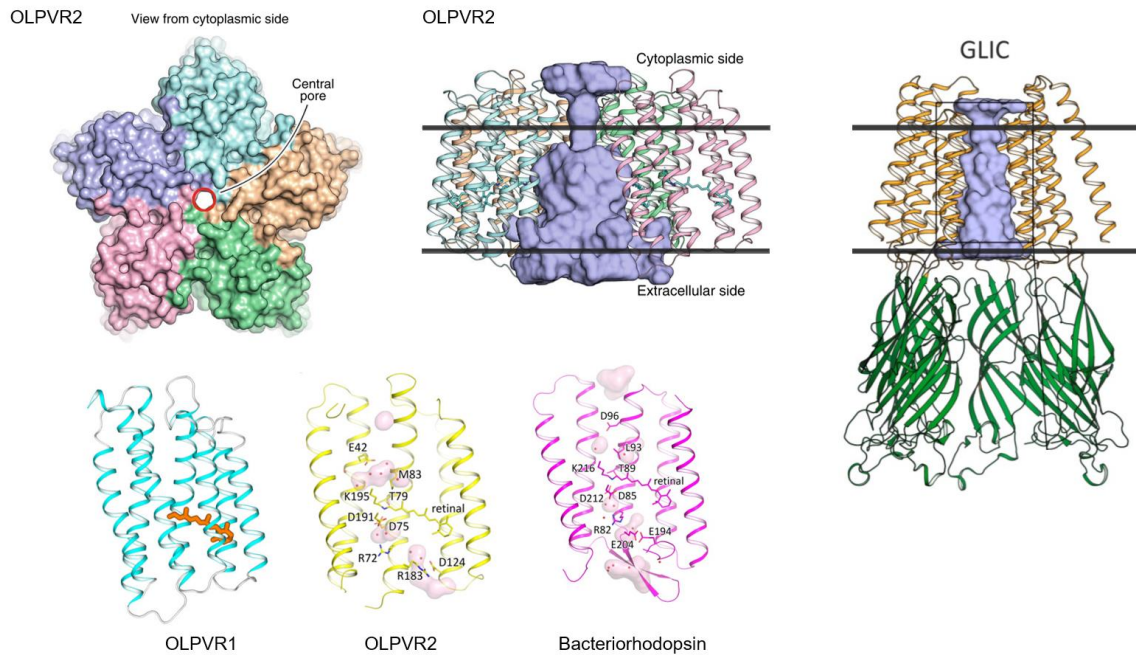


Figure b.3. Structures of OLPVR1 and OLPVR2.

GLIC - Ligand-gated ion channel. Adapted from Bratanov *et al.*, 2019 and Zabelskii *et al.*, 2020.

Nevertheless, in the same work, VirChR1 (61% sequence similarity with OLPVR1) was expressed in human neuroblastoma cells and showed Na⁺ and K⁺ currents. Contrarily to ChR2, this protein did not conduct Ca²⁺ and, in fact, was blocked by external Ca²⁺ at millimolar concentrations (50% block at ≈2 mM Ca²⁺). They further show that VirRDTS (41% sequence identity with OLPVR1), functions as a light-gated cation channel in HEK293 cells, despite being initially proposed to be an H⁺ pump by Needham *et al.* (2019).

Many aspects of the function and properties of the different viral rhodopsins are still uncertain.

An important ecological indicator and a potential novel optogenetic tool

Even if the function of viral rhodopsins remains uncertain, the extensive representation of rhodopsins in the genomes of algae-infecting viruses reflects their significance in virus-host interactions. Viruses often encode proteins that affect the functions of their host, tweaking them in a manner that favors viral reproduction. For instance, certain cyanobacteria-infecting phages encode the complete photosystems I and II (of the photosynthetic chain). These proteins support photosynthesis in infected cyanobacteria, promoting phage reproduction (Lindell *et al.*, 2005).

Thus, the hypothesis for the biological function of viral rhodopsins is that they modulate phototaxis in infected protists to promote virus reproduction. The mode of action should be analogous to the way ChR acts in *Chlamydomonas reinhardtii* (Yutin *et al.*, 2012). Photoexcitation of ChR results in cationic currents that depolarize the membrane, consequently activating voltage-gated calcium channels. The increase in local intracellular calcium is transmitted to the flagellar base leading to flagellar beating, allowing the algae to act in a phototactic manner (Schneider *et al.*, 2015).

Marine algae are the base of the marine food chain and the oxygen and carbon cycles and thus play a global role in climate and ecology. Viruses that infect marine algae regulate their population dynamics. Understanding the interactions between the virus and the host could contribute to a better understanding of their impact on global ecology and climate (Gómez-Consarnau *et al.*, 2019; Short 2012; Yau *et al.*, 2011).

Metagenomic studies have extended the catalog of microbial rhodopsin sequences. However, as mentioned before most of the microbial rhodopsins remain experimentally uncharacterized. At the same time, major efforts are being made to identify rhodopsins with new functions and properties that could be harnessed as novel optogenetic tools (López *et al.*, 2017; Berndt *et al.*, 2014), such as channels and transporters with high selectivity and conductivity for a particular ion.

Given the distant relationship between viral rhodopsins and the rest of the already characterized rhodopsins, it is expected that VRs have unique properties, which makes them an interesting target for the development of novel optogenetic tools.

3.2 Project aim

The previous section contextualizes the relevance of viral rhodopsins as a potential optogenetic tool and as an ecological factor.

The goal of this project is to characterize the function of viral rhodopsins using electrophysiology techniques.

3.3 Results

3.3.1 Photoactivation of OLPVR1 elicits a chloride current in *Xenopus* oocytes

In an attempt to study the function of viral rhodopsins, we injected *Xenopus* oocytes with mRNAs coding for different members of the viral rhodopsin family. We screened their function using TEVC and a led emitting 505 nm light. The 505-nm illumination was chosen based on the reported absorption spectra of this family of rhodopsins (Bratanov *et al.*, 2019; Zabelskii *et al.*, 2020). The different viral rhodopsins tested were: OLPVR1, VirChR1, and TARA150 of the VR1 family; OLPVR2, Baikal20, and TARA149 of the VR2 family.

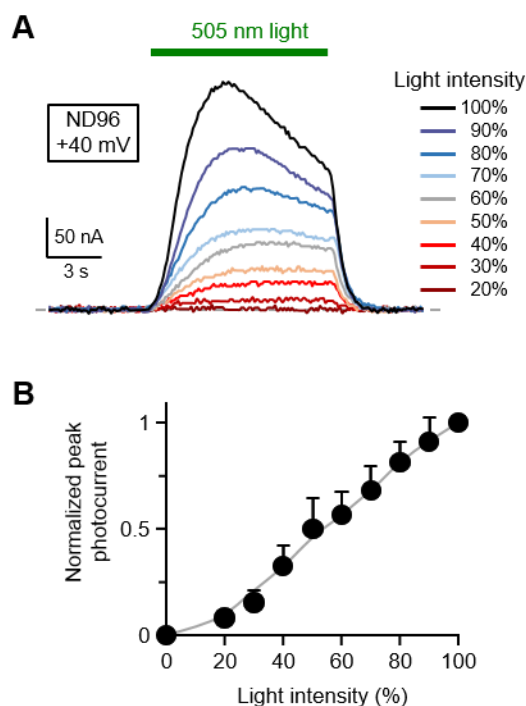


Figure b.4. Amplitude of photocurrents correlates with the intensity of applied light.

(A) Representative responses to a 10-s pulse of light of decreasing intensity. Current records were taken every 50 seconds from the same oocyte injected with 30 ng OLPVR1 RNA clamped at 40 mV. Bath solution was ND96, similar to oocyte Ringer's solution (91 mM NaCl, 2 mM KCl, 1 mM MgCl₂, 1.8 mM CaCl₂, 5 mM HEPES, pH adjusted to 7.4 with NaOH).

(B) Average peak current vs. light intensity obtained from the protocol shown in (A), applied to 4 oocytes.

After a round of optimization of expression conditions, we were able to consistently obtain photoinducible currents when injecting 7.5-30 ng of OLPVR1 RNA into *Xenopus* oocytes incubated at 19°C for 2-5 days in a 1 μ M all-trans retinal incubation solution. Figure b.4 showcases the photoinduced currents obtained for a single oocyte injected with 30 ng of OLPVR1 mRNA, where the increase in light intensity applied is proportional to the increase in current.

To identify the ions mobilized in the photoinduced currents, we subjected the same oocyte injected with OLPVR1 RNA to extracellular solutions with different ionic compositions.

Figure b.5.B shows recordings of a single oocyte in the different solutions tested, clamped between -60 and 60 mV, where we performed a cation substitution (Na^+ to K^+) and an anion substitution (100 mM Cl^- to 10 mM Cl^- +90 mM methanesulfonate-).

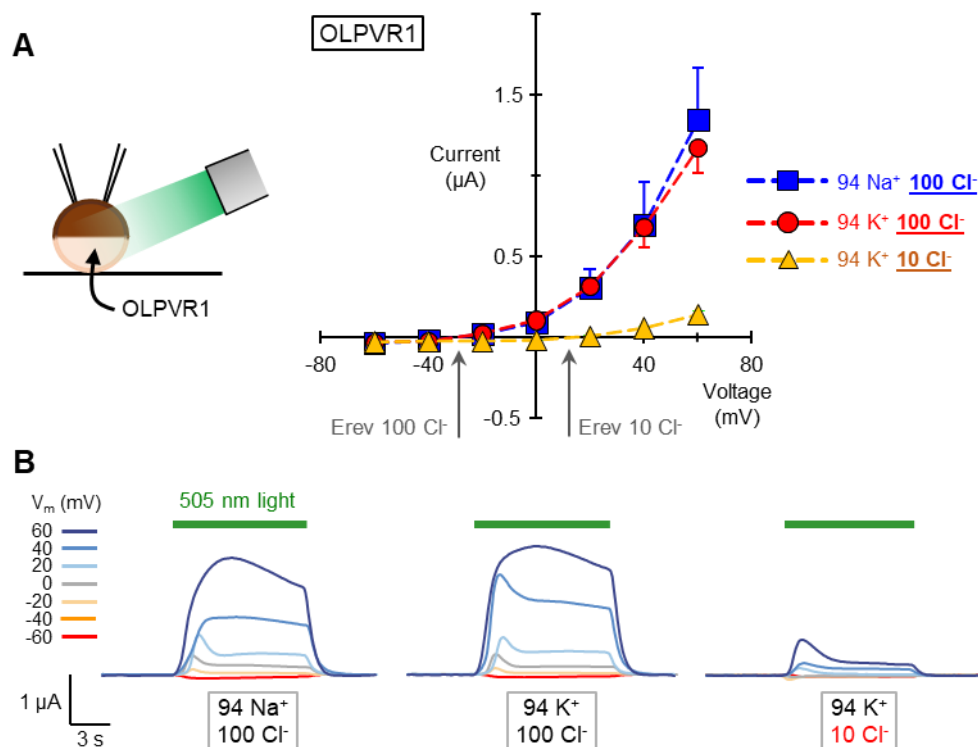


Figure b.5. Photo-activation of OLPVR1 induces chloride currents in *Xenopus* oocytes.

(A) Current-voltage relationship of OLPVR1 photo-induced stationary currents. Oocytes were injected with 30 ng of OLPVR1 RNA and incubated for 72-86h in standard physiological solution with 1 μ M all-trans retinal. Oocytes were bathed in specified solutions. 505-nm light was applied for 10 seconds. All solutions contained (in mM) 2 Ca^{2+} , 1 Mg^{2+} , 5 HEPES and the ions indicated. Each data point represents the average of 7-13 oocytes. Substituting the cation in the solution (Na^+ to K^+) did not affect the reversal potential (-30 mV). The reversal potential shifted to +13 mV when reducing Cl^- concentration from 100 to 10 mM by substitution with the impermeant ion methanesulfonate.

(B) Representative recordings of the same oocyte in the different solutions tested in (A). Leak currents were subtracted, and traces at each voltage were superimposed.

When substituting sodium ions with potassium ions, we saw virtually no changes in the current amplitude through the membrane. Moreover, between these two solutions, there was no change in the reversal potential (-30 mV) (Figure b.5.A & B). The data suggest that the currents observed are chloride currents because the chloride gradient is the same in the two solutions (100 mM extracellular chloride). Furthermore, based on the described ionic concentrations inside the oocyte (Marin, 2012), the reversal potential observed is far from what should be expected if sodium or potassium were being conducted (E_{Na} [94 mM Na^+]_o >> 36 mV; E_K [94 mM K^+]_o >> -11 mV), but close to the predicted E_{Cl} [100 mM Cl^-]_o between -35 and -12 mV).

Supplementary figure b.1 shows similar results for the cations $Tris^+$, $Arginine^+$, and Mg^{2+} .

In contrast, when we decreased extracellular Cl^- (from 100 mM to 10 mM), by substituting it with methanesulfonate (MS^-), there was a drastic reduction in current amplitudes with a change in the reversal potential to +13 mV (Figure b.5.A). The decrease in currents most likely originated from the reduction of the chloride gradient and from the fact that MS^- is a large anion that cannot cross the channel. It ultimately pushes the reversal potential towards more positive values closer to the E_{Cl} [10 Cl^-]_o, predicted to be between 22 and 46 mV.

Notably, OLPVR1 photoinduced currents were passive - shown by the reversibility imposed by the electrochemical gradient - but not symmetrical (Figure b.5.A). Positive currents were much stronger than negative currents, reflecting an outward rectification. By convention, that means the outward movement of positive charges is stronger than the inward movement of positive charges. Since chloride is a negative charge, that equates to chloride permeating more easily in the inward than in the outward direction.

Apart from being photoinduced, the strong outward rectification and chloride selectivity of the OLPVR1 currents are very similar to what has been described for *Xenopus* endogenous calcium-activated chloride channels (CaCCs) (Machaca *et al.*, 1998), discussed in section 1.2.

3.3.2 Other members of the VR1 family show identical photocurrent properties

Using the same expression conditions that allowed us to record OLPVR1, we were able to obtain photoinduced currents for the other two members of the VR1 family tested, namely VirChR1 and TARA150.

Photoinduced currents of OLPVR1, VirChR1 and TARA150 showed similar profiles (Figure b.6) with outward-rectifying currents (both peak/maximal and after 10 s of illumination) that

reversed around the predicted $E_{Cl}[100\text{mM Cl}^-]_o$ between -35 and -12 mV.

ChR2, an already described light-gated non-selective cationic channel (Nagel *et al.*, 2003), is shown in Figure b.6.A & B for comparison. Contrasting with VR1, upon illumination, ChR2 elicits currents that reverse around the predicted $E_K [94\text{mM K}^+]_o$ between -11 and 5 mV and are not outward-rectifying.

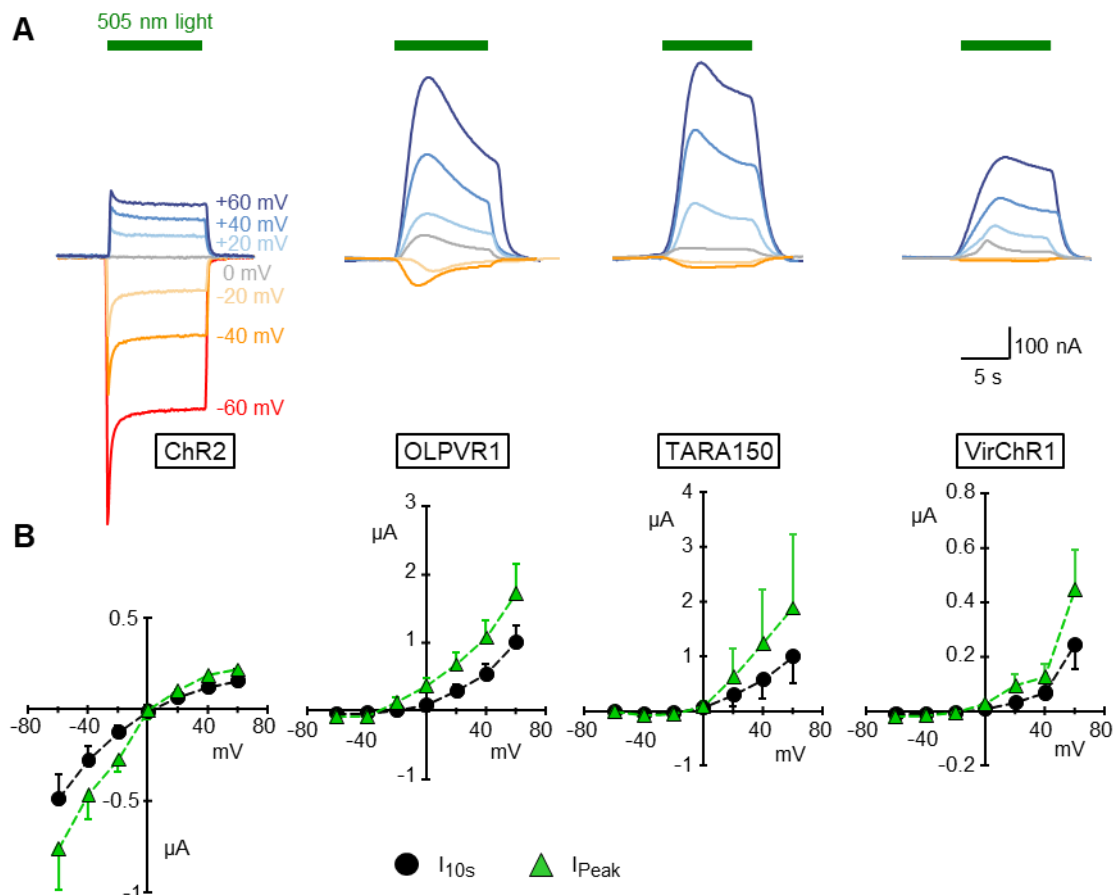


Figure b.6. Photo-induced currents of members of the VR1 family have a similar profile which is distinct from ChR2.

(A) Representative recordings from oocytes expressing the specified rhodopsins. **(B)** Current (μA) – voltage (mV) relationships of peak currents (I_{peak} , green) and currents measured after 10 seconds of illumination (I_{10s} , black). Averages are from 3-10 oocytes.

Oocytes injected with 7.5 ng of ChR2 RNA were incubated for 48h in standard physiological solution with 1 μM all-trans retinal. Oocytes expressing rhodopsins from the VR1 family (OLPVR1, TARA150, and VirChR1) were injected with 30 ng of RNA and incubated for 86h in the same solution. Recording solution (in mM) contained 94 K^+ , 100 Cl^- , 2 Ca^{2+} , 1 Mg^{2+} , and 5 HEPES. Leak currents were subtracted, and recordings at each voltage were superimposed.

3.3.3 OLPVR1 photoresponse is different from Channelrhodopsin-2

Since OLPVR1 photoinduced currents exhibited common characteristics with the *Xenopus* endogenous calcium-activated chloride channels (CaCCs), we set out to investigate if OLPVR1 was indeed triggering these channels.

ChR2 has been reported to induce CaCCs by enabling Ca^{2+} entry through the membrane. Thus, at a first stage, we compared the photo-responses of oocytes injected with ChR2 and OLPVR1 mRNAs in different extracellular calcium concentrations.

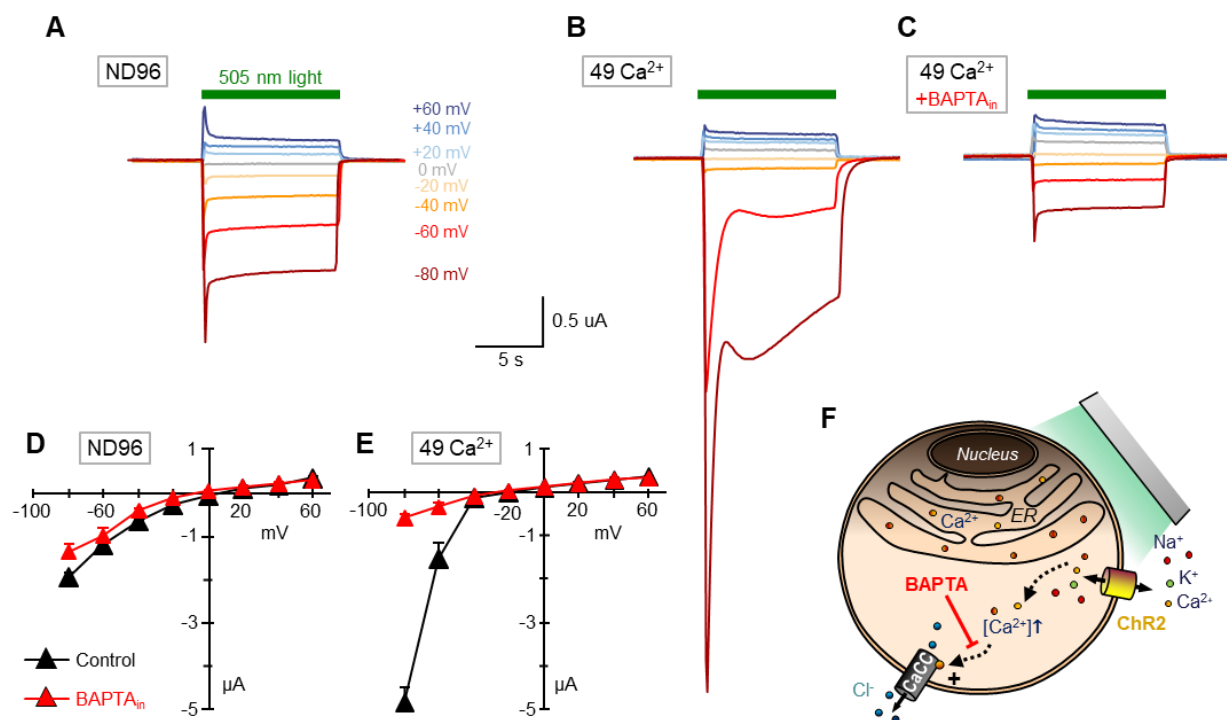


Figure b.7. ChR2 photo-activation can induce large chloride currents in *Xenopus* oocytes only at high extracellular calcium concentrations and hyperpolarizing voltages.

Oocytes injected with 7.5 ng of ChR2 RNA were incubated for 24h in standard physiological solution with 1 μM all-trans retinal.

Recordings from the same oocyte in different extracellular solutions, before and after BAPTA injection:

(A) ND96 (high sodium and low calcium)

(B) 49 mM Ca^{2+} (high calcium)

(C) 49 mM Ca^{2+} after intracellular injection of BAPTA.

Leak currents were subtracted, and recordings at each voltage were superimposed. Large peak currents appear in high extracellular calcium concentrations at -60 and -80 mV. Intracellular injection of BAPTA abrogates the large peak currents.

(D) Current-voltage relationship of ChR2 photo-induced peak currents in extracellular ND96 solution before and after intracellular injection of BAPTA. Each curve is the average of curves obtained in 5 oocytes.

(E) Current-voltage relationship of ChR2 photo-induced peak currents in high calcium extracellular solution before and after intracellular injection of BAPTA. Each curve is the average of curves obtained in 5 oocytes.

(F) Schematic representation of how ChR2 couples with *Xenopus* calcium-activated chloride channels (CaCCs): ChR2 at the plasma membrane permeates Ca^{2+} , which activates CaCCs.

Figure b.7 demonstrates the characteristic photoresponse of ChR2 when expressed in *Xenopus* oocytes. When we changed the extracellular solution from a low Ca^{2+} concentration (ND96 1.8 mM Ca^{2+} , Figure b.7.A) to a solution with a high Ca^{2+} concentration (49 mM Ca^{2+} - Figure b.7.B), additional large transient currents were generated upon light application at -60 and -80 mV. These currents were abrogated once the oocytes were injected with BAPTA, a Ca^{2+} chelator (Figure b.7.C & E).

Notably, BAPTA injection only blocked the large currents elicited in high extracellular calcium by hyperpolarizing voltages. This is seen in Figure b.7.D & E where there are no other differences in the current-voltage relationships before and after BAPTA injection.

The action of ChR2 in *Xenopus* oocytes has already been described in Nagel *et al.* (2003). Because ChR2 is a non-selective cationic channel, it allows the permeation of Na^+ and K^+ , but also Ca^{2+} . Calcium flux through the channel is modest though, but can transiently raise the internal local Ca^{2+} concentration near ChR2 channels. Only when external Ca^{2+} is elevated and the driving force for Ca^{2+} is strong enough, the entry of calcium becomes sufficient to activate endogenous Ca^{2+} -activated chloride currents (Figure b.7.F), which are responsible for the large peak currents observed. When BAPTA is injected into the oocyte, it chelates Ca^{2+} , consequently blocking the activation of CaCCs.

Figure b.8 demonstrates that, similar to ChR2, OLPVR1 photoinduced response evokes larger peak currents in high extracellular Ca^{2+} concentrations (Figure b.8.A & B). However, in contrast with ChR2, peak currents were consistently higher over the entire voltage range (Figure b.8.D). Furthermore, OLPVR1 elicited chloride currents even in low extracellular Ca^{2+} concentrations (ND96). High extracellular calcium is not required, but it does potentiate the chloride currents induced by OLPVR1.

It appears that the mechanism by which ChR2 and OLPVR1 are generating chloride currents is different.

Nevertheless, we hypothesized that OLPVR1 could be selectively permeating Ca^{2+} , either actively or passively. Ca^{2+} entry through OLPVR1 would elicit CaCCs currents with characteristics equivalent to the chloride currents observed (Figure b.8.C).

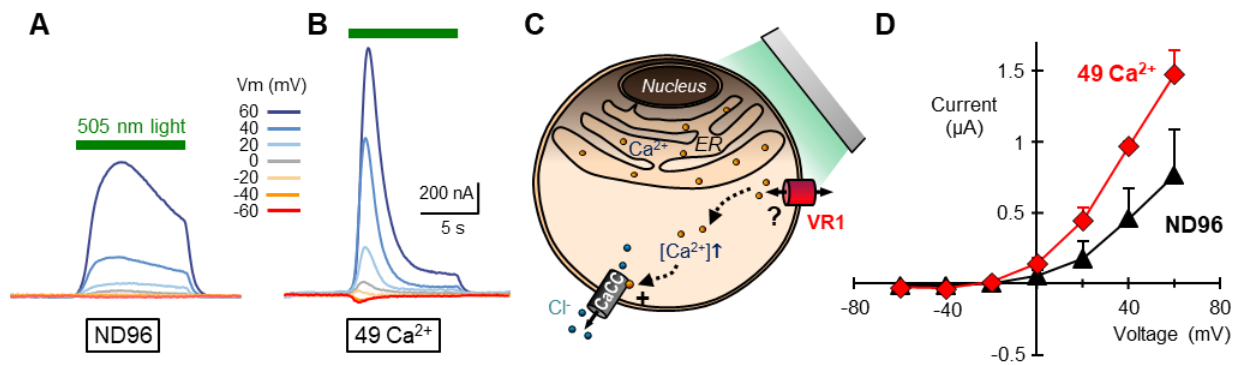


Figure b.8. OLPVR1-induced chloride currents do not require high extracellular calcium and large calcium driving forces.

Oocytes injected with 7.5 ng of OLPVR1 RNA were incubated for 48h in standard physiological solution with 1 μ M all-trans retinal.

(A-B) Recordings from the same oocyte in external 1.8 mM Ca²⁺ (ND96) **(A)** and 49 mM Ca²⁺ **(B)**. Leak currents were subtracted, and recordings at each voltage were superimposed.

(C) Hypothesis of how OLPVR1 might couple with *Xenopus* calcium-activated chloride channels (CaCCs): OLPVR1 at the plasma membrane permeates calcium, which activates CaCCs.

(D) Current-voltage relationship of OLPVR1 photo-induced peak currents in extracellular ND96 solution and high extracellular calcium concentration (49 mM Ca²⁺). The average peak currents in high calcium concentration are larger than in low calcium concentration. High extracellular calcium potentiates OLPVR1 currents, but the reversal potential remains unchanged. Each curve represents the average of curves recorded in 5 (49 mM Ca²⁺) and 9 (ND96) oocytes.

3.3.4 BAPTA abrogates OLPVR1 photocurrents in oocytes

To assess if, similar to ChR2, OLPVR1 permeates calcium through the membrane activating CaCCs, we proceeded with the intracellular injection of BAPTA. As seen in Figure b.9, the injection of BAPTA, which chelates internal calcium, completely abrogated OLPVR1 currents in both low and high extracellular calcium concentrations, which starkly differs from the ChR2 responses seen in the previous section. ChR2 in the presence of BAPTA still displays observable currents through the membrane.

The data demonstrate that OLPVR1 currents observed before BAPTA injection are solely from calcium-activated chloride channels, with no contribution of direct OLPVR1 currents.

We identified two distinct situations that could justify the response of OLPVR1:

(1) Direct Ca²⁺ currents through OLPVR1 proteins at the cell membrane are too small to be recorded but strong enough to activate CaCCs, which amplify the response into observable chloride currents. Higher extracellular Ca²⁺ increases the driving force for the entry of Ca²⁺, which is still not sufficient to be recorded but enough to activate more CaCCs.

(2) OLPVR1 localizes in intracellular membranes rather than at the cell surface. Photoactivation of OLPVR1 leads to the release of calcium from intracellular stores, which activates CaCCs. Depleting calcium from intracellular stores induces Store-Operated Calcium

Entry (SOCE). Calcium entry through SOCE amplifies the signal by further activating CaCCs. High extracellular calcium potentiates the response of OLPVR1 by entering through SOCE (Figure b.9.D).

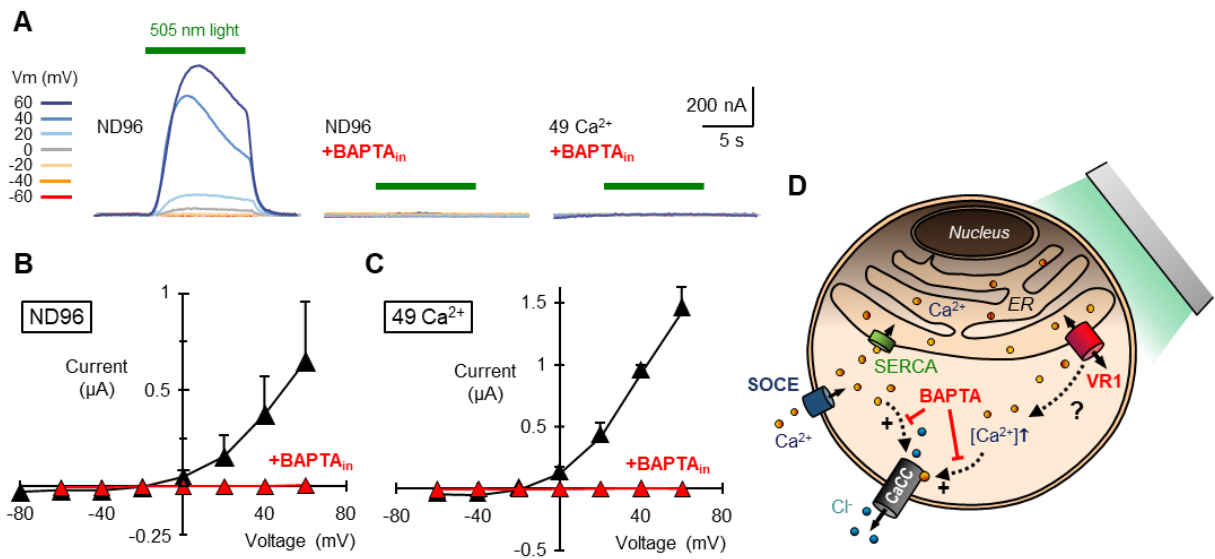


Figure b.9. OLPVR1-induced chloride currents are abrogated by intracellular injection of BAPTA.

Oocytes were injected with 7.5 ng of OLPVR1 RNA and incubated for 48h in standard physiological solution with 1 μM all-trans retinal.

(A) Representative recordings upon photo-activation of OLPVR1 with and without intracellular injection of BAPTA in external 1.8 mM Ca²⁺ (ND96) and 49 mM Ca²⁺. Leak currents were subtracted, and recordings at each voltage were superimposed.

(B) Current-voltage relationship of OLPVR1 photo-induced peak currents in extracellular ND96 solution (1.8 mM Ca²⁺) before and after intracellular injection of BAPTA. Each data point represents the average of 10 oocytes.

(C) Current-voltage relationship of OLPVR1 photo-induced peak currents in 49 mM Ca²⁺ extracellular solution before and after intracellular injection of BAPTA. Each data point represents the average of 4-5 oocytes.

(D) Hypothesis of how OLPVR1 might couple with *Xenopus* calcium-activated chloride channels (CaCCs): OLPVR1 does not express at the surface of the cell but rather in intracellular membranes. Activation of OLPVR1 leads to the release of calcium from intracellular stores, which activates CaCCs. The depletion of calcium from intracellular stores induces store-operated calcium entry (SOCE). Calcium entry through SOCE amplifies the signal by further activating CaCCs. High extracellular calcium potentiates the response of OLPVR1 by entering through SOCE.

3.3.5 OLPVR1 accumulates intracellularly rather than at the cell surface

To address the localization of OLPVR1, we employed the same technique as in Project A - XenoGlo. It relies on the luminescence produced by the complementation between the LgBit of nanoluciferase and the HiBiT-tag fused to the protein of interest. More information about this technique can be found in Annex D.

For this purpose, we created the constructs OLPVR1-HB and Chr2-HB. Each protein is fused to the 11-amino acid sequence of the HiBiT at the N-terminal (HB notation is added at the end of the name for clarity). Because the N-terminal of OLPVR1 is predicted to be extracellular, luminescence upon applying LgBiT and its substrate should function as a read-out of surface expression. Subsequently, permeabilization of the cell should enable an estimation of total protein expression.

Functional validation of the OLPVR1-HB and Chr2-HB constructs is shown in Supplementary figure b.2.

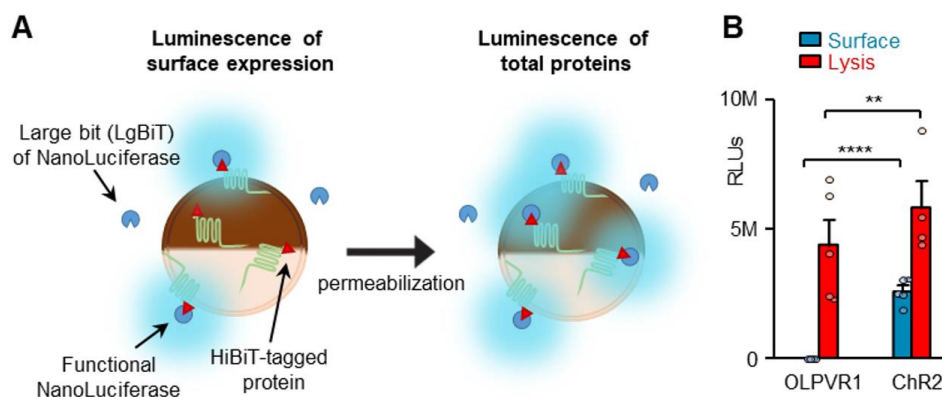


Figure b.10. OLPVR1, in contrast with Chr2, is not present at the surface of the oocytes.

(A) Illustration of protein detection in oocytes using Nanoluciferase.

(B) Mean luminescence recorded in oocytes injected with 7.5 ng RNA coding for HiBiT-tagged OLPVR1 and Chr2 before (blue) and after membrane permeabilization (red). The OLPVR1 surface luminescence value is 2846 ± 1024 , which is 1000 times smaller than Chr2. Values are averages from 4-6 batches of oocytes. For each batch, data points in each condition were obtained as the average luminescence from 3 oocytes.

Chr2 values are larger than those of OLPVR1: **P < 0.01, ****P < 0.0001, two-way ANOVA with Sidak's post hoc test.

Figure b.10 shows that surface luminescence of OLPVR1-HB ($2.8 \pm 1K$ RLUs) is approximately a thousandfold smaller than surface luminescence of Chr2-HB ($2.6 \pm 0.2M$ RLUs). In contrast, luminescence upon lysis of the cell, albeit statistically different, is only 1.5 times larger for Chr2. The data suggest that OLPVR1-HB accumulates intracellularly rather than being

trafficked to the cell surface like ChR2.

It supports the hypothesis that OLPVR1 is triggered from intracellular membranes, but it does not demonstrate that it mobilizes calcium stores – this is addressed in the next section.

3.3.6 OLPVR1 photocurrents require IP₃-dependent calcium stores

We hypothesized that OLPVR1 localizes in intracellular membranes and, upon illumination, leads to the release of calcium from intracellular stores, which activates CaCCs. We validated the predominantly intracellular localization of OLPVR1 in the previous section.

To address if OLPVR1 mobilizes Ca²⁺ stores, we coexpressed OLPVR1 and the Muscarinic Receptor 3 (M3) in *Xenopus* oocytes.

As illustrated in section 1.2, M3 is a Gq-coupled receptor that can activate phospholipase C (PLC), cleaving PIP₂ into DAG and IP₃. IP₃, in turn, acts on IP₃ receptors at the ER to trigger the release of Ca²⁺, ultimately activating CaCCs. Thus, by activating M3 with its agonist acetylcholine (ACh), Ca²⁺ is mobilized, and the intracellular Ca²⁺ stores get depleted. Depletion of calcium stores persists in conditions of no extracellular calcium, by interfering with the store-operated calcium entry.

We tested if OLPVR1 can elicit photocurrents in conditions of Ca²⁺-store depletion. This was accomplished by applying ACh in oocytes coexpressing M3 and OLPVR1, previous to an application of light. As seen in Figure b.11.B, the application of ACh triggers large chloride currents due to the release of calcium from intracellular stores. Subsequent application of 505-nm light did not enable OLPVR1 to produce a photoresponse (Figure b.11.B & C) compared to the control (Figure b.11.A & D).

To explain this data, we propose that OLPVR1 expresses and functions in intracellular membranes, where, when activated by light, it enables calcium release from calcium stores towards the cytoplasm, eventually reaching CaCCs, activating them.

Supplementary Figure b.3 further supports these findings by demonstrating that extracellular calcium is not necessary for OLPVR1 to induce photocurrents.

The most direct explanation would imply OLPVR1 permeating Ca²⁺ directly from the ER into the cytoplasm. However, VirChR1, which we have established, has a similar photoresponse

profile, has been described as a cationic channel impermeable to Ca^{2+} (Zabelskii *et al.*, 2020). We thus hypothesized that OLPVR1 might depend on another transducing pathway to activate calcium release.

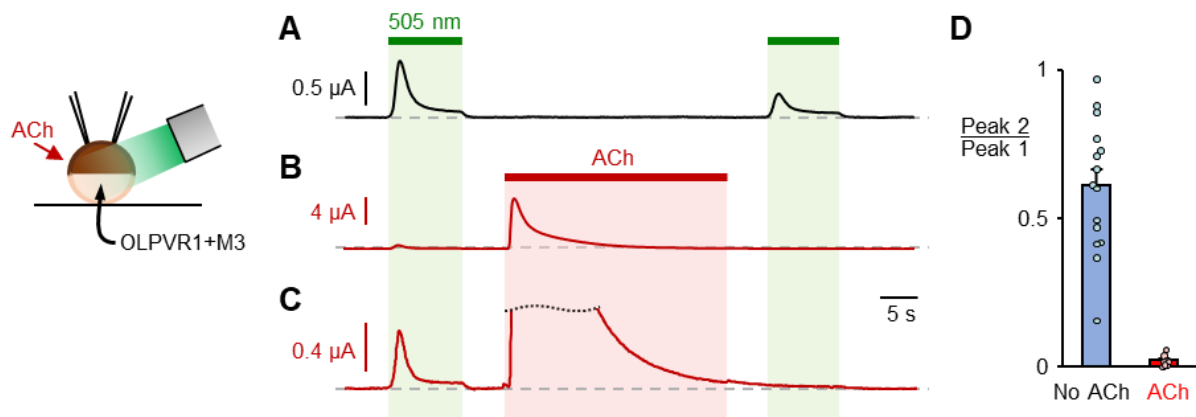


Figure b.11. OLPVR1 response is absent after intracellular calcium depletion.

(A-C) Representative traces at +40 mV (in ND96 0Ca^{2+} : 91 mM Na^+ , 5 mM K^+ , 100 mM Cl^- , 0 Ca^{2+}) from oocytes coexpressing OLPVR1 and Gq-coupled muscarinic M3 receptor. The M3 agonist ACh (5 μM) induces Ca^{2+} release and large calcium-activated chloride currents. OLPVR1 response is absent after M3 is activated and stores are depleted (B). (C) is an enlarged version of (B).

(D) Average ratios of OLPVR1 peak current induced by the second illumination over peak current of the first illumination with and without ACh application in between. Illuminations were 50 s apart.

3.3.7 OLPVR1 integrates tightly with the calcium-signaling pathway of *Xenopus* oocytes

To clarify how OLPVR1 integrates with the calcium signaling of *Xenopus*, we utilized inhibitors of different agents of this mechanism. Figure b.12.A illustrates the inhibitors used and their targets: YM-254890 targets Gq proteins (Uemura *et al.*, 2009; Peng *et al.*, 2021), Ani9 (Seo *et al.*, 2016) and MONNA (Oh *et al.*, 2013) target CaCCs, and 2-APB targets both IP_3R and SOCE (Maruyama *et al.*, 1997; Wei *et al.*, 2016; Wozniak *et al.*, 2018).

Supplementary figure b.4. shows validation tests of the inhibitors in oocytes expressing M3.

In Figure b.12, panel B presents representative recordings of oocytes before and after being subjected to the specified inhibitor. Inhibitors of CaCCs, Ani9 and MONNA, produced near-complete inhibitions on par with the control tests in M3. It further validates that OLPVR1 photocurrents through the membrane result from the triggering of CaCCs.

In contrast, the Gq inhibitor YM-254890 did not affect the OLPVR1 photocurrents. It suggests that OLPVR1 mobilizes calcium release independently of the Gq pathway.

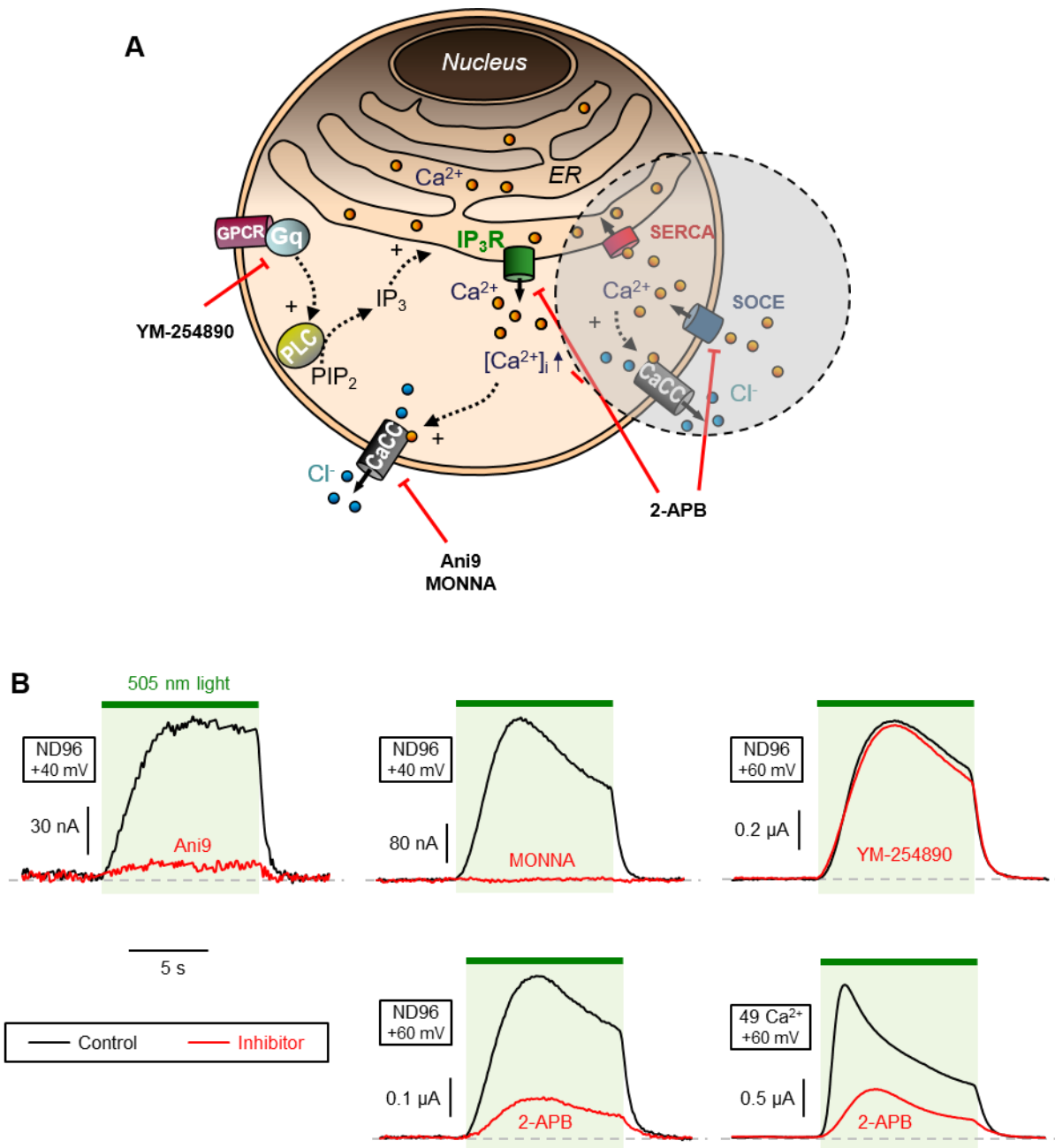


Figure b.12. Effect of the different calcium-signaling inhibitors on OLPVR1 photo-induced currents.

(A) Illustration of the targets of the different inhibitors tested.

(B) Representative traces (N between 3 and 6) at +40/+60 mV from oocytes before (black trace) and after incubation with the specified inhibitor (red trace). Oocytes were injected with 7.5-30 ng of OLPVR1 RNA and incubated for 48h in standard physiological solution with 1 μ M all-trans retinal.

Concentrations and incubation times of the inhibitors were: Ani9 (30 μ M, 60 min), MONNA (30 μ M, 60 min), YM-254890 (10 μ M, 10 min) and 2-APB (100 μ M, 60 min). Recording solutions were as indicated: ND96 (1.8 mM Ca^{2+}) or high calcium solution (49 mM Ca^{2+}).

On the other hand, 2-APB incubation decreased OLPVR1 currents considerably but far from completely. It suggests that the OLPVR1 total photocurrents are largely contributed by the action of IP₃R and SOCE, likely as a consequence of a positive feedback amplification of calcium signaling. This observation applies with the caveat that we do not know the direct effects of 2-APB on OLPVR1, which might confound our conclusions.

The fact that 2-APB blocks almost entirely (98±0.5%) currents elicited by M3 (Supplementary figureb.4) but did not fully block OLPVR1 photocurrents also suggests that OLPVR1 might be able to permeate Ca²⁺ on its own. It is, however, just a speculation at this time.

3.3.8 Addressing OLPVR1 to the membrane reveals a BAPTA-insensitive current

To record the direct activity of OLPVR1, one solution is to try to overcome the OLPVR1 propensity of accumulating intracellularly by improving its trafficking to the membrane.

Figure b.13.A shows the surface luminescence for different conditions tested to improve OLPVR1 surface expression.

We first assessed whether increasing the amount of OLPVR1 RNA injected from 7.5 ng to 30 ng affected surface expression. However, this approach did not suffice to change surface expression (7.5 ng, 3±0.7K RLU vs. 30 ng, 3±1.4K RLU, P>0.9999).

We modified OLPVR1 by inserting signal sequences previously reported to improve the surface expression of *Natronomonas pharaonis* halorhodopsin (NpHR) (Gradinaru *et al.*, 2008). Neither the fusion to the Golgi export trafficking signal of Kir2.1 (OLPVR1-MT, 6±0.7K RLU, P>0.9999), nor the fusion to the signal sequence of human nicotinic acetylcholine α-7 receptor (SS-OLPVR1, 3.1±1K RLU, P>0.9999), had significant effects on the surface expression of OLPVR1.

Similarly, a fusion of OLPVR1 to the Interleukine 6 secretion signal sequence (IL6-OLPVR1, 2.9±0.5K RLU, P>0.9999) did not improve surface expression, despite being used successfully to improve the expression of DOR in Project A.

We also tested the OLPVR1 mutant 'O1O2mut' used for protein purification, crystallization, and structural determination in Zabelskii *et al.* (2020). Like our other attempts, it did not improve surface expression (2.3±0.5K RLU, P>0.9999).

Since the genome of the Organic Lake Phycodnavirus contains both OLPVR1 from the VR1 family and OLPVR2 from the VR2 family, we hypothesized that both rhodopsins might be functioning together and require each other for surface trafficking. However, coexpressing OLPVR1 and OLPVR2 did not improve surface expression either (≈ 0 RLUs, $P=0.9998$).

Only the fusion DOR=OLPVR1 (30 ng of RNA injected) increased surface expression by approximately fifteenfold (43 ± 10 K RLUs, $P < 0.0001$).

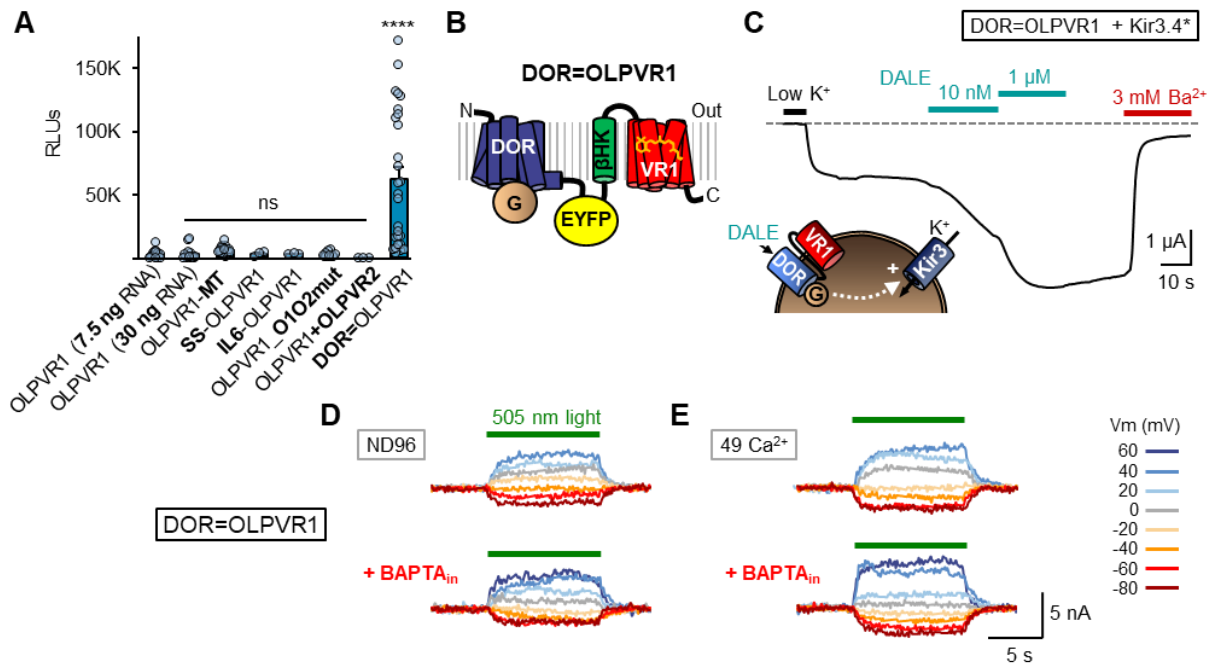


Figure b.13. Fusing OLPVR1 to a high-expressing GPCR allows the trafficking of the protein to the membrane and reveals a BAPTA-insensitive photocurrent.

(A) Mean luminescence recorded in oocytes expressing different HiBiT-tagged OLPVR1 constructs (24-72h in solution containing 1 μ M all-trans retinal). Increasing the amount of OLPVR1 RNA injected from 7.5 to 30 ng did not affect surface expression. Modifying the protein by inserting signal sequences did not improve surface expression (MT, Golgi export trafficking signal of Kir2.1 potassium channel; SS, Signal sequence of human nicotinic acetylcholine $\alpha 7$ receptor subunit; IL6, Interleukine-6 secretion signal sequence). Mutant O1O2mut used for crystallization and structural determination does not improve surface expression. Coexpressing OLPVR1 with viral rhodopsin OLPVR2 did not improve surface expression. Only the fusion DOR=OLPVR1 (30 ng) increased surface expression (≈ 15 times). Data points represent single oocytes.

**** $P < 0.0001$, ns not significant, one-way ANOVA followed by Dunnett's multiple comparison test against the control OLPVR1 (7.5 ng RNA).

(B) Design of fusion construct DOR=OLPVR1. G, G protein; EYFP, Enhanced Yellow Fluorescent Protein; β HK, Transmembrane segment of H⁺,K⁺-ATPase.

(C) TEVC recording from an oocyte coexpressing G protein-activated Kir3.4* channels and DOR=OLPVR1 fusion. Application of the DOR agonist DALE causes G protein activation and Kir3.4* current increase. Low K⁺ solution corresponds to ND96 and the rest of the recording was performed in hK⁺ solution.

(D-E) Representative current traces from a single oocyte recorded upon photoactivation of DOR=OLPVR1 at different potentials before and after intracellular BAPTA injection. Currents are mostly insensitive to BAPTA. Oocytes were injected with 30 ng of RNA and incubated in standard physiological solution with 1 μ M all-trans retinal for 72h. Leak currents were subtracted, and recordings at each voltage were superimposed.

Supplementary figure b.5. further explores the total protein expression and function of these constructs.

DOR=OLPVR1 corresponds to the fusion of the δ -opioid receptor (DOR) to OLPVR1. The reasoning behind the creation of DOR=OLPVR1 fusion was based on:

- (1) DOR has a robust surface expression in *Xenopus* oocytes and is amenable to protein engineering;
- (2) In the context of creating ICCRs - Ion channel coupled receptors (Moreau *et al.*, 2008), fusing a GPCR to an ion channel has been demonstrated by our laboratory to yield a fusion construct where both the receptor and the channel are functional;
- (3) Kleinlogel, Terpitz *et al.* (2011) created a construct where they fused two microbial rhodopsins in tandem for stoichiometric colocalization and demonstrated that both are functional;
- (4) DOR surface expression, correct folding, and membrane docking can be assessed by coexpressing Kir3 channels in *Xenopus* and verifying if, upon agonist application, Kir3 channels are activated;
- (5) Based on Project A, the level of surface expression of the fusion construct could be gauged based on the activation or inhibition of Kir3 channels.

Thus, we hypothesized that fusing DOR to OLPVR1 could generate functional DOR and OLPVR1 with improved surface expression driven by DOR at the N-terminal. Furthermore, we would be able to evaluate surface expression and correct protein folding by coexpressing Kir3 channels in *Xenopus* oocytes and using TEVC.

Supplementary figure b.2 validates the function of a similar fusion construct with Chr2.

A schematic representation of the DOR=OLPVR1 construct is shown in Figure b.13.B. It was based on the construct by Kleinlogel, Terpitz *et al.* (2011). The full-length DOR protein is at the N-terminal, followed by an Enhanced Yellow Fluorescent Protein (EYFP). The addition of β HK enables the connection of the intracellular C-terminal of DOR to the extracellular N-terminal of OLPVR1. Furthermore, this helix was demonstrated to improve membrane trafficking of bacteriorhodopsin by tenfold (Kleinlogel, Terpitz, *et al.*, 2011). It corresponds to the 105-aminoacid N-terminal fragment of the β -subunit of the rat gastric H⁺,K⁺-ATPase. The construction ends with the full-length OLPVR1 protein. Note that EYFP was shown to be required to deliver a functional fusion construct (Kleinlogel, Terpitz, *et al.*, 2011). It was suggested to act as a spacer that allows flexibility of the proteins in tandem.

As seen in Figure b.13.C, DOR=OLPVR1 coexpressed with Kir3 activates the channel upon

agonist application. This indicates that the protein is properly folded and docked at the membrane, allowing for its functionality.

Subsequently, we tested if the protein was able to produce photoinduced currents. In Figure b.13.D & E we show the photoinduced currents of DOR=OLPVR1 in low (ND96) and high (49 Ca^{2+}) extracellular calcium solution after BAPTA injection. The currents observed are different from those obtained by illuminating OLPVR1. The strong outward rectifying currents sensitive to BAPTA are not present. Instead, currents are small (low nA range at 60 mV), symmetric with little change upon BAPTA application (also seen in Figure b.14).

Figure b.14 shows the current-voltage relationships of DOR=OLPVR1 in low (ND96) and high (49 Ca^{2+}) extracellular calcium solution, before and after BAPTA injection. Both in ND96 and in 49 Ca^{2+} currents seem to reverse at around -30 mV, close to the predicted E_{Cl} . Upon BAPTA injection there is a slight shift in reversal potential towards more positive values, more pronounced in high extracellular calcium, which suggests there was a small contribution of CaCCs in the currents before BAPTA injection. The data, however, is not robust enough to enable the determination of selectivity. A full set of solution exchanges and pharmacological inhibition of CaCCs would be necessary to evaluate further aspects of this current.

Since DOR=OLPVR1 currents reverse depending on the electrochemical gradient imposed, it suggests OLPVR1 functions as a channel rather than a pump, allowing ions to follow their electrochemical gradient. The selectivity, however, could not be determined.

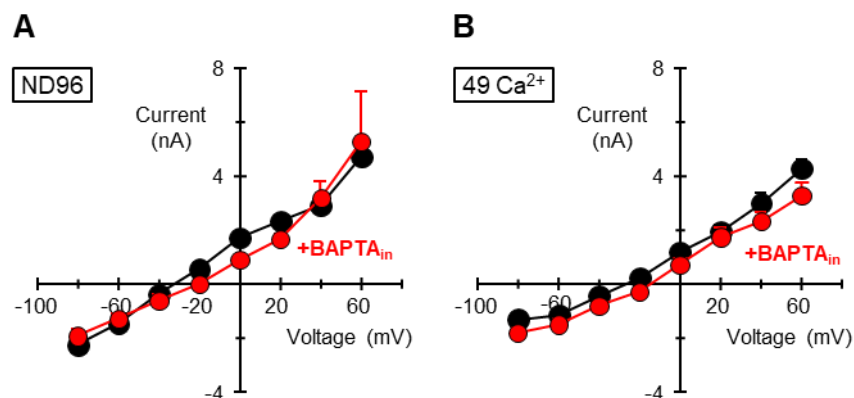


Figure b.14. Current-voltage relationships of stationary currents elicited by photo-activation of OLPVR1 fused to DOR.

Light-induced currents were recorded at different voltages in the same oocytes before (black) and after BAPTA injection (red). Stationary currents were measured after 10 seconds of illumination. Bath solution was either **(A)** ND96 (5 oocytes) or **(B)** 49 Ca^{2+} (6 oocytes). Oocytes were injected with 30 ng DOR=OLPVR1 RNA and incubated in standard physiological solution with 1 μM all-trans retinal for 72h. In both solutions, there is a positive shift of ~ 10 mV of the reversal potential after BAPTA injection.

3.3.9 OLPVR1 photoresponse elicits calcium release in HEK293T cells activating exogenous calcium-activated channels

Since the study of the function of viral rhodopsins had, as a background motivation, the objective of identifying novel optogenetic tools, we were interested in understanding if OLPVR1 could mobilize intracellular calcium signaling in mammalian cells.

To this end, OLPVR1 was expressed in HEK293T cells. Initial experiments using whole-cell patch clamp showed that light induced no detectable current in OLPVR1-expressing cells. Unlike *Xenopus* oocytes, HEK293T cells do not have endogenous Ca^{2+} -sensitive channels. To reproduce oocyte results, HEK293T cells were cotransfected with OLPVR1 and one of two different calcium-activated channels: TMEM16A¹⁵ – a gene coding for the same Ca^{2+} -activated chloride channels as the CaCCs of *Xenopus* – and SK1 – small conductance calcium-activated potassium channels.

Figure b.15 demonstrates that, just as in *Xenopus* oocytes, in HEK293T cells, OLPVR1 can induce calcium-activated chloride channels at the surface of the cell. Figure b.15.A show how the application of 505-nm light induces whole-cell outward rectifying currents, which are abrogated when EGTA, a calcium chelator, is added in the pipette/intracellular solution (Figure b.15.B).

Figure b.15.C shows peak currents induced by consecutive 5-s pulses of 505-nm light when cells are clamped at 100 mV. Figure b.15.D shows the current-voltage relationships of the currents before, during, and after light application. The light-induced currents reverse close to the expected reversal potential of chloride.

Figure b.15.E showcases how extracellular calcium is not required for OLPVR1 photoinduced chloride currents. However, the absence of extracellular Ca^{2+} decreases the photoinduced currents (Supplementary Figure b.3 shows similar results in *Xenopus* oocytes). Figure b.15.F confirms that, in all conditions, the light-induced currents reverse near E_{Cl} .

Figure b.16 describes equivalent results when SK1 is coexpressed with OLPVR1, showing an almost complete reduction of SK1 potassium currents when the pipette solution contained EGTA, and a more modest change in currents in the absence of extracellular calcium.

The results in HEK293T cells are in all aspects comparable with the results in *Xenopus* oocytes. The data strongly support the hypothesis that OLPVR1 can induce the release of

¹⁵ TMEM16A (Transmembrane protein 16A) or ANO1 (Anoctamin-1).

intracellular calcium and activate downstream Ca^{2+} -sensitive effectors in HEK293 cells, just like in oocytes.

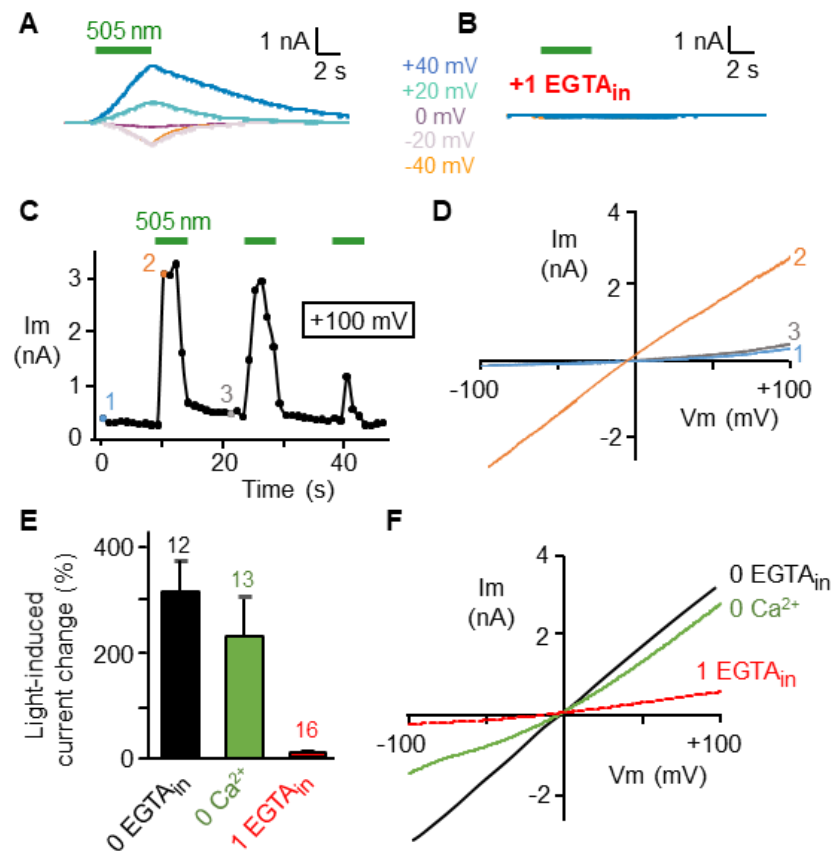


Figure b.15. OLPVR1 activates surface TMEM16A Ca^{2+} -activated Cl^- channels (CaCCs) through release of intracellular calcium in HEK293T cells.

Whole-cell currents were recorded by patch clamping HEK293T cells coexpressing TMEM16A and OLPVR1. Bath solution contained (in mM): 150 NaCl, 5 KCl and 10 HEPES with added 2 Ca^{2+} unless otherwise specified. Pipette solution contained 155 KCl, 3 MgCl_2 , 10 HEPES, with added 1 EGTA where noted.

(A) Representative current traces recorded at different potentials, without EGTA in pipette (few μM Ca^{2+} contaminant).

(B) As in A, with 1 mM EGTA in pipette (few nM free Ca^{2+}).

(C) Representative time course of the current at +100 mV and responses to 505-nm, 5-s illuminations. Currents were elicited by 1-s voltage ramps from -100 to +100 mV. No EGTA in pipette, 2 mM Ca^{2+} in bath.

(D) Representative IV traces corresponding to points 1, 2, & 3 of experiment shown in C.

(E) Histogram representing the percent changes in current elicited by 505-nm illumination in different extracellular and intracellular ionic conditions (0 EGTA_{in} = No EGTA in pipette, 2 mM Ca^{2+} in bath; 0 Ca^{2+} =No EGTA in pipette, no Ca^{2+} in bath; 1 EGTA_{in} =1 mM EGTA in pipette, no Ca^{2+} in bath). Bars represent mean \pm SEM. The numbers of cells are indicated above bars.

(F) Representative traces during illumination in different extracellular and intracellular ionic conditions. Currents were elicited by 1-s voltage ramps from -100 to +100 mV.

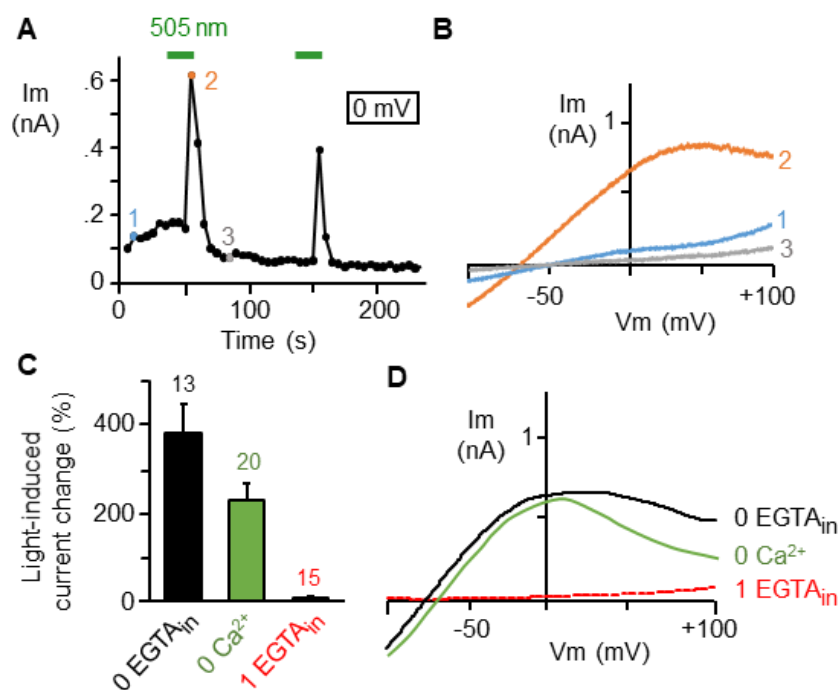


Figure b.16. OLPVR1 activates surface SK1 Ca²⁺-activated K⁺ channels through release of intracellular calcium in HEK293T cells.

Whole-cell currents were recorded by patch clamping HEK293T cells coexpressing SK1 and OLPVR1. Bath solution contained (in mM) 150 NaCl, 5 KCl and 10 HEPES with added 2 Ca²⁺ unless otherwise specified. Pipette solution contained 155 KCl, 3 MgCl₂, 10 HEPES, with added 1 EGTA where noted.

(A) Representative time course of the current at +0 mV and responses to 505-nm, 5-s illuminations. Currents were elicited by 1-s voltage ramps from -100 to +100 mV. No EGTA in pipette, 2 mM Ca²⁺ in bath.

(B) Representative IV traces corresponding to points 1, 2, & 3 of experiment shown in A.

(C) Histogram representing the percent changes in current elicited by 505-nm illumination, in different extracellular and intracellular ionic conditions (0 EGTA_{in}= No EGTA in pipette, 2 mM Ca²⁺ in bath; 0 Ca²⁺=No EGTA in pipette, no Ca²⁺ in bath; 1 EGTA_{in}=1 mM EGTA in pipette, no Ca²⁺ in bath). Bars represent mean±SEM. The numbers of cells are indicated above bars.

(D) Representative current traces during illumination in different extracellular and intracellular ionic conditions. Currents were elicited by 1-s voltage ramps from -100 to +100 mV.

3.4 Discussion

3.4.1 Photoactivation of VR1 rhodopsins elicits the release of calcium from intracellular stores coupling with calcium-signaling effectors

In this project, we set out to study the function of viral rhodopsins. By injecting VR mRNAs in *Xenopus* oocytes, after 2-5 days of incubation in the presence of 1 μM all-trans retinal, we observed photoinducible currents for the members of the VR1 family OLPVR1, TARA150 and VirChR1. The observed currents were outward-rectifying chloride currents - the hallmark characteristics of endogenous oocyte calcium-activated chloride channels (CaCCs).

The injection of BAPTA - a Ca^{2+} chelator - in oocytes expressing OLPVR1 abolished the photoinduced currents. It enabled us to establish that the large light-induced chloride currents were a secondary response arising from an increase in intracellular calcium. Interestingly, no OLPVR1 photocurrents at the cell surface were observed in the presence of BAPTA, which led us to explore the possibility that this protein was localized intracellularly and indirectly triggered endogenous CaCCs at the oocyte membrane.

Using XenoGlo, a technique optimized *in situ* for the detection of protein expression in oocytes, we observed that OLPVR1 accumulates intracellularly with no obvious expression at the surface of the cell. Furthermore, by activating M3 receptors to deplete IP_3 -triggered intracellular calcium stores, we demonstrated that the OLPVR1 response requires the release of calcium from the same calcium stores.

We assessed how OLPVR1 integrates with the *Xenopus* calcium signaling by using a battery of different inhibitors. As expected, inhibitors directed at CaCCs, such as MONNA and Ani9, abolished the currents. In contrast, incubation with the Gq inhibitor YM-254890 had no effects on the photoinduced currents, demonstrating that OLPVR1 integrates with calcium signaling downstream of Gq activation. On the other hand, 2-APB incubation decreased OLPVR1 currents severalfold but not entirely. It suggests that the OLPVR1 net photocurrents are largely contributed by the action of IP_3R and SOCE, presumably as a consequence of a positive feedback amplification of calcium signaling. However, while 2-APB is standardly used to block the actions of IP_3R and SOCE, it has shown non-specific activity on other proteins, such as

Transient Receptor Potential channels (Singh *et al.*, 2018), potassium channels (Ma *et al.*, 2011) and volume-regulated anion channels (Lemonnier *et al.*, 2004). Thus, we cannot rule out direct effects of 2-APB on OLPVR1. In that context, we could be overestimating the contribution of IP₃R and SOCE on the OLPVR1 response.

The fact that 2-APB blocks almost entirely the currents elicited by M3 but did not fully block OLPVR1 photocurrents suggests that OLPVR1 might be permeating calcium directly. The simplest explanation for our observations would be that OLPVR1 permeates calcium down its electrochemical gradient from Ca²⁺ stores towards the cytoplasm. However, that remains to be verified.

Even though we managed to increase OLPVR1 surface localization by fusing it to a high-expressing GPCR (DOR=OLPVR1), the determination of selectivity was not trivial.

Light-induced DOR=OLPVR1 currents had amplitudes in the 10 nA range, close to the limit of what is measurable in an oocyte, but were clearly distinguishable from background noise. This low amplitude is not surprising because, although clearly detectable, surface expression of DOR=OLPVR1 was still about two orders of magnitude less than that of ChR2, which produces currents in the μ A range. Contrasting with the currents of OLPVR1, DOR=OLPVR1 currents were symmetric and largely insensitive to BAPTA. BAPTA injection imposed a small shift in reversal potential towards more positive values suggesting there was a small contribution of CaCC currents. It is not clear whether the small CaCC activation was due to the calcium-release activity of intracellular DOR=OLPVR1, or to calcium entry through surface DOR=OLPVR1.

Our observations strongly support the hypothesis that OLPVR1 proteins are expressed but not trafficked to the cell surface. Green light can penetrate intracellularly and activate OLPVR1, which ultimately leads to the release of calcium from intracellular stores and the consequent activation of calcium-signaling effectors such as calcium-activated channels in *Xenopus* oocytes. Indeed, we further validated this action of OLPVR1 in mammalian HEK293T cells. When OLPVR1 was expressed alone in HEK293T cells, no light-induced current could be detected. However, strong photoresponses were obtained when OLPVR1 was cotransfected with calcium-sensitive channels, either calcium-activated chloride channels akin to *Xenopus* CaCCs (TMEM16A), or calcium-activated potassium channels (SK1).

3.4.2 OLPVR1 localizes in intracellular membranes

It is not uncommon that rhodopsins localize intracellularly. Animal rhodopsins natively localize and function in internal membranes (reviewed in Palczewsky, 2006). Even microbial rhodopsins from bacteria, which lack intracellular membranes, when expressed in multi-membrane organisms often accumulate in intracellular domains and have to be subjected to optimizations for surface membrane expression (as in Gradinaru *et al.*, 2008). On the other hand, microbial rhodopsins such as ChR2 natively localize on the plasma membrane of algae, but in delimited and specialized regions that together with the chloroplast form the eyespot of the unicellular *Chlamydomonas reinhardtii* (Boyd *et al.*, 2011).

The fact that rhodopsins seem to have preferential localizations cannot be explained by already described retention or export signal sequences. For instance, the amino acid sequence of OLPVR1 when subjected to localization prediction tools (tools reviewed in Imai & Nakai, 2020) showed no consistent result (data not shown).

Another possible reason for differential localization might arise from the dependency on the lipid context where the rhodopsins are inserted. It is well recognized that plasma membranes and organelle membranes differ in lipidic composition (Opekarová & Tanner, 2003; Shrestha *et al.*, 2014).

Curiously, both the structures of OLPVR1 and VirChR1 in Zabelskii *et al.* (2020), as well as the structure of VirRDTS in Needham *et al.* 2019, exhibited a lipid molecule blocking the pore of the proteins. Zabelskii *et al.* (2020) further demonstrated that the mutant OLPVR1_O1O2mut (nine mutations mimicking OLPVR2) successfully excluded the lipid from the pore, maintaining it in a similar structural conformation. They concluded that lipid interactions were not necessary for the stabilization of the structure of the protein and dismissed it as a presumable artifact of crystallization.

When we expressed OLPVR1_O1O2mut in *Xenopus* oocytes, we found similar expression patterns as OLPVR1, with little surface expression and high intracellular accumulation, supporting the idea that pore-lipid interaction is not required for the stabilization of the protein. However, we were not able to obtain photocurrents for the OLPVR1_O1O2mut (Supplementary figure b.5). The fact that all available VR1 structures exhibit this central lipid and that its exclusion in OLPVR1 hinders activity might reflect a modulation by lipids. We did not directly address this aspect but it opens the question of how lipid context might impact the localization and function of viral rhodopsins.

It is also curious to note that, VR2 family members Baikal20 and TARA149 (Supplementary figure b. 6) also accumulate intracellularly but showed no photocurrents (data not shown), suggesting a common localization predisposition but different function from VR1 rhodopsins.

As we have demonstrated, ChR2 also accumulates intracellularly to a certain extent (the ratio lysis/surface luminescence is ≈ 2), even though it is not its predominant localization. One asks why ChR2 does not have the same effect of consistently activating CaCCs as OLPVR1, since it could potentially permeate Ca^{2+} from intracellular stores. Indeed our observations, as well as Nagel *et al.* (2003) show that the activation of CaCCs by ChR2 occurs only when the driving force for Ca^{2+} entry through the membrane is high.

We first hypothesized that ChR2 was unable to function in the lipid context of the ER since it is ultimately a plasma membrane protein. However, the lipid context might not explain the difference. Asano *et al.* (2018) have demonstrated that ChR2 can in fact be retained and function from the ER, once it is fused to the fourth transmembrane helix of the ryanodine receptor, and lead to the release of intracellular calcium.

To explain the difference in the results we obtained for ChR2 and OLPVR1, one possibility is that retention of ChR2 in intracellular membranes is not strong or long-lived enough.

Another possibility is that ChR2 expression at the surface, bound to retinal molecules, acts as a light absorption barrier that blocks green light from penetrating into deeper regions of the cell, similar to how melanin acts for UV light. In that situation, intracellular ChR2 is not photoactivated and thus cannot activate CaCCs. We did not address this question, but co-expression of both ChR2 and OLPVR1 could tell us if this is the case, if in this situation OLPVR1 is unable to activate CaCCs.

3.4.3 OLPVR1 selectivity remains to be fully elucidated

The most parsimonious explanation for our observations would imply OLPVR1 permeating Ca^{2+} directly from the calcium stores into the cytoplasm down its electrochemical gradient. However, we were not able to determine with confidence the selectivity of OLPVR1. Expression at the surface of OLPVR1 was accomplished by fusing it to DOR but photocurrents were still low and difficult to record reliably.

The measurement of calcium entry is often complicated by the close arrangement between calcium-entry channels and CaCCs. For instance, Kolesnikov *et al.* (2021) have shown that

BAPTA was inefficient to stop CaCCs activation induced by Ca^{2+} entry through SOCE channels. Indeed, to record SOCE channels the protocols require the use of both BAPTA and La^{3+} – a blocker of SOCE. Only the La^{3+} -inhibited current corresponds to SOCE current (Machaca & Haun, 2000). This is due to the fact that Ca^{2+} entry through a channel can raise Ca^{2+} levels transiently to hundreds of μM in the immediate vicinity of the channel, with a flow too fast to be captured by BAPTA (reviewed in Rizutto & Pozzan, 2006). Parekh (2008) estimated using fluorescent dyes that 1 mM BAPTA restricts the micro-domain of calcium entry to 22.4 nm, which justifies the inefficiency in uncoupling closely-arranged calcium channels and calcium effectors.

In our experiments, assuming the oocyte is a sphere with a radius of 0.55 mm and a consequent total volume of 0.7 μl , the injection of 50 nl of 40 mM BAPTA yields an estimated intracellular BAPTA concentration of 3 mM. We could hypothesize that, if OLPVR1 is permeating Ca^{2+} at the membrane, we might not be able to fully block its activation of CaCCs. These are however speculations. We cannot exclude with certainty the possibility that OLPVR1 might depend on another transducing pathway to activate calcium release.

It is important to note that VirChR1, which we have established, has a photoresponse profile similar to OLPVR1 in *Xenopus* oocytes, has been described as a cationic channel impermeable to Ca^{2+} (Zabelskii *et al.*, 2020). VirChR1 (61% sequence similarity with OLPVR1) was expressed in human neuroblastoma cells and showed Na^+ and K^+ currents (but not Ca^{2+}) blocked by external Ca^{2+} at millimolar concentrations (50% block at ≈ 2 mM Ca^{2+}).

This observation does not fit with our data. Even assuming OLPVR1 would be impermeant to Ca^{2+} , its activity seems unlikely to be blocked by Ca^{2+} , since during calcium release it is bound to be exposed to high calcium concentrations. Furthermore, DOR=OLPVR1, when exposed to much higher extracellular calcium concentrations (49 mM Ca^{2+}) still exhibited observable currents.

Curiously, Yellen (1982) described a class of non-selective cation channels in neuroblastoma cells activated by micromolar concentrations of Ca^{2+} on the intracellular face of the membrane. The channels were equally permeable to Na^+ , K^+ but practically impermeable to Ca^{2+} . One could question if VirChR1 is acting in neuroblastoma cells as OLPVR1 acts in *Xenopus* oocytes or HEK293T cells, i.e., leading to the release of intracellular Ca^{2+} that acts on Ca^{2+} effectors at the membrane.

Another possibility to explain the response of OLPVR1 involves the intracellular acidification of the oocyte. Intracellular acidification induced by exposing the oocyte to an extracellular

acidic medium has been shown to trigger both calcium release and calcium influx (Marin *et al.*, 2010).

Both OLPVR1 (Zabelskii *et al.*, 2020) and VirRDTS (Needham *et al.*, 2019) seem to pump protons when expressed in *E. coli*. Furthermore, VirChR1 also channels protons (Zabelskii *et al.*, 2020). It is not uncommon that rhodopsins show some level of proton pumping, which is also true for ChR2 (Feldbauer *et al.*, 2009). However, intracellular acidification with the consequent activation of CaCCs has not been reported when coexpressing proton channels in *Xenopus*. For instance, ChR1 (Nagel *et al.*, 2001) can produce large (several μA) currents from proton entry without eliciting CaCCs. We did not explore the possibility of proton channeling by OLPVR1, and we cannot exclude that proton pumping/channeling from organelles might trigger calcium release.

If OLPVR1 directly permeates calcium or activates endogenous calcium channels through another transducing pathway remains to be verified.

Even if our observations do not match those in Zabelskii *et al.* (2020) what seems clear is that these proteins have an intricate relationship with calcium. A full battery of solution exchanges, as well as pharmacological inhibition of endogenous channels, might be necessary to disclose the true selectivity of VR1.

3.5 Conclusion and perspectives

In this project, we were able to detect the photoresponse of three members of the VR1 family. This was only made possible by the fact that their activity coupled with the calcium-activated endogenous channels of *Xenopus*, which acted as reporters and amplifiers of the calcium release mediated by VR1 proteins.

Interestingly, OLPVR1 is acting in oocytes in a manner analogous to the proposed biological function of VRs and Channelrhodopsins (Harz & Hegemann, 1991). That is, their activation upon irradiation induces the release of calcium from intracellular stores, which in algae is instead transmitted to the flagellar base (rather than chloride channels), allowing phototactic motion of the host.

We were not able to fully understand the selectivity of OLPVR1 but it is clear OLPVR1 has the ability to integrate with calcium signaling, both in *Xenopus* as well as in mammalian HEK293T cells.

Ca²⁺ is a ubiquitous intracellular messenger. The precise release of calcium from intracellular stores mediates a panoply of transduction cascades and cellular processes such as gene expression, neurotransmitter release, hormone release, or muscle contraction (reviewed in Demarex *et al.*, 2003). It relies on the large driving force created by maintaining the Ca²⁺ concentrations in the cytoplasm low (<100 nM) compared to the extracellular (1-2 mM) or intracellular store Ca²⁺ concentrations (hundreds of μM in the ER lumen). Mobilization of intracellular calcium has been made possible by pharmacological approaches. However, leveraging the spatiotemporal resolution of light delivery could enable more precise control of calcium release with potential advantages on our understanding of calcium signaling.

The propensity of the VR1 to accumulate in internal storages and modulate calcium release, in a tunable manner depending on the light intensity, makes it a great candidate as a novel optogenetic tool, with potential applications in the manipulation of numerous aspects of cell activity. Precisely identifying the selectivity of VRs would be a necessary milestone to understand the full scope of its utility as an optogenetic tool, but experiments are already on the way to test the OLPVR1 effects both in DRG neurons (Dr. Guillaume Sandoz lab) as well as in muscle fibers of mice (Dr. Bruno Allard lab).

4. Materials and Methods

4.1 Molecular Biology

Genes and expression vectors

All genes, except for M2 and M3, were subcloned in the oocyte high-expression vector pXOOM (Jespersen *et al.*, 2002), which contains untranslated regulatory regions (UTR) of the β -globin gene of *Xenopus laevis* (Krieg *et al.*, 1984) to boost expression (Figure 4.1). Genes coding for M2 and M3 were subcloned in pGEMHE-derived pGH2 vector (Kan^R) containing the same UTRs. Both pXOOM and pGH2 plasmids contain a Kanamycin resistance gene. Genes were inserted by PCR after the T7 promoter and in between the 5'UTR and 3'UTR of β -globin.

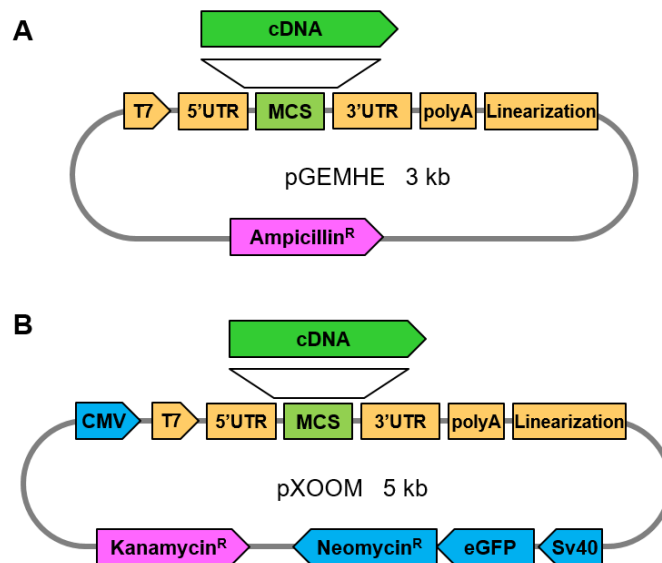


Figure 4.1. *Xenopus* oocyte expression vectors.

(A) The pGEMHE vector incorporates the 5' and 3' untranslated regions of the *Xenopus* β -globin gene. These flanking sequences enhance expression of the gene cloned in the multiple cloning sites region (MCS). The upstream T7 promoter is used to initiate *in vitro* transcription by the T7 RNA polymerase. The linearization region contains several rare restriction sites that are used to linearize the plasmid before transcription.

(B) The pXOOM vector retains the features of pGEMHE while adding a cytomegalovirus (CMV) promoter to drive expression in mammalian cells when necessary, as well as GFP-fused neomycin resistance gene for identification and selection of transfected mammalian cells.

From Vivaudou *et al.*, 2017.

Annex C Table c.1 & 2 list information on all genes/constructs used in Projects A & B, respectively, including names, origins, and accession numbers, when applicable, as well as annotations about protein size, design, and molecular manipulation performed.

Mutagenesis

Mutagenesis of genes in Tables C.1 & 2 was performed by PCR using the QuickChange Lightning site-directed mutagenesis kit (#210519, Agilent), unless when annotated with 'GeneCust' or 'GenScript'. In that case, the construct was produced by the specified company.

The different types of molecular manipulations performed can be divided into point mutations, codon insertions, and large fragment insertions/substitutions.

Point mutations and codon insertions were obtained by a single PCR round with symmetric primers (20-24 nucleotides) containing the desired residues at the center of the primer sequence.

Large fragment insertions/substitutions were obtained through two sequential PCRs. The first PCR amplifies the insertion fragment of interest from a template, while simultaneously adding flanking regions on both sides of the fragment. For that purpose, each primer comprises a stretch of 20 nucleotides that hybridize with the fragment of interest and 30 flanking nucleotides. The second PCR uses the product of the first PCR as primers. The 30-nucleotide flanking regions will hybridize to the left and right insertion sites on the recipient vector priming amplification while introducing the new fragment.

All primers were synthesized by Eurofins. PCR mix and conditions were as per the supplier's instructions.

For strategies that comprised two PCR steps, the product of the first PCR was separated by electrophoresis in a TAE (Tris-acetate-ethylenediamine tetraacetic acid) 0.8% agarose gel stained with GelRed (#41002, Biotium). Purification of the PCR product was performed using the QIAquick Gel Extraction Kit (#28706, Qiagen) as per the supplier's instructions. The purified DNA was quantified by spectrophotometry using a NanoDrop 2000c and 700 ng was used as primers for the second PCR.

Protein constructs annotated with the tag 'SS-' were fused, at the N-terminal after the first methionine, with the signal sequence of the human nicotinic acetylcholine $\alpha 7$ receptor (Amino

acid sequence = RCSPGGVWLALAASLLHVSLQGEF). Protein constructs annotated with the tag '-MT' -were fused at the C-terminal, before the stop codon, with the Golgi export trafficking signal sequence from human Kir2.1 potassium channels (Amino acid sequence = KSRITSEGEYIPLDQIDINV). Insertions of the corresponding nucleotidic sequences were performed by PCR.

Subcloning

Subcloning of genes in Tables C.1 & 2 from an original plasmid into pXOOM was performed by PCR, using the QuickChange Lightning site-directed mutagenesis kit (#210519, Agilent).

Subcloning was achieved through two sequential PCRs. The first PCR amplifies the gene of interest from the original plasmid, while simultaneously adding flanking regions on both sides of the gene. The flanking regions correspond to the left and right insertion sites on the new plasmid. A second PCR uses the product of the first PCR as primers. Flanking regions will hybridize with the new plasmid and allow insertion of the gene. Purification of the product of the first PCR and PCR conditions were as described in the previous section.

Selection of positive clones and amplification of genetic material

The final PCR product was digested with the restriction enzyme DpnI for 20-120 min, and transformed into XL10-Gold ultra-competent cells, provided in the QuickChange Lightning site-directed mutagenesis kit (#210519, Agilent). The transformation was performed as per the supplier's instructions and cells were plated in LB Agar medium supplemented with kanamycin (50 µg/ml) and incubated overnight at 37°C.

Individual colonies were inoculated into 15 mL of LB Broth supplemented with kanamycin (50 µg/ml) and incubated overnight at 37°C and 180 RPM. Small-scale plasmid purification was performed using the NucleoSpin Plasmid Quick Pure Kit (#740615, Macherey-Nagel) as per the supplier's instructions.

Purified plasmids were assessed by Sanger sequencing of the mutagenized regions. Sanger sequencing was performed by GeneWiz.

Colonies hosting the plasmid with the correct gene sequence were re-picked from the original plate into 50 ml LB Broth supplemented with kanamycin (50 µg/ml) and incubated overnight at 37°C and 180 RPM. Large-scale DNA extraction was performed using the QIAfilter Plasmid

Midi Kit (#12245, Qiagen) as per the supplier's instructions.

The integrity of the coding sequences in the purified plasmid was accessed by fully sequencing the genes from the promotor T7 until the stop codon.

***In vitro* transcription**

In vitro transcription was performed with nuclease-free and sterile materials in a dedicated fumehood cleansed with RNase decontamination solution.

Plasmid DNA (3 µg) was digested for 60-180 min with a restriction enzyme with a single-cutting site after the PolyA sequence of the plasmid (Linearization region in Figure 4.1). The linearized plasmid was then purified with phenol/chloroform and resuspended in 10 µl of autoclaved DEPC¹⁶-treated (RNase-free) water. A sample of the purified DNA was quantified by spectrophotometry using a NanoDrop 2000c.

mRNA was prepared following the protocol supplied with the mMessage mMACHINE T7 Transcription Kit (#AM1344, Invitrogen) using 1 µg of purified linearized template DNA. RNA was purified either by phenol/chloroform or using the NucleoSpin RNA XS purification kit (#740902, Macherey-Nagel). mRNA was resuspended in 20 µl of DEPC-treated water and stored at -80°C until use. When not at -80°C, RNAs were kept on ice.

A sample of the purified mRNA was quantified by spectrophotometry using a NanoDrop 2000c. Only samples with absorption ratios A₂₆₀/A₂₈₀ and A₂₆₀/A₂₃₀ equal or above 2 were kept. The integrity of the mRNA samples was assessed through electrophoresis in a TAE 0.8% agarose gel stained with GelRed (#41002, Biotium).

¹⁶ Diethyl pyrocarbonate.

4.2 Heterologous expression in *Xenopus* oocytes

Preparation of oocytes

Xenopus laevis ovary lobes were available from two sources:

- (1) collected from animals maintained in the animal facilities of the Commissariat à l'Énergie atomique - Grenoble, France;
- (2) received from the commercial seller CRB Xénopes Université de Rennes 1 - Rennes, France.

Using forceps, the ovarian lobes were gently pulled apart in a 60-mm plastic Petri dish with Collagenase Solution.

Collagenase Solution was prepared with:

88 mM NaCl, 1 mM KCl, 2.4 mM NaHCO₃, 0.82 mM MgSO₄, 16 mM NaOH-HEPES (pH 7.4) + 2 mg/ml of collagenase (#C9891, Sigma-Aldrich).

The dish was incubated at 19°C and 80 RPM for approximately 120 min and frequently checked under a microscope for completion of digestion. Digestion was halted once most oocytes were free from the ovary conjunctive tissue and with no apparent blood vessels on the surface. At this stage, the oocytes were subjected to several washes in the same solution without collagenase. Once the solution appeared free of debris, the oocytes were washed and transferred to a new Petri dish with Ringer's oocyte solution:

88 mM NaCl, 1 mM KCl, 2.4 mM NaHCO₃, 0.82 mM MgSO₄, 0.3 mM Ca(NO₃)₂, 0.41 mM CaCl₂, 16 mM NaOH-HEPES (pH 7.4).

The oocytes were sorted under a binocular microscope with a 40X magnification. Only intact oocytes at stages V–VI oocytes (1-1.2 mm with contrasted cream and dark brown hemispheres separated by a light equatorial line) were selected. The selected oocytes were transferred to a sterile Petri dish with Ringer's oocyte solution supplemented with 100 U/ml penicillin, 100 µg/ml streptomycin, and 100 µg/ml gentamycin. Oocytes were kept at 19°C until use.

Figure 4.2 shows a graphical representation of the general experimental procedures for the characterization of membrane proteins using *Xenopus* oocytes.

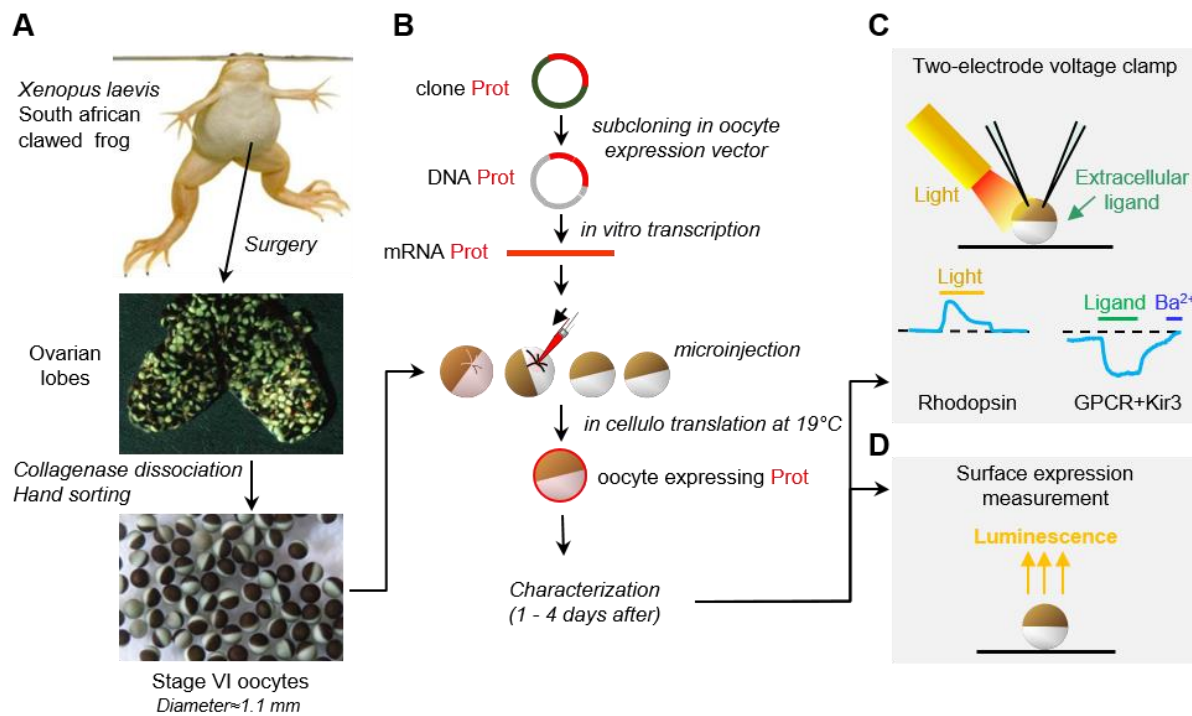


Figure 4.2. Experimental protocol for *in vitro* characterization of potassium channels and light-regulated transporters in *Xenopus* oocytes.

(A) Oocytes are harvested weekly from *Xenopus* frogs.

(B) Wild-type and mutant protein genes are inserted in a pGEMHE or pXOOM vector. Oocytes injected with the constructs RNA are maintained at 19°C and characterized by electrophysiological techniques 1 to 4 days later.

(C) Whole-oocyte currents are measured using the TEVC technique using manual or robotic setups.

(D) Surface and total expression can be measured using XenoGlo technique.

RNA microinjection

In vitro transcribed RNAs were quantified by spectrophotometry with a NanoDrop 2000c and a working dilution was prepared in DEPC-treated water. The concentration of the working dilutions was calculated such that the injection of 50 nl corresponds to the amount of RNA injected per oocyte specified in the results.

The amount of Kir3.4* mRNA was adjusted through the months to account for oocyte expression variability. In months where oocytes displayed higher expression the amount was decreased to avoid K⁺ depletion in the oocyte and the consequent loss of viability due to the large basal activity of Kir3.4*.

To prepare microinjection pipettes, borosilicate glass capillaries with 0.53 mm inner diameter (#3-000-203-G/X, Drummond Scientific) were pulled using a laser pipette puller Model P-2000 (Sutter Instrument Co.) with the following parameters:

Heat=290, Fil=5, Vel=100, Del=200, Pul=125.

These parameters were optimized empirically to produce an injection pipette with an elongated shank with a gradual uniform taper and a submicron tip. The pipettes were then broken under a microscope equipped with a calibrated eyepiece reticle to yield a $\approx 20 \mu\text{m}$ diameter tip.

The injection pipettes were backfilled with light mineral oil (#M5904, Sigma-Aldrich) using 30G hypodermic needles (#3-000-027, Drummond Scientific) and mounted on the piston of a Microinjector NanoJect II (Drummond Scientific). The use of mineral oil avoids evaporation of the sample. The microinjection pipette was then filled with RNA by aspirating a 1-3 μl droplet of the working dilution of RNA.

Already dissociated and selected oocytes were placed in a 35-mm Petri dish with Ringer's oocyte solution and positioned on a $\approx 0.8 \text{ mm}$ nylon mesh grid glued at the bottom to hold the oocytes. Using a 3-axis manual manipulator mounted to the microinjector and a binocular microscope with a 40X magnification, oocytes were injected one by one with 50 nl of working dilution of RNA.

Once injected, the oocytes were transferred to 96-well plates with conical bottoms (#732-0812, NUNC) filled with 230 μl of incubation solution.

For Project A the incubation solution was a Ringer's oocyte solution supplemented with 100 U/ml penicillin, 100 $\mu\text{g/ml}$ streptomycin, and 100 $\mu\text{g/ml}$ gentamycin. Oocytes were kept at 19°C until use.

For Project B the incubation solution was the same solution as in Project A supplemented with 1 μM all-trans retinal (#R2500, Sigma-Aldrich).

All-trans retinal stock was prepared as a 10 mM solution in ethanol (#4145872, CARLO ERBA Reagents) and stored at -20°C in black polypropylene tubes until use. Oocytes were kept at 19°C and in the dark until use.

4.3 Protein expression measurement by luminescence assays in *Xenopus* oocytes

This section focus on the methodological details of a protocol for protein expression detection based on Nanoluciferase and optimized for the use in *Xenopus* oocytes.

The principle and validation of the method can be found in Annex D.

Design of HiBiT fusion constructs

HiBiT fusion constructs correspond to the proteins of interest fused to the HiBiT tag which, by complementation with the LgBit of Nanoluciferase and in the presence of its substrate, can produce strong luminescence. To be able to detect the surface expression of a protein through this system, the HiBiT tag has to be in an extracellular domain of the protein.

Protein constructs annotated with the tag '-HB' were fused at the extracellular N-terminal after the first methionine, with the HiBiT tag, followed by a flexible GS linker. The amino acid sequence of the HiBiT tag is VSGWRLFKKIS and that of the linker was GSSGGS or GSSGGSSG.

Protein constructs annotated with the tag 'IL6-' were further fused, upstream of the HiBiT tag, with the Interleukin-6 secretion signal peptide (IL6; Amino acid sequence = NSFSTSAFGPVAFSLGLLLVLPAAFPAP). To ensure the integrity of the HiBiT tag upon signal peptide removal, a two amino acid linker (VS) was added between IL6 and HiBiT tag.

Insertions of the corresponding nucleotidic sequences in the genes of interest were performed by PCR.

Experimental conditions

Oocytes injected with mRNA coding for HiBiT-tagged proteins were kept at 19°C for 24-48 h to allow for expression. After the incubation period, the oocytes were transferred and positioned with the animal pole (dark brown pole) facing up in a white round-bottom 96-well plate (#054311, NUNC Dutscher) containing 100 µl of Ringer's oocyte solution in each well.

Three wells with 100 µl of Ringer's oocyte solution without oocyte were used as blanks. Three wells with oocytes expressing untagged proteins were used as a control.

For surface luminescence measurement the kit used was Nano-Glo HiBiT Extracellular Detection System (#N2421, Promega).

The Nano-Glo HiBiT Extracellular reagent was prepared as a master mix with a total volume of 100 µl/oocyte + 600 µl for triplicate blank and control wells. The reagent comprised a 1:100 dilution of the LgBiT protein and 1:50 dilution of HiBiT Extracellular Substrate in the HiBiT Extracellular Buffer, all provided in the kit. The mix was vortexed, spun down, and distributed in the wells using a dispenser pipette set to 100 µl.

After 10 minutes of incubation at 19°C and 200 RPM the plate was transferred to a CLARIOstar plate reader (BMG Labtech). Relative luminescence units were recorded for each well from a top optic with a focal height of 11 mm and the gain set to 3500.

For luminescence measurement of lysed cells the kit used was Nano-Glo HiBiT Lytic Detection System (#N3040, Promega).

Oocytes subjected to surface luminescence measurements were washed for ≈30 seconds in Ringer's oocyte solution with gentle agitation and transferred to a new white round-bottom 96-well plate (#054311, NUNC Dutscher) containing 100 µl of Ringer's oocyte solution in each well. The protocol for luminescence measurement of lysed oocytes was the same as for surface luminescence measurement, except for the solutions which are specific for the lytic kit, namely HiBiT Lytic Substrate and HiBiT Lytic Buffer.

Analysis of luminescence data

Relative luminescence units for each well were extracted from the CLARIOstar software into a .txt file. Blank correction, outlier exclusion, and data plotting were automated by the use of the excel macro eeDataStat developed by Dr. Michel Vivaudou.

Results are shown as histograms of averaged blank-corrected RLUs of single oocytes, or triplicates when indicated. Most experiments were performed with at least two different batches of oocytes. Experiments where N was less than 6 oocytes were performed with a single batch of oocytes. Error bars represent the standard error of the mean (SEM). Statistical analysis was done using GraphPad Prism 8.

4.4 Functional study of membrane proteins by electrophysiology techniques in *Xenopus* oocytes

Configuration of the TEVC setup

In a standard TEVC setup, an oocyte is immobilized in a recording chamber and manually impaled by 2 microelectrodes under a microscope. The microelectrode measuring heads are mounted on two manual manipulators inside a Faraday cage and connected to an amplifier - digitizer - computer on the outside. For stable recordings, the recording chamber with the impaled oocyte is perfused continuously with a bath solution and the voltage is clamped to a chosen value. Test compounds are applied by switching the bath solutions perfused. Because the flow speed needs to be high to achieve rapid exchange of the bathing solution in the chamber, large volumes of solutions are necessary (20-40 ml for a full day of experiments). In our lab, the TEVC setup uses an Amplifier GeneClamp 500B from Axon Instruments (Molecular Devices), a Digitizer Digidata 1440A from Axon Instruments, and a ValveLink8 eight-channel perfusion system with a manually operated controller (ValveLink8.2 Controller) from AutoMate Scientific.

In contrast, automated TEVC relies on the HiClamp Robot (MultiChannel Systems, Germany) (see Figure 4.3) connected to a computer with the HiClamp software where a protocol for the recordings can be pre-set. The design of the protocol requires the identification and plate position of the oocytes/solutions, value of membrane potential to impose, the time of recording in each solution as well as sampling and filtering rates.

A typical recording on HiClamp follows the following steps:

- (1) Transfer of the oocyte from the 96-well plate with conical bottoms (#732-0812, NUNC) into a miniature movable basket.
- (2) Wash of the oocyte in a central chamber perfused by a standard bath solution under continuous flow.
- (3) Impalement of the oocyte, voltage clamp, and measurement of current in a standard bath solution. If the oocyte does not pass the quality control check it is discarded.
- (4) If the oocyte passes the quality control point it is sequentially transferred, while recording, to the wells of a flat-bottom 96-well plate (#353072, BD Falcon) containing the different solutions to be tested (250 μ l). The homogeneity of the solution is maintained by using

magnetic microstirrers inside of each test well.

(5) At the end of the recording the oocyte is transferred back to the original plate and the robot repeats the protocol with the next oocyte in line.

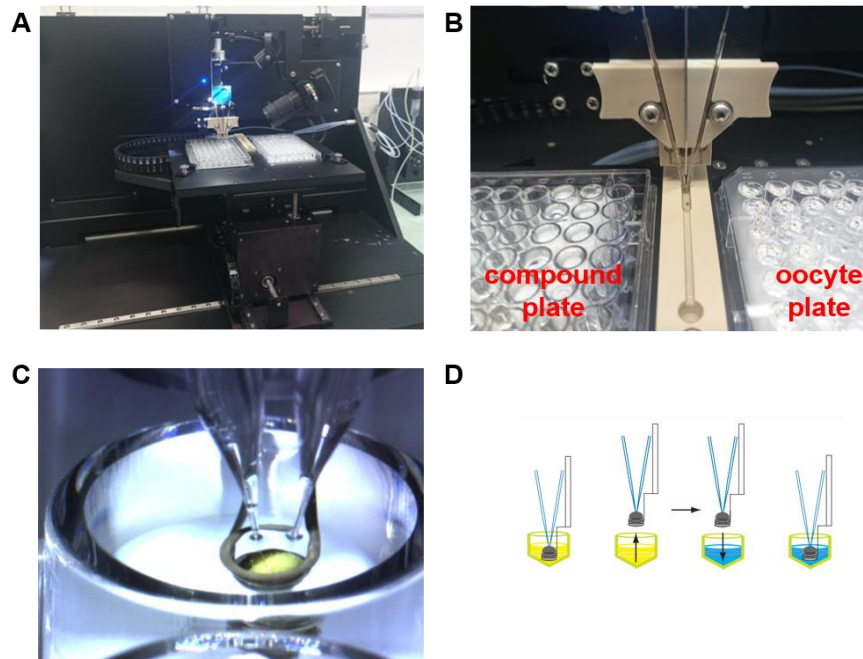


Figure 4.3. HiClamp robot.

(A) Overview of the HiClamp robot.

(B) Close-up of A showing the compound plate on the left, the wash chamber in the center, and the oocyte plate on the right. The oocyte is impaled by the electrodes in the wash chamber.

(C) Close-up showing the wire basket with an oocyte which is impaled by the 2 recording glass microelectrodes. The oocyte is in a compound well above a white magnetic microstirrer, necessary to guarantee homogeneous application of compound.

(D) Schematics illustrating how an oocyte travels from one well to the next (drawing courtesy of MultiChannel Systems). Adapted from Vivaudou *et al.*, 2017.

To prepare the recording microelectrodes, thin-wall capillaries with filament (#TW150F-4, World Precision Instruments) were pulled using a laser puller Sutter Instrument Co. Model P-2000 with the following parameters:

Heat=375, Fil=4, Vel=35, Del=250, Pul=90.

These parameters were optimized empirically to yield a microelectrode with a resistance of $\approx 0.3 \text{ M}\Omega$.

The microelectrodes were 1/3 backfilled with filtered ($0.22 \mu\text{m}$) 3 M KCl using a needle and ensuring no air bubbles form at the tip that could increase the resistance. Microelectrodes were then mounted around the wire silver chloride electrodes on the measuring heads of the TEVC setups.

Project A

Experimental conditions

Whole-cell currents were recorded by TEVC using the HiClamp Robot 24-48 h after injection. Voltage was generally clamped at -50 mV, current was filtered at 500 Hz and sampled at 1000 Hz. Time in the different solutions tested is indicated in the results.

Bath solutions

An adaption of the ND96 solution, defined by Dascal *et al.* (1993), was used as a low K⁺ solution:

91 mM NaCl, 2 mM KCl, 1.8 mM CaCl₂, 1 mM MgCl₂, 0.3 mM Niflumic acid, 5 mM HEPES (pH 7.4). pH was adjusted with NaOH.

All recordings started with a measurement of currents in ND96. Oocytes with large currents (< -1 μA) were rejected since it is expected that healthy oocytes have no significant ion permeability in these conditions.

High K⁺ solution (hK⁺) was prepared with:

91 mM KCl, 1.8 mM CaCl₂, 1 mM MgCl₂, 0.3 mM Niflumic acid, 5 mM HEPES (pH 7.4). pH was adjusted with KOH.

In these conditions, Kir3 channel potassium currents are inward and are represented by convention by negative values.

Ba²⁺ solution was applied at the end of each recording and it was prepared with:

hK⁺ solution + 3 mM BaCl₂ (pH 7.4).

Ba²⁺ is a generic K⁺ channel blocker which serves to estimate the amount of observable current generated specifically by potassium channels.

Agonists

All agonists were prepared with hK⁺ solution in the specified concentrations except when oocytes tested were solely injected with M3 mRNA. In that case, the agonist (acetylcholine) was prepared with ND96.

Table 4.1. List of agonists used in Project A

Agonist	Stock concentration	Solvent	Storage conditions
Acetylcholine (#A6625, Sigma-Aldrich)	5 mM	nuclease-free water	-20°C
Adenosine (# 3624, Tocris)	10 mM	nuclease-free water	-20°C
DADLE (#E7131, Sigma-Aldrich)	1 mM	nuclease-free water	-20°C
DALE (#E5008, Sigma-Aldrich)	1 mM	nuclease-free water	-20°C
DAMGO (#ab120674, Abcam)	1 mM	nuclease-free water	-20°C
SNC80 (#sc-203267, Santa Cruz Biotechnology, Inc.)	1 mM	DMSO (Dimethylsulfoxide, #D8418, Sigma-Aldrich)	4°C

Inhibitors

Stock solutions of all the inhibitors were kept at -20°C until use. All inhibitors were prepared to a working concentration with oocyte Ringer's solution.

Table 4.2. List of inhibitors used in Project A

Inhibitor	Stock concentration	Solvent	Working concentration	Incubation time
CMPD101 (#5642, Tocris)	1 mM	DMSO	200 µM	60 min
Gallein (#3090, Tocris)	75 mM	DMSO	200 µM	60 min
SU 6656 (#6475, Tocris)	10 mM	DMSO	30 µM	120 min
PP1 (#1397, Tocris)	10 mM	DMSO	30 µM	120 min
YM-254890 (#21910-1590, Tebu-BIO)	1 mM	DMSO	10 µM	10 min

Data processing and analysis

HiClamp export software (custom made for this project by MultiChannel Systems) was used to convert HiClamp files (proprietary file format) into Microsoft Excel-readable files. To reduce the dataset sizes, HiClamp recordings transferred to Excel were undersampled to 10 Hz, a frequency sufficient to resolve the fastest events in our experiments.

Annotation, plotting and analysis of the recording traces were performed in Microsoft Excel 2016 and automated by the use of Excel macros eeTEVC, eeSTAT and eeFIT developed by Dr. Michel Vivaudou (Vivaudou *et al.*, 2017; Vivaudou, 2019; see Figure 4.4).

Most experiments were performed with at least two different batches of oocytes. Experiments where N was less than 6 oocytes were performed with a single batch of oocytes. Error bars represent the standard error of the mean (SEM). Statistical analysis was done using GraphPad Prism 8.

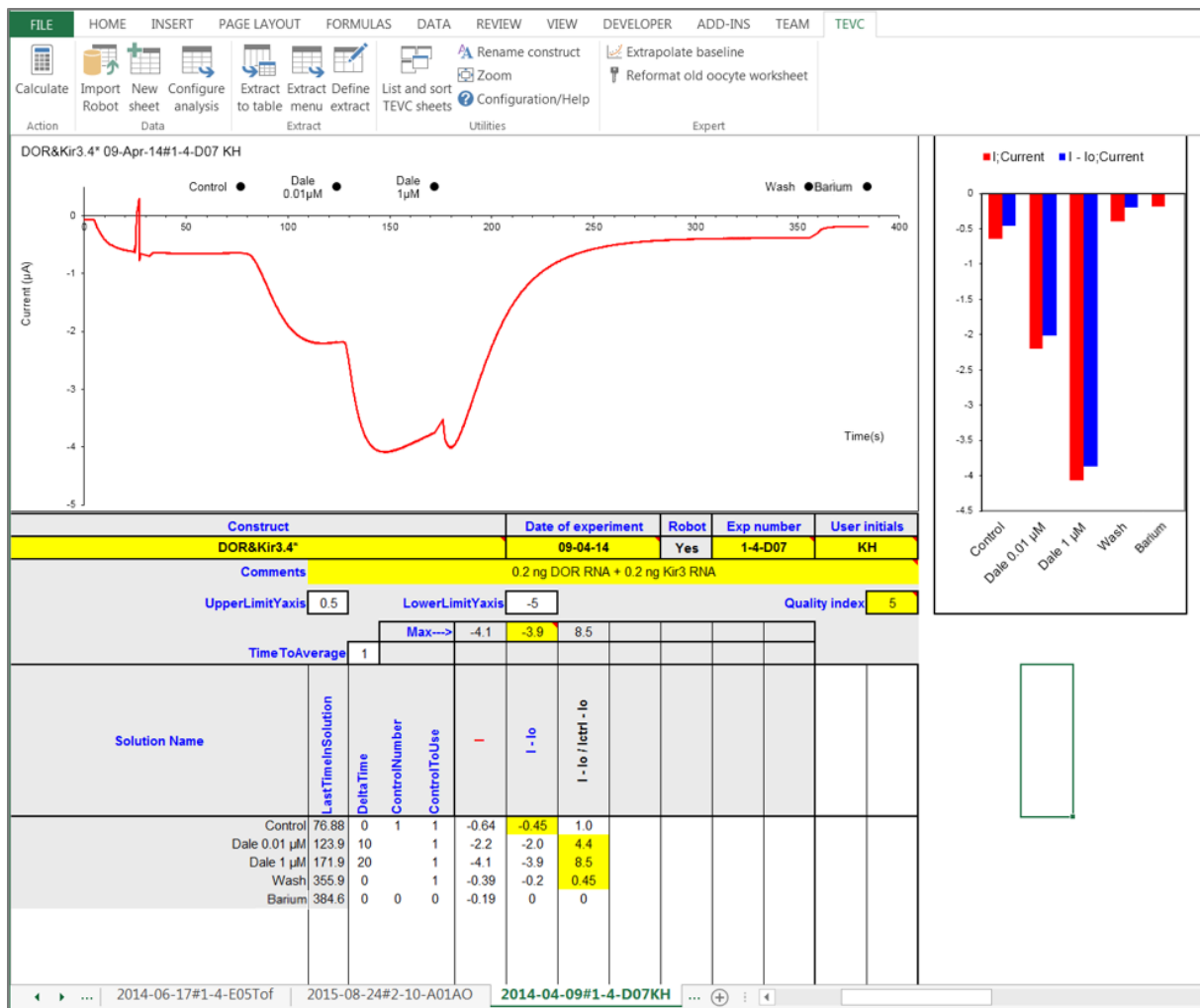


Figure 4.4. Example of GIRK data obtained with the HiClamp robot.

The full-length DOR was co-expressed with the GIRK channel Kir3.4*.

The 385-second test sequence consisted of:

- 1) Wash with Low-K⁺ solution for 5 s;
- 2) Wash with High-K⁺ solution for 30 s (with an IV curve recorded at t=25 s);
- 3) In-well Control (i.e., High-K⁺ solution) for 40 s;
- 4) In-well application of agonist DALE at 10 nM for 40 s;
- 5) In-well application of agonist DALE at 1 µM for 40 s;
- 6) In-well wash-out for 180 s;
- 7) In-well application of blocker Barium at 3 mM for 30 s.

The figure is a screen capture of Microsoft Excel running the eeTEVC macro, after import of robot-recorded data.

From Vivaudou *et al.*, 2017.

Project B

Experimental conditions

Oocyte whole-cell ionic currents were recorded by TEVC 24-96 h after injection using a GeneClamp 500B Amplifier from Axon Instruments, a Digitizer Digidata 1440A from Axon Instruments and an eight-channel perfusion system with a manually operated controller from AutoMate Scientific. Currents were filtered at 3 KHz and sampled at 10 KHz.

Voltage was clamped at the specified values in different bath solutions. 505 nm-light was applied for 10 seconds with an OPTOLED LITE dual LED light source from CAIRN, placed 3 cm above the oocyte (input power consumption of 1 Watt).

Bath solutions

Table 4.3. List of bath solutions used in Project B.

Concentration are presented in mM.

Solution	NaCl	KCl	CaCl ₂	MgCl ₂	TrisCl	ArginineCl	HEPES ¹⁷	Glucose	EGTA
ND96	91	2	1.8	1	0	0	5	0	0
ND96 0 Ca ²⁺	91	2	0	1	0	0	5	0	0
49 Ca ²⁺	0	0	49	1	0	0	5	47	0
94 K ⁺ 100Cl ⁻	0	94	2	1	0	0	5	0	0
94 K ⁺ 100 Cl ⁻ EGTA	0	94	0	1	0	0	5	0	1
94 Na ⁺ 100 Cl ⁻	94	0	2	1	0	0	5	0	0
94 Tris ⁺ 100 Cl ⁻	0	0	2	1	94	0	0	5	0
94 Arginine ⁺ 100 Cl ⁻	0	0	1	1	0	94	5	0	0
48 Mg ²⁺ 100 Cl ⁻	0	0	2	48	0	0	5	47	0

All bath solutions had a pH of 7.4. The solutions pH was adjusted with Tris or Citric acid, except for ND96 and ND96 0 Ca²⁺ where NaOH was used.

Inhibitors

BAPTA (#2786, Tocris) 40 mM stock solution was prepared in 160 mM KOH (pH 7) and kept at -20°C. In experiments with BAPTA_{in}, oocytes were injected with 50 nl of stock solution of 40 mM K-BAPTA pH 7 and were left incubating in oocyte Ringer's solution for at least 30 min before recording.

Stock solutions of all the inhibitors were kept at -20°C until use. Working dilutions of the

¹⁷ 4-(2-Hydroxyethyl)-1-piperazineethanesulfonic acid.

remaining inhibitors tested were prepared in the specified solutions (either ND96 or 49 Ca²⁺).

Table 4.4. List of inhibitors used in Project B

Inhibitor	Stock concentration	Solvent	Working concentration	Incubation time
2-APB (#1224, Tocris)	100 mM	DMSO	200 μ M	20-180 min
Ani9 (#6076, Tocris)	10 mM	DMSO	30 μ M	30-180 min
BAPTA-AM (#A1076, Sigma-Aldrich)	100 mM	DMSO	100 μ M	240 min
MONNA (#5770, Tocris)	10 mM	DMSO	30 μ M	120 min
Niflumic acid (#N0630, Sigma-Aldrich)	300 mM	DMSO	0.3-3 mM	60-300 min
YM-254890 (#21910-1590, Tebu-BIO)	1 mM	DMSO	10 μ M	10 min

Data processing and analysis

Data acquisition was performed using pClamp software (Molecular Devices). Data points from recordings were extracted from pClamp files into Excel using Clampfit. Extraction imposed a reduction of the data sampling to 10 Hz. Annotation, plotting, and analysis of the recording traces was automated by the use of Excel macros eeTEVC and eeSTAT developed by Michel Vivaudou (Vivaudou *et al.*, 2017). Basal leak currents were subtracted for clarity and varied in amplitude depending on the batch of the oocytes ($E_{rev} \approx E_{Cl}$).

Most experiments were performed with at least two different batches of oocytes. Experiments where N was less than 6 oocytes were performed with a single batch of oocytes. Error bars represent the standard error of the mean (SEM). Statistical analysis was done using GraphPad Prism 8.

4.5 Functional validation of OLPVR1 by electrophysiology techniques in HEK293T cells

The experiments to validate the function of OLPVR1 in mammalian cells were performed by the team of Dr. Guillaume Sandoz at the Institut de Biologie Valrose, Université Nice Sophia Antipolis.

HEK293T cells (ATCC, #CRL11268) were maintained in DMEM¹⁸ supplemented with 10% FBS¹⁹ in 35-mm dishes. At 70–80% confluency cells were transiently cotransfected with plasmids encoding OLPVR1 (in vector pIRES2-EGFP) with either mouse TMEM16A variant "a" (ANO1; in pmCherry-N1 from Clontech), or human SK1 (isoform 1, KCNN1; in pcDNA3.1) using the calcium phosphate method (CaCl₂ 2.5M) with a total amount of 1.2 and 2.4 mg of DNA, respectively, and seeded on 35 mm diameter plates.

HEK293T cell electrophysiology was performed 24-48h after transfection. For whole-cell patch-clamp experiments, cells were recorded in a bath solution containing 150 mM NaCl, 5 mM KCl and 10 mM HEPES, with or without 2 mM CaCl₂, pH 7.4. The glass pipettes (2-5 MΩ resistance) were filled with 155 mM KCl, 3 mM MgCl₂, 10 mM HEPES, with or without 1 mM EGTA, pH 7.3.

HEK293T cells were recorded at room temperature in voltage-clamp mode using an Axopatch 200B (Molecular Devices) amplifier. Signals were filtered at 10 kHz and digitalized at 20 kHz. Whole-cell currents were elicited by voltage ramps from -100 to +100 mV (1 s), or voltage steps from -100 to +100 mV in 20 mV increments (1 s each pulse), holding the cells at -80 mV. Current densities were measured at +100 mV for TMEM16A and 0 mV for SK1. Cell recordings, data acquisition and analysis were performed using pClamp software (Molecular Devices).

¹⁸ Gibco Dulbecco's Modified Eagle *Medium*.

¹⁹ Fetal bovine serum.

References

- Adamantidis, A. R., Zhang, F., Aravanis, A. M., Deisseroth, K., & De Lecea, L. (2007). Neural substrates of awakening probed with optogenetic control of hypocretin neurons. *Nature*, 450(7168), 420–424.
- Airan, R. D., Thompson, K. R., Fenno, L. E., Bernstein, H., & Deisseroth, K. (2009). Temporally precise *in vivo* control of intracellular signalling. *Nature*, 458(7241), 1025–1029.
- Ågren, R., & Sahlholm, K. (2021). G protein-coupled receptor kinase-2 confers isoform-specific calcium sensitivity to dopamine D2 receptor desensitization. *FASEB Journal*, 35(11), e22013.
- Aguado, C., Colón, J., Ciruela, F., Schlaudraff, F., Cabañero, M. J., Perry, C., Watanabe, M., Liss, B., Wickman, K., & Luján, R. (2008). Cell type-specific subunit composition of G protein-gated potassium channels in the cerebellum. *Journal of Neurochemistry*, 105(2), 497–511.
- Al-Hasani, R., & Bruchas, M. R. (2011). Molecular mechanisms of opioid receptor-dependent signaling and behavior. *Anesthesiology*, 115(6), 1363–1381.
- Allouche, S., Noble, F., Marie, N., & Mollereau, C. (2014). Opioid receptor desensitization : mechanisms and its link to tolerance. *Frontiers in Pharmacology*, 5, 280.
- Asano, T., Igarashi, H., Ishizuka, T., & Yawo, H. (2018). Organelle optogenetics: Direct manipulation of intracellular Ca²⁺ dynamics by light. *Frontiers in Neuroscience*, 12(AUG), 1–8.
- Audet, N., Galés, C., Archer-Lahlou, É., Vallières, M., Schiller, P. W., Bouvier, M., & Pineyro, G. (2008). Bioluminescence resonance energy transfer assays reveal ligand-specific conformational changes within preformed signaling complexes containing δ -opioid receptors and heterotrimeric G proteins. *Journal of Biological Chemistry*, 283(22), 15078–15088.
- Barish, M. E. (1983). A transient calcium-dependent chloride current in the immature *Xenopus* oocyte. *Journal of Physiology*, 342, 309–325.
- Beddell, C. R., Clark, R. B., Hardy, G. W., Lowe, L. A., Ubatuba, F. B., Vane, J. R., & Wilkinson, S. (1977). Structural requirements for opioid activity of analogues of the enkephalins. *Proceedings of the Royal Society of London - Biological Sciences*, 198(1132), 249–265.
- Béjà, O., Aravind, L., Koonin, E. V., Suzuki, M. T., Hadd, A., Nguyen, L. P., Jovanovich, S. B., Gates, C. M., Feldman, R. A., Spudich, J. L., Spudich, E. N., & DeLong, E. F. (2000). Bacterial rhodopsin: Evidence for a new type of phototrophy in the sea. *Science*, 289(5486), 1902–1906.
- Berlin, S., Artzy, E., Handklo-Jamal, R., Kahanovitch, U., Parnas, H., Dascal, N., & Yakubovich, D. (2020). A collision coupling model governs the activation of neuronal GIRK1/2 channels by Muscarinic-2 receptors. *Frontiers in Pharmacology*, 11, 1216.
- Berndt, A., Lee, S. Y., Ramakrishnan, C., & Deisseroth, K. (2014). Structure-Guided Transformation of Channelrhodopsin into a Light-Activated Chloride Channel. *Science*, 344(6182), 420–424.

- Berndt, A., Yizhar, O., Gunaydin, L. A., Hegemann, P., & Deisseroth, K. (2009). Bi-stable neural state switches. *Nature Neuroscience*, 12(2), 229–234.
- Bichet, D., Haass, F. A., Jan, L. Y., & Medical, H. H. (2003). Merging functional studies with structures of inward-rectifier K⁺ channels. *Nature Reviews Drug Discovery*, 4(12), 957–967.
- Blanchet, C., & Lüscher, C. (2002). Desensitization of mu-opioid receptor-evoked potassium currents: initiation at the receptor, expression at the effector. *Proceedings of the National Academy of Sciences of the United States of America*, 99(7), 4674–4679.
- Blednov, Y. A., Stoffel, M., Alva, H., & Harris, R. A. (2003). A pervasive mechanism for analgesia: Activation of GIRK2 channels. *Proceedings of the National Academy of Sciences of the United States of America*, 100(1), 277–282.
- Boorman, J. P. B., Groot-Kormelink, P. J., & Sivilotti, L. G. (2000). Stoichiometry of human recombinant neuronal nicotinic receptors containing the $\beta 3$ subunit expressed in *Xenopus* oocytes. *Journal of Physiology*, 529(3), 565–577.
- Boursier, M. E., Levin, S., Zimmerman, K., MacHleidt, T., Hurst, R., Butler, B. L., Eggers, C. T., Kirkland, T. A., Wood, K. V., & Ohana, R. F. (2020). The luminescent HiBiT peptide enables selective quantitation of G protein-coupled receptor ligand engagement and internalization in living cells. *Journal of Biological Chemistry*, 295(15), 5124–5135.
- Boyd, J. S., Mittelmeier, T. M., & Dieckmann, C. L. (2011). New insights into eyespot placement and assembly in *Chlamydomonas*. *BioArchitecture*, 1(4), 196–199.
- Boyden, E. S., Zhang, F., Bamberg, E., Nagel, G., & Deisseroth, K. (2005). Millisecond-timescale, genetically targeted optical control of neural activity. *Nature Neuroscience*, 8(9), 1263–1268.
- Brackley, A. D., Gomez, R., Akopian, A. N., Henry, M. A., & Jeske, N. A. (2016). GRK2 constitutively governs peripheral Delta Opioid Receptor activity. *Cell Reports*, 16(10), 2686–2698.
- Brandt, M. R., Furness, M. S., Rice, K. C., Fischer, B. D., & Negus, S. S. (2001). Studies of tolerance and dependence with the delta-opioid agonist SNC80 in rhesus monkeys responding under a schedule of food presentation. *The Journal of Pharmacology and Experimental Therapeutics*, 299(2), 629–637.
- Bratanov, D., Kovalev, K., Machtens, J. P., Astashkin, R., Chizhov, I., Soloviov, D., Volkov, D., Polovinkin, V., Zabelskii, D., Mager, T., Gushchin, I., Rokitskaya, T., Antonenko, Y., Alekseev, A., Shevchenko, V., Yutin, N., Rosselli, R., Baeken, C., Borshchevskiy, V., ... Gordeliy, V. (2019). Unique structure and function of viral rhodopsins. *Nature Communications*, 10(1), 4939.
- Broom, D. C., Nitsche, J. F., Pintar, J. E., Rice, K. C., Woods, J. H., & Traynor, J. R. (2002). Comparison of receptor mechanisms and efficacy requirements for delta-agonist-induced convulsive activity and antinociception in mice. *The Journal of Pharmacology and Experimental Therapeutics*, 303(2), 723–729.
- Bukiya, A. N., Durdagim, S., Noskov, S., & Rosenhouse-Dantske, A. (2017). Cholesterol up-regulates neuronal G protein-gated inwardly rectifying potassium (GIRK) channel activity in the hippocampus. *Journal of Biological Chemistry*, 292(15), 6135–6147.
- Cahill, C. M., Holdridge, S. V., & Morinville, A. (2007). Trafficking of δ -opioid receptors and other G protein-coupled receptors: implications for pain and analgesia. *Trends in Pharmacological Sciences*, 28(1), 23–31.

- Cahill, C.M., McClellan, K., Morinville, A., Hoffert, C., Hubatsch, D., O'Donnell, D., & Beaudet, A. (2001). Immunohistochemical distribution of delta opioid receptors in the rat central nervous system: Evidence for somatodendritic labeling and antigen-specific cellular compartmentalization. *Journal of Comparative Neurology*, 440(1), 65–84.
- Cahill, C. M., Morinville, A., Lee, M. C., Vincent, J. P., Collier, B., & Beaudet, A. (2001). Prolonged morphine treatment targets δ opioid receptors to neuronal plasma membranes and enhances δ -mediated antinociception. *Journal of Neuroscience*, 21(19), 7598–7607.
- Casey, L. M., Pistner, A. R., Belmonte, S. L., Migdalovich, D., Stolpnik, O., Nwakanma, F. E., Vorobiof, G., Dunaevsky, O., Mavel, A., Lopes, C., Smrcka, A. V., & Blaxall, B. C. (2010). Small molecule disruption of G $\beta\gamma$ signaling inhibits the progression of heart failure. *Circulation Research*, 107(4), 532–539.
- Castonguay, A., & Robitaille, R. (2002). Xestospongine C is a potent inhibitor of SERCA at a vertebrate synapse. *Cell Calcium*, 32(1), 39–47.
- Cen, B., Yu, Q., Guo, J., Wu, Y., Ling, K., Cheng, Z., & Ma, L. (2001). Direct binding of beta-arrestins to two distinct intracellular domains of the delta opioid receptor. *Journal of Neurochemistry*, 76(6), 1887–1894.
- Chan, K. W., Sui, J.-L., Vivaudou, M., & Logothetis, D. E. (1996). Control of channel activity through a unique amino acid residue of a G protein-gated inwardly rectifying K⁺ channel subunit. *Proceedings of the National Academy of Sciences of the United States of America*, 93(24), 14193–14198.
- Charbogne, P., Kieffer, B. L., & Befort, K. (2014). 15 years of genetic approaches *in vivo* for addiction research: Opioid receptor and peptide gene knockout in mouse models of drug abuse. *Neuropharmacology*, 76(B), 204–217.
- Charfi, I., Audet, N., Bagheri Tudashki, H., & Pineyro, G. (2015). Identifying ligand-specific signalling within biased responses: focus on δ opioid receptor ligands. *British Journal of Pharmacology*, 172(2), 435–448.
- Chen, Y., Mestek, A., Liu, J., Hurley, J. A., & Yu, L. (1993). Molecular cloning and functional expression of a mu opioid receptor from rat brain. *Molecular Pharmacology*, 44(1), 8–12.
- Chow, B. Y., Han, X., Dobry, A. S., Qian, X., Chuong, A. S., Li, M., Henninger, M. A., Belfort, G. M., Lin, Y., Monahan, P. E., & Boyden, E. S. (2010). High-performance genetically targetable optical neural silencing by light-driven proton pumps. *Nature*, 463(7277), 98–102.
- Chuang, H. H., Yu, M., Jan, Y. N., & Jan, L. Y. (1998). Evidence that the nucleotide exchange and hydrolysis cycle of G proteins causes acute desensitization of G-protein gated inward rectifier K⁺ channels. *Proceedings of the National Academy of Sciences of the United States of America*, 95(20), 11727–11732.
- Chung, M. K., Cho, Y. S., Bae, Y. C., Lee, J., Zhang, X., & Ro, J. Y. (2014). Peripheral G protein-coupled inwardly rectifying potassium channels are involved in δ opioid receptor-mediated anti-hyperalgesia in rat masseter muscle. *European Journal of Pain (United Kingdom)*, 18(1), 29–38.
- Chung, P. C. S., & Kieffer, B. L. (2013). Delta opioid receptors in brain function and diseases. *Pharmacology & Therapeutics*, 140(1), 112–120.

- Chuong, A. S., Miri, M. L., Busskamp, V., Matthews, G. A. C., Acker, L. C., Sørensen, A. T., Young, A., Klapoetke, N. C., Henninger, M. A., Kodandaramaiah, S. B., Ogawa, M., Ramanlal, S. B., Bandler, R. C., Allen, B. D., Forest, C. R., Chow, B. Y., Han, X., Lin, Y., Tye, K. M., ... Boyden, E. S. (2014). Noninvasive optical inhibition with a red-shifted microbial rhodopsin. *Nature Neuroscience*, 17(8), 1123–1129.
- Ciruela, F., Fernández-Dueñas, V., Sahlholm, K., Fernández-Alacid, L., Nicolau, J. C., Watanabe, M., & Luján, R. (2010). Evidence for oligomerization between GABAB receptors and GIRK channels containing the GIRK1 and GIRK3 subunits. *European Journal of Neuroscience*, 32(8), 1265–1277
- Clancy, S. M., Fowler, C. E., Finley, M., Suen, K. F., Arrabit, C., Berton, F., Kosaza, T., Casey, P. J., & Slesinger, P. A. (2005). Pertussis-toxin-sensitive G α subunits selectively bind to C-terminal domain of neuronal GIRK channels: Evidence for a heterotrimeric G-protein-channel complex. *Molecular and Cellular Neuroscience*, 28(2), 375–389.
- Colman, A., Bhamra, S., & Valle, G. (1984). Post-translational modification of exogenous proteins in *Xenopus laevis* oocytes. *Biochemical Society Transactions*, 12(6), 932–937.
- Copits, B. A., Pullen, M. Y., & Gereau IV, R. W. (2016). Spotlight on pain: optogenetic approaches for interrogating somatosensory circuits. *Pain*, 157(11), 2424–2433.
- Corder, G., Castro, D. C., Bruchas, M. R., & Scherrer, G. (2018). Endogenous and exogenous opioids in pain. *Annual Review of Neuroscience*, 41, 453–473.
- Courjaret, R., & Machaca, K. (2016). *Xenopus* oocyte as a model system to study store-operated Ca²⁺ entry (SOCE). *Frontiers in Cell and Developmental Biology*, 4, 66.
- Cruz, H. G., Ivanova, T., Lunn, M. L., Stoffel, M., Slesinger, P. A., & Lüscher, C. (2004). Bi-directional effects of GABAB receptor agonists on the mesolimbic dopamine system. *Nature Neuroscience*, 7(2), 153–159.
- Cvejic, S., & Devi, L. A. (1997). Dimerization of the δ Opioid Receptor: Implications for a role in receptor internalization. *Journal of Biological Chemistry*, 272(43), 26959–26964.
- Dascal, N., Lim, N. F., Schreibmayer, W., Wang, W., Dascal, N., Lim, N. F., Schreibmayert, W., Wang, W., Davidson, N., & Lester, H. A. (1993). Expression of an atrial G-Protein-Activated Potassium Channel in *Xenopus* Oocytes. *Proceedings of the National Academy of Sciences of the United States of America*, 90(14), 6596–6600.
- Deisseroth, K. (2015). Optogenetics: 10 years of microbial opsins in neuroscience. *Nature Neuroscience*, 18(9), 1213–1225.
- Deisseroth, K., Feng, G., Majewska, A. K., Miesenböck, G., Ting, A., & Schnitzer, M. J. (2006). Next-generation optical technologies for illuminating genetically targeted brain circuits. *Journal of Neuroscience*, 26(41), 10380–10386.
- Demaurex, N., & Frieden, M. (2003). Measurements of the free luminal ER Ca²⁺ concentration with targeted “cameleon” fluorescent proteins. *Cell Calcium*, 34(2), 109–119.
- De Robertis, E. M., & Gurdon, J. B. (2021). A Brief history of *Xenopus* in Biology. *Cold Spring Harbor Protocols*, 2021(12), pdb.top107615.

- Doupnik, C. A. (2015). Chapter 3 - RGS redundancy and implications in GPCR-GIRK signaling. In P. A. Slesinger & W. Kevin (Eds.), *International Review of Neurobiology* (1st ed., Vol. 123, pp. 87–116). Academic Press.
- Doupnik, C. A., Davidson, N., Lester, H. A., & Kofuji, P. (1997). RGS proteins reconstitute the rapid gating kinetics of G $\beta\gamma$ -activated inwardly rectifying K⁺ channels. *Proceedings of the National Academy of Sciences of the United States of America*, 94(19), 10461–10466.
- Dripps, I. J., Wang, Q., Neubig, R. R., Rice, K. C., Traynor, J. R., & Jutkiewicz, E. M. (2017). The role of regulator of G protein signaling 4 in delta-opioid receptor-mediated behaviors. *Psychopharmacology*, 234(1), 29–39.
- Durisic, N., Godin, A. G., Wever, C. M., Heyes, C. D., Lakadamyali, M., & Dent, J. A. (2012). Stoichiometry of the human glycine receptor revealed by direct subunit counting. *Journal of Neuroscience*, 32(37), 12915–12920.
- Ernst OP, Lodowski DT, Elstner M, Hegemann P, Brown LS, Kandori H (2014). Microbial and Animal Rhodopsins: Structures, Functions, and Molecular Mechanisms. *Chemical Reviews*, 114(1), 126–163.
- Evans, C. J., Keith, D. E., Morrison, H., Magendzo, K., & Edwards, R. H. (1992). Cloning of a delta opioid receptor by functional expression. *Science*, 258(5090), 1952–1955.
- Fagerberg, L., Hallstro, M., Oksvold, P., Kampf, C., Djureinovic, D., Odeberg, J., Habuka, M., Tahmasebpoor, S., Danielsson, A., Edlund, K., Asplund, A., Sjo, E., Lundberg, E., Szigartyo, C. A., Skogs, M., Ottosson, J., Berling, H., Tegel, H., Mulder, J., ... Uhle, M. (2014). Analysis of the human tissue-specific expression by genome-wide integration of transcriptomics and antibody-based proteomics. *Molecular and Cellular Proteomics*, 13(2), 397–406. <https://www.proteinatlas.org/> Version:21 updated: 2021-11-18.
- Feldbauer, K., Zimmermann, D., Pintschovius, V., Spitz, J., Bamann, C., & Bamberg, E. (2009). Channelrhodopsin-2 is a leaky proton pump. *Proceedings of the National Academy of Sciences of the United States of America*, 106(30), 12317–12322.
- Fenalti G, Giguere PM, Katritch V, Huang X-P, Thompson AA, Cherezov V, Stevens RC (2014). Molecular control of δ -opioid receptor signalling. *Nature*, 506(7487), 191–196.
- Ferenczi, E. A., Tan, X., & Huang, C. L. H. (2019). Principles of optogenetic methods and their application to cardiac experimental systems. *Frontiers in Physiology*, 10, 1096.
- Fernández-Alacid, L., Watanabe, M., Molnár, E., Wickman, K., & Luján, R. (2011). Developmental regulation of G protein-gated inwardly-rectifying K⁺ (GIRK/Kir3) channel subunits in the brain. *The European Journal of Neurosciences*, 34(11), 1724–1736.
- Fourie, C., Li, D., & Montgomery, J. M. (2014). The anchorin protein SAP97 influences the trafficking and localisation of multiple membrane channels. *Biochimica et Biophysica Acta (BBA) - Biomembranes*, 1838(2), 589–594.
- Galés, C., Van Durm, J. J. J., Schaak, S., Pontier, S., Percherancier, Y., Audet, M., Paris, H., & Bouvier, M. (2006). Probing the activation-promoted structural rearrangements in preassembled receptor-G protein complexes. *Nature Structural & Molecular Biology*, 13(9), 778–786.
- Gendron, L., Cahill, C. M., Zastrow, M. Von, Schiller, P. W., & Pineyro, G. (2016). Molecular pharmacology of δ -opioid receptors. *Pharmacological Reviews*, 68(3), 631–700.

- George, S. R., Fan, T., Xie, Z., Tse, R., Tam, V., Varghese, G., & O'Dowd, B. F. (2000). Oligomerization of μ - and δ -opioid receptors: Generation of novel functional properties. *Journal of Biological Chemistry*, 275(34), 26128–26135.
- Gilman, A. G. (1987). G proteins: transducers of receptor-generated signals. *Annual Review of Biochemistry*, 56(1), 615–649.
- Glaaser, I. W., & Slesinger, P. A. (2015). Chapter Four - Structural insights into GIRK channel function. In P. A. Slesinger & W. Kevin (Eds.), *International Review of Neurobiology* (1st ed., Vol. 123, pp. 117–160). Academic Press.
- Gomes, I., Jordan, B. A., Gupta, A., Trapaidze, N., Nagy, V., & Devi, L. A. (2000). Heterodimerization of mu and delta opioid receptors: A role in opiate synergy. *The Journal of Neuroscience*, 20(22), RC110.
- Gómez-Consarnau, L., Raven, J. A., Levine, N. M., Cutter, L. S., Wang, D., Seegers, B., Arístegui, J., Fuhrman, J. A., Gasol, J. M., & Sañudo-Wilhelmy, S. A. (2019). Microbial rhodopsins are major contributors to the solar energy captured in the sea. *Science Advances*, 5(8), eaaw8855.
- Gradinaru, V., Thompson, K. R., & Deisseroth, K. (2008). eNpHR: A *Natronomonas halorhodopsin* enhanced for optogenetic applications. *Brain Cell Biology*, 36(1–4), 129–139.
- Granier, S., Manglik, A., Kruse, A. C., Kobilka, T. S., Thian, F. S., Weis, W. I., & Kobilka, B. K. (2012). Structure of the δ -opioid receptor bound to naltrindole. *Nature*, 485(7398), 400–404.
- Greiner, T., Moroni, A., Van Etten, J. L., & Thiel, G. (2018). Genes for membrane transport proteins: Not so rare in viruses. *Viruses*, 10(9), 456.
- Gross, W., & Lohse, M. J. (1991). Mechanism of activation of A2 adenosine receptors. II. A restricted collision-coupling model of receptor-effector interaction. *Molecular Pharmacology*, 39(4), 524–530.
- Gunaydin, L. A., Yizhar, O., Berndt, A., Sohal, V. S., Deisseroth, K., & Hegemann, P. (2010). Ultrafast optogenetic control. *Nature Neuroscience*, 13(3), 387–392.
- Guo, J., Wu, Y., Zhang, W., Zhao, J., Devi, L. A., Pei, G., & Ma, L. (2000). Identification of G protein-Coupled Receptor Kinase 2 phosphorylation sites responsible for agonist-stimulated δ -Opioid receptor phosphorylation. *Molecular Pharmacology*, 58(5), 1050–1056.
- Gupta, A., Mulder, J., Gomes, I., Rozenfeld, R., Bushlin, I., Ong, E., Lim, M., Maillet, E., Junek, M., Cahill, C. M., Harkany, T., & Devi, L. A. (2010). Increased abundance of opioid receptor heteromers after chronic morphine administration. *Science Signaling*, 3(131), 1–8.
- Gurdon, J. B., Lane, C. D., Woodland, H. R., & Marbaix, G. (1971). Use of frog eggs and oocytes for the study of messenger RNA and its translation in living cells. *Nature*, 233, 177–182.
- Gurevich, V. V., & Gurevich, E. V. (2019). GPCR signaling regulation: The role of GRKs and arrestins. *Frontiers in Pharmacology*, 10, 125.
- Gushchin, I., Shevchenko, V., Polovinkin, V., Kovalev, K., Alekseev, A., Round, E., Borshchevskiy, V., Balandin, T., Popov, A., Gensch, T., Fahlke, C., Bamann, C., Willbold, D., Büldt, G., Bamberg, E., & Gordeliy, V. (2015). Crystal structure of a light-driven sodium pump. *Nature Structural and Molecular Biology*, 22(5), 390–396.

- Hagiwara, S., Miyazaki, S., Moody, W., & Patlak, J. (1978). Blocking effects of barium and hydrogen ions on the potassium current during anomalous rectification in the starfish egg. *The Journal of Physiology*, 279, 167–185.
- Hagiwara, S., Miyazaki, S., & Rosenthal, N. P. (1976). Potassium current and the effect of cesium on this current during anomalous rectification of the egg cell membrane of a starfish. *Journal of General Physiology*, 67(6), 621–638.
- Hamacher, K., Greiner, T., Ogata, H., van Etten, J. L., Gebhardt, M., Villarreal, L. P., Cosentino, C., Moroni, A., & Thiel, G. (2012). Phycodnavirus potassium ion channel proteins question the virus molecular piracy hypothesis. *PLOS ONE*, 7(6), e38826.
- Han, X., & Boyden, E. S. (2007). Multiple-color optical activation, silencing, and desynchronization of neural activity, with single-spike temporal resolution. *PLOS ONE*, 2(3), e299.
- Hartzell, H. C. (1996). Activation of different Cl currents in *Xenopus* oocytes by Ca liberated from stores and by capacitative Ca influx. *Journal of General Physiology*, 108(3), 157–175.
- Harz, H., & Hegemann, P. (1991). Rhodopsin-regulated calcium currents in *Chlamydomonas*. In *Nature* (Vol. 351, Issue 6326, pp. 489–491).
- Hatcher-Solis, C., Fribourg, M., Spyridaki, K., Younkin, J., Ellaithy, A., Xiang, G., Liapakis, G., Gonzalez-Maeso, J., Zhang, H., Cui, M., & Logothetis, D. E. (2014). G protein-coupled receptor signaling to Kir channels in *Xenopus* oocytes. *Current Pharmaceutical Biotechnology*, 15(10), 987–995.
- Headrick, J. P., See Hoe, L. E., Du Toit, E. F., & Peart, J. N. (2015). Opioid receptors and cardioprotection - “opioidergic conditioning” of the heart. *British Journal of Pharmacology*, 172(8), 2026–2050.
- Heginbotham, L., Lu, Z., Abramson, T., & Mackinnon, R. (1994). Mutations in the K⁺ channel signature sequence. *Biophysical Journal*, 66(4), 1061–1067.
- Hibino, H., Inanobe, A., Furutani, K., Murakami, S., Findlay, I., & Kurachi, Y. (2010). Inwardly rectifying potassium channels: their structure, function, and physiological roles. *Physiological Reviews*, 90(1), 291–366.
- Hight AE, Kozin ED, Darrow K, Lehmann A, Boyden E, Brown MC, Lee DJ (2015) Superior temporal resolution of Chronos versus Channelrhodopsin-2 in an optogenetic model of the auditory brainstem implant, *Hear Res.*, 322, 235-241.
- Hille, B. (2001). *Ion Channels of Excitable Membranes* (Third Edit). Sinauer Associates, Inc.
- Ho, I. H., & Murrell-Lagnado, R. D. (1999). Molecular determinants for sodium-dependent activation of G protein-gated K⁺ channels. *The Journal of Biological Chemistry*, 274(13), 8639–8648.
- Hofherr, A., Fakler, B., & Klöcker, N. (2005). Selective Golgi export of Kir2.1 controls the stoichiometry of functional Kir2.x channel heteromers. *Journal of Cell Science*, 118(9), 1935–1943.
- Hong, M. H., Xu, C., Wang, Y. J., Ji, J. L., Tao, Y. M., Xu, X. J., Chen, J., Xie, X., Chi, Z. Q., & Liu, J. G. (2009). Role of Src in ligand-specific regulation of δ -opioid receptor desensitization and internalization. *Journal of Neurochemistry*, 108(1), 102–114.

- Husson, S. J., Liewald, J. F., Schultheis, C., Stirman, J. N., Lu, H., & Gottschalk, A. (2012). Microbial light-activatable proton pumps as neuronal inhibitors to functionally dissect neuronal networks in *C. elegans*. *PLOS ONE*, 7(7), e40937.
- Imai, K., & Nakai, K. (2020). Tools for the recognition of sorting signals and the prediction of subcellular localization of proteins from their amino acid sequences. *Frontiers in Genetics*, 11, 607812.
- Ikeda, K., Kobayashi, T., Kumanishi, T., Niki, H., & Yano, R. (2000). Involvement of G protein-activated inwardly rectifying K⁺ (GIRK) channels in opioid-induced analgesia. *Neuroscience Research*, 38(1), 113–116.
- Inanobe, A., Yoshimoto, Y., Horio, Y., Morishige, K. I., Hibino, H., Matsumoto, S., Tokunaga, Y., Maeda, T., Hata, Y., Takai, Y., & Kurachi, Y. (1999). Characterization of G protein-gated K⁺ channels composed of Kir3.2 Subunits in dopaminergic neurons of the substantia nigra. *Journal of Neuroscience*, 19(3), 1006–1017.
- Jeremic, D., Sanchez-rodriguez, I., Jimenez-diaz, L., & Navarro-lopez, J. D. (2021). Therapeutic potential of targeting G protein-gated inwardly rectifying potassium (GIRK) channels in the central nervous system. *Pharmacology and Therapeutics*, 223, 107808.
- Jespersen, T., Grunnet, M., Angelo, K., Klærke, D. A., & Olesen, S. P. (2002). Dual-function vector for protein expression in both mammalian cells and *Xenopus laevis* oocytes. *BioTechniques*, 32(3), 536–540.
- Jimenez-Vargas, N. N., Gong, J., Wisdom, M. J., Jensen, D. D., Latorre, R., Hegron, A., Teng, S., DiCello, J. J., Rajasekhar, P., Veldhuis, N. A., Carbone, S. E., Yu, Y., Lopez-Lopez, C., Jaramillo-Polanco, J., Canals, M., Reed, D. E., Lomax, A. E., Schmidt, B. L., Leong, K. W., ... Poole, D. P. (2020). Endosomal signaling of delta opioid receptors is an endogenous mechanism and therapeutic target for relief from inflammatory pain. *Proceedings of the National Academy of Sciences of the United States of America*, 117(26), 15281–15292.
- Jin, W., & Lu, Z. (1998). A novel high-affinity inhibitor for inward-rectifier K⁺ channels. *Biochemistry*, 37(38), 13291–13299.
- Johnston, J. M., Aburi, M., Provasi, D., Bortolato, A., Urizar, E., Lambert, N. A., Javitch, J. A., & Filizola, M. (2011). Making structural sense of dimerization interfaces of delta opioid receptor homodimers. *Biochemistry*, 50(10), 1682–1690.
- Jutkiewicz, E. M., Rice, K. C., Traynor, J. R., & Woods, J. H. (2005). Separation of the convulsions and antidepressant-like effects produced by the delta-opioid agonist SNC80 in rats. *Psychopharmacology*, 182(4), 588–596.
- Kimura, M., Shiokawa, H., Karashima, Y., Sumie, M., Hoka, S., & Yamaura, K. (2020). Antinociceptive effect of selective G protein-gated inwardly rectifying K⁺ channel agonist ML297 in the rat spinal cord. *PLOS ONE*, 15(9 September), 1–14.
- Kahanovitch, U., Tsemakhovich, V., Berlin, S., Rubinstein, M., Styr, B., Castel, R., Peleg, S., Tabak, G., Dessauer, C. W., Ivanina, T., & Dascal, N. (2014). Recruitment of Gβγ controls the basal activity of G protein coupled inwardly rectifying potassium (GIRK) channels: Crucial role of distal C terminus of GIRK1. *Journal of Physiology*, 592(24), 5373–5390.
- Kapur, A., Derry, J. M. C., & Hansen, R. S. (2007). Expression and study of ligand-gated ion channels in *Xenopus laevis* oocytes. In A. Lajtha, G. Baker, S. Dunn, & A. Holt (Eds.), *Handbook of Neurochemistry and Molecular Neurobiology* (pp. 323–340). Springer Boston.

- Karoussiotis, C., Marti-Solano, M., Stepniewski, T. M., Symeonof, A., Selent, J., & Georgoussi, Z. (2020). A highly conserved δ -opioid receptor region determines RGS4 interaction. *FEBS Journal*, 287(4), 736–748.
- Karschin, C., Dißmann, E., Stühmer, W., & Karschin, A. (1996). IRK(1-3) and GIRK(1-4) inwardly rectifying K^+ channel mRNAs are differentially expressed in the adult rat brain. *Journal of Neuroscience*, 16(11), 3559–3570.
- Kato, H. E., Zhang, F., Yizhar, O., Ramakrishnan, C., Nishizawa, T., Hirata, K., Ito, J., Aita, Y., Tsukazaki, T., Hayashi, S., Hegemann, P., Maturana, A. D., Ishitani, R., Deisseroth, K., & Nureki, O. (2012). Crystal structure of the channelrhodopsin light-gated cation channel. *Nature*, 482(7385), 369–374.
- Keiper, B. D. (2003). Translation of mRNAs in *Xenopus* Oocytes. In *Encyclopedia of Life Sciences* (p. <http://www.els.net>). John Wiley & Sons, Ltd.
- Kieffer, B. L., Befort, K., Gaveriaux-Ruff, C., & Hirth, C. G. (1992). The δ -opioid receptor: Isolation of a cDNA by expression cloning and pharmacological characterization. *Proceedings of the National Academy of Sciences of the United States of America*, 89(24), 12048–12052.
- Kiehn, J., Lacerda, A. E., Wible, B., & Brown, A. M. (1996). Molecular physiology and pharmacology of HERG. Single-channel currents and block by dofetilide. *Circulation*, 94(10), 2572–2579.
- Kimura, M., Shiokawa, H., Karashima, Y., Sumie, M., Hoka, S., & Yamaura, K. (2020). Antinociceptive effect of selective G protein-gated inwardly rectifying K^+ channel agonist ML297 in the rat spinal cord. *PLOS ONE*, 15(9 September), 1–14.
- Kleinlogel S, Feldbauer K, Dempski RE, Fotis H, Wood PG, Bamann C, Bamberg E. (2011) Ultra light-sensitive and fast neuronal activation with the Ca^{2+} - permeable channelrhodopsin CatCh, *Nat. Neurosci.*, 14, 513-518.
- Kleinlogel, S., Terpitz, U., Legrum, B., Göckbuget, D., Boyden, E. S., Bamann, C., Wood, P. G., & Bamberg, E. (2011). A gene-fusion strategy for stoichiometric and co-localized expression of light-gated membrane proteins. *Nature Methods*, 8(12), 1083–1091.
- Kobrinisky, E., Mirshahi, T., Zhang, H., Jin, T., & Logothetis, D. E. (2000). Receptor-mediated hydrolysis of plasma membrane messenger PIP_2 leads to K^+ -current desensitization. *Nature Cell Biology*, 2(8), 507–514.
- Koehl, A., Hu, H., Maeda, S., Zhang, Y., Qu, Q., Paggi, J. M., Latorraca, N. R., Hilger, D., Dawson, R., Matile, H., Schertler, G. F. X., Granier, S., Weis, W. I., Dror, R. O., Manglik, A., Skiniotis, G., & Kobilka, B. K. (2018). Structure of the μ -opioid receptor-Gi protein complex. *Nature*, 558(7711), 547–552.
- Kolesnikov, D., Perevoznikova, A., Gusev, K., Glushankova, L., Kaznacheyeva, E., & Shalygin, A. (2021). Electrophysiological properties of endogenous single Ca^{2+} activated Cl^- channels induced by local Ca^{2+} entry in HEK293. *International Journal of Molecular Sciences*, 22(9), 4767.
- Kouhen, O. M., Wang, G., Solberg, J., Erickson, L. J., Law, P. Y., & Loh, H. H. (2000). Hierarchical phosphorylation of delta-opioid receptor regulates agonist-induced receptor desensitization and internalization. *The Journal of Biological Chemistry*, 275(47), 36659–36664.
- Kovoor, A., Nappey, V., Kieffer, B. L., & Chavkin, C. (1997). μ and δ opioid receptors are differentially desensitized by the coexpression of β -adrenergic receptor kinase 2 and β -arrestin 2 in *Xenopus* oocytes. *Journal of Biological Chemistry*, 272(44), 27605–27611.

- Koyrakh, L., Luján, R., Colón, J., Karschin, C., Kurachi, Y., Karschin, A., & Wickman, K. (2005). Molecular and cellular diversity of neuronal G protein-gated potassium channels. *Journal of Neuroscience*, 25(49), 11468–11478.
- Kramer, H. K., Andria, M. L., Kushner, S. A., Esposito, D. H., Hiller, J. M., & Simon, E. J. (2000). Mutation of tyrosine 318 (Y318F) in the delta-opioid receptor attenuates tyrosine phosphorylation, agonist-dependent receptor internalization, and mitogen-activated protein kinase activation. *Molecular Brain Research*, 79(1–2), 55–66.
- Kramer, R. H., Mouroto, A., & Adesnik, H. (2013). Optogenetic pharmacology for control of native neuronal signalin G proteins. *Nature Neuroscience*, 16(7), 816–823.
- Krapivinsky, G., Gordon, E. A., Wickman, K., Velimirović, B., Krapivinsky, L., & Clapham, D. E. (1995). The G protein-gated atrial K⁺ channel IK_{ACh} is a heteromultimer of two inwardly rectifying K⁺-channel proteins. *Nature*, 374, 135–141.
- Krieg, P. A., & Melton, D. A. (1984). Functional messenger RNAs are produced by SP6 *in vitro* transcription of cloned cDNAs. *Nucleic Acids Research*, 12(18), 7057–7070.
- Kyung, T., Lee, S., Kim, J. E., Cho, T., Park, H., Jeong, Y. M., Kim, D., Shin, A., Kim, S., Baek, J., Kim, J., Kim, N. Y., Woo, D., Chae, S., Kim, C. H., Shin, H. S., Han, Y. M., Kim, D., & Heo, W. Do. (2015). Optogenetic control of endogenous Ca²⁺ channels *in vivo*. *Nature Biotechnology*, 33(10), 1092–1096
- Labouèbe, G., Lomazzi, M., Cruz, H. G., Creton, C., Luján, R., Li, M., Yanagawa, Y., Obata, K., Watanabe, M., Wickman, K., Boyer, S. B., Slesinger, P. A., & Lüscher, C. (2007). RGS2 modulates coupling between GABAB receptors and GIRK channels in dopamine neurons of the ventral tegmental area. *Nature Neuroscience*, 10(12), 1559–1568.
- Law, P. Y., Maestri-EI Kouhen, O., Solberg, J., Wang, W., Erickson, L. J., & Loh, H. H. (2000). Deltorphin II-induced rapid desensitization of δ-opioid receptor requires both phosphorylation and internalization of the receptor. *Journal of Biological Chemistry*, 275(41), 32057–32065.
- Leaney, J. L., Benians, A., Brown, S., Nobles, M., Kelly, D., & Tinker, A. (2004). Rapid desensitization of G protein-gated inwardly rectifying K⁺ currents is determined by G protein cycle. *American Journal of Physiology - Cell Physiology*, 287(1), C182–C191.
- Leaney, J. L., Dekker, L. V., & Tinker, A. (2001). Regulation of a G protein-gated inwardly rectifying K⁺ channel by a Ca²⁺-independent protein kinase C. *Journal of Physiology*, 534(2), 367–379.
- Lechleiter, J., Girard, S., Clapham, D., & Peralta, E. (1991). Subcellular patterns of calcium release determined by G protein-specific residues of muscarinic receptors. *Nature*, 350, 505–508.
- Lehmann, D. M., Seneviratne, A. M. P. B., & Smrcka, A. V. (2009). Small molecule disruption of G protein beta gamma subunit signaling inhibits neutrophil chemotaxis and inflammation. *Molecular Pharmacology*, 73(2), 410–418.
- Lei, Q., Jones, M. B., Talley, E. M., Garrison, J. C., & Bayliss, D. A. (2003). Molecular mechanisms mediating inhibition of G protein-coupled inwardly-rectifying K⁺ channels. *Molecules and Cells*, 15(1), 1–9.
- Lemonnier, L., Prevarskaya, N., Mazurier, J., Shuba, Y., & Skryma, R. (2004). 2-APB inhibits volume-regulated anion channels independently from intracellular calcium signaling modulation. *FEBS Letters*, 556(1–3), 121–126.

- Leontiadis, L. J., Papakonstantinou, M. P., & Georgoussi, Z. (2009). Regulator of G protein signaling 4 confers selectivity to specific G proteins to modulate μ - and δ -opioid receptor signaling. *Cellular Signalling*, 21(7), 1218–1228.
- Lewohl, J. M., Wilson, W. R., Mayfield, R. D., Brozowski, S. J., Morrisett, R. A., & Harris, R. A. (1999). G protein-coupled inwardly rectifying potassium channels are targets of alcohol action. *Nature Neuroscience*, 2(12), 1084–1090.
- Liggett, S. B. (2011). Phosphorylation barcoding as a mechanism of directing GPCR signaling. *Science Signaling*, 4(185), 2–5.
- Lindell D, Jaffe JD, Johnson ZI, Church GM, Chisholm SW. Photosynthesis genes in marine viruses yield proteins during host infection. *Nature*. 2005;438(7064):86–89.
- Logothetis, D. E., Kurachi, Y., Galper, J., Neer, E. J., & Clapham, D. E. (1987). The $\beta\gamma$ subunits of GTP-binding proteins activate the muscarinic K^+ channel in heart. *Nature*, 325(6102), 321–326.
- Logothetis, D. E., Mahajan, R., Adney, S. K., Ha, J., Kawano, T., Meng, X. Y., & Cui, M. (2015). Chapter One - Unifying mechanism of controlling Kir3 channel activity by G proteins and phosphoinositides. In P. A. Slesinger & W. Kevin (Eds.), *International Review of Neurobiology* (1st ed., Vol. 123, pp. 1–26). Academic Press.
- Lopatin, A. N., Makhina, E. N., & Nichols, C. G. (1995). The mechanism of inward rectification of potassium channels: “long-pore plugging” by cytoplasmic polyamines. *The Journal of General Physiology*, 106(5), 923–955.
- López JL, Golemba M, Hernández E, Lozada M, Dionisi H, Jansson JK, Cormack, WP (2017). Microbial and viral-like rhodopsins present in coastal marine sediments from four polar and subpolar regions. *FEMS Microbiology Ecology*, 93(1), fiw216.
- Lowe, J. D., Celver, J. P., Gurevich, V. V., & Chavkin, C. (2002). Mu-opioid receptors desensitize less rapidly than delta-opioid receptors due to less efficient activation of arrestin. *Journal of Biological Chemistry*, 277(18), 15729–15735.
- Luik, R. M., Wang, B., Prakriya, M., Wu, M. M., & Lewis, R. S. (2008). Oligomerization of STIM1 couples ER calcium depletion to CRAC channel activation. *Nature*, 454(7203), 538–542.
- Lüscher, C., Jan, L. Y., Stoffel, M., Malenka, R. C., & Nicoll, R. A. (1997). G protein-coupled inwardly rectifying K^+ channels (GIRKs) mediate postsynaptic but not presynaptic transmitter actions in hippocampal neurons. *Neuron*, 19(3), 687–695.
- Lüscher, C., & Slesinger, P. A. (2010). Emerging roles for G protein-gated inwardly rectifying potassium (GIRK) channels in health and disease. *Nature Reviews Neuroscience*, 11(5), 301–315.
- Ma, H. T., Venkatachalam, K., Li, H. S., Montell, C., Kurosaki, T., Patterson, R. L., & Gill, D. L. (2001). Assessment of the Role of the Inositol 1,4,5-Trisphosphate Receptor in the Activation of Transient Receptor Potential Channels and Store-operated Ca^{2+} Entry Channels. *Journal of Biological Chemistry*, 276(22), 18888–18896.
- Ma, K. T., Guan, B. C., Yang, Y. Q., Nuttall, A. L., & Jiang, Z. G. (2011). 2-Aminoethoxydiphenyl borate blocks electrical coupling and inhibits voltage-gated K^+ channels in guinea pig arteriole cells. *American Journal of Physiology - Heart and Circulatory Physiology*, 300(1), 335–346.

- Ma, Y., Huang, J., Ali, S., Lowry, W., & Huang, X. (2000). Src tyrosine kinase is a novel direct effector of G proteins. *Cell*, 102(5), 635–646.
- Machaca, K., & Hartzell, H. C. (1998). Asymmetrical distribution of Ca-activated Cl channels in *Xenopus* oocytes. *Biophysical Journal*, 74(3), 1286–1295.
- Machaca, K., & Haun, S. (2000). Store-operated calcium entry inactivates at the germinal vesicle breakdown stage of *Xenopus* meiosis. *Journal of Biological Chemistry*, 275(49), 38710–38715.
- Machaca, K., Qu, Z., Kuruma, A., Criss Hartzell, H., & McCarty, N. (2002). The endogenous calcium-activated Cl channel in *Xenopus* oocytes: A physiologically and biophysically rich model system. In C. M. Fuller (Ed.), *Current Topics in Membranes - Calcium-Activated Chloride Channels* (Vol. 53, pp. 3–39). Academic Press.
- Manglik, A., Kruse, A. C., Kobilka, T. S., Thian, F. S., Mathiesen, J. M., Sunahara, R. K., Pardo, L., Weis, W. I., Kobilka, B. K., & Granier, S. (2012). Crystal structure of the μ -opioid receptor bound to a morphinan antagonist. *Nature*, 485(7398), 321–326.
- Mann, A., Liebetrau, S., Klima, M., Dasgupta, P., Massotte, D., & Schulz, S. (2020). Agonist-induced phosphorylation bar code and differential post-activation signaling of the delta opioid receptor revealed by phosphosite-specific antibodies. *Scientific Reports*, 10(1), 8585.
- Mao, J., Wang, X., Chen, F., Wang, R., Rojas, A., Shi, Y., Piao, H., & Jiang, C. (2004). Molecular basis for the inhibition of G protein-coupled inward rectifier K⁺ channels by protein kinase C. *Proceedings of the National Academy of Sciences of the United States of America*, 101(4), 1087–1092.
- Marin, M. (2012). Chapter 49 Calcium Signaling in *Xenopus* oocyte. In S. Islam (Ed.), *Advances in Experimental Medicine and Biology: Calcium signaling* (1st ed., pp. 1073–1094). Springer International Publishing.
- Marin, M., Sellier, C., Paul-Antoine, A. F., Cailliau, K., Browaeys-Poly, E., Bodart, J. F., & Vilain, J. P. (2010). Calcium dynamics during physiological acidification in *Xenopus* oocyte. *Journal of Membrane Biology*, 236(3), 233–245.
- Marker, C. L., Luján, R., Loh, H. H., & Wickman, K. (2005). Spinal G protein-Gated Potassium channels contribute in a dose-dependent manner to the analgesic effect of μ - and δ but not κ -opioids. *Journal of Neuroscience*, 25(14), 3551–3559.
- Marmont, G. (1949). Studies on the axon membrane. *Journal of Cellular and Comparative Physiology*, 34(3), 351–382.
- Maruyama, T., Kanaji, T., Nakade, S., Kanno, T., & Mikoshiba, K. (1997). 2APB, 2-aminoethoxydiphenyl borate, a membrane-penetrable modulator of Ins(1,4,5)P₃-induced Ca²⁺ release. *Journal of Biochemistry*, 122(3), 498–505.
- Machelska, H., & Celik, M. (2018). Advances in achieving opioid analgesia without side effects. *Frontiers in Pharmacology*, 9, 1388.
- Medina, I., Krapivinsky, G., Arnold, S., Kovoov, P., Krapivinsky, L., & Clapham, D. E. (2000). A switch mechanism for G $\beta\gamma$ activation of IKACH. *Journal of Biological Chemistry*, 275(38), 29709–29716.
- Miesenböck G. (2011). Optogenetic Control of Cells and Circuits. *Annual Review of Cell and Developmental Biology*, 27(1), 731–758.

- Miledi, R., & Parker, I. (1984). Chloride current induced by injection of calcium into *Xenopus* oocytes. *The Journal of Physiology*, 357, 173–183.
- Mirshahi, T., & Logothetis, D. E. (2004). Molecular determinants responsible for differential cellular distribution of G protein-gated Inwardly Rectifying K⁺ Channels. *Journal of Biological Chemistry*, 279(12), 11890–11897.
- Mirshahi, T., Robillard, L., Zhang, H., Hébert, T. E., & Logothetis, D. E. (2002). Gβ residues that do not interact with Gα underlie agonist-independent activity of K⁺ channels. *Journal of Biological Chemistry*, 277(9), 7348–7355.
- Mitrovic, I., Margeta-Mitrovic, M., Bader, S., Stoffel, M., Jan, L. Y., & Basbaum, A. I. (2003). Contribution of GIRK2-mediated postsynaptic signaling to opiate and α2-adrenergic analgesia and analgesic sex differences. *Proceedings of the National Academy of Sciences of the United States of America*, 100(1), 271–276.
- Molinari, P., Vezzi, V., Sbraccia, M., Grò, C., Riitano, D., Ambrosio, C., Casella, I., & Costa, T. (2010). Morphine-like opiates selectively antagonize receptor-arrestin interactions. *Journal of Biological Chemistry*, 285(17), 12522–12535.
- Nagi, K., Charfi, I., & Pineyro, G. (2015). Kir3 channels undergo arrestin-dependant internalization following delta opioid receptor activation. *Cellular and Molecular Life Sciences*, 72(18), 3543–3557.
- Mollereau, C., Parmentier, M., Mailleux, P., Butour, J.-L., Moisand, C., Chalon, P., Caput, D., Vassart, G., & Meunier, J.-C. (1994). ORL1, a novel member of the opioid receptor family. *FEBS Letters*, 341(1), 33–38.
- Mora, S. I., & Escobar, L. I. (2005). Phosphorylation of a tyrosine at the N-terminus regulates the surface expression of GIRK5 homomultimers. *FEBS Letters*, 579(14), 3019–3023.
- Moreau, C. J., Dupuis, J. P., Revilloud, J., Arumugam, K., & Vivaudou, M. (2008). Coupling ion channels to receptors for biomolecule sensing. *Nature Nanotechnology*, 3(10), 620–625.
- Müllner, C., Yakubovich, D., Dessauer, C. W., Platzer, D., & Schreiber, W. (2003). Single channel analysis of the regulation of GIRK1/GIRK4 channels by protein phosphorylation. *Biophysical Journal*, 84(2 I), 1399–1409.
- Mutneja, M., Berton, F., Suen, K. F., Lüscher, C., & Slesinger, P. A. (2005). Endogenous RGS proteins enhance acute desensitization of GABAB receptor-activated GIRK currents in HEK-293T cells. *Pflügers Archiv European Journal of Physiology*, 450(1), 61–73.
- Nagel, G., Ollig, D., Fuhrmann, M., Kateriya, S., Musti, A. M., Bamberg, E., & Hegemann, P. (2002). Channelrhodopsin-1: A Light-Gated Proton Channel in Green Algae. *Science*, 296(5577), 2395–2398.
- Nagel, G., Szellas, T., Huhn, W., Kateriya, S., Adeishvili, N., Berthold, P., Bamberg, E. (2003). Channelrhodopsin-2, a directly light-gated cation-selective membrane channel. *Proceedings of the National Academy of Sciences*, 100(24), 13940–13945.
- Nassirpour, R., Bahima, L., Lalive, A. L., Lüscher, C., Luján, R., & Slesinger, P. A. (2010). Morphine- and CaMKII-dependent enhancement of GIRK channel signaling in hippocampal neurons. *Journal of Neuroscience*, 30(40), 13419–13430.
- Needham, D. M., Yoshizawa, S., Hosaka, T., Poirier, C., Choi, C. J., Hehenberger, E., Irwin, N. A. T., Wilken, S., Yung, C.-M., Bachy, C., Kurihara, R., Nakajima, Y., Kojima, K., Kimura-Someya, T., Leonard, G., Malmstrom, R. R., Mende, D. R., Olson, D. K., Sudo, Y., ... Worden, A. Z. (2019). A distinct lineage of giant viruses brings a rhodopsin photosystem to unicellular marine

- predators. *Proceedings of the National Academy of Sciences of the United States of America*, 116(41), 20574–20583.
- Neer, E. J. (1995). Heterotrimeric G proteins: Organizers of transmembrane signals. *Cell*, 80(2), 249–257.
- Nobles, M., Benians, A., & Tinker, A. (2005). Heterotrimeric G proteins precouple with G protein-coupled receptors in living cells. *Proceedings of the National Academy of Sciences of the United States of America*, 102(51), 18706–18711.
- Nelson, M. E., Kuryatov, A., Choi, C. H., Zhou, Y., & Lindstrom, J. (2003). Alternate stoichiometries of $\alpha 4\beta 2$ nicotinic acetylcholine receptors. *Molecular Pharmacology*, 63(2), 332–341.
- Neubig, R. (1994). Membrane organization in G protein mechanisms. *The FASEB Journal*, 8(12), 939–946.
- Niu, Y., Tao, X., Touhara, K. K., & Mackinnon, R. (2020). Cryo-EM analysis of PIP₂ regulation in mammalian GIRK channels. *ELife*, 9, e60552.
- North, R. A., Williams, J. T., Surprenant, A., & Christie, M. J. (1987). Mu and delta receptors belong to a family of receptors that are coupled to potassium channels. *Proceedings of the National Academy of Sciences of the United States of America*, 84(15), 5487–5491.
- Oh, S.-J., Hwang, S. J., Jung, J., Yu, K., Kim, J., Choi, J. Y., Hartzell, H. C., Roh, E. J., & Lee, C. J. (2013). MONNA, a potent and selective blocker for transmembrane protein with unknown function 16/anoctamin-1. *Molecular Pharmacology*, 84(5), 726–735.
- Opekarová, M., & Tanner, W. (2003). Specific lipid requirements of membrane proteins - A putative bottleneck in heterologous expression. *Biochimica et Biophysica Acta - Biomembranes*, 1610(1), 11–22.
- Oppermann, J., Fischer, P., Silapetere, A., Liepe, B., Rodriguez-Rozada, S., Flores-Urbe, J., Peter, E., Keidel, A., Vierock, J., Kaufmann, J., Broser, M., Luck, M., Bartl, F., Hildebrandt, P., Wiegert, J. S., Bèjà, O., Hegemann, P., & Wietek, J. (2019). MerMAIDs: a family of metagenomically discovered marine anion-conducting and intensely desensitizing channelrhodopsins. *Nature Communications*, 10(1), 3315.
- Palczewski, K. (2006). G protein–Coupled Receptor rhodopsin. *Annual Review of Biochemistry*, 75, 743–767.
- Parekh, A. B. (2008). Ca²⁺ microdomains near plasma membrane Ca²⁺ channels: impact on cell function. *The Journal of Physiology*, 586(Part 13), 3043–3054.
- Patil, N., Cox, D. R., Bhat, D., Faham, M., Myers, R. M., & Peterson, A. S. (1995). A potassium channel mutation in weaver mice implicates membrane excitability in granule cell differentiation. *Nature Genetics*, 11(2), 126–129.
- Peng, Q., Alqahtani, S., Nasrullah, M. Z. A., & Shen, J. (2021). Functional evidence for biased inhibition of G protein signaling by YM-254890 in human coronary artery endothelial cells. *European Journal of Pharmacology*, 891, 173706.
- Pfaffinger, P. J., Martin, J. M., Hunter, D. D., Nathanson, N. M., & Hille, B. (1985). GTP-binding proteins couple cardiac muscarinic receptors to a K channel. *Nature*, 317(6037), 536–538.
- Pfleger, J., Gresham, K., & Koch, W. J. (2019). G protein-coupled receptor kinases as therapeutic targets in the heart. *Nature Reviews Cardiology*, 16(10), 612–622.

- Pradhan, A. A. A., Becker, J. A. J., Scherrer, G., Tryoen-Toth, P., Filliol, D., Matifas, A., Massotte, D., Gavériaux-Ruff, C., & Kieffer, B. L. (2009). *In vivo* delta opioid receptor internalization controls behavioral effects of agonists. *PLOS ONE*, 4(5), e5425.
- Pradhan, A. A., Befort, K., Nozaki, C., Gavériaux-Ruff, C., & Kieffer, B. L. (2011). The delta opioid receptor: an evolving target for the treatment of brain disorders. *Trends in Pharmacological Sciences*, 32(10), 581–590.
- Pradhan, A. A., Tawfik, V. L., Tipton, A. F., & Scherrer, G. (2015). *In vivo* techniques to investigate the internalization profile of opioid receptors. *Methods in Molecular Biology*, 1230, 87–104.
- Pradhan, A. A., Walwyn, W., Nozaki, C., Filliol, D., Erbs, E., Matifas, A., Evans, C., & Kieffer, B. L. (2010). Ligand-directed trafficking of the δ -opioid receptor *in vivo*: Two paths toward analgesic tolerance. *Journal of Neuroscience*, 30(49), 16459–16468.
- Qiu, Y., Loh, H. H., & Law, P. (2007). Phosphorylation of the delta-opioid receptor regulates its beta-arrestins selectivity and subsequent receptor internalization and adenylyl cyclase desensitization. *Journal of Biological Chemistry*, 282(31), 22315–22323.
- Quirion, B., Bergeron, F., Blais, V., & Gendron, L. (2020). The Delta-Opioid Receptor; a target for the treatment of pain. *Frontiers in Molecular Neuroscience*, 13, 52. <https://doi.org/10.3389/fnmol.2020.00052>
- Raveh, A., Cooper, A., Guy-David, L., & Reuveny, E. (2010). Nonenzymatic rapid control of GIRK channel function by a G protein-coupled receptor kinase. *Cell*, 143(5), 750–760.
- Raveh, A., Riven, I., & Reuveny, E. (2009). Elucidation of the gating of the GIRK channel using a spectroscopic approach. *The Journal of Physiology*, 587(22), 5331–5335.
- Rebois, R. V., Robitaille, M., Galés, C., Dupré, D. J., Baragli, A., Trieu, P., Ethier, N., Bouvier, M., & Hébert, T. E. (2006). Heterotrimeric G proteins form stable complexes with adenylyl cyclase and Kir3.1 channels in living cells. *Journal of Cell Science*, 119(13), 2807–2818.
- Rifkin, R. A., Moss, S. J., & Slesinger, P. A. (2017). G protein-Gated Potassium Channels: A Link to drug addiction. *Trends in Pharmacological Sciences*, 38(4), 378–392.
- Rizzuto, R., & Pozzan, T. (2006). Microdomains of intracellular Ca^{2+} : Molecular determinants and functional consequences. *Physiological Reviews*, 86(1), 369–408.
- Robitaille, M., Ramakrishnan, N., Baragli, A., & Hébert, T. E. (2009). Intracellular trafficking and assembly of specific Kir3 channel/G protein complexes. *Cellular Signalling*, 21(4), 488–501.
- Rogalski, S. L., Appleyard, S. M., Pattillo, A., Terman, G. W., & Chavkin, C. (2005). TrkB activation by brain-derived Neurotrophic Factor inhibits the G protein-gated Inward Rectifier Kir3 by tyrosine phosphorylation of the channel. *Journal of Biological Chemistry*, 275(33), 25082–25088.
- Romero, G., von Zastrow, M., & Friedman, P. A. (2011). Role of PDZ proteins in regulating trafficking, signaling, and function of GPCRs: means, motif, and opportunity. *Advances in Pharmacology*, 62, 279–314.
- Rosenbaum, D. M., Cherezov, V., Hanson, M. A., Rasmussen, S. G. F., Foon, S. T., Kobilka, T. S., Choi, H. J., Yao, X. J., Weis, W. I., Stevens, R. C., & Kobilka, B. K. (2007). GPCR engineering yields high-resolution structural insights into β 2-adrenergic receptor function. *Science*, 318(5854), 1266–1273.

- Rosenhouse-dantsker, A., Sui, J. L., Zhao, Q., Rusinova, R., Zhang, Z., & Logothetis, D. E. (2014). A sodium-mediated structural switch that controls the sensitivity of Kir channels to PIP₂. *Nature Chemical Biology*, 4(10), 624–631.
- Rubinstein, M., Peleg, S., Berlin, S., Brass, D., Keren-Raifman, T., Dessauer, C. W., Ivanina, T., & Dascal, N. (2009). Divergent regulation of GIRK1 and GIRK2 subunits of the neuronal G protein gated K⁺ channel by GαiGDP and Gβγ. *Journal of Physiology*, 587(14), 3473–3491.
- Rusinova, R., Shen, Y.-M. A., Dolios, G., Padovan, J., Yang, H., Kirchberger, Madeleine, Wang, R., & Logothetis, D. E. (2009). Mass spectrometric analysis reveals a functionally important PKA phosphorylation site in a Kir3 channel subunit. *Pflügers Archiv European Journal of Physiology*, 458(2), 303–314.
- Sadja, R., Smadja, K., Alagem, N., & Reuveny, E. (2001). Coupling Gβγ-dependent activation to channel opening via pore elements in inwardly rectifying potassium channels. *Neuron*, 29(3), 669–680.
- Sahel, J. A., Boulanger-Scemama, E., Pagot, C., Arleo, A., Galluppi, F., Martel, J. N., Esposti, S. D., Delaux, A., de Saint Aubert, J. B., de Montleau, C., Gutman, E., Audo, I., Duebel, J., Picaud, S., Dalkara, D., Blouin, L., Tiel, M., & Roska, B. (2021). Partial recovery of visual function in a blind patient after optogenetic therapy. *Nature Medicine*, 27(7), 1223–1229.
- Saitoh, O., Kubo, Y., & Miyatani, Y. (1997). RGS8 accelerates G protein-mediated modulation of K⁺ currents. *Nature*, 390(6659), 525–529.
- Scherrer, G., Tryoen-Tóth, P., Filliol, D., Matifas, A., Laustriat, D., Cao, Y. Q., Basbaum, A. I., Dierich, A., Vonesh, J.-L., Gavériaux-Ruff, C., & Kieffer, B. L. (2006). Knockin mice expressing fluorescent delta-opioid receptors uncover G protein-coupled receptor dynamics *in vivo*. *Proceedings of the National Academy of Sciences of the United States of America*, 103(25), 9691–9696.
- Seo, Y., Lee, H. K., Park, J., Jeon, D., Jo, S., Jo, M., & Namkung, W. (2016). Ani9, a novel potent small-molecule ANO1 inhibitor with negligible effect on ANO2. *PLOS ONE*, 11(5), e0155771.
- Schneider F, Grimm C, Hegemann P (2015). Biophysics of Channelrhodopsin. *Annual Review of Biophysics*, 44(1), 167–186.
- Schroeder, B. C., Cheng, T., Jan, Y. N., & Jan, L. Y. (2008). Expression cloning of TMEM16A as a Calcium-Activated Chloride Channel subunit. *Cell*, 134(6), 1019–1029.
- Siarey, R. J., Carlson, E. J., Epstein, C. J., Balbo, A., Rapoport, S. I., & Galdzicki, Z. (1999). Increased synaptic depression in the Ts65Dn mouse, a model for mental retardation in Down syndrome. *Neuropharmacology*, 38(12), 1917–1920.
- Sickmann, T., & Alzheimer, C. (2003). Short-term desensitization of G protein-activated, inwardly rectifying K⁺ (GIRK) currents in pyramidal neurons of rat neocortex. *Journal of Neurophysiology*, 90(4), 2494–2503.
- Signorini, S., Liao, Y. J., Duncan, S. A., Jan, L. Y., & Stoffel, M. (1997). Normal cerebellar development but susceptibility to seizures in mice lacking G protein-coupled, inwardly rectifying K⁺ channel GIRK2. *Proceedings of the National Academy of Sciences of the United States of America*, 94(3), 923–927.
- Singh, A. K., Saotome, K., McGoldrick, L. L., & Sobolevsky, A. I. (2018). Structural bases of TRP channel TRPV6 allosteric modulation by 2-APB. *Nature Communications*, 9(1), 1–11.

- Siotto, F., Martin, C., Rauh, O., Van Etten, J. L., Schroeder, I., Moroni, A., & Thiel, G. (2014). Viruses infecting marine picoplankton encode functional potassium ion channels. *Virology*, 466–467, 103–111.
- Siuda, E. R., Copits, B. A., Schmidt, M. J., Baird, M. A., Al-Hasani, R., Planer, W. J., Funderburk, S. C., McCall, J. G., Gereau, R. W., & Bruchas, M. R. (2015). Spatiotemporal control of opioid signaling and behavior. *Neuron*, 86(4), 923–935.
- Shirasaki, T., Abe, K., Soeda, F., & Takahama, K. (2004). δ -Opioid receptor antagonists inhibit GIRK channel currents in acutely dissociated brainstem neurons of rat. *Brain Research*, 1006(2), 190–197.
- Short, S. M. (2012). The ecology of viruses that infect eukaryotic algae. *Environmental Microbiology*, 14(9), 2253–2271.
- Shrestha, B., Sripadi, P., Reschke, B. R., Henderson, H. D., Powell, M. J., Moody, S. A., & Vertes, A. (2014). Subcellular metabolite and lipid analysis of *Xenopus laevis* eggs by LAESI mass spectrometry. *PLOS ONE*, 9(12), 1–22.
- Shukla, A. K., Westfield, G. H., Xiao, K., Reis, R. I., Huang, L. Y., Tripathi-Shukla, P., Qian, J., Li, S., Blanc, A., Oleskie, A. N., Dosey, A. M., Su, M., Liang, C. R., Gu, L. L., Shan, J. M., Chen, X., Hanna, R., Choi, M., Yao, X. J., ... Lefkowitz, R. J. (2014). Visualization of arrestin recruitment by a G protein-coupled receptor. *Nature*, 512(7513), 218–222.
- Sobczak, K., Bangel-Ruland, N., Leier, G., & Weber, W. M. (2010). Endogenous transport systems in the *Xenopus laevis* oocyte plasma membrane. *Methods*, 51, 183–189.
- Stival, C., La Spina, F. A., Graf, C. B., Arcelay, E., Arranz, S. E., Ferreira, J. J., Le Grand, S., Dzikunu, V. A., Santi, C. M., Visconti, P. E., Buffone, M. G., & Krapf, D. (2015). Src kinase is the connecting player between Protein Kinase A (PKA) activation and hyperpolarization through SLO3 potassium channel regulation in mouse sperm. *Journal of Biological Chemistry*, 290(30), 18855–18864.
- Sui, J. L., Petit-Jacques, J., & Logothetis, D. E. (1998). Activation of the atrial K ACh channel by the B γ subunits of G proteins or intracellular Na⁺ ions depends on the presence of phosphatidylinositol phosphates. *Proceedings of the National Academy of Sciences of the United States of America*, 95(3), 1307–1312.
- Sungkaworn, T., Jobin, M. L., Burnecki, K., Weron, A., Lohse, M. J., & Calebiro, D. (2017). Single-molecule imaging reveals receptor-G protein interactions at cell surface hot spots. *Nature*, 550(7677), 543–547.
- Suzuki, K., Ritchie, K., Kajikawa, E., Fujiwara, T., & Kusumi, A. (2005). Rapid hop diffusion of a G protein-coupled receptor in the plasma membrane as revealed by single-molecule techniques. *Biophysical Journal*, 88(5), 3659–3680.
- Suzuki, K., Ritchie, K., Kajikawa, E., Fujiwara, T., & Kusumi, A. (2005). Rapid hop diffusion of a G protein-coupled receptor in the plasma membrane as revealed by single-molecule techniques. *Biophysical Journal*, 88(5), 3659–3680.
- Svoboda, K. R., & Lupica, C. R. (1998). Opioid inhibition of hippocampal interneurons via modulation of potassium and hyperpolarization-activated cation (I(h)) currents. *Journal of Neuroscience*, 18(18), 7084–7098.
- Szücs, M., Di Gleria, K., & Medzihradzsky, K. (1985). Melphalan potently substitutes the N-terminal Tyr of D-Ala²-Leu⁵-enkephalin methyl ester. *FEBS Letters*, 179(1), 87–90.

- Terhag, J., Cavara, N. A., & Hollmann, M. (2010). Cave Canalem: How endogenous ion channels may interfere with heterologous expression in *Xenopus* oocytes. *Methods*, 51(1), 66–74.
- Tian, W. N., Duzic, E., Lanier, S. M., & Deth, R. C. (1994). Determinants of alpha2-adrenergic receptor activation of G proteins: Evidence for a precoupled receptor/G protein state. *Molecular Pharmacology*, 45(3), 524–531.
- Tischer, D., & Weiner, O. (2014). Illuminating cell signalling with optogenetic tools. *Nature Reviews Molecular Cell Biology*, 15, 551–558.
- Theodoulou, F. L., & Miller, A. J. (1995). *Xenopus* oocytes as a heterologous expression system. In H. Jones (Ed.), *Methods in Molecular Biology - Plant Gene Transfer and Expression Protocols* (pp. 317–340). Springer Totowa.
- Thiel, G., Greiner, T., Dunigan, D. D., Moroni, A., & Van Etten, J. L. (2015). Large dsDNA chloroviruses encode diverse membrane transport proteins. *Virology*, 479–480, 38–45.
- Thomas, A. M., Brown, S. G., Leaney, J. L., & Tinker, A. (2006). Differential phosphoinositide binding to components of the G protein-gated K⁺ channel. *Journal of Membrane Biology*, 211(1), 43–53.
- Thompson, A. A., Liu, W., Chun, E., Katritch, V., Wu, H., Vardy, E., Huang, X. P., Trapella, C., Guerrini, R., Calo, G., Roth, B. L., Cherezov, V., & Stevens, R. C. (2012). Structure of the nociceptin/orphanin FQ receptor in complex with a peptide mimetic. *Nature*, 485(7398), 395–399.
- Thomsen, A. R. B., Jensen, D. D., Hicks, G. A., Bunnett, N. W., City, Y., & Street, L. (2018). Therapeutic targeting of endosomal G protein-Coupled Receptors. *Trends in Pharmacological Sciences*, 39(10), 879–891.
- Tokmakov, A. A., Sato, K. I., Iwasaki, T., & Fukami, Y. (2002). Src kinase induces calcium release in *Xenopus* egg extracts via PLC γ and IP₃-dependent mechanism. *Cell Calcium*, 32(1), 11–20.
- Touhara, K. K., & Mackinnon, R. (2018). Molecular basis of signaling specificity between GIRK channels and GPCRs. *ELife*, 7, e42908.
- Trapaidze, N., Keith, D. E., Cvejic, S., Evans, C. J., & Devi, L. A. (1996). Sequestration of the δ opioid receptor: Role of the C terminus in agonist-mediated internalization. *Journal of Biological Chemistry*, 271(46), 29279–29285.
- Tsai, H.-C., Zhang, F., Adamantidis, A., Stuber, G. D., Bonci, A., Lecea, L. de, & Deisseroth, K. (2009). Phasic firing in dopaminergic neurons is sufficient for behavioral conditioning. *Science*, 324(5930), 1080–1084.
- Tso, P. H., Yung, L. Y., & Wong, Y. H. (2000). Regulation of adenylyl cyclase, ERK1/2, and CREB by G(z) following acute and chronic activation of the δ -opioid receptor. *Journal of Neurochemistry*, 74(4), 1685–1693.
- Turecek, R., Schwenk, J., Fritzius, T., Ivankova, K., Zolles, G., Adelfinger, L., Jacquier, V., Besseyrias, V., Gassmann, M., Schulte, U., Fakler, B., & Bettler, B. (2014). Auxiliary GABAB receptor subunits uncouple G protein $\beta\gamma$ subunits from effector channels to induce desensitization. *Neuron*, 82(5), 1032–1044.
- Tye, K. M., & Deisseroth, K. (2012). Optogenetic investigation of neural circuits underlying brain disease in animal models. *Nature Reviews Neuroscience*, 13(4), 251–266.

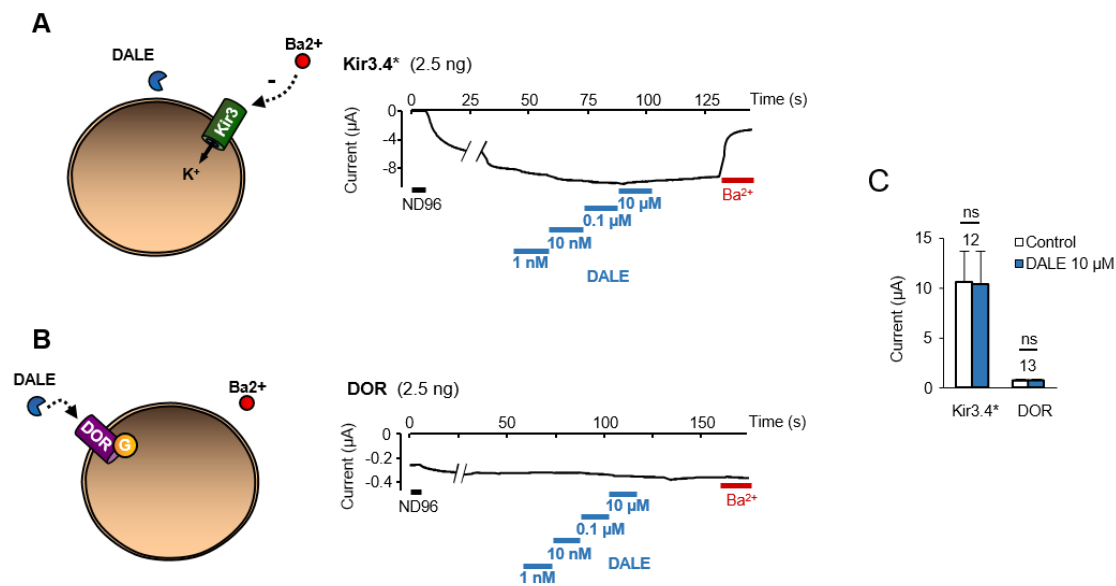
- Uemura, T., Kawasaki, T., Taniguchi, M., Moritani, Y., Hayashi, K., Saito, T., Takasaki, J., Uchida, W., & Miyata, K. (2009). Biological properties of a specific Gαq/11 inhibitor, YM-254890, on platelet functions and thrombus formation under high-shear stress. *British Journal of Pharmacology*, 148(1), 61–69.
- Van't Veer, A., & Carlezon Jr, W. A. (2013). Role of kappa-opioid receptors in stress and anxiety-related behavior. *Psychopharmacology*, 229(3), 435–452.
- Verkhatsky, A., & Parpura, V. (2014). History of electrophysiology and the patch clamp. In M. Martina & S. Taverna (Eds.), *Methods in Molecular Biology - Patch-Clamp* (Vol. 1183, pp. 1–19). Humana Press.
- Vivaudou, M. (2019). eeFit: a Microsoft Excel-embedded program for interactive analysis and fitting of experimental dose-response data. *Biotechniques* 66, 186-193.
- Vivaudou, M., Chan, K. W., Sui, J., Jan, L. Y., Reuveny, E., Logothetis, D. E., Chan, G., Natl, D. E. P., & Sci, A. (1997). Probing the G-protein regulation of GIRK1 and GIRK4, the two subunits of the K_{ACh} Channel, using functional homomeric mutants. *Journal of Biological Chemistry*, 272(50), 31553–31560.
- Vivaudou, M., Todorov, Z., Reyes-Mejia, G. C., & Moreau, C. (2017). Ion channels as reporters of membrane receptor function: Automated analysis in *Xenopus* Oocytes. In J.-J. Lacapere (Ed.), *Membrane Protein Structure and Function Characterization: Methods and Protocols* (pp. 283–301). Springer New York.
- Vorobiov, D., Bera, A. K., Keren-Raifman, T., Barzilai, R., & Dascal, N. (2000). Coupling of the muscarinic m2 receptor to G protein-activated K⁺ channels via Galpha(z) and a receptor-Galpha(z) fusion protein. Fusion between the receptor and Galpha(z) eliminates catalytic (collision) coupling. *The Journal of Biological Chemistry*, 275(6), 4166–4170.
- Walwyn, W., John, S., Maga, M., Evans, C. J., & Hales, T. G. (2009). Delta receptors are required for full inhibitory coupling of mu-receptors to voltage-dependent Ca²⁺ channels in dorsal root ganglion neurons. *Molecular Pharmacology*, 76(1), 134–143.
- Wang, Q., Chao, D., Chen, T., Sandhu, H., & Xia, Y. (2014). δ-Opioid Receptors and Inflammatory Cytokines in Hypoxia: differential regulation between glial and neuron-Like cells. *Translational Stroke Research*, 5(4), 476–483.
- Wang, Q., Liu-Chen, L. Y., & Traynor, J. R. (2009). Differential modulation of μ- and δ-opioid receptor agonists by endogenous RGS4 protein in SH-SY5Y cells. *Journal of Biological Chemistry*, 284(27), 18357–18367.
- Wang, W., Touhara, K. K., Weir, K., Bean, B. P., & Mackinnon, R. (2016). Cooperative regulation by G proteins and Na⁺ of neuronal GIRK2 K⁺ channels. *ELife*, 5, e15751.
- Wang, W., Whorton, M. R., & MacKinnon, R. (2014). Quantitative analysis of mammalian GIRK2 channel regulation by G proteins, the signaling lipid PIP₂ and Na⁺ in a reconstituted system. *ELife*, 3, e03671.
- Wang, Y., Van Bockstaele, E. J., & Liu-Chen, L.-Y. (2008). *In vivo* trafficking of endogenous opioid receptors. *Life Sciences*, 83(21–22), 693–699.
- Wei M, Zhou Y, Sun A, Ma G, He L, Zhou L, Zhang S, Liu J, Zhang SL, Gill DL, W. Y. (2016). Molecular mechanisms underlying inhibition of STIM1-Orai1-mediated Ca²⁺ entry induced by 2-aminoethoxydiphenyl borate. *Pflugers Archiv European Journal of Physiology*, 468(11–12), 2061–2074.

- Wickman, K., Nemeč, J., Gendler, S. J., & Clapham, D. E. (1998). Abnormal heart rate regulation in GIRK4 knockout mice. *Neuron*, 20(1), 103–114.
- Wietek, J., Wiegert, J. S., Adeishvili, N., Schneider, F., Watanabe, H., Tsunoda, S. P., Vogt, A., Elstner, M., Oertner, T. G., & Hegemann, P. (2014). Conversion of channelrhodopsin into a light-gated chloride channel. *Science*, 344(6182), 409–412.
- Wilden, U. (1995). Duration and amplitude of the light-induced cGMP hydrolysis in vertebrate photoreceptors are regulated by multiple phosphorylation of rhodopsin and by arrestin binding. *Biochemistry*, 34(4), 1446–1454.
- White, M. M., & Aylwin, M. (1990). Niflumic and flufenamic acids are potent reversible blockers of Ca²⁺-activated Cl⁻ channels in *Xenopus* oocytes. *Molecular Pharmacology*, 37(5), 720–724.
- Willems, J., & Kelly, E. (2001). Desensitization of endogenously expressed δ -opioid receptors: no evidence for involvement of G protein-coupled receptor kinase 2. *European Journal of Pharmacology*, 431(2), 133–141.
- Whorton, M. R., & MacKinnon, R. (2011). Crystal structure of the mammalian GIRK2 K⁺ channel and gating regulation by G proteins, PIP₂ and sodium. *Cell*, 147(1), 199–208.
- Whorton, M. R., & MacKinnon, R. (2013). X-ray structure of the mammalian GIRK2 – $\beta\gamma$ G protein complex. *Nature*, 498(7453), 190–197.
- Woodland, H. (1982). The translational control phase of early development. *Bioscience Reports*, 2, 471–491.
- Wooten, D., Christopoulos, A., Marti-Solano, M., Babu, M. M., & Sexton, P. M. (2018). Mechanisms of signalling and biased agonism in G protein-coupled receptors. *Nature Reviews Molecular Cell Biology*, 19(10), 638–653.
- Wozniak, K. L., Tembo, M., Phelps, W. A., Lee, M. T., & Carlson, A. E. (2018). PLC and IP₃-evoked Ca²⁺ release initiate the fast block to polyspermy in *Xenopus laevis* eggs. *Journal of General Physiology*, 150(9), 1239–1250.
- Wreggett, K. A., & De Léan, A. (1984). The ternary complex model. Its properties and application to ligand interactions with the D₂-dopamine receptor of the anterior pituitary gland. *Molecular Pharmacology*, 26(2), 214–227.
- Wu, H., Wacker, D., Mileni, M., Katritch, V., Han, G. W., Vardy, E., Liu, W., Thompson, A. A., Huang, X. P., Carroll, F. I., Mascarella, S. W., Westkaemper, R. B., Mosier, P. D., Roth, B. L., Cherezov, V., & Stevens, R. C. (2012). Structure of the human κ -opioid receptor in complex with JDTic. *Nature*, 485(7398), 327–332.
- Wydeven, N., Young, D., Mirkovic, K., & Wickman, K. (2012). Structural elements in the Girik1 subunit that potentiate G protein-gated potassium channel activity. *Proceedings of the National Academy of Sciences of the United States of America*, 109(52), 21492–21497.
- Xiang, B., Yu, G. H., Guo, J., Chen, L., Hu, W., Pei, G., & Ma, L. (2001). Heterologous activation of protein kinase C stimulates phosphorylation of delta-opioid receptor at serine 344, resulting in beta-arrestin- and clathrin-mediated receptor internalization. *Journal of Biological Chemistry*, 276(7), 4709–4716.
- Yasuda, K., Raynor, K., Kong, H., Breder, C. D., Takeda, J., Reisine, T., & Bell, G. I. (1993). Cloning and functional comparison of κ and δ opioid receptors from mouse brain. *Proceedings of the National Academy of Sciences of the United States of America*, 90(14), 6736–6740.

- Yau, S., Lauro, F. M., DeMaere, M. Z., Brown, M. V., Thomas, T., Raftery, M. J., Andrews-Pfannkoch, C., Lewis, M., Hoffman, J. M., Gibson, J. A., & Cavicchioli, R. (2011). Virophage control of antarctic algal host-virus dynamics. *Proceedings of the National Academy of Sciences of the United States of America*, 108(15), 6163–6168.
- Yellen, G. (1982). Single Ca^{2+} -activated nonselective cation channels in neuroblastoma. *Nature*, 296(5855), 357–359.
- Yi, B. A., Lin, Y. F., Jan, Y. N., & Jan, L. Y. (2001). Yeast screen for constitutively active mutant G protein-activated potassium channels. *Neuron*, 29(3), 657–667.
- Yutin, N., & Koonin, E. V. (2012). Proteorhodopsin genes in giant viruses. *Biology Direct*, 7, 34.
- Zabelskii, D., Alekseev, A., Kovalev, K., Rankovic, V., Balandin, T., Soloviov, D., Bratanov, D., Savelyeva, E., Podolyak, E., Volkov, D., Vaganova, S., Astashkin, R., Chizhov, I., Yutin, N., Rulev, M., Popov, A., Eria-Oliveira, A. S., Rokitskaya, T., Mager, T., ... Gordeliy, V. (2020). Viral rhodopsins 1 are an unique family of light-gated cation channels. *Nature Communications*, 11(1), 5707.
- Zhang, F., Prigge, M., Beyrière, F., Tsunoda, S. P., Mattis, J., Yizhar, O., Hegemann, P., & Deisseroth, K. (2008). Red-shifted optogenetic excitation: A tool for fast neural control derived from *Volvox carteri*. *Nature Neuroscience*, 11(6), 631–633.
- Zhang F, Vierock J, Yizhar O, Fenno LE, Tsunoda S, Kianianmomeni A, Deisseroth K(2011, December 23). The microbial opsin family of optogenetic tools. *Cell*, Vol. 147, pp. 1446–1457.
- Zhang, F., Wang, L. P., Brauner, M., Liewald, J. F., Kay, K., Watzke, N., Wood, P. G., Bamberg, E., Nagel, G., Gottschalk, A., & Deisseroth, K. (2007). Multimodal fast optical interrogation of neural circuitry. *Nature*, 446(7136), 633–639.
- Zhang, H., He, C., Yan, X., Mirshahi, T., & Logothetis, D. E. (1999). Activation of inwardly rectifying K^+ channels by distinct $\text{PtdIns}(4,5)\text{P}_2$ interactions. *Nature Cell Biology*, 1(3), 183–188.
- Zhang, X., Wang, F., Chen, X., Chen, Y., & Lan, M. (2008). Post-endocytic fates of δ -opioid receptor are regulated by GRK2-mediated receptor phosphorylation and distinct β -arrestin isoforms. *Journal of Neurochemistry*, 106(2), 781–792.
- Zhang, X., Wang, F., Chen, X., Li, J., Xiang, B., Zhang, Y. Q., Li, B. M., & Ma, L. (2005). B-Arrestin1 and B-Arrestin2 Are Differentially Required for Phosphorylation-Dependent and -Independent Internalization of Δ -Opioid Receptors. *Journal of Neurochemistry*, 95(1), 169–178.
- Zhao, J., Pei, G., Huang, Y. L., Zhong, F. M., & Ma, L. (1997). Carboxyl terminus of delta opioid receptor is required for agonist-dependent receptor phosphorylation. *Biochemical and Biophysical Research Communications*, 238(1), 71–76.
- Zhao, Y., Gameiro-Ros, I., Glaaser, I. W., & Slesinger, P. A. (2021). Advances in targeting GIRK channels in disease. *Trends in Pharmacological Sciences*, 42(3), 203–215.
- Zheng, S., Abreu, N., Levitz, J., & Kruse, A. C. (2019). Structural basis for KCTD-mediated rapid desensitization of GABAB signalling. *Nature*, 567(7746), 127–131.

Annexes

A - Supplementary figures – Project A



Supplementary figure a.1. No unspecific effects of opioid agonists in *Xenopus* oocytes.

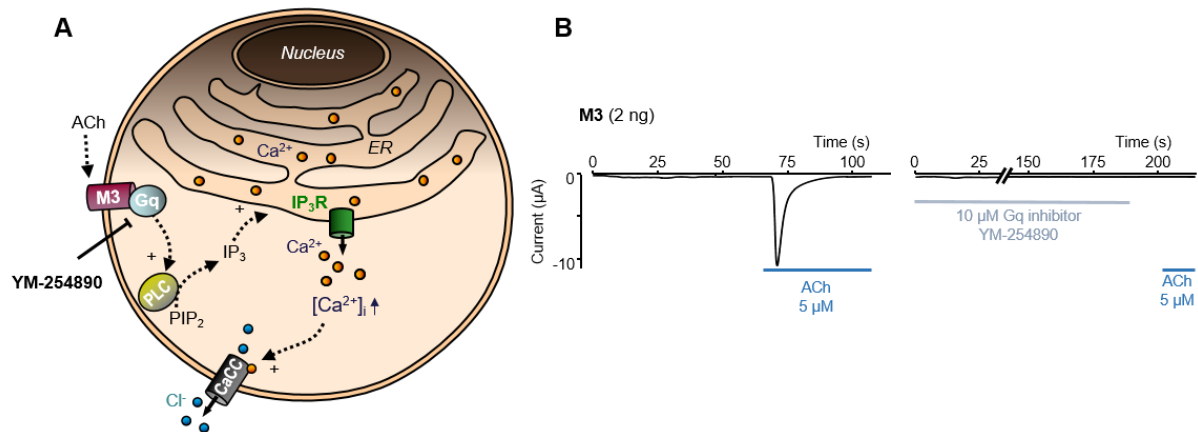
Representative recordings at -50 mV of oocytes expressing either Kir3.4* (A) or DOR (B) and subjected to extracellular DALE application. Oocytes were injected with the RNA amounts indicated. Recordings start in ND96 bath solution (91 mM Na⁺, 2 mM K⁺) and proceed in hK⁺ (0 Na⁺, 91 mM K⁺) until the end. DALE was applied at concentrations ranging from 1 nM to 10 μM.

(A) There is no evident direct effect of the opioid agonist DALE on Kir3.4* currents.

(B) Opioid agonist DALE does not act through DOR to activate endogenous oocyte currents.

(C) Average current values before (Control) and after application of 10 μM DALE for oocytes injected with either Kir3.4* or DOR RNA. ns: not significant, Two-tailed Student's t-test.

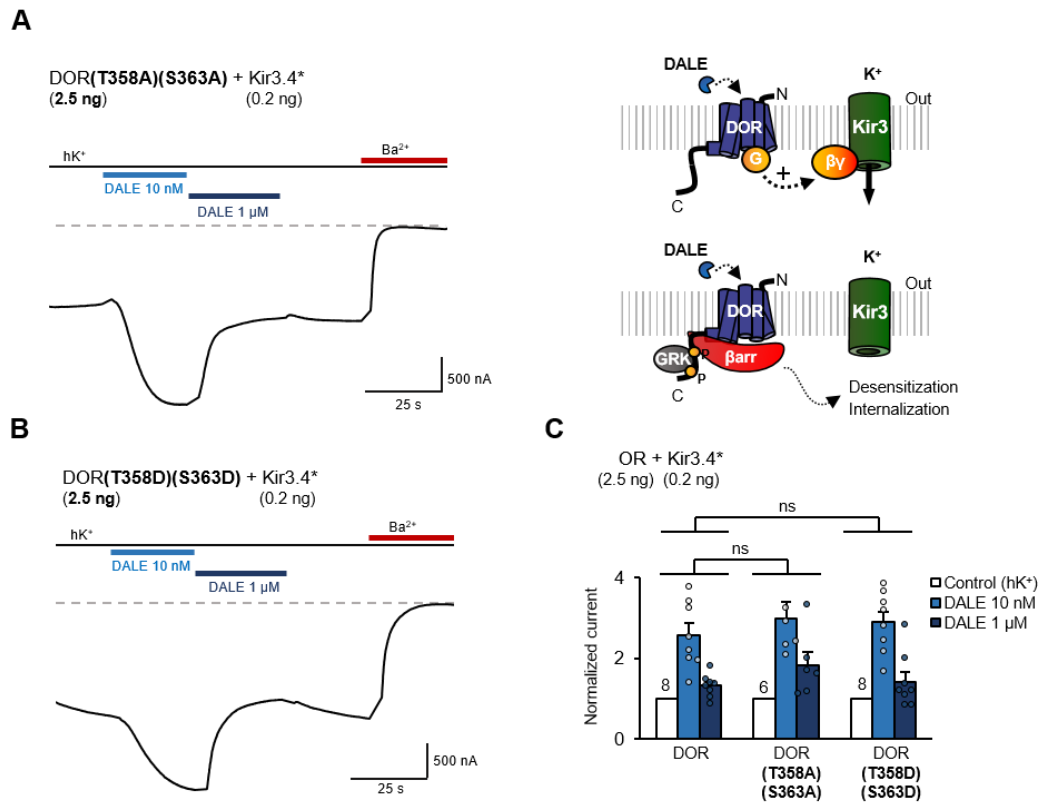
Inhibition of potassium currents therefore requires DOR and Kir3 channels to be coexpressed.



Supplementary figure a.2. Control test of the Gq/Gs inhibitor YM-254890.

(A) Exogenous Muscarinic 3 receptor (M3) couples with the calcium signaling of *Xenopus* oocytes by activating Gq upon agonist binding. Gq induces calcium release from intracellular stores, which in turn triggers large calcium-activated chloride currents.

(B) Representative traces at -50 mV in ND96 (see methods) from oocytes expressing Gq-coupled muscarinic M3 receptor without (left) and with (right) application of YM-254890. The M3 agonist ACh (5 µM) can no longer induce chloride currents after incubation with 10 µM YM-254890 for 10 min.



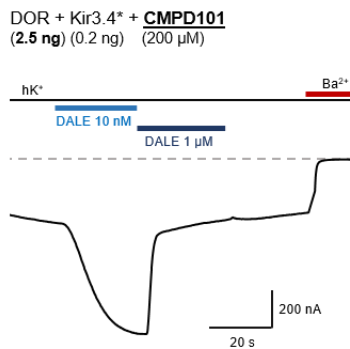
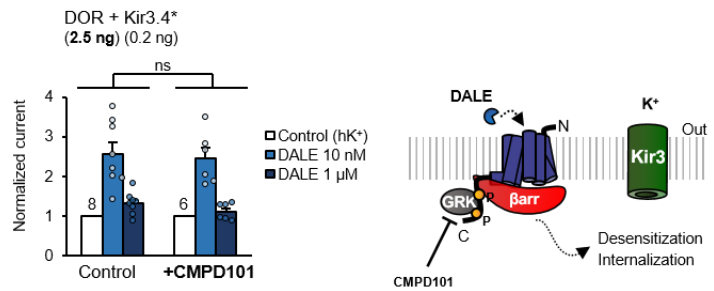
Supplementary figure a.3. Inhibition of Kir3.4* channels by DOR does not involve the phosphorylation of the receptor by GRK2/3 on residues Thr-358 and Ser-363.

Residues Thr-358 and Ser-363 are recognized targets of GRK2/3 phosphorylation and are involved in rapid receptor desensitization and internalization mediated by β -arrestins. Mutant DOR(T58A,S363A) has been shown to block GRK2 phosphorylation, while mutant (T358D,S363D) mimicks phosphorylation.

(A,B) Representative recordings of oocytes injected with 0.2 ng Kir3.4* RNA and 2.5 ng DOR(T358A,S363A) (A) or DOR(T358D,S363D) (B) RNA. Recordings show currents in hK⁺ (0 Na⁺, 91mM K⁺) while voltage is clamped at -50 mV. DALE was applied at the concentrations indicated, and 3 mM Ba²⁺ was applied at the end of the recording. Inhibition elicited by 1 μ M DALE is present in both DOR mutants.

(C) Average normalized currents of oocytes tested in the same conditions as in (A) vs. oocytes expressing Kir3.4* (0.2 ng RNA) and wt DOR (2.5 ng RNA). The numbers above the bars represent the number of oocytes tested. The responses of oocytes expressing wt DOR and oocytes expressing the DOR mutants are not statistically different. ns: not significant, 2-way ANOVA.

The phosphorylation of residues Thr-358 and Ser-363 at the C-terminal of DOR is not required for the inhibition. The data suggest that inhibition is not dependent on the phosphorylation by GRK2/3, and the associated receptor desensitization.

A**B**

Supplementary figure a.4. Inhibition of Kir3.4* channels by DOR does not involve the kinase activity of GRK2/3.

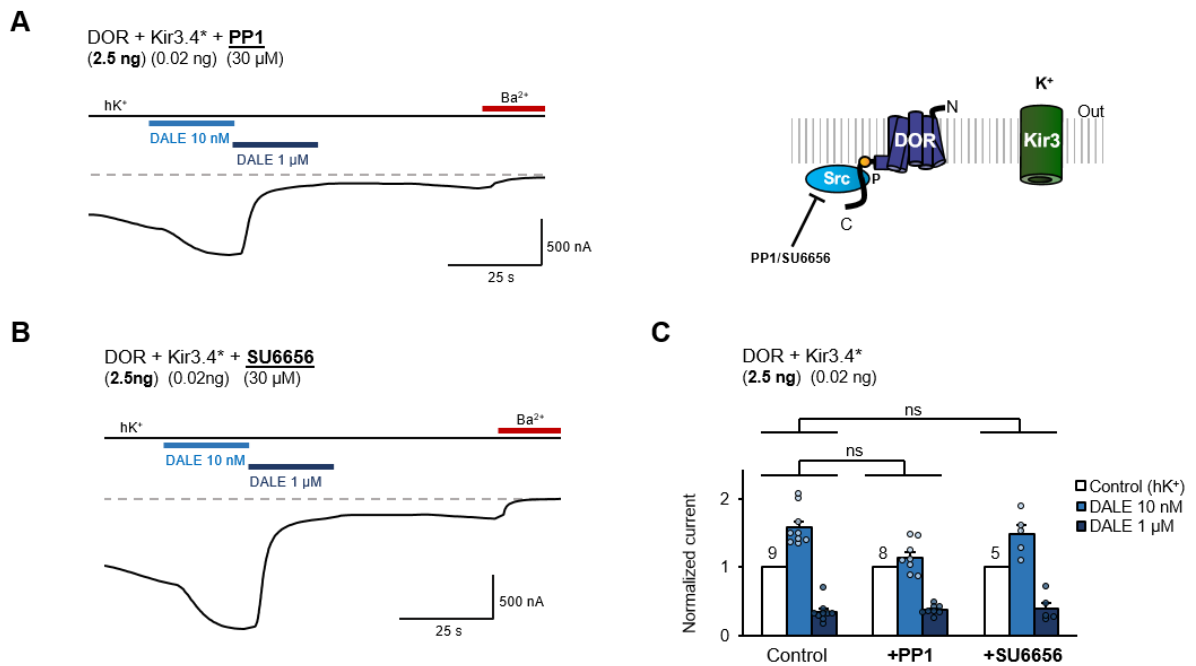
GRK2/3 phosphorylation upon receptor activation is involved in rapid receptor desensitization and internalization mediated by β-arrestins.

(A) Representative recording of an oocyte injected with 0.2 ng Kir3.4* RNA and 2.5 ng DOR RNA after incubation for 60 minutes with the inhibitor of the kinase activity of GRK2/3 - CMPD101 (200 μM). Recording shows currents in hK⁺ (0 Na⁺, 91mM K⁺) while voltage is clamped at -50 mV. DALE was applied at the concentrations indicated, and 3 mM Ba²⁺ was applied at the end of the recordings.

(B) Average normalized currents of oocytes tested in the same conditions as in (A) vs. oocytes not exposed to the inhibitor (Control). The numbers above the bars represent the number of oocytes tested. The response of control oocytes and oocytes subjected to CMPD101 is not statistically different. ns: not significant, 2-way ANOVA.

Note that the use of the inhibitor CMPD101 in oocytes was validated elsewhere (Ågren & Sahlholm, 2021).

There is no effect of the GRK2/GRK3 inhibitor, suggesting that DOR-mediated inhibition is not dependent on the phosphorylation by GRK2/GRK3. This data is in agreement with experiments using phosphorylation mutants DOR(T358A,S363A) and DOR(T358D,S363D).



Supplementary figure a.5. Inhibition of Kir3.4* channels by DOR does not require the activity of Src tyrosine kinases.

Src tyrosine kinases have been implicated in the phosphorylation of DOR at the beginning of the C-terminal in an activation-independent manner, modulating its activity.

(A,B) Representative recording of an oocyte injected with 0.02 ng Kir3.4* RNA and 2.5 ng DOR RNA after incubation for 120 minutes with the inhibitors of Src tyrosine kinases PP1 at 30 μ M (A) or SU6656 at 30 μ M (B). Recordings show currents in hK⁺ (0 Na⁺, 91mM K⁺) while voltage is clamped at -50 mV. DALE was applied at the concentrations indicated, and 3 mM Ba²⁺ was applied at the end of the recordings.

(C) Average normalized currents of oocytes tested in the same conditions as in (A) vs. oocytes not exposed to the inhibitors (Control). The numbers above the bars represent the number of oocytes tested. The responses of control oocytes and oocytes subjected to either of the inhibitors are not statistically different. There is no effect of the Src-inhibitors on the inhibition of Kir3.4* by DOR.

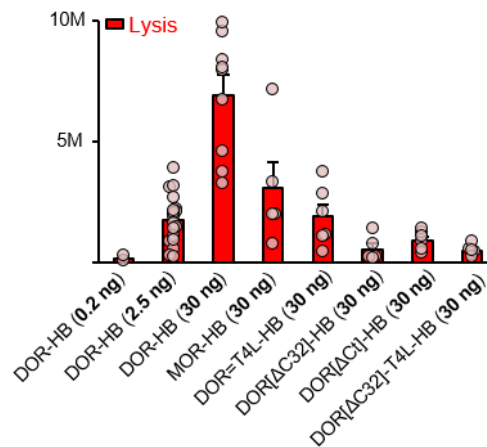
ns: not significant, 2-way ANOVA.

Note that the use of the inhibitors SU6656 and PP1²⁰ in oocytes was validated elsewhere (Stival *et al.*, 2015; Tokmakov *et al.*, 2002).

The data suggest that DOR-mediated inhibition is not dependent on the phosphorylation by Src tyrosine kinases.

²⁰PP1 4-amino-5-(4-methylphenyl)-7-(t-butyl)pyrazolo[3,4-d]- pyrimidine.

SU6656 (3Z)-N,N-Dimethyl-2-oxo-3-(4,5,6,7-tetrahydro-1H-indol-2-ylmethylidene)-2,3-dihydro-1H-indole-5-sulfonamide.



Supplementary figure a.6. DOR[ΔC32], which inhibits Kir3.4* currents, has not only low surface expression, but also low total expression.

Mean luminescence recorded in permeabilized oocytes expressing the specified HiBiT-tagged (HB) receptors and 0-0.2 ng of Kir3.4* RNA. Each point represents a single oocyte.

Receptor-HB corresponds to the receptor with the HiBiT-tag fused to the N-terminal.

DOR=T4L corresponds to the fusion of the Lysozyme of bacteriophage T4 (T4L) to the intracellular loop 3 (ICL3) of DOR.

DOR[ΔC32] corresponds to the deletion of the last 32 residues of the C-terminal of DOR.

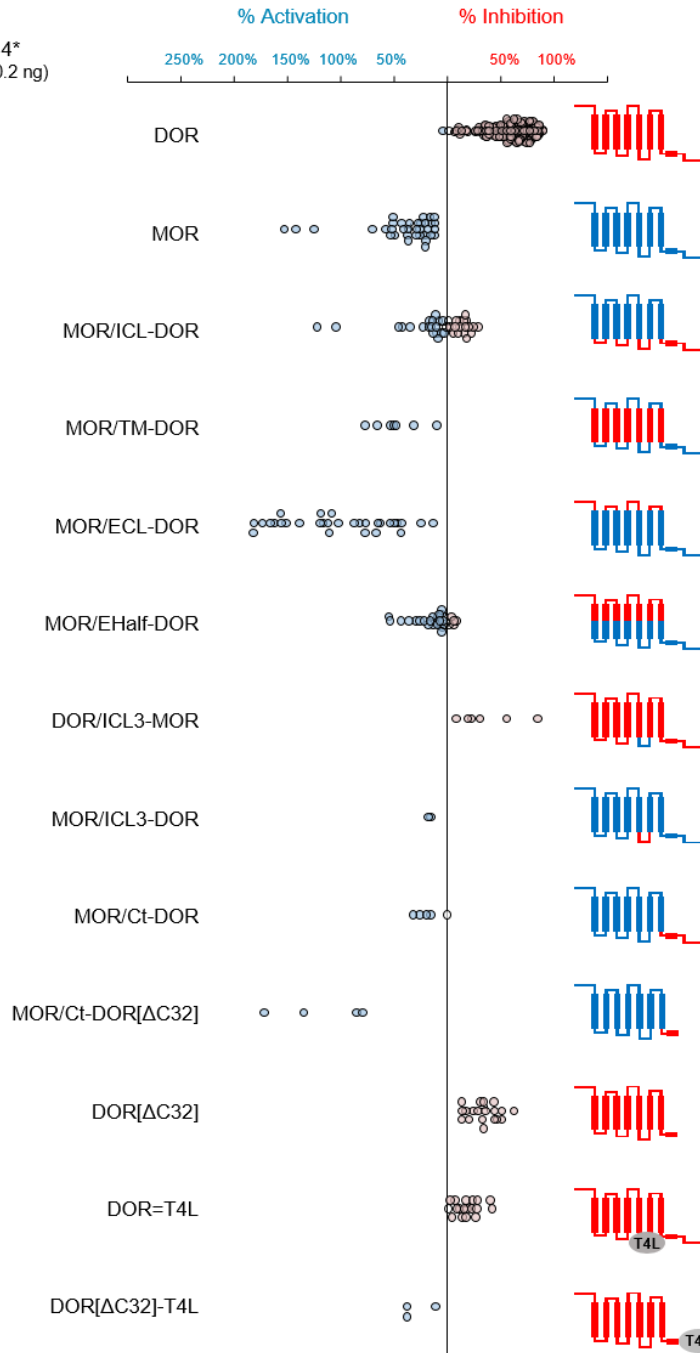
DOR[ΔCt] corresponds to the deletion of the full C-terminal of DOR (51 residues).

DOR[ΔC32]-T4L corresponds to DOR[ΔC32] fused at the C-terminal to T4L. See Supplementary figure a.7. for the topology of the different constructs.

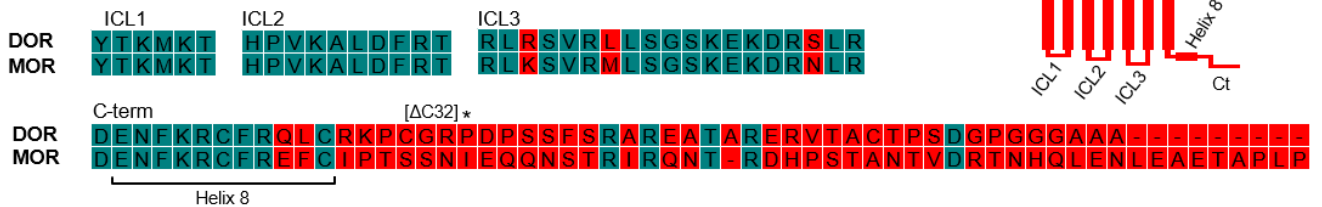
The inhibition of Kir3.4* channels depends on the DOR RNA amount injected. An increase in RNA amount of DOR (from 0.2 to 30 ng) leads to an increase in total expression, seen by the increase in luminescence of permeabilized oocytes. One hypothesis could be that inhibition arises from intracellular signaling of DOR, and it would be thus potentiated by an intracellular accumulation of DOR in high expression conditions. DOR-HB (30 ng) can inhibit Kir3.4* currents (seen in Figure a.19.) and it is in fact, the receptor with the highest total expression (≈7M RLUs). However, note that DOR[ΔC32]-HB has very low total expression (≈600K RLUs) and can still inhibit Kir3.4* currents. Intracellular accumulation of DOR does not seem to fully justify the inhibitory behavior.

A

OR + Kir3.4*
(2.5-30 ng) (0.02-0.2 ng)



B



Supplementary figure a.7. Topology of different MOR/DOR chimeras and summary of their effects on Kir3.4* currents.

Different DOR constructions and chimeras between MOR and DOR were created in an attempt to identify the molecular domain involved in the inhibition. The schematic topology of the constructs is shown on the right, and the nomenclature (on the left) refers to:
ICL – Intracellular loops

TM – Transmembrane domain

ECL – Extracellular loops

Ehalf – Extracellular half

ICL3 – Intracellular loop 3

Ct - C-terminal

Δ C32 - Truncation of the last 32 residues of the C-terminal

T4L - Lysozyme of bacteriophage T4 (T4L)

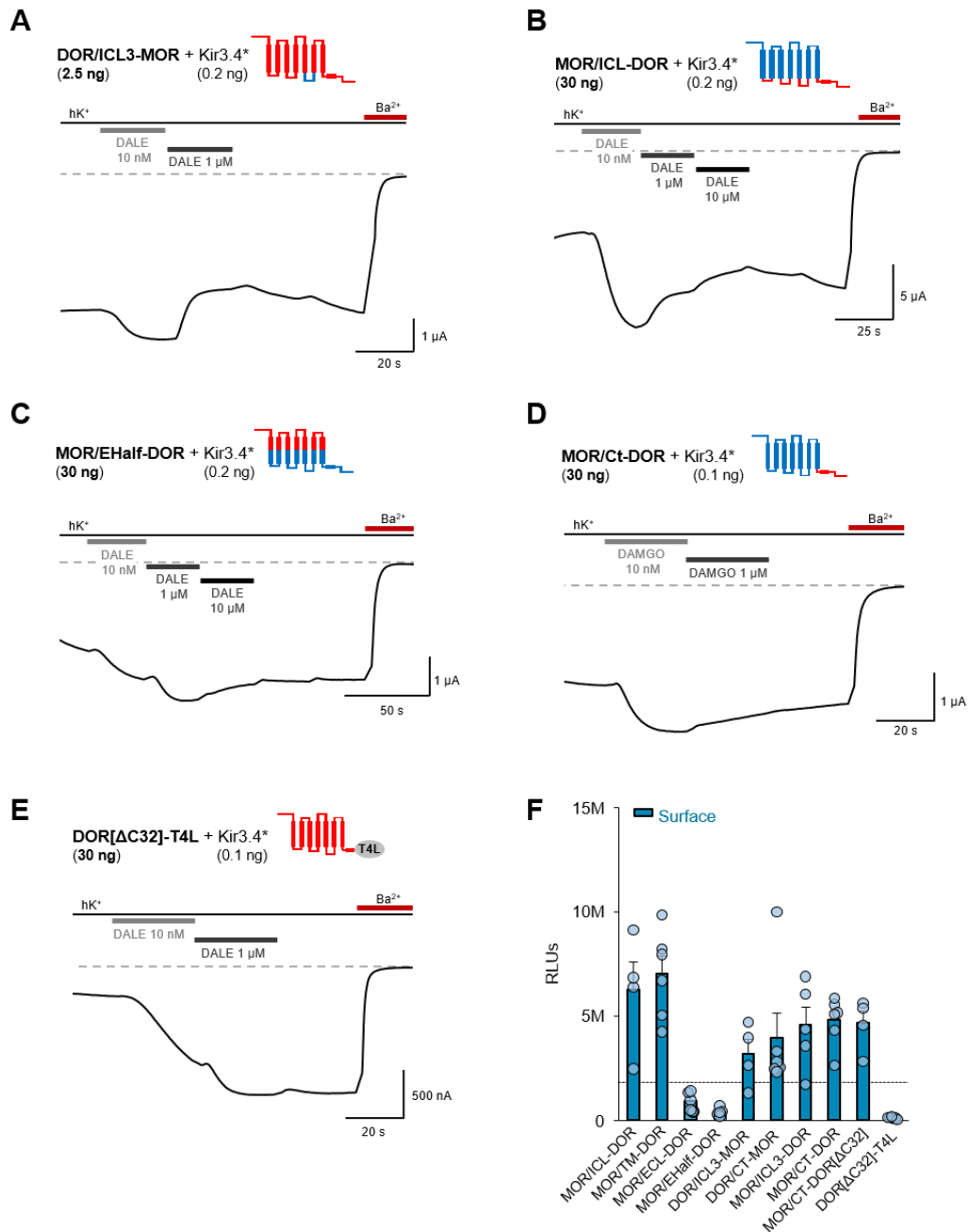
(A) Summary of the responses in 1 μ M DALE of oocytes injected with RNA of the specified receptor constructs and Kir3.4* RNA. Data points represent the response of single oocytes. % Inhibition or activation is calculated by the % decrease or increase of current, respectively, elicited by 1 μ M DALE, with respect to the current in 10 nM DALE. The response varies greatly in different oocytes injected with the same construct. Constructs that show clear inhibition in some of the tested oocytes are DOR/ICL3-MOR and MOR/ICL-DOR.

DOR/ICL3-MOR corresponds to the DOR where the ICL3 was substituted by that of the MOR. The ICL3s of the two receptors differ only in 3 residues. Simply interchanging the ICL3s of the receptors did not change the inhibitory behavior of MOR (MOR/ICL3-DOR) or DOR (DOR/ICL3-MOR). MOR/ICL-DOR corresponds to the MOR receptor where all the intracellular loops and C-terminal were substituted by those of DOR. The intracellular loops of the two receptors differ in the ICL3 (3 residues) but mostly in the C-terminal.

(B) Alignment of the intracellular regions of MOR and DOR. * Indicates the last residue of DOR[Δ C32].

Together with the data on the DOR[Δ C32], which retains inhibitory capability, this seems to suggest that the inhibitory capability arises from differences in the C-terminal around the region of the intracellular short helix 8. The importance of said domain for the inhibition is further supported by the results of construct DOR[Δ C32] fused to T4L at the C-terminal (DOR[Δ C32]-T4L). T4L obstructs access to the C-terminal disabling inhibition (few data points). However, simply exchanging the C-terminal region of MOR with that of DOR (MOR/Ct-DOR) did not suffice to transfer inhibitory capability. More experiments are necessary to deconvolute these results.

See Supplementary figure a.8 for recordings of the relevant constructs.



Supplementary figure a.8. Recordings and surface expression of different MOR/DOR chimeras discussed in Supplementary figure a.7.

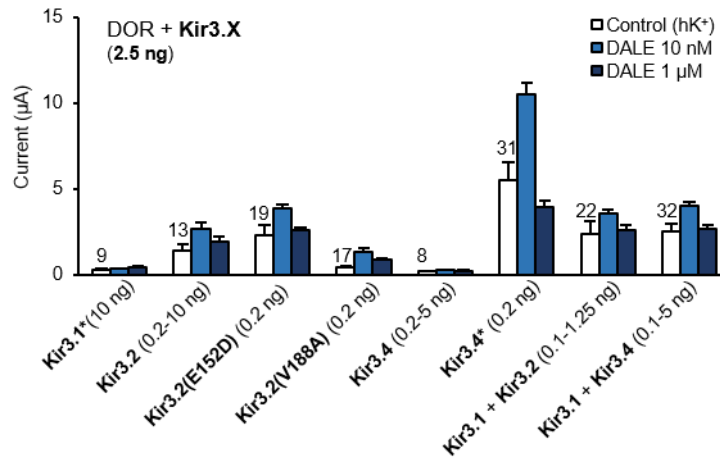
(A-E) Representative recordings of oocytes injected with 0.1-0.2 ng Kir3.4* RNA and RNA of the specified receptors (not tagged to HiBiT). Recordings show currents in hK⁺ (0 Na⁺, 91mM K⁺) while voltage is clamped at -50 mV. DALE or DAMGO were applied at the concentrations indicated, and 3 mM Ba²⁺ was applied at the end of the recordings. Note that (A) DOR/ICL3-MOR (2.5 ng RNA) and (B) MOR/ICL-DOR (30 ng RNA) can inhibit Kir3.4* currents upon application of 1 μM DALE.

(C) In a few oocytes, MOR/Ehalf-DOR shows a small reduction in currents upon application of 1-10 μM DALE. However, it does not show the fast kinetics of DOR inhibition.

(D) Exchanging the C-terminal region of MOR with that of DOR (MOR/Ct-DOR) did not suffice to transfer inhibitory capability.

(E) DOR[ΔC32] fused to T4L at the C-terminal (DOR[ΔC32]-T4L) did not show inhibition.

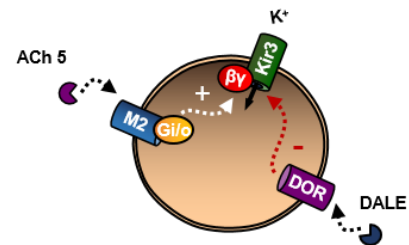
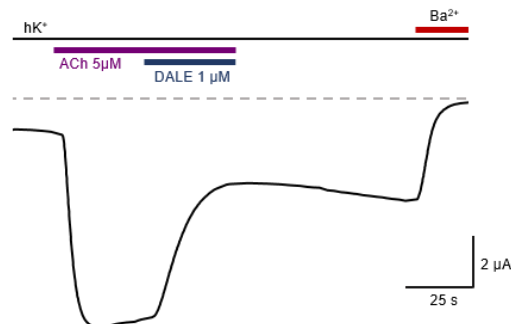
(F) Mean luminescence recorded in oocytes expressing the specified receptors (tagged to HiBiT on the N-terminal) and 0-0.2 ng of Kir3.4* RNA. Each point represents a single oocyte. Dashed line marks the surface luminescence level of oocytes injected with 2.5 ng IL6-DOR-HB RNA (DOR-HB construction with an added secretion signal sequence). DOR[ΔC32]-T4L (98±18K RLU) has a similar surface expression level as DOR[ΔC32] (108±15K RLU), shown in Figure a.19, but lost inhibitory capability (E).



Supplementary figure a.9. Average current values of different Kir3 channels coexpressed with DOR show intrinsic differences between the different channels.

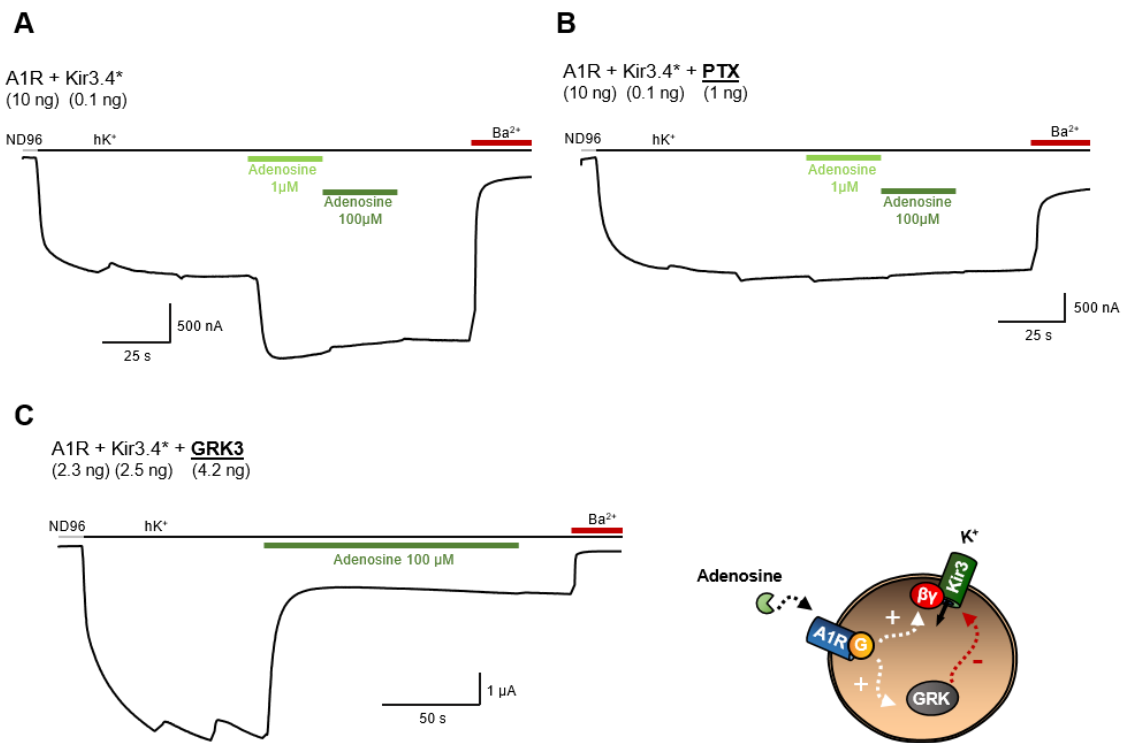
Average normalized currents of oocytes injected with the specified Kir3 RNA and 2.5 ng DOR RNA. The numbers above the bars represent the number of oocytes tested. Note that both homotetrameric channels of Kir3.4 or Kir3.1* show small currents under 1 µA. However, as seen in Figure a.20., Kir3.4 can be inhibited by DOR while Kir3.1* cannot.

DORF + Kir3.4* + M2
(0.2 ng) (0.02 ng) (2.5 ng)



Supplementary figure a.10. DOR can inhibit Kir3.4* currents activated by other Gi/o-coupled GPCRs.

Representative recording (N=7) of an oocyte injected with 0.02 ng Kir3.4* RNA, 0.2 ng DOR RNA, and 2.5 ng Gi/o-coupled Muscarinic 2 receptor (M2). Recording shows currents in hK⁺ (0 Na⁺, 91mM K⁺) while voltage is clamped at -50 mV. 1 µM DALE was applied in combination with 5 µM Acetylcholine (ACh 5 µM) after the first application of 5 µM ACh. Upon application of 5 µM ACh, M2 can activate and elicit an increase of Kir3.4* currents. The subsequent application of 1 µM DALE acts through DOR to inhibit M2-activated Kir3.4* currents. Furthermore, inhibition was evident even at low expression of DOR (0.2 ng RNA injected).

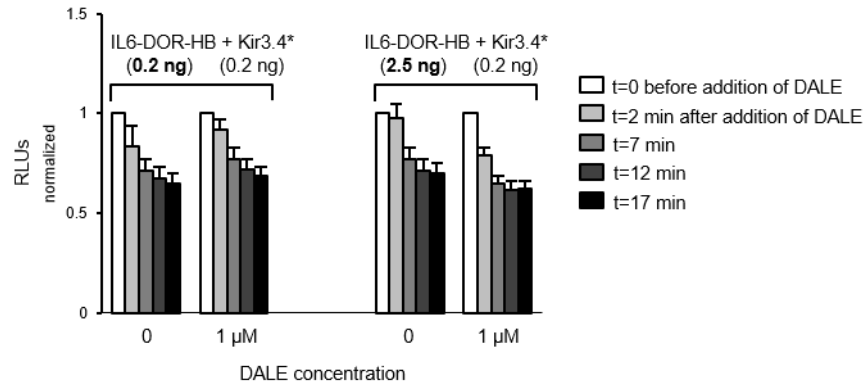


Supplementary figure a.11. A1R can inhibit Kir3.4* currents when coexpressed with GRK3.

(A,B) Representative recordings (of N=2) of oocytes injected with 0.1 ng Kir3.4* RNA and 10 ng Adenosine 1 Receptor (A1R) without (A) or with (B) the coexpression of PTX (1 ng of RNA). Recordings start in ND96 bath solution (91 mM Na⁺, 2 mM K⁺) and proceeds in hK⁺ (0 Na⁺, 91mM K⁺). Voltage is clamped at -50 mV. 100 μM Adenosine was applied where indicated, and 3 mM Ba²⁺ was applied at the end of the recording. 100 μM Adenosine elicits activation of Kir3.4* (A) which is abrogated by the coexpression of PTX (B). The coexpression of PTX effectively blocks Gi/o signaling and, consequently, the activation of Kir3.4* by A1R. The presence of PTX does not reveal any hidden inhibition even if A1R is highly expressed (10 ng RNA).

(C) Representative recording (N=10) of an oocyte injected with 2.5 ng Kir3.4* RNA, 2.3 ng A1R RNA, and 4.2 ng GRK3 RNA. Adenosine 100 μM elicits a fast and robust inhibition of Kir3.4* through A1R when coexpressed with GRK3.

This data is in agreement with Raveh *et al.* (2010) description of the non-enzymatic effects of GRK2/3 on A1R activation of Kir3. In the conditions tested here, further than desensitizing, A1R effectively inhibits Kir3.4* currents to a level under the initial basal current, similar to the inhibition of Kir3.4* by DOR.

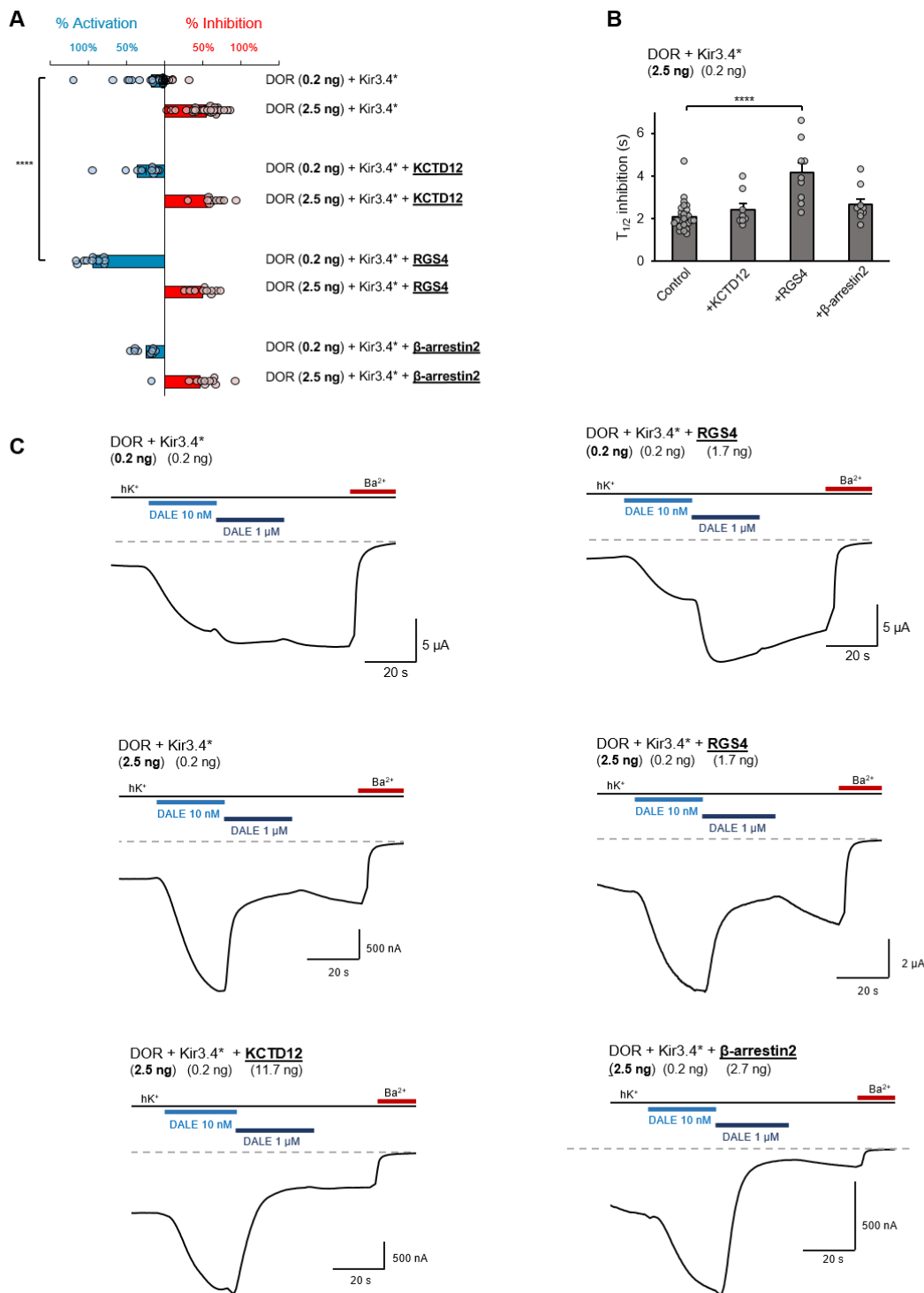


Supplementary figure a.12. Application of 1 μM DALE does not acutely affect the amount of surface DOR.

Mean luminescence was recorded in oocytes from the same batch expressing IL6-DOR-HB (0.2 or 2.5 ng RNA) with Kir3.4* (0.2 ng RNA). IL6-DOR-HB corresponds to the DOR fused with the HiBiT tag at the N-terminal, and an extra secretion signal sequence of Interleukine 6 (IL6) to improve surface expression. The function of this construct was validated (see Figure a.19). Values of luminescence for all conditions were normalized to the initial luminescence value t=0.

Oocytes were incubated with either 1 μM DALE or no agonist (0), and luminescence was recorded at the indicated times. Values represent the means of 3-4 oocytes. Two-way ANOVA shows no significant differences between the 4 groups.

There is a decrease in the luminescence signal with time, which is uniform for all the conditions tested. The data suggest that the inhibition of Kir3 at 1 μM DALE is not the result of DOR internalization.



Supplementary figure a.13. Coexpressing regulatory proteins KCTD12, RGS4 and β -arrestin2 with Kir3.4* and DOR has no major impact on the inhibition.

KCTD12, RGS4 and, β -arrestin2 have been implicated in the regulation of Kir3.4* and/or DOR activity. KCTD12 can act under the control of GABA_B receptors and sequester G $\beta\gamma$ subunits from activated Kir3 channels, blocking said activation. RGS4 can lead to fast desensitization of Kir3 currents by accelerating the G protein cycle. β -arrestin2 can desensitize and lead to the internalization of DOR, obstructing G protein signaling and activation of Kir3.

(A) Summary of responses to 1 μ M DALE of oocytes injected with the indicated mix of RNAs. For all conditions, Kir3.4* RNA was 0.2 ng. RNA amounts for the regulatory proteins impose a protein stoichiometry of 1:1 to DOR 2.5 ng, and were as follows: 11.7 ng for KCTD12, 1.7 ng for RGS4, 2.7 ng for β -arrestin2.

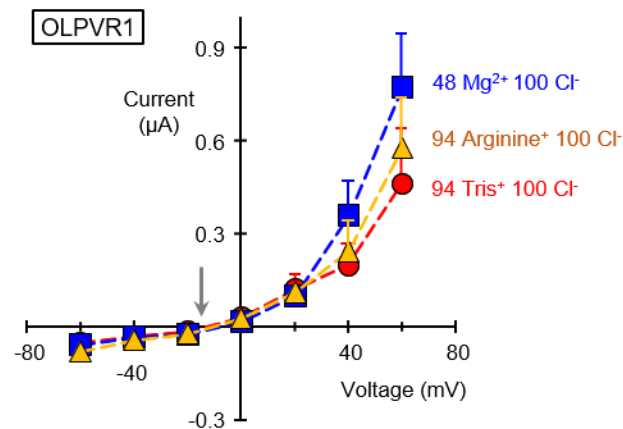
Bars represent the average response, while data points represent the response of single oocytes. % Inhibition or activation is calculated by the % decrease or increase of current, respectively, elicited by 1 μ M DALE with respect to the current in 10 nM DALE. % Activation was compared by one-way ANOVA with Dunnett's multiple comparison tests against the control (DOR 0.2 ng + Kir3.4* 0.2 ng). Only the response of the control condition and coexpression of RGS4 were significantly different. **** $P < 0.0001$. % Inhibition was compared by one-way ANOVA with Dunnett's multiple comparison tests against the control (DOR 2.5 ng + Kir3.4* 0.2 ng). The responses are not significantly different.

(B) Average half-time values of the inhibition by 1 μ M DALE for oocytes injected with 0.2 ng Kir3.4*, 2.5 ng DOR, and the RNA of the specified regulatory protein. Coexpressing RGS4 significantly slows down the inhibition. **** $P < 0.0001$, one-way ANOVA with Dunnett's post hoc test.

(C) Representative recordings of oocytes injected with the specified RNA ratios of Kir3.4*, DOR and regulatory proteins RGS4, KCTD12 or β -arrestin2. Recording shows currents in hK⁺ (0 Na⁺, 91mM K⁺) while voltage is clamped at -50 mV. DALE was applied at the concentrations indicated, and 3 mM Ba²⁺ was applied at the end of the recording.

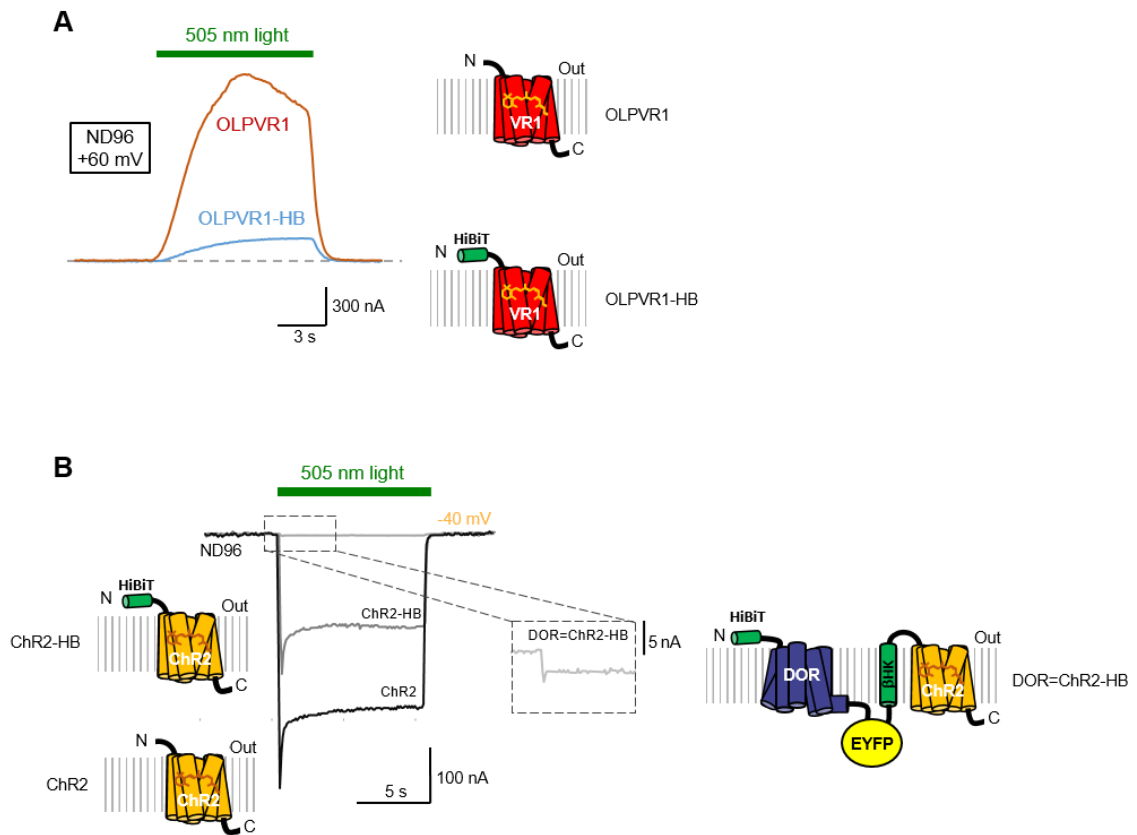
Inhibition elicited by 1 μ M DALE is present and equally effective in oocytes expressing 2.5 ng DOR and any of the specified regulatory proteins. The data suggest RGS4, KCTD12 or β -arrestin2 are not the major players in the inhibition of Kir3.4* by DOR. The increase in % activation observed when coexpressing RGS4 is most likely connected to the slowing down of the inhibition. It is not clear if RGS4 directly slows down inhibition and consequently increases apparent activation or the other way around, i.e., directly increases activation slowing down apparent inhibition. Regardless, the effects of RGS4, most likely on the G-protein activation cycle, seem to impact the equilibrium between activation and inhibition of Kir3.4* by DOR, but not the maximal effect of inhibition.

B - Supplementary figures – Project B



Supplementary figure b.1. Substitution of the cation in the extracellular solution does not affect the reversal potential of OLPVR1 photo-induced currents.

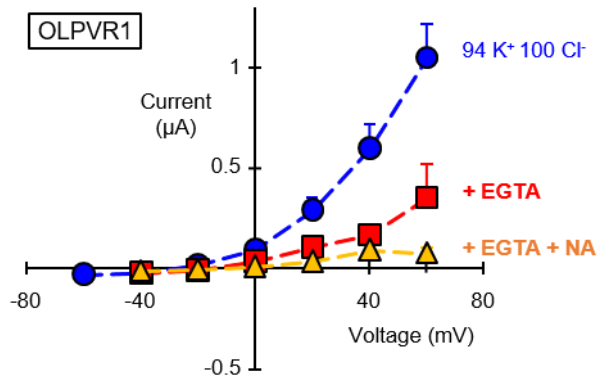
Current-voltage relationships of OLPVR1 photo-induced stationary currents. Oocytes were injected with 30 ng OLPVR1 RNA and incubated for 72-96h in standard physiological solution with 1 μM all-trans retinal. Oocytes were bathed in the specified solutions. 505-nm light was applied for 10 seconds. All solutions contained 2 mM Ca²⁺ and 5 mM HEPES as well as the ions indicated (concentrations in mM). Arginine and Tris solutions also contained 1 mM Mg²⁺. Each data point represents the average of 4-11 oocytes. Reversal potential in the different solutions was approximately -18 mV which is closer to the predicted reversal potential of Cl⁻ (between -36 mV and -12 mV) than that of Mg²⁺ (≈58mV). Tris and Arginine are impermeant cationic species. The data supports the hypothesis that OLPVR1 photo-activation induces chloride currents in *Xenopus* oocytes.



Supplementary figure b.2. Functional validation of HiBiT and DOR fusion constructs.

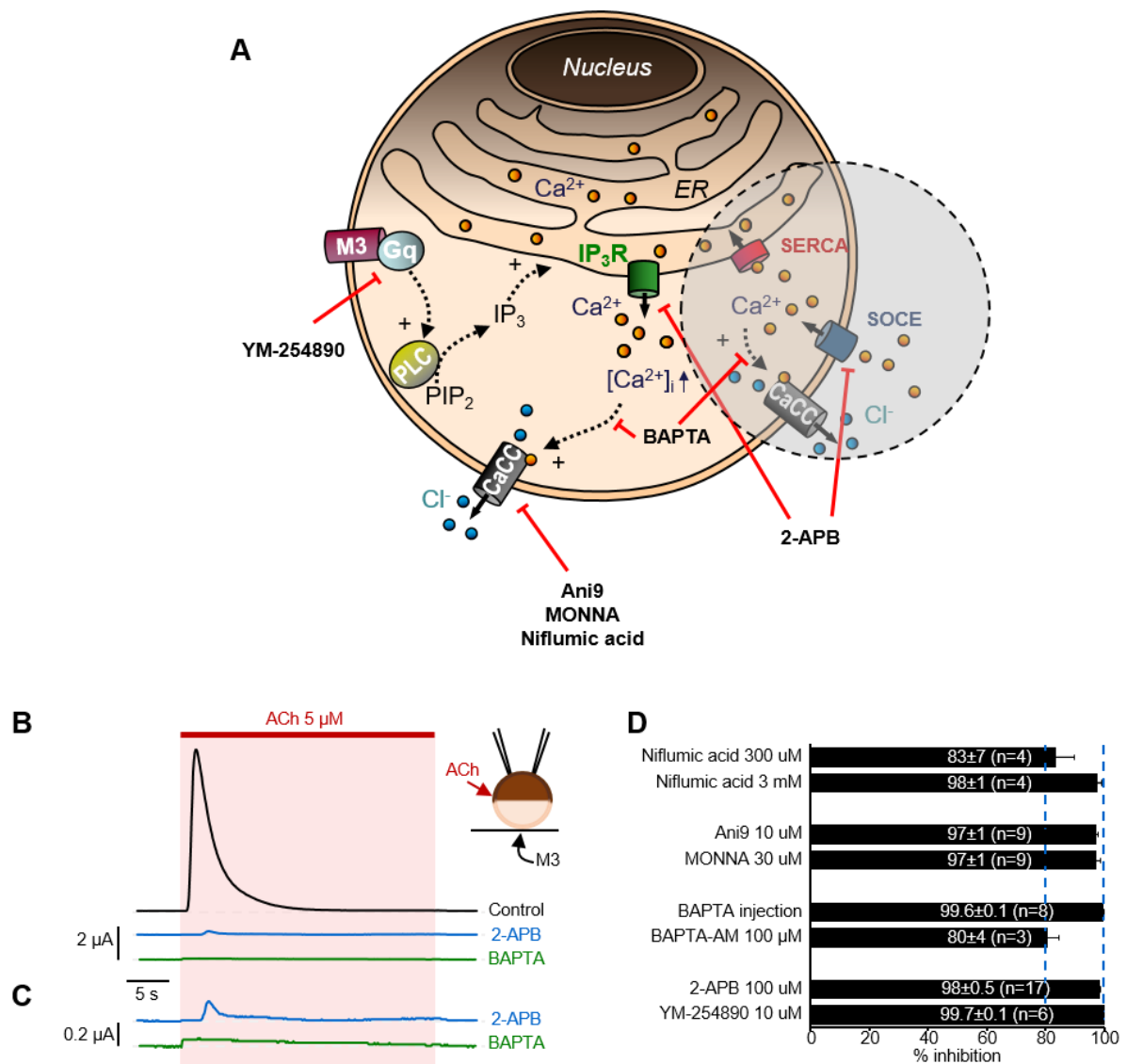
(A) OLPVR1 tagged with HiBiT is functional, albeit expression is reduced. Representative traces of oocytes from the same batch injected with the same amount of RNA (30 ng) of the two different constructs.

(B) Fusing ChR2 with HiBiT or DOR maintains the functional properties of the protein. HiBiT-tag decreases the expression but less than the fusion to DOR. Representative traces of oocytes expressing the different ChR2 constructs after 72h incubation with 1 μ M all-trans retinal. Oocytes were injected with 7.5 ng RNA except for DOR=ChR2 (30 ng).



Supplementary figure b.3. Extracellular EGTA, as well as extracellular Niflumic Acid, reduce the average peak currents induced by OLPVR1.

Current-voltage relationships of OLPVR1 photo-induced peak currents. Oocytes were injected with 30 ng OLPVR1 RNA and incubated for 96h in standard physiological solution with 1 μ M all-trans retinal. Oocytes were clamped at the specified voltage and solution. 505-nm light was applied for 10 seconds. All solutions contained 1 mM Mg^{2+} and 5 mM HEPES as well as the ions indicated (concentrations in mM). Solution in blue also contained 2 mM Ca^{2+} . The same 3 oocytes were tested in the different solutions. Reversal potential in the different solutions was -20 mV, which is close to the predicted reversal potential of Cl^- (between -36 mV and -12 mV). 1 mM EGTA chelates extracellular calcium, and 300 μ M of Niflumic Acid (NA) partially blocks chloride channels. The data supports the hypothesis that OLPVR1 photo-activation induces calcium release from intracellular stores and consequent activation of chloride channels in *Xenopus* oocytes.



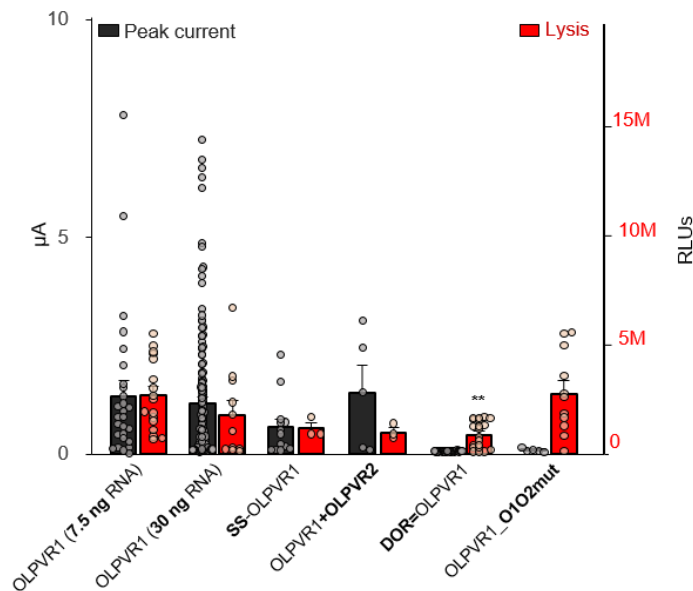
Supplementary figure b.4. Control tests of inhibitors used in this study.

(A) Illustration of the targets of the different inhibitors tested.

(B) Representative traces at +40 mV in ND96 (see methods) from oocytes expressing Gq-coupled muscarinic M3 receptor. The M3 agonist ACh (5 μ M) induces Ca^{2+} release via activation of Gq and IP_3 receptors, and triggers large calcium-activated chloride currents. Traces illustrate the effects of oocyte incubation in 100 μ M 2-APB for 60 minutes (blue) or injection of BAPTA 30 minutes (green) before recording.

(C) Same traces as in (A), stretched vertically 10-fold.

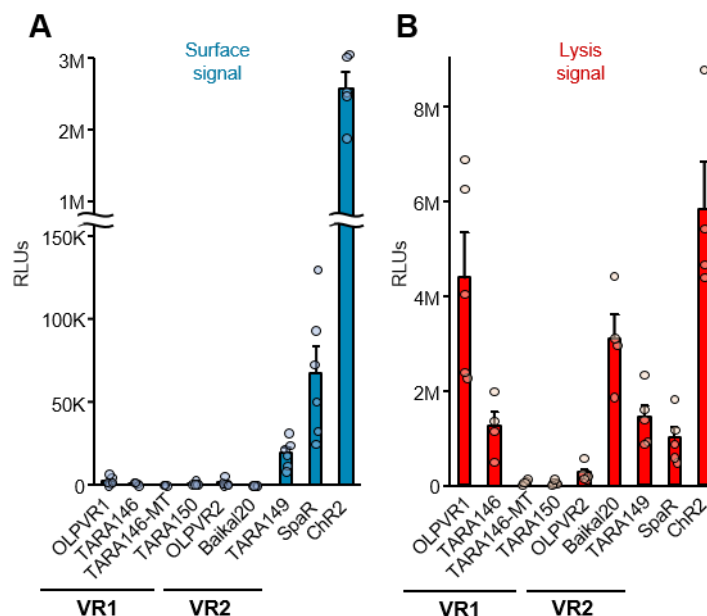
(D) Average inhibition of ACh-induced peak currents by indicated compounds. Targets, concentrations and incubation times were: Niflumic acid (Cl^- channels, 300-3000 μ M, 60-300'), Ani9 (CaCCs, 10-30 μ M, 30-180'), MONNA (CaCCs, 30 μ M, 20-180'), BAPTA injection (Ca^{2+} chelator, 50 nl of a 40-nM solution per oocyte, 30-120'), BAPTA-AM (Ca^{2+} chelator, 100 μ M, 240'), 2-APB (IP₃ receptors and SOCE, 100 μ M, 20-180'), YM-254890 (Gq proteins, 10 μ M, 10'). 2-APB and YM-254890 were also tested in the same bath solution without Ca^{2+} with similar results. All compounds were also tested at -50 mV with similar results.



Supplementary figure b.5. Comparison of peak currents of different OLPVR1 constructs with the luminescence after lysis of their HiBiT-tagged counterparts.

Luminescence values of lysed oocytes expressing 7.5-30 ng of HiBiT-tagged constructs are represented in red bars (right axis). Each data point represents a single oocyte. **P < 0.01, one-way ANOVA followed by Dunnett's multiple comparison test against the control OLPVR1 (7.5 ng). When not indicated, the difference is not significant.

Peak photo-induced currents of untagged constructs at +60 mV (all solutions) are represented as black bars (left axis). Note that OLPVR1_O1O2mut, which does not have surface expression (seen in Figure b.13), is not functional despite accumulating intracellularly like wt OLPVR1.



Supplementary figure b.6. Surface and intracellular expressions of different rhodopsins compared to ChR2.

Mean luminescence was recorded in oocytes injected with 7.5 ng RNA coding for HiBiT-tagged VRs and ChR2 before (panel A with dual-scale axis) and after membrane permeabilization (panel B). Values are averages from 4-6 batches of oocytes. For each batch, data points in each condition were obtained as the average luminescence from 3 oocytes. Viral rhodopsins have low or no surface expression compared to other rhodopsins such as SpaR from bacteria *Shingomonas paucimobilis* or ChR2 from algae *Chlamydomonas reinhardtii*.

C - Extended information on the molecular biology and protein engineering

Table c.1. Detailed information about the design of the different proteins used in Project A.

'GeneCust' or 'GenScript' indicates that the specified company prepared the constructions.


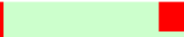

Construct	Molecular manipulation	Protein size	Protein origin	Comments
A1R	Subcloning	326	Human	NM_000674.3
DOR	Subcloning	372	Human	NP_000902.3 with Phe-27
DOR(Δ C32)	Truncation of last 32 residues at C-terminal of DOR	340	Human	Cys-27
DOR(Δ C32)-HB	Insertion of HB tag on DOR(Δ C32)	357	Human	
DOR(Δ C32)-T4L	Fusion of T4L at C-terminal of DOR(Δ C32)	500	Human, T4 phage	T4L from Granier <i>et al.</i> , 2012
DOR(Δ C32)-T4L-HB	Insertion of HB tag on DOR(Δ C32)-T4L	517	Human, T4 phage	
DOR(Δ Ct)	Stop codon insertion after residue 321 of DOR(Δ C32) (GeneCust)	321	Human	Full C-terminal truncation
DOR(Δ Ct)-HB	Insertion of HB tag on DOR(Δ Ct)	338	Human	
DOR(T358A,S363A)	Mutagenesis of DOR at positions 358 and 363 to A (GeneCust)	372	Human	NP_000902.3 with Phe-27
DOR(T358D,S363D)	Mutagenesis of DOR at positions 358 and 363 to D (GeneCust)	372	Human	NP_000902.3 with Phe-27
DOR/Ct-MOR	DOR(M1-R330)-MOR(E351-P400)	380	Human MOR and DOR	
DOR/Ct-MOR-HB	Insertion of HB tag on DOR/Ct-MOR	397	Human MOR and DOR	
DOR=T4L	Insertion of T4L at ICL3 of DOR. DOR(M1-V243)-T4L-DOR(E251-A372).	526	Human, T4 phage	NP_000902.3 with Phe-27. Based on construction used in Granier <i>et al.</i> , 2012.
DOR=T4L-HB	Insertion of HB tag on DOR=T4L	543	Human, T4 phage	Phe-27
DOR/ICL3-MOR	Mutagenesis (R241K)(L245M)(S255N)	372	Human MOR and DOR	Phe-27
DOR/ICL3-MOR-HB	Insertion of HB tag on DOR/ICL3-MOR	389	Human MOR and DOR	Mutagenesis (R241K)(L245M)(S255N)
DOR-HB	Insertion of HB tag on DOR	389	Human	
GRK2	Subcloning	689	Human	NM_001619.5
GRK3	Subcloning	688	Human	NM_005160.4
HiBiT-DOR ^C	Mutagenesis F27C on HiBiT-DORF	389	Human	
HiBiT-DOR ^F		389	Human	Same as DOR-HB
HiBiT-Kir3.4(S143T)	Synthesized by GeneCust.	521	Human	IL6-(VS)-HB-(GSSGGSSG)-M2(M1-L53)-Kir3.4(S143T)
IL6-DOR-HB	Insertion of IL6 and a (VS) linker on DOR-HB	421	Human	
KCTD12	Subcloning	325	Human	NM_004313.4
Kir3.1	Already in the lab	501	Human	Original from Dr. Diomedes Logothetis.
Kir3.1(F137S) or Kir3.1*	Already in the lab	501	Human	Original from Dr. Diomedes Logothetis.
Kir3.2	Already in the lab	414	<i>Mus musculus</i>	NP_001020755.1
Kir3.2(E152D)	Mutagenesis (E152D) on Kir3.2	414	<i>Mus musculus</i>	
Kir3.2(V188A)	Mutagenesis (V188A) on Kir3.2	414	<i>Mus musculus</i>	
Kir3.4	Already in the lab	419	Human	U39195.1
Kir3.4(S143T) or Kir3.4*	Already in the lab	419	Human	Mutagenesis of NP_000881.3



Construct	Molecular manipulation	Protein size	Protein origin	Comments
Kir3.4(S143T)(D223N)	Mutagenesis (D223N) on Kir3.4(S143T)	419	Human	
Kir3.4(S143T)(I229L)	Mutagenesis (I229L) on Kir3.4(S143T)	419	Human	
Kir3.4(S143T)(R196A)	Mutagenesis (R196A) on Kir3.4(S143T)	419	Human	
Kir3.4(S143T)(S176P)	Mutagenesis (S176P) on Kir3.4(S143T)	419	Human	
Kir3.4(S143T)(S191A)	Mutagenesis (S191A) on Kir3.4(S143T)	419	Human	
Kir3.4(S143T)/CT-Kir3.1	Substitution of Kir3.4(S143T) C-terminal by Kir3.1 C-terminal	507	Human	Kir3.4(S143T) from M1 to R375 and Kir3.1 from P370 to T501.
M2	Subcloning	466	Human	NP_001365901.1
M3	Subcloning	590	Human	NP_001362913.1
MOR	Subcloning	400	Human	
MOR/Ct[Δ32]-DOR	Truncation of 32 residues from the C-terminal of MOR/Ct-DOR	360	Human MOR and DOR	
MOR/Ct[Δ32]-DOR - HB	Insertion of HB tag on MOR/Ct[Δ32]-DOR -	377	Human MOR and DOR	
MOR/Ct-DOR	MOR(M1-R350)-DOR(Q331-A372)	392	Human MOR and DOR	
MOR/Ct-DOR-HB	Insertion of HB tag on MOR/Ct-DOR	409	Human MOR and DOR	
MOR/ECL-DOR	Synthesized by GenScript	380	Human MOR and DOR	See alignment for more details (Supp figure c.1)
MOR/ECL-DOR-HB	Insertion of HB tag on MOR/ECL-DOR	397	Human MOR and DOR	
MOR/EHalf-DOR	Synthesized by GenScript	380	Human MOR and DOR	See alignment for more details (Supp figure c.1)
MOR/EHalf-DOR-HB	Insertion of HB tag on MOR/EHalf-DOR	397	Human MOR and DOR	
MOR/ICL3-DOR	Mutagenesis (K262R)(M266L)(N276S)	400	Human MOR and DOR	
MOR/ICL3-DOR-HB	Insertion of HB tag on MOR/ICL3-DOR	417	Human MOR and DOR	
MOR/ICL-DOR	Synthesized by GenScript	392	Human MOR and DOR	See alignment for more details (Supp figure c.1)
MOR/ICL-DOR-HB	Insertion of HB tag on MOR/ICL-DOR	409	Human MOR and DOR	
MOR/TM-DOR	Synthesized by GenScript	400	Human MOR and DOR	See alignment for more details (Supp figure c.1)
MOR/TM-DOR-HB	Insertion of HB tag on MOR/TM-DOR	417	Human MOR and DOR	
MOR-HB	Insertion of HB tag on MOR (GeneCust)	417	Human	
PTX S1		269	<i>Bordetella pertussis</i>	From Vivaudou <i>et al.</i> , 1997
RGS4	Subcloning	205	Human	NM_005613.5
β-arrestin2	Subcloning	409	Human	NM_004313.4



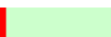
Supplementary figure c.1. Alignment of the protein sequences of MOR/DOR chimeras.


Structural annotation of the different domains appears on top of the alignment. Green – extracellular; blue - intracellular, red -transmembrane helix; yellow- intracellular helix VIII; Residues in brown differ between MOR and DOR. Grey delimits the regions of the constructs selected to be equivalent to DOR.




DOR Structure			
MOR Structure			
MOR/ECL-DOR	- - - - -	M E P A P S A G A	9
DOR	- - - - -	M E P A P S A G A	9
DOR/ICL3-MOR	- - - - -	M E P A P S A G A	9
MOR/EHALF-DOR	- - - - -	M E P A P S A G A	9
DOR/Ct-MOR	- - - - -	M E P A P S A G A	9
MOR/TM-DOR	M D S S A A P T N A S N C T D A L A Y S S	C S P A P S P G S	30
MOR	M D S S A A P T N A S N C T D A L A Y S S	C S P A P S P G S	30
MOR/ICL3-DOR	M D S S A A P T N A S N C T D A L A Y S S	C S P A P S P G S	30
MOR/ICL-DOR	M D S S A A P T N A S N C T D A L A Y S S	C S P A P S P G S	30
MOR/Ct-DOR	M D S S A A P T N A S N C T D A L A Y S S	C S P A P S P G S	30
MOR/C{Δ32}-DOR	M D S S A A P T N A S N C T D A L A Y S S	C S P A P S P G S	30
DOR Structure			
MOR Structure			
MOR/ECL-DOR	E L Q P P L F A N A S D A Y P S A F P S A G A N A S G P P G		39
DOR	E L Q P P L F A N A S D A Y P S A F P S A G A N A S G P P G		39
DOR/ICL3-MOR	E L Q P P L F A N A S D A Y P S A F P S A G A N A S G P P G		39
MOR/EHALF-DOR	E L Q P P L F A N A S D A Y P S A F P S A G A N A S G P P G		39
DOR/Ct-MOR	E L Q P P L F A N A S D A Y P S A F P S A G A N A S G P P G		39
MOR/TM-DOR	W V N L S H L D G N L S D P C G P N R T D L G G R D S L C P		60
MOR	W V N L S H L D G N L S D P C G P N R T D L G G R D S L C P		60
MOR/ICL3-DOR	W V N L S H L D G N L S D P C G P N R T D L G G R D S L C P		60
MOR/ICL-DOR	W V N L S H L D G N L S D P C G P N R T D L G G R D S L C P		60
MOR/Ct-DOR	W V N L S H L D G N L S D P C G P N R T D L G G R D S L C P		60
MOR/C{Δ32}-DOR	W V N L S H L D G N L S D P C G P N R T D L G G R D S L C P		60
DOR Structure			
MOR Structure			
MOR/ECL-DOR	A R S A S S M I T A I T I M A L Y S I V C V V G L F G N F L		69
DOR	A R S A S S L A L A I A I T A L Y S A V C A V G L L G N V L		69
DOR/ICL3-MOR	A R S A S S L A L A I A I T A L Y S A V C A V G L L G N V L		69
MOR/EHALF-DOR	A R S A S S L A L A I A I T A L Y S A V C A V G L F G N F L		69
DOR/Ct-MOR	A R S A S S L A L A I A I T A L Y S A V C A V G L L G N V L		69
MOR/TM-DOR	P T G S P S L A L A I A I T A L Y S A V C A V G L L G N V L		90
MOR	P T G S P S M I T A I T I M A L Y S I V C V V G L F G N F L		90
MOR/ICL3-DOR	P T G S P S M I T A I T I M A L Y S I V C V V G L F G N F L		90
MOR/ICL-DOR	P T G S P S M I T A I T I M A L Y S I V C V V G L F G N F L		90
MOR/Ct-DOR	P T G S P S M I T A I T I M A L Y S I V C V V G L F G N F L		90
MOR/C{Δ32}-DOR	P T G S P S M I T A I T I M A L Y S I V C V V G L F G N F L		90
DOR Structure			
MOR Structure			
MOR/ECL-DOR	V M Y V I V R Y T K M K T A T N I Y I F N L A L A D A L A T		99
DOR	V M F G I V R Y T K M K T A T N I Y I F N L A L A D A L A T		99
DOR/ICL3-MOR	V M F G I V R Y T K M K T A T N I Y I F N L A L A D A L A T		99
MOR/EHALF-DOR	V M Y V I V R Y T K M K T A T N I Y I F N L A L A D A L A T		99
DOR/Ct-MOR	V M F G I V R Y T K M K T A T N I Y I F N L A L A D A L A T		99
MOR/TM-DOR	V M F G I V R Y T K M K T A T N I Y I F N L A L A D A L A T		120
MOR	V M Y V I V R Y T K M K T A T N I Y I F N L A L A D A L A T		120
MOR/ICL3-DOR	V M Y V I V R Y T K M K T A T N I Y I F N L A L A D A L A T		120
MOR/ICL-DOR	V M Y V I V R Y T K M K T A T N I Y I F N L A L A D A L A T		120
MOR/Ct-DOR	V M Y V I V R Y T K M K T A T N I Y I F N L A L A D A L A T		120
MOR/C{Δ32}-DOR	V M Y V I V R Y T K M K T A T N I Y I F N L A L A D A L A T		120



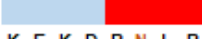
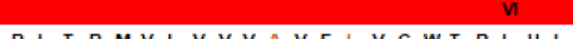
DOR Structure																															
MOR Structure				III																											
MOR/ECL-DOR	S	T	L	P	F	Q	S	V	N	Y	L	M	E	T	W	P	F	G	E	L	L	C	K	I	V	I	S	I	D	Y	129
DOR	S	T	L	P	F	Q	S	A	K	Y	L	M	E	T	W	P	F	G	E	L	L	C	K	A	V	L	S	I	D	Y	129
DOR/ICL3-MOR	S	T	L	P	F	Q	S	A	K	Y	L	M	E	T	W	P	F	G	E	L	L	C	K	A	V	L	S	I	D	Y	129
MOR/EHALF-DOR	S	T	L	P	F	Q	S	A	K	Y	L	M	E	T	W	P	F	G	E	L	L	C	K	A	V	L	S	I	D	Y	129
DOR/Ct-MOR	S	T	L	P	F	Q	S	A	K	Y	L	M	E	T	W	P	F	G	E	L	L	C	K	A	V	L	S	I	D	Y	129
MOR/TM-DOR	S	T	L	P	F	Q	S	A	K	Y	L	M	G	T	W	P	F	G	T	I	L	C	K	A	V	L	S	I	D	Y	150
MOR	S	T	L	P	F	Q	S	V	N	Y	L	M	G	T	W	P	F	G	T	I	L	C	K	I	V	I	S	I	D	Y	150
MOR/ICL3-DOR	S	T	L	P	F	Q	S	V	N	Y	L	M	G	T	W	P	F	G	T	I	L	C	K	I	V	I	S	I	D	Y	150
MOR/ICL-DOR	S	T	L	P	F	Q	S	V	N	Y	L	M	G	T	W	P	F	G	T	I	L	C	K	I	V	I	S	I	D	Y	150
MOR/Ct-DOR	S	T	L	P	F	Q	S	V	N	Y	L	M	G	T	W	P	F	G	T	I	L	C	K	I	V	I	S	I	D	Y	150
MOR/Ct(Δ32)-DOR	S	T	L	P	F	Q	S	V	N	Y	L	M	G	T	W	P	F	G	T	I	L	C	K	I	V	I	S	I	D	Y	150


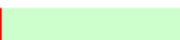


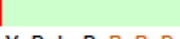

DOR Structure																															
MOR Structure			ICL2																												
MOR/ECL-DOR	Y	N	M	F	T	S	I	F	T	L	C	T	M	S	V	D	R	Y	I	A	V	C	H	P	V	K	A	L	D	F	159
DOR	Y	N	M	F	T	S	I	F	T	L	T	M	M	S	V	D	R	Y	I	A	V	C	H	P	V	K	A	L	D	F	159
DOR/ICL3-MOR	Y	N	M	F	T	S	I	F	T	L	T	M	M	S	V	D	R	Y	I	A	V	C	H	P	V	K	A	L	D	F	159
MOR/EHALF-DOR	Y	N	M	F	T	S	I	F	T	L	C	T	M	S	V	D	R	Y	I	A	V	C	H	P	V	K	A	L	D	F	159
DOR/Ct-MOR	Y	N	M	F	T	S	I	F	T	L	T	M	M	S	V	D	R	Y	I	A	V	C	H	P	V	K	A	L	D	F	159
MOR/TM-DOR	Y	N	M	F	T	S	I	F	T	L	T	M	M	S	V	D	R	Y	I	A	V	C	H	P	V	K	A	L	D	F	180
MOR	Y	N	M	F	T	S	I	F	T	L	C	T	M	S	V	D	R	Y	I	A	V	C	H	P	V	K	A	L	D	F	180
MOR/ICL3-DOR	Y	N	M	F	T	S	I	F	T	L	C	T	M	S	V	D	R	Y	I	A	V	C	H	P	V	K	A	L	D	F	180
MOR/ICL-DOR	Y	N	M	F	T	S	I	F	T	L	C	T	M	S	V	D	R	Y	I	A	V	C	H	P	V	K	A	L	D	F	180
MOR/Ct-DOR	Y	N	M	F	T	S	I	F	T	L	C	T	M	S	V	D	R	Y	I	A	V	C	H	P	V	K	A	L	D	F	180
MOR/Ct(Δ32)-DOR	Y	N	M	F	T	S	I	F	T	L	C	T	M	S	V	D	R	Y	I	A	V	C	H	P	V	K	A	L	D	F	180

DOR Structure																															
MOR Structure		IV																													
MOR/ECL-DOR	R	T	P	R	N	A	K	I	I	N	V	C	N	W	I	L	S	S	A	I	G	L	P	V	M	F	M	A	V	T	189
DOR	R	T	P	A	K	A	K	L	I	N	I	C	I	W	V	L	A	S	G	V	G	V	P	I	M	V	M	A	V	T	189
DOR/ICL3-MOR	R	T	P	A	K	A	K	L	I	N	I	C	I	W	V	L	A	S	G	V	G	V	P	I	M	V	M	A	V	T	189
MOR/EHALF-DOR	R	T	P	R	N	A	K	I	I	N	V	C	N	W	I	L	S	S	A	I	G	L	P	V	M	F	M	A	V	T	189
DOR/Ct-MOR	R	T	P	A	K	A	K	L	I	N	I	C	I	W	V	L	A	S	G	V	G	V	P	I	M	V	M	A	V	T	189
MOR/TM-DOR	R	T	P	A	K	A	K	L	I	N	I	C	I	W	V	L	A	S	G	V	G	V	P	I	M	V	M	A	T	T	210
MOR	R	T	P	R	N	A	K	I	I	N	V	C	N	W	I	L	S	S	A	I	G	L	P	V	M	F	M	A	T	T	210
MOR/ICL3-DOR	R	T	P	R	N	A	K	I	I	N	V	C	N	W	I	L	S	S	A	I	G	L	P	V	M	F	M	A	T	T	210
MOR/ICL-DOR	R	T	P	R	N	A	K	I	I	N	V	C	N	W	I	L	S	S	A	I	G	L	P	V	M	F	M	A	T	T	210
MOR/Ct-DOR	R	T	P	R	N	A	K	I	I	N	V	C	N	W	I	L	S	S	A	I	G	L	P	V	M	F	M	A	T	T	210
MOR/Ct(Δ32)-DOR	R	T	P	R	N	A	K	I	I	N	V	C	N	W	I	L	S	S	A	I	G	L	P	V	M	F	M	A	T	T	210

DOR Structure																															
MOR Structure		V																													
MOR/ECL-DOR	R	P	R	D	G	A	V	V	C	M	L	Q	F	P	S	P	T	W	Y	W	E	N	L	L	K	I	C	V	F	I	219
DOR	R	P	R	D	G	A	V	V	C	M	L	Q	F	P	S	P	S	W	Y	W	D	T	V	T	K	I	C	V	F	L	219
DOR/ICL3-MOR	R	P	R	D	G	A	V	V	C	M	L	Q	F	P	S	P	S	W	Y	W	D	T	V	T	K	I	C	V	F	L	219
MOR/EHALF-DOR	R	P	R	D	G	A	V	V	C	M	L	Q	F	P	S	P	S	W	Y	W	D	T	V	T	K	I	C	V	F	L	219
DOR/Ct-MOR	R	P	R	D	G	A	V	V	C	M	L	Q	F	P	S	P	S	W	Y	W	D	T	V	T	K	I	C	V	F	L	219
MOR/TM-DOR	K	Y	R	Q	G	S	I	D	C	T	L	T	F	S	H	P	S	W	Y	W	D	T	V	T	K	I	C	V	F	L	240
MOR	K	Y	R	Q	G	S	I	D	C	T	L	T	F	S	H	P	T	W	Y	W	E	N	L	L	K	I	C	V	F	I	240
MOR/ICL3-DOR	K	Y	R	Q	G	S	I	D	C	T	L	T	F	S	H	P	T	W	Y	W	E	N	L	L	K	I	C	V	F	I	240
MOR/ICL-DOR	K	Y	R	Q	G	S	I	D	C	T	L	T	F	S	H	P	T	W	Y	W	E	N	L	L	K	I	C	V	F	I	240
MOR/Ct-DOR	K	Y	R	Q	G	S	I	D	C	T	L	T	F	S	H	P	T	W	Y	W	E	N	L	L	K	I	C	V	F	I	240
MOR/Ct(Δ32)-DOR	K	Y	R	Q	G	S	I	D	C	T	L	T	F	S	H	P	T	W	Y	W	E	N	L	L	K	I	C	V	F	I	240

DOR Structure			
MOR Structure		ICL3	
MOR/ECL-DOR	F A F I M P V L I I T V C Y G L M I L R L K S V R M L S G S		249
DOR	F A F V V P I L I I T V C Y G L M L L R L R S V R L L S G S		249
DOR/ICL3-MOR	F A F V V P I L I I T V C Y G L M L L R L K S V R M L S G S		249
MOR/EHALF-DOR	F A F V V P V L I I T V C Y G L M I L R L K S V R M L S G S		249
DOR/Ct-MOR	F A F V V P I L I I T V C Y G L M L L R L R S V R L L S G S		249
MOR/TM-DOR	F A F V V P I L I I T V C Y G L M L L R L K S V R M L S G S		270
MOR	F A F I M P V L I I T V C Y G L M I L R L K S V R M L S G S		270
MOR/ICL3-DOR	F A F I M P V L I I T V C Y G L M I L R L R S V R L L S G S		270
MOR/ICL-DOR	F A F I M P V L I I T V C Y G L M I L R L R S V R L L S G S		270
MOR/Ct-DOR	F A F I M P V L I I T V C Y G L M I L R L K S V R M L S G S		270
MOR/Ct(Δ32)-DOR	F A F I M P V L I I T V C Y G L M I L R L K S V R M L S G S		270

DOR Structure			
MOR Structure			VI
MOR/ECL-DOR	K E K D R N L R R I T R M V L V V V A V F I V C W T P I H I		279
DOR	K E K D R S L R R I T R M V L V V V G A F V V C W A P I H I		279
DOR/ICL3-MOR	K E K D R N L R R I T R M V L V V V G A F V V C W A P I H I		279
MOR/EHALF-DOR	K E K D R N L R R I T R M V L V V V G A F V V C W A P I H I		279
DOR/Ct-MOR	K E K D R S L R R I T R M V L V V V G A F V V C W A P I H I		279
MOR/TM-DOR	K E K D R N L R R I T R M V L V V V G A F V V C W A P I H I		300
MOR	K E K D R N L R R I T R M V L V V V A V F I V C W T P I H I		300
MOR/ICL3-DOR	K E K D R S L R R I T R M V L V V V A V F I V C W T P I H I		300
MOR/ICL-DOR	K E K D R S L R R I T R M V L V V V A V F I V C W T P I H I		300
MOR/Ct-DOR	K E K D R N L R R I T R M V L V V V A V F I V C W T P I H I		300
MOR/Ct(Δ32)-DOR	K E K D R N L R R I T R M V L V V V A V F I V C W T P I H I		300

DOR Structure				
MOR Structure				VII
MOR/ECL-DOR	Y V I I K A L V D I D R R D T F Q T V S W H F C I A L G Y T			309
DOR	F V I V W T L V D I D R R D P L V V A A L H L C I A L G Y A			309
DOR/ICL3-MOR	F V I V W T L V D I D R R D P L V V A A L H L C I A L G Y A			309
MOR/EHALF-DOR	F V I V W T L V D I D R R D P L V V A A L H L C I A L G Y A			309
DOR/Ct-MOR	F V I V W T L V D I D R R D P L V V A A L H L C I A L G Y A			309
MOR/TM-DOR	F V I V W T L V T I P E - T P L V V A A L H L C I A L G Y A			329
MOR	Y V I I K A L V T I P E - T T F Q T V S W H F C I A L G Y T			329
MOR/ICL3-DOR	Y V I I K A L V T I P E - T T F Q T V S W H F C I A L G Y T			329
MOR/ICL-DOR	Y V I I K A L V T I P E - T T F Q T V S W H F C I A L G Y T			329
MOR/Ct-DOR	Y V I I K A L V T I P E - T T F Q T V S W H F C I A L G Y T			329
MOR/Ct(Δ32)-DOR	Y V I I K A L V T I P E - T T F Q T V S W H F C I A L G Y T			329




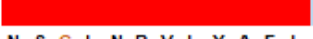
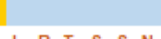
DOR Structure				
MOR Structure		VII		
MOR/ECL-DOR	N S C L N P V L Y A F L D E N F K R C F R E F C I P T S S N			339
DOR	N S S L N P V L Y A F L D E N F K R C F R Q L C R K P C G R			339
DOR/ICL3-MOR	N S S L N P V L Y A F L D E N F K R C F R Q L C R K P C G R			339
MOR/EHALF-DOR	N S C L N P V L Y A F L D E N F K R C F R E F C I P T S S N			339
DOR/Ct-MOR	N S S L N P V L Y A F L D E N F K R C F R E F C I P T S S N			339
MOR/TM-DOR	N S S L N P V L Y A F L D E N F K R C F R E F C I P T S S N			359
MOR	N S C L N P V L Y A F L D E N F K R C F R E F C I P T S S N			359
MOR/ICL3-DOR	N S C L N P V L Y A F L D E N F K R C F R E F C I P T S S N			359
MOR/ICL-DOR	N S C L N P V L Y A F L D E N F K R C F R Q L C R K P C G R			359
MOR/Ct-DOR	N S C L N P V L Y A F L D E N F K R C F R Q L C R K P C G R			359
MOR/Ct(Δ32)-DOR	N S C L N P V L Y A F L D E N F K R C F R Q L C R K P C G R			359

Table c.2. Detailed information about the design of the different proteins used in Project B.

'GeneCust' indicates that the specified company prepared the constructions.

Construct	Molecular manipulation	Protein size	Protein origin	Comments
Baikal20-HB	Subcloning of Baikal20 and insertion of HiBIT tag by PCR. Original supplied by Dr. Valentin Gordeliy.	264	Type 2 VR of unknown virus. From metagenomic study.	
Chr2	Subcloning. Original supplied by Dr. Arne Julich.	586	<i>Chlamydomonas reinhardtii</i>	Optimized for mammalian cell expression. It is fused to a red fluorescent protein mKate.
Chr2-HB	Insertion of HB tag on Chr2 (GeneCust).	603	<i>Chlamydomonas reinhardtii</i>	
DOR=Chr2-HB	Synthesized by GeneCust.	1045	Human DOR, mutant of GFP from <i>Aequorea victoria</i> , rat gastric H ⁺ K ⁺ -ATPase β-subunit, and <i>Chlamydomonas reinhardtii</i>	Construction based on Kleinlogel <i>et al.</i> , 2011 (JN836740.1)
DOR=OLPVR1	Synthesized by GenScript.	942	Human DOR, mutant of GFP from <i>Aequorea victoria</i> , rat gastric H ⁺ K ⁺ -ATPase β-subunit, and Organic Lake Phycodnavirus (OLP)	Construction based on Kleinlogel <i>et al.</i> , 2011 (JN836740.1)
DOR=OLPVR1-HB	Insertion of HB tag by PCR on DOR=OLPVR1.	959	Human DOR, mutant of GFP from <i>Aequorea victoria</i> , rat gastric H ⁺ K ⁺ -ATPase β-subunit, and Organic Lake Phycodnavirus (OLP)	
IL6-OLPVR1-HB	Insertion of IL6 tag and a (VS) linker upstream the HB tag. (GeneCust)	272	Organic Lake Phycodnavirus (OLP)	
OLPVR1	Subcloning. Original supplied by Valentin Gordeliy.	223	Organic Lake Phycodnavirus (OLP)	ADX06642.1
OLPVR1_O1O2mut	Synthesized by GenScript.	223	Organic Lake Phycodnavirus (OLP)	7AKW_A, Mutations: I169L, Y172G, F173A, V177L, F179A, V202F, I206F, Y207V, I211F and S208G
OLPVR1_O1O2mut-HB	Insertion of HB tag by PCR on OLPVR1_O1O2mut.	240	Organic Lake Phycodnavirus (OLP)	
OLPVR1-HB	Insertion of HB tag on OLPVR1 (GeneCust).	240	Organic Lake Phycodnavirus (OLP)	
OLPVR1-MT-HB	Insertion of MT and HB tag by PCR on OLPVR1.	263	Organic Lake Phycodnavirus (OLP)	
OLPVR2-HB	Subcloning of OLPVR2 and insertion of HiBIT tag by PCR. Original supplied by Dr. Valentin Gordeliy.	228	Organic Lake Phycodnavirus (OLP)	6SQG_E
SpaR-HB	Subcloning of SpaR and insertion of HB tag by PCR. Original supplied by Dr. Valentin Gordeliy.	254	<i>Sphingomonas paucimobilis</i>	WP_037567788.1
SS-OLPVR1	Insertion of SS by PCR.	247	Organic Lake Phycodnavirus (OLP)	
SS-OLPVR1-HB	Insertion of HB tag on SS-OLPVR1 (GeneCust).	268	Organic Lake Phycodnavirus (OLP)	SS-(GS)-HB-(GSSGGSSG)-OLPVR1
TARA149-HB	Subcloning of TARA149 and insertion of HB tag by PCR. Original supplied by Dr. Valentin Gordeliy.	303	Type 2 VR of unknown virus. From metagenomic study.	
TARA150	Subcloning and insertion of SS by PCR (SS-TARA150). Original supplied by Dr. Valentin Gordeliy.	254	Type 1 VR of unknown virus. From metagenomic study.	
TARA150-HB	Insertion of HB tag by PCR and deletion of SS from TARA150	247	Type 1 VR of unknown virus. From metagenomic study.	
VirChR1	Subcloning and insertion of SS by PCR (SS-VirChR1-MT). Original construct already fused to MT supplied by Valentin Gordeliy.	289	Type 1 VR of unknown virus. From metagenomic study.	
VirChR1-HB	Insertion of HB tag by PCR on VirChR1 and deletion of SS and MT.	259	Type 1 VR of unknown virus. From metagenomic study.	
VirChR1-MT-HB	Insertion of HB tag (GeneCust). Original construct supplied by Valentin Gordeliy containing MT and mKate at the C-terminal (VirChR1-MT-mKate-HB).	570	Type 1 VR of unknown virus. From metagenomic study.	Original construct is fused to a red fluorescent protein mKate.

D – XenoGlo: Exploiting Nanoluc technology for non-destructive surface-expression measurements of single-cell *Xenopus* oocytes

We developed a new technique to measure surface expression in *Xenopus* oocytes, which we name XenoGlo.

The assessment of expression levels is often desirable and necessary when studying proteins. It is the case when comparing the properties of wild-type vs. mutant proteins or when studying mechanisms that depend on the protein density or stoichiometry.

In the specific case of *Xenopus* oocytes, where variability in expression is often considerable, performing functional assays and determining expression level on a single oocyte might be required to integrate both pieces of information accurately.

The most common techniques used to determine protein expression in single oocytes are western blotting, fluorescent microscopy of GFP-fused proteins, and chemiluminescent detection of an external epitope using horseradish peroxidase-coupled antibodies.

Western blotting utilizes antibodies to detect specific proteins from a pool that has been separated by gel electrophoresis. While western blotting is widely used with many cell types, *Xenopus* presents some particular constraints to using this technique. *Xenopus* are large cells that can express close to 125 µg of a particular protein, facilitating single-cell protein detection. However, it comes with the caveat that it contains large amounts of yolk platelet proteins in the cytoplasm. Separation by electrophoresis is unfeasible unless a protocol is used to firstly exclude them from the pool. It is possible to perform western blotting in *Xenopus*, but it is a challenging and time-consuming task that prerequisites the destruction of the cell (Jørgensen, Nour-Eldin & Halkier 2016; Lin-Moshier & Marchant, 2013).

The green fluorescent protein (GFP) from the jellyfish *Aequorea victoria*, fused to the protein of interest, can serve as a marker for protein expression and localization in *Xenopus* oocytes (Lee & Bezanilla, 2019; Mirshahi *et al.*, 2001). Contrary to western blotting, which requires small or no tags linked to the protein, the fusion to GFP modifies the protein significantly. Potential artifacts on trafficking and function have to be scrutinized through stringent controls.

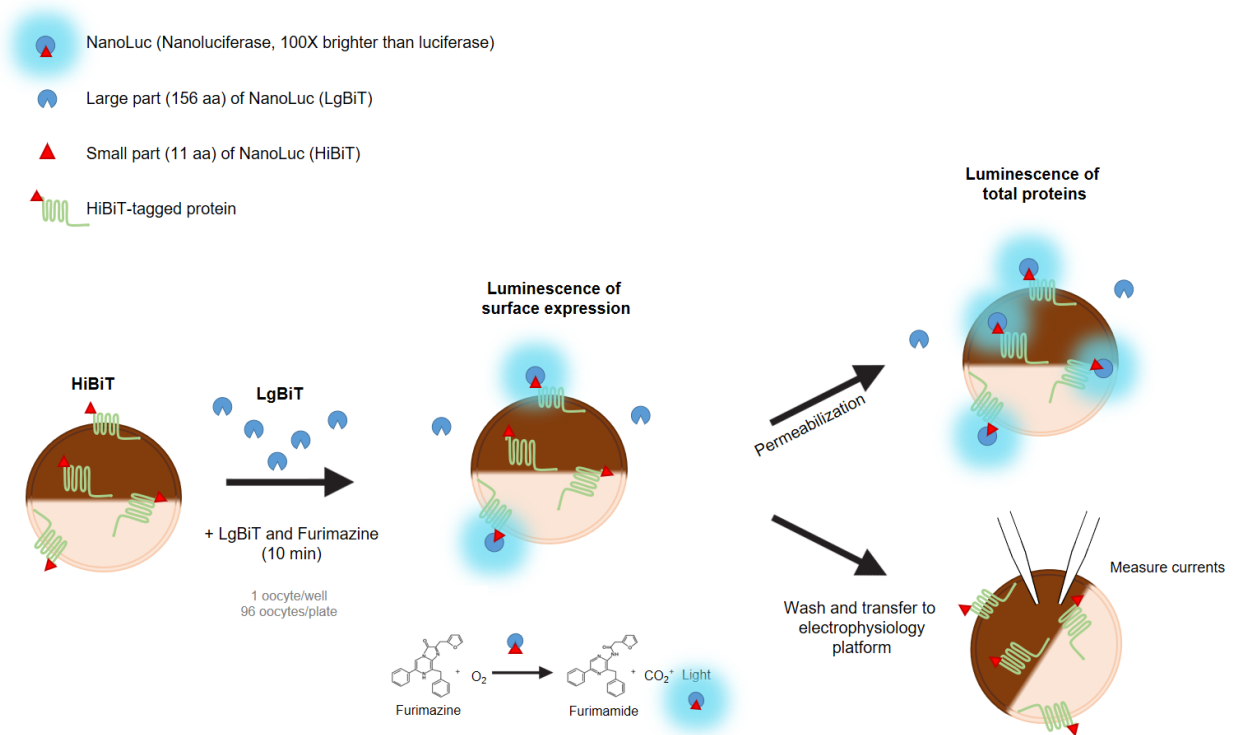
In the particular case of oocytes, their unusually high background autofluorescence imposes another limitation to this method since it impairs sensitivity. Because oocytes are large and opaque, paraformaldehyde fixation and sectioning are necessary for confocal or wide-field epifluorescence microscopy.

Chemiluminescent detection of an external epitope using horseradish peroxidase (HRP)-coupled antibodies was introduced by Zerangue *et al.* (1999) to measure surface expression of Kir6.2 channels in single oocytes. They inserted an HA tag in an extracellular loop of Kir6.2. When Kir6.2 is addressed to the surface membrane, the HA epitope is exposed and can be labeled with a monoclonal antibody to HA, and subsequently with a HRP-conjugated secondary antibody, which can produce a luminescence signal in the presence of luminol. Oocytes are large enough that the chemiluminescence of single oocytes can be measured. This technique has been used successfully in a number of studies, following the original work. It proved however difficult to implement, in particular in our laboratory where, in spite of many attempts, we were unable to obtain reproducible results, even using the original Kir6.2 construct. Furthermore, this technique is relatively expensive and time consuming, and requires highly-trained personnel.

These methods allow the measurement of protein expression in single oocytes, albeit with complex multi-step protocols associated with problems of reproducibility. The use of the same oocyte for functional studies and protein expression measurements is permitted, as long as functional studies are done first, since the three protein detection methods are destructive.

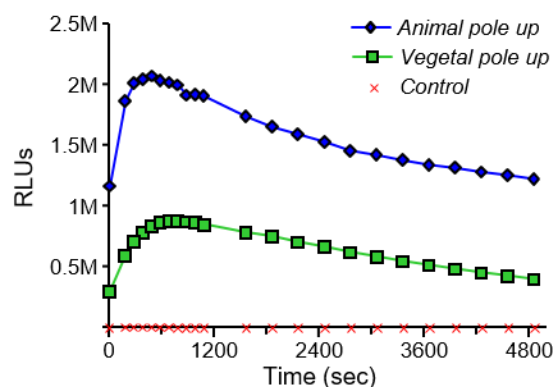
We sought to optimize a protein expression detection system for the oocytes that overcomes some of the disadvantages of western blotting, GFP fusions, or enzyme-coupled antibodies. For that, we relied on Nanoluciferase, in particular the HiBiT system offered by Promega (Nano-Glo®).

The HiBiT tag is a small 11–amino acid peptide that produces bright luminescence upon high-affinity complementation with LgBiT - the large subunit of Nanoluciferase. Quantification of HiBiT-tagged proteins can be performed in less than 20 minutes, by measuring luminescent upon addition of a reagent containing the LgBiT and the substrate for the luciferase (Supplementary figure d.1). In oocytes, luminescence signal peaks at 10 minutes after addition of the reagent. Furthermore, it reaches higher values when the animal pole (dark pole) is facing the light detector. This is in agreement with the polarized protein distribution in *Xenopus* oocytes (Supplementary figure d.2).



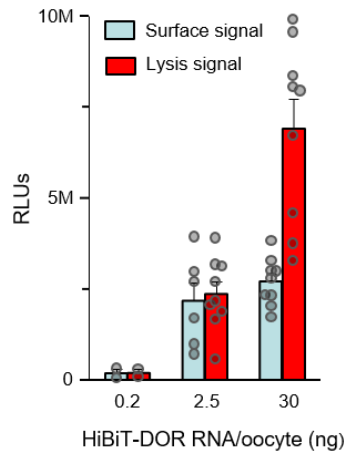
Supplementary figure d.1. Schematic protocol for the detection of protein expression in *Xenopus* oocytes using Nanoluciferase.

The protein of interest is tagged with the 11 amino-acid sequence of HiBiT on the extracellular terminal. The short HiBiT peptide can complement the LargeBiT (LgBiT) of nanoluciferase and yield a functional protein (NanoLuc). Once applied, the substrate furimazine is converted by NanoLuc producing a luminescence signal. Intact cells only present luminescence if expressing HiBiT-tagged proteins at the surface. Permeabilization of the cells allows detection of HiBiT-tagged proteins intracellularly. Surface detection is non-destructive, and oocytes can be reused for electrophysiological recordings after a ≈ 30 s wash in oocyte Ringer's solution.



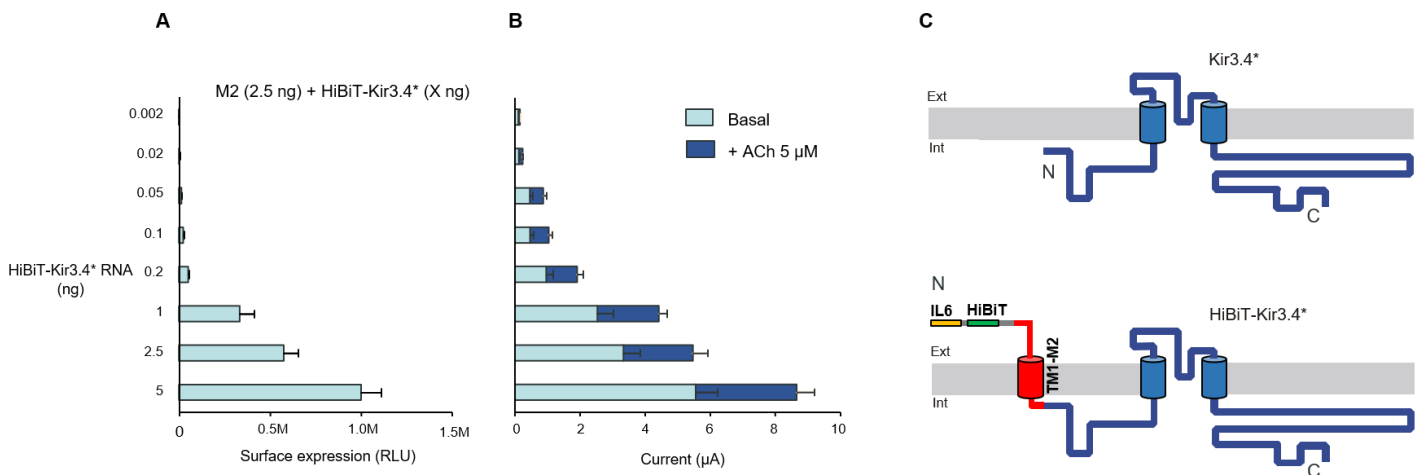
Supplementary figure d.2. Luminescence signal reaches the peak at 10 minutes and depends on oocyte placement.

Mean luminescence recorded in intact oocytes expressing HiBiT-tagged δ -opioid receptors (HiBiT-DOR). Each oocyte was injected with 2.5 ng RNA coding for HiBiT-DOR and 0.1 ng coding for Kir3.4*. Oocytes expressing untagged M3 receptors were used as a negative control. After 48-hour incubation, oocytes were positioned in a 96-well plate, and luminescence was monitored for 80 minutes after adding the nanoluciferase substrate. Oocytes were positioned either with the vegetal or animal (dark) pole facing the luminescence detector (*Vegetal pole up* or *Animal pole up*). Each point represents the average luminescence from 3 oocytes. Receptor proteins express better in the animal pole than the vegetal pole of oocytes. The *Animal pole up* peak signal was 2.4-fold larger than the *Vegetal pole up* peak signal.



Supplementary figure d.3. Expression of DOR increases with the amount of RNA injected and can be followed using HiBiT tagged proteins.

Blue bars represent the mean luminescence recorded in intact oocytes vs. the quantity of RNA coding for HiBiT-tagged DOR (HiBiT-DOR). Oocytes were coinjected with 0.1 ng of Kir3.4* RNA. Red bars represent the mean luminescence measured in the oocytes after permeabilization.



Supplementary figure d.4. Luminescence of HiBiT-tagged Kir3.4* channel increases with the amount of RNA injected and correlates with an increase in measured currents.

(A) Bars represent the mean luminescence recorded in intact oocytes injected with different RNA amounts of HiBiT-tagged Kir3.4* and 2.5 ng of M2 receptor. Error bars represent the SEM of 2-12 oocytes.

(B) Light blue bars represent the basal currents recorded by TEVC for the same RNA amounts of the tagged channel. Dark blue bars represent the induced current by the application of acetylcholine – ACh. Error bars represent the SEM of 2-12 oocytes.

(C) Topology of the Kir3.4* channel tagged with HiBiT. Wt Kir3.4 has intracellular N- and C-terminals. The tagged construct is first fused to the transmembrane helix 1 (TM1) of the human Muscarinic Receptor 2 (M2) to create an extracellular N-terminal. HiBiT is then fused to the N-terminal, allowing for extracellular detection. Interleukine 6 secretion signal sequence (IL6) is used to improve the expression of the construct.

The insertion of the HiBiT tag on an extracellular domain of a membrane protein allows for the measurement of its surface expression. Promega claims the amount of luminescence generated is proportional to the amount of HiBiT-tagged protein accessible over seven orders

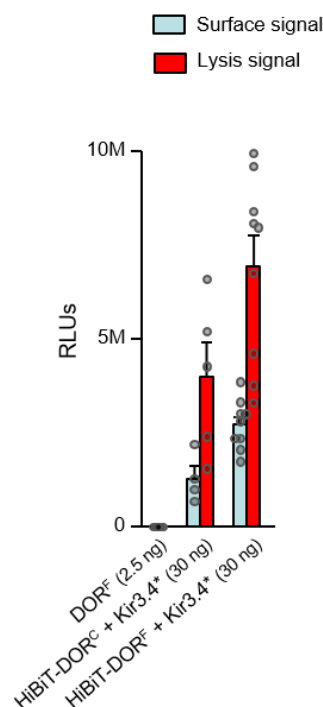
of magnitude. We found that in oocytes, increasing the amount of RNA injected correlates with an increase in luminescence (surface and total) as seen in Supplementary figure d.3.

By permeabilizing the cells, the total amount of HiBiT-protein can be assessed. Alternatively, oocytes can be washed and used for functional studies. See Supplementary figure d.4. where HiBiT-tagged channels are subjected to protein surface detection and functional analyses.

Contrary to GFP, the small size of the HiBiT tag facilitates its fusion to the protein of interest with minimal impact on trafficking or function.

Boursier *et al.* (2020) showed that HiBiT-fused GPCRs had the same pharmacological properties as wild-type receptors. Adding an IL6 secretion signal sequence upstream of the HiBiT tag further promoted the efficient translocation of the GPCRs to the cell surface, similarly to unmodified proteins. The results of Boursier *et al.* (2020) in PC3 cell lines are consistent with the results we found in *Xenopus* oocytes.

Throughout the thesis, we validated the use of this technique in oocytes and illustrated its utility.



Supplementary figure d.5. Expression of DOR is regulated by the identity of residue 27 and can be distinguished using HiBiT tagged proteins.

Blue bars represent the mean luminescence recorded in intact oocytes expressing HiBiT-tagged DOR^{Phe-27} (HiBiT-DOR^F) or DOR^{Cys-27} (HiBiT-DOR^C). Untagged DOR^{Phe-27} (DOR^F) was used as a negative control. The amount of receptor RNA injected in each oocyte is indicated in parenthesis. Where specified, 0.1 ng of Kir3.4* RNA was coinjected. Red bars represent the mean luminescence measured in the oocytes after permeabilization. Error bars represent the SEM of 4-15 oocytes.

We surveyed, with the same HiBiT-tagged proteins, multiple aspects related to protein expression, including differences in surface expression of polymorphic proteins (Supplementary figure d.5), internalization (Supplementary figure a.13), differences in intracellular vs. surface expression (Figure b.10). Furthermore, we confirmed the functionality of the different proteins tagged to HiBiT, including ion channels (Supplementary figure d.4), rhodopsins (Supplementary figure b.2) and GPCRs (Figure a.19).

Fusion of IL6 upstream the HiBiT tag promoted a response of the GPCRs (Figure a.19) and the ions channels (Supplementary figure d.4), which was similar to wild-type proteins (as in Boursier *et al.*, 2020). In contrast, it did not improve surface expression of rhodopsins that accumulate intracellularly (Figure b.13).

The XenoGlo assay is a simple, reproducible, versatile, and non-destructive method to evaluate surface protein expression levels in single oocytes enabling prior or subsequent functional testing.

Being able to estimate protein surface expression easily and simultaneously measure current amplitude in a single oocyte might further expand the usefulness of these model cells.

- Boursier, M. E., Levin, S., Zimmerman, K., Machleidt, T., Hurst, R., Butler, B. L., Eggers, C. T., Kirkland, T. A., Wood, K. V., & Ohana, R. F. (2020). The luminescent HiBiT peptide enables selective quantitation of G protein-coupled receptor ligand engagement and internalization in living cells. *Journal of Biological Chemistry*, 295(15), 5124–5135.
- Jørgensen, M. E., Nour-Eldin, H. H., & Halkier, B. A. (2016). A Western Blot protocol for detection of proteins heterologously expressed in *Xenopus laevis* oocytes. In A. Fett-Neto (Ed.), *Methods in Molecular Biology - Biotechnology of Plant Secondary Metabolism* (Vol. 1405, pp. 99–107). Humana Press.
- Lee, E. E. L., & Bezanilla, F. (2019). Methodological improvements for fluorescence recordings in *Xenopus laevis* oocytes. *The Journal of General Physiology*, 151(2), 264–272.
- Leskelä TT, Markkanen PM, Alahuhta IA, Tuusa JT, P.-R. U. (2009). Phe27Cys polymorphism alters the maturation and subcellular localization of the human delta opioid receptor. *Traffic*, 10(1), 116–129.
- Lin-Moshier, Y., & Marchant, J. S. (2013). A rapid Western blotting protocol for the *Xenopus* oocyte. *Cold Spring Harbor Protocols*, 2013(3), pdb.prot072793.
- Mirshahi, T., Logothetis, D. E., & Sassaroli, M. (2001). Localization and quantification of GFP-tagged ion channels expressed in *Xenopus* oocytes. In A. N. Lopatin & C. G. Nichols (Eds.), *Ion Channel Localization: Methods and Protocols* (pp. 215–231). Humana Press.

Sarajärvi T, Tuusa JT, Haapasalo A, Lackman JJ, Sormunen R, Helisalmi S, Roehr JT, Parrado AR, Mäkinen P, Bertram L, Soininen H, Tanzi RE, Petäjä-Repo UE, H. M. (2011). Cysteine 27 variant of the delta-opioid receptor affects amyloid precursor protein processing through altered endocytic trafficking. *Molecular and Cellular Biology*, 31(11), 2326–2340.

Zerangue, N., Schwappach, B., Jan, Y. N., and Jan, L. Y. (1999). A new ER trafficking signal regulates the subunit stoichiometry of plasma membrane K(ATP) channels. *Neuron* 22, 537-548